A Variable Material Property Approach for Elastic-Plastic Analysis of Proportional and Nonproportional Loading

by

Hamid Jahed

A thesis
presented to the University of Waterloo
in fulfilment of the
thesis requirement for the degree of
Doctor of Philosophy
in
Mechanical Engineering

Waterloo, Ontario, Canada, 1997

© Hamid Jahed, 1997

National Library of Canada
Acquisitions and Bibliographic Services
395 Wellington Street
Ottawa ON K1A 0N4
Canada

Bibliothèque nationale du Canada
Acquisitions et services bibliographiques
395, rue Wellington
Ottawa ON K1A 0N4
Canada

Your file Votre référence

Our file Notre référence

The author has granted a non-exclusive licence allowing the National Library of Canada to reproduce, loan, distribute or sell copies of this thesis in microform, paper or electronic formats.

The author retains ownership of the copyright in this thesis. Neither the thesis nor substantial extracts from it may be printed or otherwise reproduced without the author's permission.

L'auteur a accordé une licence non exclusive permettant à la Bibliothèque nationale du Canada de reproduire, prêter, distribuer ou vendre des copies de cette thèse sous la forme de microfiche/film, de reproduction sur papier ou sur format électronique.

L'auteur conserve la propriété du droit d'auteur qui protège cette thèse. Ni la thèse ni des extraits substantiels de celle-ci ne doivent être imprimés ou autrement reproduits sans son autorisation.

0-612-22211-X

Canada

The University of Waterloo requires the signatures of all persons using or photocopying this thesis. Please sign below, and give address and date.

ABSTRACT

A linear elastic solution of a boundary value problem is used as the basis to generate the corresponding inelastic solution. This method treats the material parameters as field variables, and their distribution is obtained as part of the solution in an iterative manner. Five different schemes to update these material parameters are discussed and compared. A procedure for the calculation of the residual stress field is presented.

In this context, a general axisymmetric method of elastic-plastic analysis is proposed. Application of this method to the residual stress prediction for an autofrettaged cylinder and a cold worked fastener hole is presented. Lamé's linear elastic solution is used in these applications. Residual stress calculations based on the actual material curve, isotropic or kinematic hardening models, and a variable Bauschinger effect factor (BEF) is carried out. It is concluded that the consideration of the dependency of the BEF on plastic strain makes significant changes to the residual hoop stress near the bore for low-level autofrettage. However, this dependency is insignificant for high level autofrettage. Results obtained here are shown to be in good agreement with experiment, and finite element results.

A total deformation theory capable of analyzing a sequence of linear nonproportional loading is proposed. Each linear loading path is defined with reference to its previous loading path, analogous to proportional loading. The application of the proposed formulation to tension-torsion loading of thin tubes and pressure-torsion loading of thick-walled cylinders is carried out. It is shown that for stress controlled processes, the proposed method gives the same plastic strain field as does incremental plasticity. For load controlled processes, where stresses are not known a priori, a method to estimate the plastic strain for linear hardening materials is proposed. This method calculates the necessary stress fields using conventional deformation plasticity. These stresses are then

used in the proposed total deformation formulation to predict plastic strains. The plastic strain field resulting from this method is compared with finite element results using incremental plasticity. The results are in very good agreement. The proposed method significantly reduces computation time.

ACKNOWLEDGMENTS

I would like to express my sincere thanks to my supervisors Professor R. N. Dubey for his insightful ideas on the theory of plasticity, continuing support, encouragement, and guidance; and Professor S. B. Lambert for his valuable suggestions and helpful advices during the course of this study.

I wish to thank my thesis committee members, especially, Professor G. Glinka for his technical advices and encouragement; and Professor C. Thompson of Civil Engineering Department, for his concerns and valuable advices during the course of this project.

I also wish to express my gratitude to Professor R. Sethuraman of Indian Institute of Technology, Madras, for hours of discussion during his stay in Waterloo.

Thanks are also due to all of my fellow graduate students in solid mechanics group for creating a friendly environment where ideas are openly exchanged. Special thanks are due to A. Kiciak, for friendly discussions on almost everything; W. Reinhardt, for helpful discussions on plasticity; R. Chen , for critical review of this manuscript and discussions on ABAQUS, X. Wang, for discussions on finite element method, and D. Cronin for discussions on ABAQUS.

The valuable financial support of Iran University of Science and Technology and Ministry of Higher Education of Iran is gratefully acknowledged. Thanks are also offered to the Natural Science and Engineering Research Council of Canada for financial assistance.

Last, but definitely not least, I would like to thank my wife, Pary, for her sacrifices, understanding and patience, particularly for her strength in single-handedly raising our children while I was spending week-ends and nights preparing this thesis.

Intrinsically, man seeks to attain absolute perfection. An artist is seeking for ultimate beauty, a politician is seeking for ultimate power, a scientist is seeking for ultimate knowledge. It is "Him" whom they all seek, however, he may not be aware of it!

in his letter to president Gorbachev,

Late Imam Khomeini, 1989

TABLE OF CONTENTS

Abstract iv

Acknowledgments vi

Dedication vii

Table of Contents viii

List of Tables xiii

List of Figures xiv

List of Symbols xviii

1. INTRODUCTION 1

1.1 OBJECTIVES AND PROBLEM IDENTIFICATION 2

1.1.1 Inelastic Analysis Based on Linear Elastic Solutions 2

1.1.2 Application of Total Deformation Theory of Plasticity to Nonproportional Loading 4

1.2 OUTLINE 6

2. BACKGROUND 8

2.1 STRESS-STRAIN CURVES 8

2.1.1 Moduli involved in elastic-plastic analysis (E, E_s, E_t, and E_p) 9

2.1.2 Modeling of the uniaxial behavior in plasticity 11

2.1.2.1 Elastic-perfectly plastic model 11

2.1.2.2 Elastic-linear hardening model 12

2.1.2.3 Ramberg-Osgood model 13

2.1.2.4 Piecewise linear model 14

2.2 YIELD CRITERIA 15

2.2.1 Tresca yield criterion 15

2.2.2 Von Mises yield criterion 16

2.3 STRESS-STRAIN RELATIONS 18

2.3.1 Linear elastic 18

2.3.2 Deformation plasticity 19

2.3.3 Incremental plasticity 20

2.3.4 Deformation versus incremental plasticity theories 21

2.4 HARDENING RULES 25

2.4.1 Isotropic hardening 25

2.4.2 Kinematic hardening 28

2.5 BOUNDARY VALUE PROBLEM 28

2.5.1 Equilibrium 29

2.5.2 Compatibility 30

2.5.3 Constitutive relations 31

2.6 ELASTIC-PLASTIC METHOD OF SOLUTION BASED ON ELASTIC SOLUTION 31

2.6.1 Modified elastic solution in elastic-plastic notch analysis 32

2.6.2 Method of successive elastic solution 35

2.6.3 Reduced modulus method 36

3. VARIABLE MATERIAL PROPERTY METHOD 40

3.1 FORMULATION 40

3.1.1 Pseudo linear elastic points 42

3.1.2 Effective moduli forms 44

3.1.3 Implementation 45

3.1.4 Moduli evaluation 47

3.1.4.1 Projection method 47

3.1.4.2 Arc-length method 49

3.1.4.3 Energy methods 50

3.1.4.3.1 Neuber's method 50

3.1.4.3.2 Glinka's Method 51

3.1.4.3.3 Combined method 53

3.1.5 Unloading and reversed yielding 55

3.2 AN AXISYMMETRIC METHOD OF ELASTIC-PLASTIC ANALYSIS 57

3.2.1 Lamé solution 58

3.2.2 Implementation for elastic-plastic analysis 62

3.2.2.1 Residual stresses calculation 65

3.3 CONVERGENCE COMPARISON 65

3.3.1 Evaluation of methods for updating the moduli 66

3.3.2 Number of strips 70

4. APPLICATIONS 75

4.1 LOADING OF THICK-WALLED CYLINDERS 75

4.1.1 Literature review 75

4.1.1.1 Elastic-perfectly plastic Tresca cylinder 76

4.1.2 Elastic-plastic behavior of nonhardening materials 85

4.1.3 Elastic-plastic behavior of hardening materials 87
4.2 AUTOFRETTAGE 93
4.2.1 Literature review 94
4.2.2 Actual stress-strain unloading curve 97
4.2.3 Isotropic and kinematic hardening models 105
4.2.4 Variable Bauschinger effect 109
4.3 LOADING AND UNLOADING OF FASTENER HOLES 113
4.3.1 Literature Review 115
4.3.1.1 Loading 115
4.3.1.2 Residual stress calculations 117
4.3.2 Loading of a fastener hole 125
4.3.3 Residual stresses in cold worked fastener holes 130
4.3.3.1 Actual stress-strain unloading curve 130
4.3.3.2 Elastic-plastic boundary prediction 134
4.4 MULTIAXIAL LOADING OF A THICK-WALLED CYLINDER 138

5. TOTAL DEFORMATION FORMULATION FOR NONPROPORTIONAL LOADING ... 145

5.1. INTRODUCTION 145
5.2. FORMULATION 146
5.2.1 Linear hardening materials 149
5.2.2 Hardening materials obeying Ramberg-Osgood relation 150
5.3. APPLICATIONS 153
5.3.1 Thin tubes under tension and torsion 153
5.3.1.1 Linear hardening materials 157
5.3.1.1.1 Tension-torsion (path OCB) 158
5.3.1.1.2 Torsion-tension (path OAB) 160
5.3.1.2 Materials obeying the Ramberg-Osgood relation 162
5.3.1.2.1 Tension-torsion (path OCB) 162
5.3.1.2.2 Torsion-tension (path OAB) 163

5.3.2 Nonproportional loading of thick-walled cylinders 165
5.3.2.1 Plastic strain field 171
5.3.2.1.1 Torsion-pressure 172
5.3.2.1.2 Pressure-torsion 174

6. CONCLUSIONS AND RECOMMENDATIONS 176

6.1 CONCLUSIONS 176
6.2 RECOMMENDATIONS 178

APPENDIX A: FORTRAN CODE FOR AXISYMMETRIC PROBLEMS 179

APPENDIX B: MAPLE V.4 OUTPUT 199

APPENDIX C: PLASTIC STRAIN CALCULATION FOR A SEQUENCE OF LINEAR NONPROPORTIONAL LOADING 202

REFERENCES 216

LIST OF TABLES

Table 3.1: Convergence comparison (plane stress) 68
Table 3.2: Convergence comparison (plane strain) 69

Table 4.1: Comparison of several theories for plastic analysis of thick cylinders 77
Table 4.2: Comparison of several autofrettage theories 98
Table 4.3: Uniaxial stress-strain data (Chen & O'Hara, 1984) 106
Table 4.4: Data for loading behavior of Al 7075 T6 135
Table 4.5: Present method results of elastic-plastic boundary location 136

LIST OF FIGURES

Figure 1.1: Elastic-plastic analysis based on linear elastic solutions 3

Figure 1.2: Nonproportional loading OB, defined as a sequence of two linear loading OA (torsion) and AB (compression) 5

Figure 2.1: Elastic, secant, tangent, and plastic moduli definition based on a)stress-strain or b) stress-plastic strain curves 9

Figure 2.2: Idealized stress-strain curves 12

Figure 2.3: Yield locus for Tresca and von Mises yield criterion 16

Figure 2.4: Nonproportional loading path 22

Figure 2.5: AISI 4333 M4 loading-unloading curve 26

Figure 2.6: Isotropic hardening 27

Figure 2.7: Isotropic and kinematic hardening 27

Figure 2.8: Kinematic hardening 29

Figure 3.1: Pseudo linear elastic points 43

Figure 3.2: Projection method 48

Figure 3.3: Arc-length method 50

Figure 3.4: Neuber's method 52

Figure 3.5: Glinka's method 54

Figure 3.6: Thick-walled cylinder 57

Figure 3.7: Strip in a thick-walled cylinder 58

Figure 3.8: Convergence of the pseudo elastic solution to the elastic-plastic solution ... 66

Figure 3.9: Effective moduli variation 67
Figure 3.10: Convergence behavior at the bore 70
Figure 3.11: Effect of number of elements (hoop stress) 72
Figure 3.12: Effect of number of elements (radial stress) 72
Figure 3.13: Effect of number of elements (axial stress) 73
Figure 3.14: Effect of number of elements (hoop strain) 73
Figure 3.15: Effect of number of elements (radial strain) 74
Figure 3.16: Effect of number of elements (displacement) 74

Figure 4.1: Comparison of present method and analytical solution 85
Figure 4.2: Comparison of present method and finite element solution 86
Figure 4.3: Stress variation in internally loaded cylinder 88
Figure 4.4: Strain variation in internally loaded cylinder 88
Figure 4.5: Hoop stress variation in externally loaded cylinder 89
Figure 4.6: Axial stress variation in externally loaded cylinder 89
Figure 4.7: Comparison of present method and finite element solution (stress field) 90
Figure 4.8: Comparison of present method and finite element solution (strain field) 91
Figure 4.9: Stress variation in internally loaded cylinder 91
Figure 4.10: Strain variation in internally loaded cylinder 92
Figure 4.11: Comparison of plane strain and plane stress results 92
Figure 4.12: AISI 4333 M4 material curve 101
Figure 4.13: Residual stress field induced by manufacturing 102
Figure 4.14: Residual stress comparison 103
Figure 4.15: Comparison of different material models 104
Figure 4.16: Comparison of different yield criteria 104
Figure 4.17: Stress-strain curve used in the analysis 106
Figure 4.18: Residual hoop stress comparison 107
Figure 4.19: Residual radial and axial stresses comparison 107
Figure 4.20: Comparison of the boundary displacements (IH) 108
Figure 4.21: Comparison of the boundary displacements (KH) 108
Figure 4.22: Bauschinger effect factor in 4330 Steel 110

Figure 4.23: Variable Bauschinger effect factor vs constant Bauschinger effect factor (Autofrettage level = 16%) 111
Figure 4.24: Variable Bauschinger effect factor vs constant Bauschinger effect factor (Autofrettage level = 30%) 111
Figure 4.25: Variable Bauschinger effect factor vs constant Bauschinger effect factor (Autofrettage level = 50%) 112
Figure 4.26: Variable Bauschinger effect factor vs constant Bauschinger effect factor (Autofrettage level = 90%) 112
Figure 4.27: Importance of fastener holes in failure of aircraft 113
Figure 4.28: Circular hole under uniform tension 125
Figure 4.29: Comparison of concentration factors 126
Figure 4.30: Comparison of concentration factors 126
Figure 4.31: Stress and strain concentration factors 128
Figure 4.32: Hoop and radial stress distributions 128
Figure 4.33: Equivalent stress distribution near the notch 129
Figure 4.34: Hoop stress distribution near the notch 129
Figure 4.35: Uniaxial loading-unloading response of Al 2024 T351 131
Figure 4.36: Comparison of calculated and measured residual stress distribution for 4.5% cold expanded hole in Al 2024 alloy plate 132
Figure 4.37: Comparison of residual stress distribution for 4% cold expanded hole in Al 2024 alloy plate 133
Figure 4.38: Comparison of predicted elastic-plastic boundaries with measurements for 7075 T6 Aluminum 137
Figure 4.39: Internal moment in a thick-walled cylinder 138
Figure 4.40: Comparison of radial stresses in multiaxial loading of a cylinder 140
Figure 4.41: Comparison of hoop stresses in multiaxial loading of a cylinder..... 140
Figure 4.42: Comparison of axial stresses in multiaxial loading of a cylinder..... 141
Figure 4.43: Comparison of shear stresses in multiaxial loading of a cylinder 141
Figure 4.44: Comparison of equivalent stresses in multiaxial loading of a cylinder 142
Figure 4.45: Comparison of plastic hoop strains in multiaxial loading of a cylinder ... 142
Figure 4.46: Comparison of plastic radial strains in multiaxial loading of a cylinder .. 143

Figure 4.47: Comparison of plastic shear strains in multiaxial loading of a cylinder... 143
Figure 4.48: Comparison of equivalent plastic strains in multiaxial loading of a cylinder 144

Figure 5.1: A typical sequence of linear loading 147
Figure 5.2: Thin tube under tension and torsion 154
Figure 5.3: Different loading paths 154
Figure 5.4: Linear hardening material 158
Figure 5.5: Loading path for von Mises isotropic material under consideration 159
Figure 5.6: Finite element mesh (undeformed configuration) 165
Figure 5.7: Finite element mesh (deformed configuration) 166
Figure 5.8: Comparison of plastic hoop strain predictions of the two plasticity theories (deformation and incremental) for a nonproportional loading 168
Figure 5.9: Stress comparison (proportional vs nonproportional), equivalent stress 169
Figure 5.10: Stress comparison (proportional vs nonproportional), hoop stress 169
Figure 5.11: Stress comparison (proportional vs nonproportional), radial stress 170
Figure 5.12: Stress comparison (proportional vs nonproportional), axial stress 170
Figure 5.13: Stress comparison (proportional vs nonproportional), shear stress 171
Figure 5.14: Strain comparison (incremental vs present method; torsion-pressure), hoop strain 172
Figure 5.15: Strain comparison (incremental vs present method; torsion-pressure), radial strain 173
Figure 5.16: Strain comparison (incremental vs present method; torsion-pressure), shear strain 173
Figure 5.17: Strain comparison (incremental vs present method; pressure-torsion), shear strain 174
Figure 5.18: Strain comparison (incremental vs present method; pressure-torsion), hoop strain 175
Figure 5.19: Strain comparison (incremental vs present method; pressure-torsion), radial strain 175

LIST OF SYMBOLS

a	hole radius
A	material constant in power law relation
A_1, A_2	constants
BEF	Bauschinger effect factor
C_1, C_2	coefficients in Lamé solution
C_{ij}	components of coefficient matrix
[C]	coefficient matrix
d	hole initial diameter
D	mandrel diameter
dW^p	increment of plastic work
E	elastic modulus
E_∞	far field secant modulus
E_{eff}	effective modulus
E_o	reference modulus
E_p	plastic modulus
E_R	reduced modulus
E_s	secant modulus
E_t	tangent modulus
G	shear modulus
G_{eff}	effective shear modulus
$\overline{G}$	general measure of strain tensor
H	material constant

$\overline{H}$	response function
i, j, k	tensor component indices (range: *1*, *2*, and *3*)
K	proportionality function
$K_\epsilon, K_\varepsilon$	strain concentration factors
K_σ, K_σ	stress concentration factors
K_t, K_t	elastic stress concentration factors
m, n	hardening exponents
n_i	unit outward normal to the surface
${}^{o}S_{ij}$	reference deviatoric stress tensor
p_1	internal pressure
p_2	external pressure
$\{p\}$	traction vector
r	radius
r_1, r_i, a	internal radius
r_2, r_o, b	external radius
r_p	elastic-plastic radius
S	remote tension
${}^{A}S_{ij}, {}^{B}S_{ij}$	deviatoric stress tensor at the end of a linear loading
S_{ij}	deviatoric stress tensor
ΔS_{ij}	change in deviatoric stress tensor
t	sleeve thickness
T	torque
$\overline{T}$	general measure of stress tensor
t_i^*	boundary traction
u	displacement
u_{aE}	maximum elastic displacement at hole
u_i^*	boundary displacement
$\{U\}$	displacement vector
W^{SE}	strain energy density
W^{TE}	total strain energy density

α	yield offset
α_{ij}	shift tensor
${}^{A}\sigma_e$, ${}^{B}\sigma_e$	equivalent stress at the end of a linear loading
$d\varepsilon$	total strain increment
$d\varepsilon^e$	elastic strain increment
$d\varepsilon_{eq}^{\ p}$	equivalent plastic strain increment
$\Delta\varepsilon_{ij}$	change in strain tensor
$d\varepsilon^p$	plastic strain increment
$d\varepsilon^p$	uniaxial plastic strain increment
$\Delta\phi$	change in scalar function
$d\gamma^p$	plastic shear strain increment
δ_{ij}	Kronecker delta
$d\sigma$	stress increment
$\Delta\sigma_e$	change in equivalent stress
$d\sigma_e$	equivalent stress increment
$d\sigma_{eq}$	equivalent stress increment
ε	uniaxial strain
$\varepsilon_{eq}^{\ p}$, ε_e	equivalent total plastic strain
ε_{ij}	total strain tensor
$\varepsilon_{ij}^{\ e}$	elastic strain tensor
$\varepsilon_{ij}^{\ p}$	plastic strain tensor
ε_o	strain at initial yield
ε^{SE}	uniaxial strain defined by strain energy density
ε^{TE}	uniaxial strain defined by total strain energy density
ϕ	scalar function
Γ	boundary
γ	shear strain
$\gamma_{r\theta}$	shear strain tensor

ν	Poisson's ratio
ν_{eff}	effective Poisson's ratio
${}^{\circ}\sigma_{ij}$	reference stress tensor
σ	uniaxial stress
σ_{∞}	remote biaxial tension
σ_{eq}, σ_{e}	von Mises equivalent stress
σ_{eq}^{T}	Tresca equivalent stress
σ_{i}	principal stresses (i=*1,2* and *3)*
σ_{ij}	stress tensor
σ_{H}	hydrostatic stress
σ_{max}	maximum principal stress
σ_{min}	minimum principal stress
σ_{o}	initial yield stress
σ_{o}^{u}	first yield stress reached during unloading
σ_{θ}	hoop stress
σ_{θ}^{R}	residual hoop stress
σ_{θ}^{u}	hoop stress due to unloading
σ_{r}	radial stress
σ_{r}^{R}	residual radial stress
σ_{r}^{u}	radial stress due to unloading
σ_{Y}	yield stress
σ_{z}	axial stress
σ_{z}^{R}	residual axial stress
σ_{z}^{u}	axial stress due to unloading
τ	torsional stress
$\tau_{r\theta}$	shear stress tensor
Ω	body volume

1. INTRODUCTION

In the design and analysis of components, it has become increasingly important to develop methods that are less sophisticated, more understandable, and easy to apply: but still accurate.

Design of components such as high pressure tubing in mechanical, chemical and armament industries, or fastener joints in aircraft industries requires elastic-plastic analysis. One reason for this is the need to accurately predict residual stresses. Compressive residual stresses in many applications such as autofrettage of cylinders and fastener holes, apart from increasing the pressure bearing capacity of the component, enhanc the component's fatigue life. The presence of these beneficial residual stresses reduces the probability of crack initiation and slows the growth of fatigue cracks.

Reliable prediction of the influence of residual stresses on the critical crack length and fatigue life of the components requires an accurate prediction of the actual residual stress field in the component. It is therefore essential to develop accurate and reliable methods to calculate residual stresses induced by pre-loads.

The theories of plasticity are not fully exploited by practicing engineers because of the difficulties in applying these mathematically sophisticated techniques. Usually it takes considerable effort to understand and implement techniques for plastic analysis. In most cases, industries are not convinced of the resulting economy and hence consider such analysis unaffordable.

Alternative methods of elastic-plastic analysis have attracted special attention recently. These methods provide simpler techniques to approximate the elastic-plastic behavior of components and therefore are more attractive to practicing engineers.

1.1 OBJECTIVES AND PROBLEM IDENTIFICATION

The objectives of this study are twofold. The first objective is to establish a method of elastic-plastic analysis based on linear elastic solutions. This method should be capable of predicting the stress, plastic strain and displacement for proportional loading. It should also be capable of accurately predicting mechanically induced residual stress, strain and displacement fields. The method, unlike conventional methods of residual stress calculation, should be able to employ the actual material stress-strain unloading curve to produce a close approximation to the real fields.

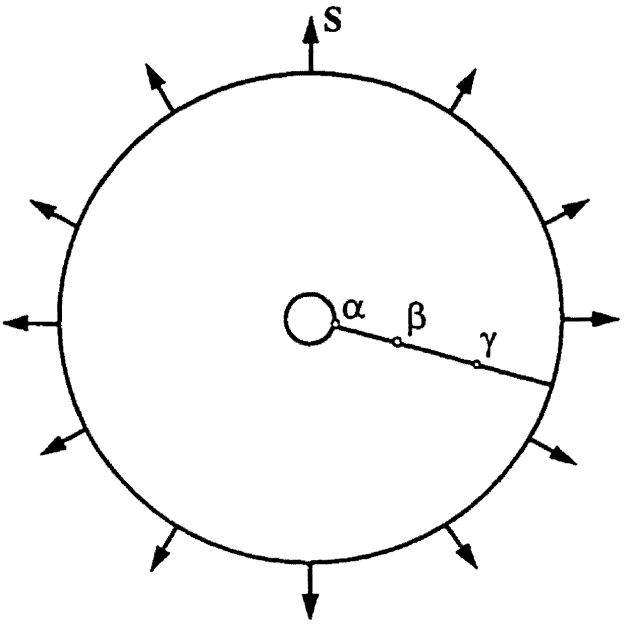
The second objective is to develop a total deformation theory applicable to nonproportional loading. This method should provide a proper way of representing a sequence of linear (but nonproportional) loadings such that total deformation theory can be employed for the analysis. The method should provide techniques for handling different deformation processes such as stress and load controlled deformations. The main focus should be devoted to reasonable plastic strain prediction in nonproportional loading where either stresses or loads are known a priori.

1.1.1 Inelastic Analysis Based on Linear Elastic Solutions

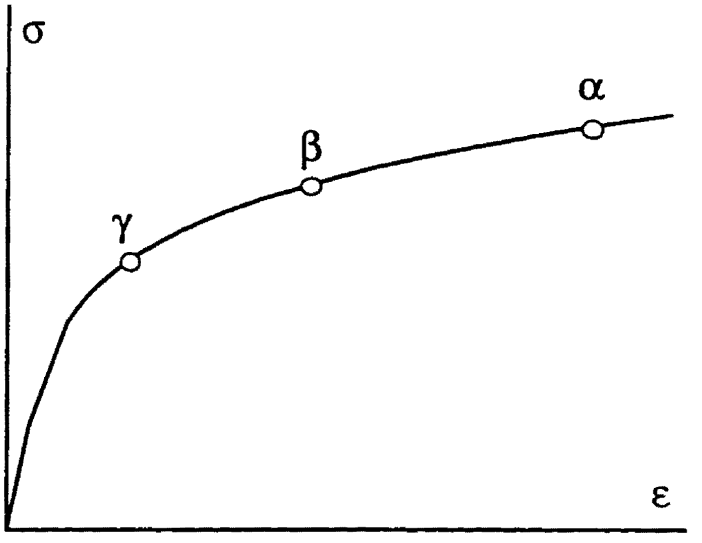
An attempt is made in this investigation to develop a mathematical model that can generate an inelastic solution using linear elastic results. This model should be able to : 1) accurately predict the elastic-plastic solution and 2) accurately predict the residual stress field due to unloading.

In order to do this, the problem to be solved can be outlined as follows. In a body under load as shown in Fig. 1.1a, different material points such as α, β and γ, shown in Fig. 1.1 (a), are at different levels of stress. Let the material behavior be represented in a general manner as shown in Fig. 1.1(b). Based on their stress levels, the material points α, β and γ may be represented by the points α, β and γ on the uniaxial stress-strain curve (Fig. 1.1 b). The problem may now be defined as follows: instead of performing a nonlinear analysis (following the nonlinear stress-strain curve) to arrive at points α, β and γ, use

known linear solutions with modified properties to reach the same points (Fig. 1.1c). It should be emphasized that the functional form of such linear dependency at each point will be the same as the functional form of the linear elastic solution.

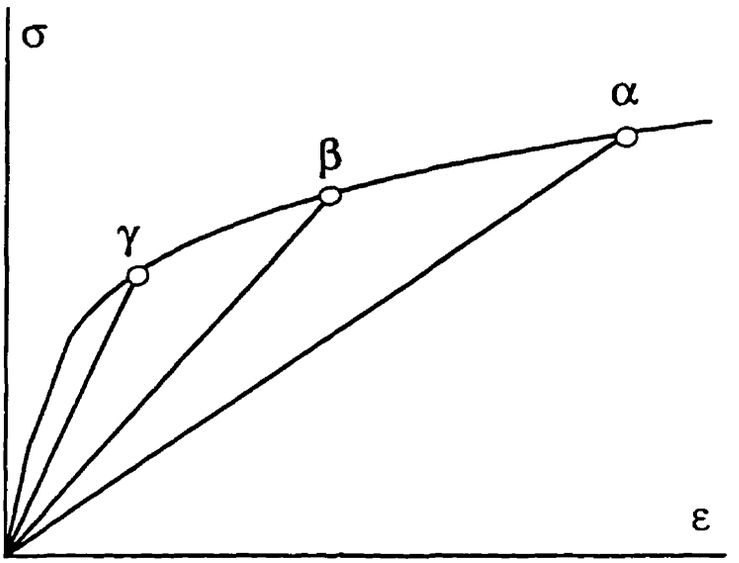


(a)



(b)

Figure 1.1(a): Elastic-plastic analysis based on linear elastic solutions



(c)

Figure 1.1 (cont.): Elastic-plastic analysis based on linear elastic solutions

1.1.2 Application of Total Deformation Theory of Plasticity to Nonproportional Loading

There are two theories of elastic plastic analysis, deformation plasticity and incremental plasticity.

Incremental theory of plasticity provides the most satisfactory basis for treating plasticity problems. However, this theory is incremental and leads to mathematical and computational complexities. Considerable simplifications are often achieved by using deformation theory of plasticity which depends only on the end values of stresses and is independent of stress history. Nevertheless, experimental results indicate that plastic strains depend not only on the current value of stress but also on the stress history. Therefore, total deformation plasticity gives inaccurate plastic strain fields for many situations involving nonproportional loading.

Despite the general inappropriateness of deformation theory, it is preferred in many practical fields of engineering because of its simplicity over incremental theory. For example, total deformation theory is widely used in fatigue design analysis (Dowling, 1993).

The validity of total deformation theory can be mathematically proven for proportional loading (Hill, 1950), and its physical soundness can be shown for limited degrees of nonproportional loading (Budiansky, 1959). However, to the authors knowledge, the applicability of total deformation theory to a sequence of linear nonproportional loadings such as the one shown in Fig 1.2, has not been adequately addressed in general.

An attempt is made to examine the validity of total deformation theory to nonproportional loading that can be defined as a sequence of linear loadings (Fig. 1.2). In order to do this the problem to be solved is defined as follows. Let a linear loading OA (simple torsion), as shown in Fig. 1.2, be followed by another linear loading AB (simple compression). The aim is to find a proper way of defining the second linear loading (AB) such that total values of plastic strain at A and B can be calculated from the stress values at A and B.

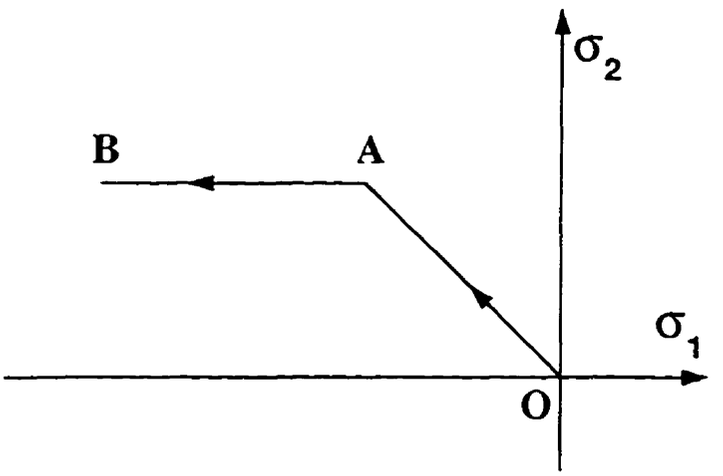


Figure 1.2: Nonproportional loading OB, defined as a sequence of two linear loading OA (torsion) and AB (compression)

1.2 OUTLINE

The thesis consists of six chapters. The present chapter describes the motivation, objectives and problem definition. The fundamental concepts which governs the theory of plasticity are reviewed in chapter 2. Only those subjects of the theory of plasticity which are appropriate for the subsequent discussions are selected. The literature on methods of elastic-plastic solutions based on elastic analysis is reviewed at the end of chapter 2. This review includes some of the frequently used approximate elastic-plastic methods.

The variable material property method is proposed in chapter 3. This is applied to obtain a general axisymmetric method of elastic-plastic analysis. Numerical implementation of this method and proper treatment of unloading are also discussed in chapter 3.

In chapter 4 the models derived in the previous chapter are applied to different axisymmetric problems. Loading of thick-walled cylinders and a plate with a circular hole are studied for different material behavior and stress states. Results are compared with other analytical methods. The ABAQUS finite element program has been used by the author for comparison purposes. The present approach results for the cases where no other solutions were available are compared to the results obtained by ABAQUS. Applications, including the autofrettage of cylinders is studied extensively in chapter 4. The application of the variable material property approach to the residual stress field around a cold worked fastener hole is also studied in chapter 4.

Application of the proposed axisymmetric analysis is extended to multiaxial loading of a thick tube. Pressure and torsion are applied proportionally to a thick cylinder. Since there are no other methods available for solving this problem, the results are compared with finite element results obtained by the author using ABAQUS.

Chapter 5 examines the validity of total deformation theory of plasticity to the situations involving nonproportional loading. Application of this method to nonproportional loading of a thin tube under tension and torsion is carried out for a linear hardening material and a material obeying the Ramberg-Osgood relation. The application of

proposed total deformation formulation to nonproportional loading of a thick-walled cylinder under pressure and torsion is also examined in chapter 5.

Chapter 6 summarizes the results and the major conclusions of this work. Recommendations are made for future work.

Appendix A gives the listing of the FORTRAN program for the elastic-plastic analysis of axisymmetric problems.

Appendix B gives the details of the integration of the Prandtl-Reuss equation for a sequence of linear loadings, based on the output from MAPLE V.

Appendix C gives the subroutine that utilizes the proposed total deformation formulation to calculate the plastic strain field using the variable material property method. The MAPLE V worksheet which performs the integration for any Ramberg-Osgood relation is included. This MAPLE program automatically generates a FORTRAN code out of the integration results which are used by the subroutine listed in this appendix.

2. BACKGROUND

Plasticity theory aims to quantify and predict the behavior of solids, generally metals, under permanent deformation. The four major components needed for such a prediction are: 1) a stress-strain relation, which describes the uniaxial loading behavior of material, 2) a yield criterion, which distinguishes between multiaxial elastic and elastic-plastic behavior, 3) a flow or deformation rule, which relates the stresses to the corresponding strains or strain increments, and 4) a hardening rule, which describes the changes of the yield criterion during the course of deformation. A boundary value problem is constituted once the above components are defined. A brief description of each component is given in this chapter. More detail on these subjects can be found in many publications, some of which are given in the references, and more or less follow the book on plasticity by R. Hill (1950).

Also, a comparison of the two major methods of plastic analysis, incremental and deformation plasticity, is discussed. The literature on methods of elastic-plastic analysis which depend on elastic solutions is reviewed at the end of this chapter.

2.1 STRESS-STRAIN CURVES

A knowledge of material properties is essential to elastic-plastic analysis. They are used in constitutive equations which relate stresses to strains. Material properties, such as the elastic modulus, Poisson's ratio, plastic modulus, secant modulus, and tangent modulus, are obtained from a uniaxial stress-strain experiment. Hence, it is important to understand and model stress-strain curves obtained experimentally.

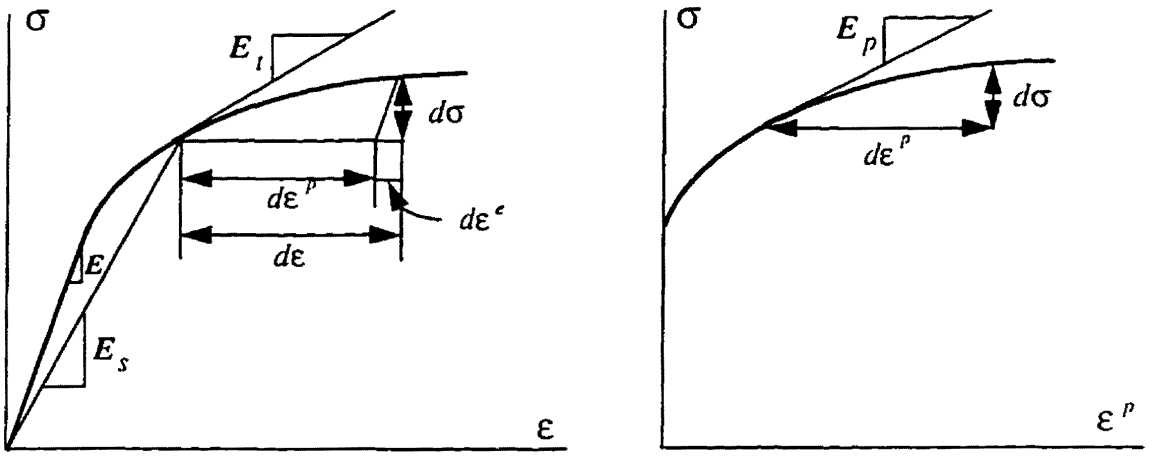


Figure 2.1: Elastic, secant, tangent, and plastic moduli definition based on a) stress-strain or b)stress-plastic strain curves

2.1.1 Moduli involved in elastic-plastic analysis (E, E_s, E_t and E_p)

Figure 2.1 (a) shows a typical uniaxial stress-strain curve. There are different modulus definitions associated with this curve. The elastic modulus, E, is the slope of the initial proportional part of the stress-strain curve. It has a constant value. The secant modulus, E_s, varies from point to point and depends on the total values of strain and stress. It is defined as

$$E_s = \frac{\sigma}{\varepsilon} \tag{2.1}$$

Clearly, when the stresses and strains remain within the proportional limit, the secant modulus is the same as the elastic modulus. The secant modulus is well suited to plasticity formulations based on total values of stress and strain. However, because the elastic-plastic stress-strain curve of the material is nonlinear in nature, an incremental procedure is often adopted. In this regard, the increment of plastic strain is considered to be the sum of an elastic part, $d\varepsilon^e$, and a plastic part, $d\varepsilon^p$:

$$d\varepsilon = d\varepsilon^e + d\varepsilon^p \tag{2.2}$$

The infinitesimal stress increment, $d\sigma$, is related to the infinitesimal strain increment, $d\varepsilon$, by

$$d\sigma = E_t d\varepsilon \tag{2.3}$$

where E_t is the tangent modulus which varies during plastic deformation. The instantaneous slope of the stress-strain curve shown in Fig. 2.1 (a) is the tangent modulus. If the plastic strain, ε^p, is separated from the total strain, ε, then the plastic strain increment and the stress increment are related by

$$d\sigma = E_p d\varepsilon^p \tag{2.4}$$

where E_p is referred to as the plastic modulus, which in the case of uniaxial loading is the slope of the σ–ε^p curve shown in Fig. 2.1 (b). Clearly, the modulus of elasticity, E, relates elastic strain increment, $d\varepsilon^e$, to the increment of stress by

$$d\sigma = E\, d\varepsilon^e \tag{2.5}$$

Substitution of $d\varepsilon$ (in Eq. 2.3), $d\varepsilon^p$ (in Eq. 2.4), and $d\varepsilon^e$ (in Eq. 2.5) into Eq. (2.2) lead to the relationship between the three moduli E_t, E and E_p:

$$\frac{1}{E_t} = \frac{1}{E} + \frac{1}{E_p} \tag{2.6}$$

Another material parameter which is not explicitly defined by the stress-strain curve is Poisson's ratio. This parameter describes the lateral behavior of materials under axial load. Poisson's ratio is defined as

$$\nu = -\frac{\varepsilon_{lateral}}{\varepsilon_{axial}} \tag{2.7}$$

This material parameter can also be measured during a simple uniaxial loading.

2.1.2 Modeling of the uniaxial behavior in plasticity

To make the uniaxial stress-strain curve more compatible with the method of solution used, it is often necessary to idealize the stress-strain curve. Four types of idealized stress-strain curve are discussed here in.

2.1.2.1 Elastic-perfectly plastic model

In some cases, it is permissible and convenient to neglect the effect of work hardening and assume that the plastic flow occurs when the stress reach its yield value, σ_o. Thus, the uniaxial stress-strain relation may be expressed as

$$\begin{aligned} \varepsilon &= \frac{\sigma}{E} && \text{for } \sigma < \sigma_o \\ \varepsilon &= \frac{\sigma}{E} + \varepsilon^p && \text{for } \sigma > \sigma_o \end{aligned} \tag{2.8}$$

Figure 2.2 (a) shows this model.

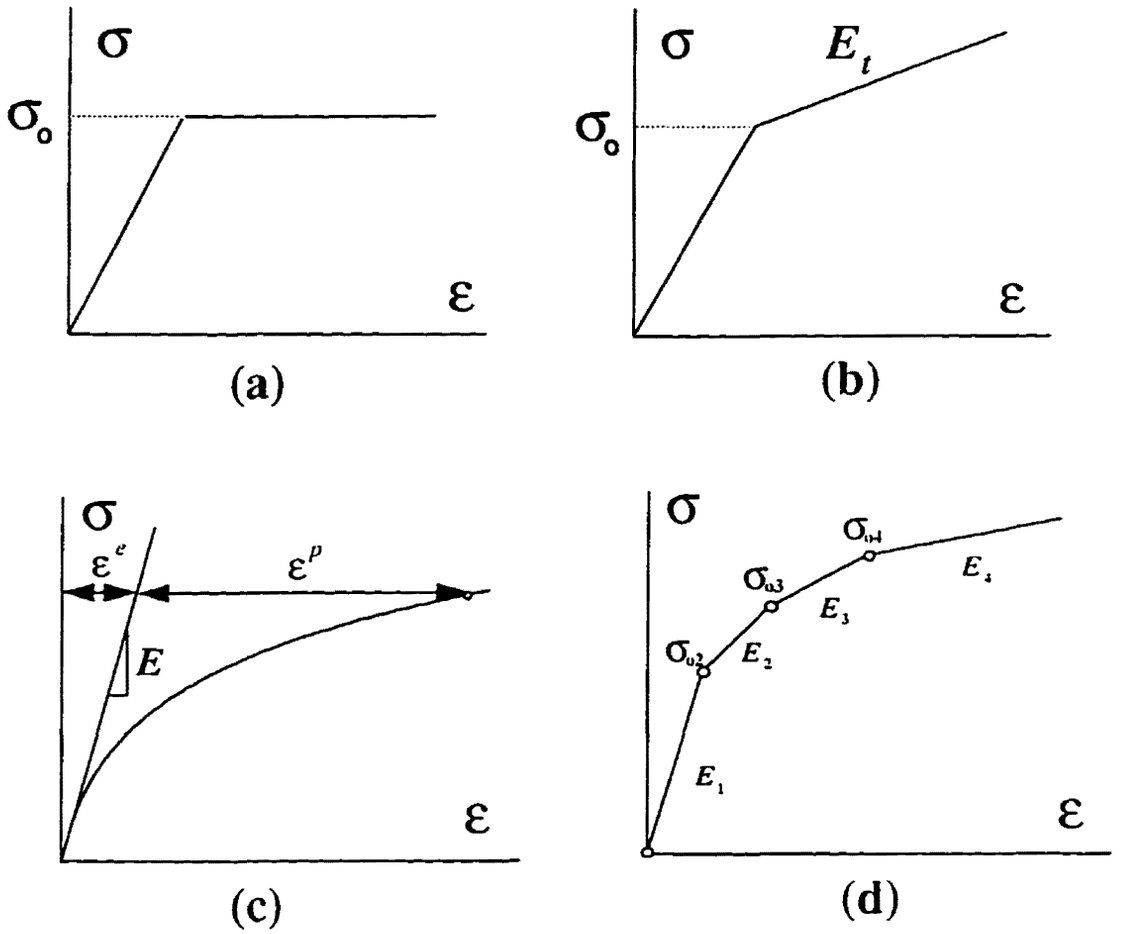


Figure 2.2: Idealized stress-strain curves

2.1.2.2 Elastic-linear hardening model

In the elastic-linear hardening model, the stress-strain curve is approximated by two straight lines, thus replacing the smooth transition by a sharp corner. The ordinate of this corner is the yield stress σ_o. The first linear branch of the idealized diagram (Fig. 2.2 b) has a slope equal to the elastic modulus. The second branch, representing the idealized hardening behavior, has a slope equal to the tangent modulus E_t. The stress-strain relation has the following form:

$$\varepsilon = \frac{\sigma}{E} \qquad \text{for } \sigma < \sigma_o$$
$$\varepsilon = \frac{\sigma_o}{E} + \frac{1}{E_t}(\sigma - \sigma_o) \qquad \text{for } \sigma > \sigma_o \tag{2.9}$$

2.1.2.3 Ramberg-Osgood model

Ramberg and Osgood (1943) suggested the following relation for representation of the nonlinear stress-strain curve shown in Fig. 2. 2 (c)

$$\varepsilon = \frac{\sigma}{E} + \alpha \frac{\sigma}{E}\left(\frac{\sigma}{\sigma_o}\right)^{m-1} \tag{2.10}$$

in which material constants α and m are the yield offset and the hardening exponent, respectively. The initial slope of the curve takes the value of elastic modulus at σ=0, and decreases monotonically with increasing load. Since the model has three parameters (σ_o , α, and m), it allows for a better fit of real stress-strain curves.

It is sometimes convenient to work with a plastic strain-stress relation in the following form

$$\sigma = H(\varepsilon^p)^n \tag{2.11}$$

where H is a material constant and n is the corresponding hardening exponent. These constants for a particular set of stress-strain data are obtained by making a log-log plot of stress versus plastic strain, σ vs. ε^p. Taking logarithms of both sides of Eq. (2.11) gives

$$\log\sigma = n\log\varepsilon^p + \log H \tag{2.12}$$

This is a straight line on a log-log plot ($y=nx+b$). The constant H is therefore the value of stress at $\varepsilon^p=1$, and n is the slope of the log-log plot.

This method of idealization is usually utilized in the deformation theory of plasticity which will be discussed later.

2.1.2.4 Piecewise linear model

A stress-strain curve, which in general is nonlinear, can be modeled by approximating it as a series of piecewise linear segments as illustrated in Fig. 2.2 (d). The first linear segment ends at the yield strength. Each subsequent line segment describes the response of the material from one yield point to the subsequent yield point. The slope of the line represents the stiffness of the associated segment.

The stress and strain for a point in the ith segment is given by

$$\left.\begin{aligned} \sigma &= \sigma_{o_i} + E_i \varepsilon_i \\ \varepsilon_i &= \frac{\sigma - \sigma_{o_i}}{E_i} \end{aligned}\right\} \quad \sigma_{o_i} < \sigma < \sigma_{o_{i+1}} \tag{2.13}$$

where E_i is the slope and ε_i is the increase in strain within that segment. The total strain up to a point in the nth segment is

$$\varepsilon = \sum_{i=1}^{n} \frac{\sigma - \sigma_{o_i}}{E_i} \tag{2.14}$$

with $\sigma_{o1}=0$, and E_1 being the Young's modulus.

The piecewise linear approximation of the actual stress-strain curve is often used in the incremental theory of plasticity which will be discussed later.

2.2 YIELD CRITERIA

The yield condition for a material defines the limit of purely elastic behavior under any combination of stresses. For complicated loading with a multiaxial stress state, a yield criterion describes how each stress component contributes to yielding at a particular material point.

It is generally agreed that yielding, especially for metals, is independent of hydrostatic stresses. Though many initial yield conditions have been proposed, the Tresca yield criterion (1864), also known as the maximum shear stress criterion, and the von Mises yield condition (1913), also referred to as the maximum distortion energy criterion, best represent actual material behavior (Davis, 1945; Naghdi et al., 1958) while preserving mathematical tractability.

2.2.1 Tresca yield criterion

According to this criterion, a material point yields when the maximum shear stress at that point reaches the maximum shear stress in a uniaxial tension specimen at yield. The Tresca yield criterion, shown in Fig. 2.3 by a hexagon, is expressed as

$$\left|\sigma_{max} - \sigma_{min}\right| = \sigma_o \tag{2.15}$$

where σ_{max}, σ_{min} are the maximum and minimum principal stresses, and σ_o is the yield stress in tension. The drawback of this criterion is that it is independent of the intermediate principal stress.

Note that, when not concerned with the initial yielding, the left hand side of Eq. (2.15) may be taken as a representation of the state of stress (i.e., an equivalent stress) at a given material point. The definition of equivalent stress is essential when working with hardening materials. The hardening characteristics of a material follow from the uniaxial stress-strain curve. For hardening materials some function of stresses, called equivalent

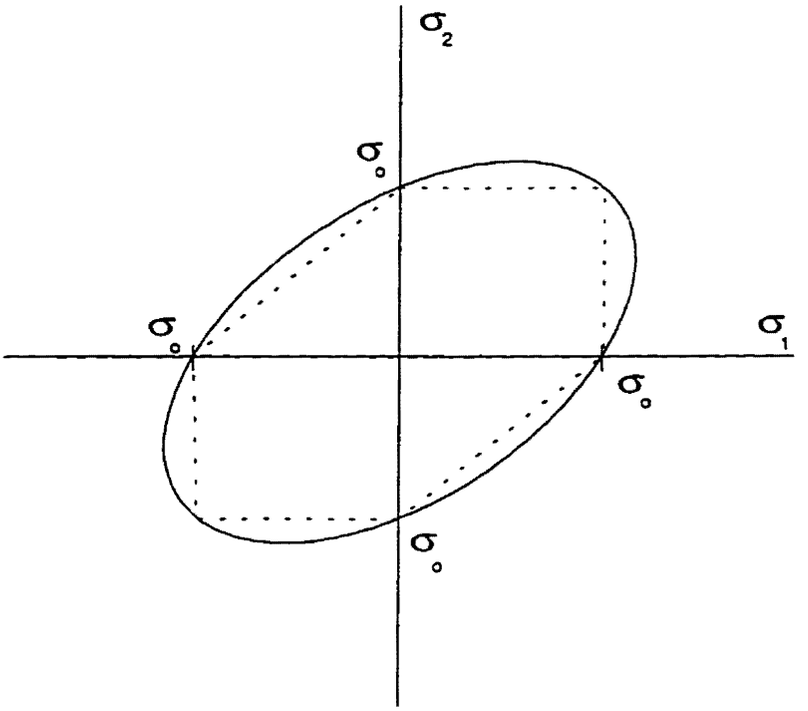


Figure 2.3: Yield locus for Tresca and von Mises yield criterion

stress, and some function of the plastic strains, called equivalent strain, are used to correlate the test results obtained for different loading programs. Tresca's equivalent stress, σ_{eq}^{T}, may be defined in the following form:

$$\sigma_{eq}^{T} = |\sigma_{max} - \sigma_{min}| \tag{2.16}$$

The equivalent plastic strain will be defined later.

2.2.2 Von Mises yield criterion

According to this criterion, yielding begins when the distortion energy for a complex stress state is equal to the distortion energy at yield in a tension specimen. The von Mises yield condition is represented using the deviatoric stress tensor, S_{ij} , and the yield stress σ_o which are defined as follows:

$$S_{ij} = \sigma_{ij} - \frac{\sigma_{kk}}{3}\delta_{ij} \tag{2.17}$$

and

$$\sigma_e^2 = \frac{3}{2} S_{ij} S_{ij} \tag{2.18}$$

where δ_{ij} is the Kronecker delta and the usual summation convention over repeated indices is adopted. The von Mises criterion in terms of principal stresses is

$$\sqrt{\frac{1}{2}\left\{(\sigma_1 - \sigma_2)^2 + (\sigma_1 - \sigma_3)^2 + (\sigma_3 - \sigma_2)^2\right\}} = \sigma_e \tag{2.19}$$

where σ_1, σ_2, and σ_3 are the principal stresses. The planar view of this surface for $\sigma_3=0$ is an ellipse in principal stress space as shown in Fig. 2.3.

Note that, when not concerned with the initial yielding, the left hand side of Eq. (2.19) may be taken as a representation of the stress state at a given material point, specifically the von Mises equivalent stress, σ_{eq}, is defined by

$$\sigma_{eq} = \sqrt{\frac{1}{2}\left\{(\sigma_1 - \sigma_2)^2 + (\sigma_1 - \sigma_3)^2 + (\sigma_3 - \sigma_2)^2\right\}} \tag{2.20}$$

The Tresca and von Mises yield criteria never give dramatically different predictions of the yield behavior under combined stress, there being no state of stress where the difference exceeds approximately 15%. The maximum distances from the origin to the Mises ellipse and the Tresca hexagon in Fig. 3.3 have the ratio of 1.155. Hill (1950)

suggested that a solution obtained using the Tresca criterion may be scaled by this factor to give an estimation based on Mises.

2.3 STRESS-STRAIN RELATIONS

Three stress-strain relations are considered here. The first one describes the linear elastic response of the material during elastic and plastic deformation. The other two describe the plastic response of the material. These are: 1) deformation plasticity, which relates the total plastic strains to the stresses, and 2) incremental or flow plasticity, which relates the plastic strain increments to the stresses. A comparison of these two plasticity theories on the basis of validity, accuracy, simplicity, and computational preferences is made.

2.3.1 Linear elastic

The generalized Hooke's law constitutes the linear elastic relationship.

$$\varepsilon_{ij}^{e} = \frac{1}{2G}\sigma_{ij} - \frac{\nu}{E}\sigma_{kk}\delta_{ij} \tag{2.21}$$

where G, E and ν are the shear modulus, Young's modulus, and Poisson's ratio, respectively.

These relationships apply not only prior to yielding but also after yielding, except that in the latter case they give only the elastic portions of the strains. Superscript e in Eq. (2.21) indicates elastic strains, and the plastic portion of strains must be added to them to obtain the total strains.

$$\varepsilon_{ij} = \varepsilon_{ij}^{e} + \varepsilon_{ij}^{p} \tag{2.22}$$

2.3.2 Deformation plasticity

Hencky (1924) proposed a relationship between total plastic strains and stresses. Assuming small strains, the plastic stress-strain relation proposed by Hencky may be written as

$$\varepsilon_{ij}^{p} = \phi \; S_{ij} \tag{2.23}$$

where ϕ is a scalar valued function. For hardening materials, ϕ depends on the equivalent stress (e.g. Mises equivalent stress), σ_{eq} , which may be regarded as a function of an equivalent total plastic strain, ε_{eq}^{p} , defined as

$$\varepsilon_{eq}^{p} = \sqrt{\frac{2}{3}\varepsilon_{ij}^{p}\varepsilon_{ij}^{p}} \tag{2.24}$$

A key feature of deformation theory is that a single curve, i.e., the uniaxial stress-strain curve, relates equivalent stress and equivalent plastic strain for all states of stress. Some tests on thin walled copper tubes conducted by Davis (1943) verify this approximately. Equation (2.23), Eq. (2.18) and Eq. (2.24) are used to determine the function ϕ:

$$\phi = \frac{3}{2}\frac{\varepsilon_{eq}^{p}}{\sigma_{eq}} \tag{2.25}$$

The stress-strain relation may therefore be expressed in the following form

$$\varepsilon_{ij}^{p} = \frac{3\varepsilon_{eq}^{p}}{2\sigma_{eq}} S_{ij} = \frac{3}{2}\left(\frac{1}{E_s} - \frac{1}{E}\right) S_{ij} \tag{2.26}$$

where E_s is the secant modulus of the uniaxial stress-strain curve.

2.3.3 Incremental plasticity

Levy (1871) and von Mises (1913) independently proposed a relationship between total strain increments (sum of elastic and plastic strain increments) and the current state of stress. The modified form of this relation, which uses plastic strain increments, was proposed by Prandtl (1924) for plane strain and by Reuss (1930) for an arbitrary state of strain in the following form

$$d\varepsilon_{ij}^{p} = d\phi \; S_{ij} \tag{2.27}$$

or in component form

$$\frac{d\varepsilon_{11}^{p}}{S_{11}} = \frac{d\varepsilon_{22}^{p}}{S_{22}} = \frac{d\varepsilon_{33}^{p}}{S_{33}} = \frac{d\varepsilon_{12}^{p}}{S_{12}} = \frac{d\varepsilon_{13}^{p}}{S_{13}} = \frac{d\varepsilon_{23}^{p}}{S_{23}} = d\phi \tag{2.28}$$

where $d\phi$ is a factor of proportionality, which may be found by considering plastic work increments. It can be shown (Hill, 1950) that the increment of plastic work per unit volume for the von Mises yield criterion is

$$dW^{p} = S_{ij} d\varepsilon_{ij}^{p} = \sigma_{eq} d\varepsilon_{eq}^{p} \tag{2.29}$$

where the equivalent plastic strain increment is defined as

$$d\varepsilon_{eq}^{p} = \sqrt{\frac{2}{3} d\varepsilon_{ij}^{p} d\varepsilon_{ij}^{p}} \tag{2.30}$$

Substituting Eq. (2.27) into Eq. (2.29), gives

$$d\phi = \frac{3}{2}\frac{d\varepsilon_{eq}^{p}}{\sigma_{eq}} = \frac{3}{2}\frac{1}{E_p}\frac{d\sigma_{eq}}{\sigma_{eq}} \tag{2.31}$$

where E_p is the plastic modulus defined by Eq. (2.4). The Prandtl-Ruess rule is completely defined by Eq. (2.27) and Eq. (2.31).

2.3.4 Deformation versus incremental plasticity theories

Both plasticity theories have been used for plastic analysis of materials. Nadai (1950) and Sokolovsky (1969) have used Hencky's deformation stress-strain relation extensively. On the other hand, Hill (1950) and Prager and Hodge (1951) focused on the theoretical shortcomings of the deformation theory and used the Prandtl-Reuss equation to handle plastic deformation.

Experimental results (Mroz and Olszak, 1963) indicate that plastic strains depend not only on the values of the stresses reached but also on the history of stressing. For example, consider a thin walled tube loaded to particular values of axial load $P=P`$ and torque $T=T`$, either of which is sufficient to cause yielding by itself (Fig. 2.4). If the axial load to cause yielding is applied first and then the torsion, the plastic strains that result differ from those that occur if the torsion is instead applied first. Also, a third result is obtained if the tension and torsion are increased proportionally, so that the ratio P/T remains constant until $P`$ and $T`$ are simultaneously reached. This suggests that deformation plasticity, which is independent of the loading path, leads to incorrect strain field calculations. In Hencky's theory, paths $OP`A$, $OT`A$, and OA give identical strain fields. Thus, in order to get the correct strain field, one has to adopt an incremental formulation to allow for the effect of the loading path. Experimental results (Mroz and Olszak, 1963) show that the Prandtl-Reuss equation, which is path dependent, is the most accurate relationship.

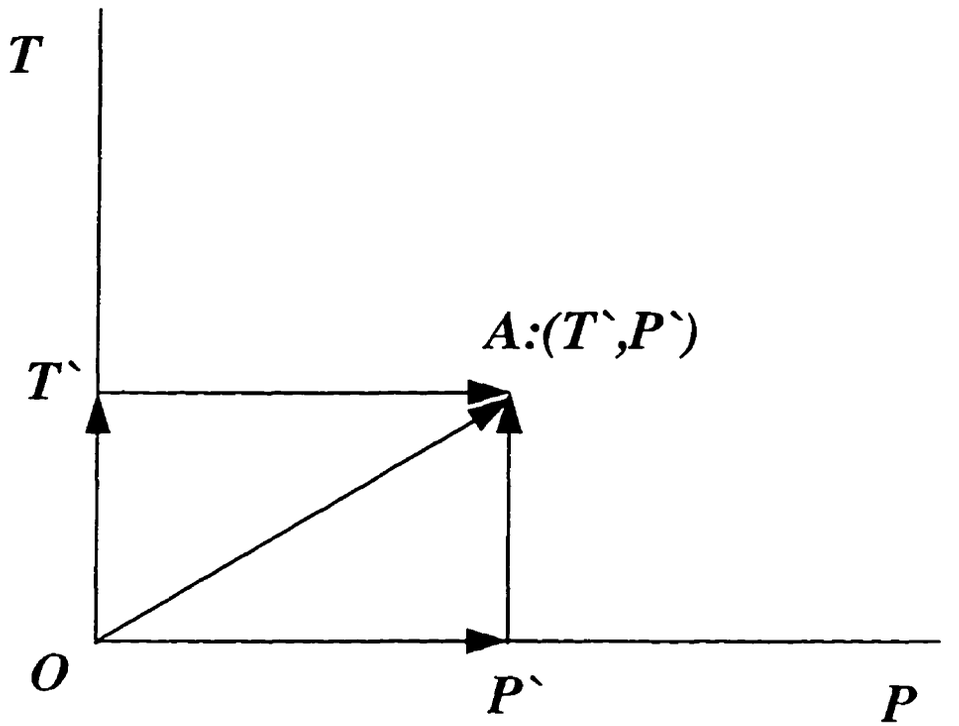


Figure 2.4: Nonproportional loading path

There have been many studies, especially during the 50's and 60's, comparing the two theories on the basis of the physical correctness of Hencky's theory. Many of these studies (Morrison et al. 1950, Hundy and Green 1954) emphasized the incorrect predictions of deformation theory, while some (Hodge and White 1952, Budiansky 1959, Chen 1973) pointed out the applicability of deformation theory for a range of loading.

For proportional loading where the components of the deviatoric stress maintain proportionality throughout the load history, the two theories are the same. A proportional loading is represented by a straight line passing through the origin in the principal stress space. The components of deviatoric stresses for a proportional loading are given as

$$S_{ij} = K \, {}^{*}S_{ij} \tag{2.32}$$

where K is a monotonically increasing function and ${}^{\circ}S_{ij}$ is an arbitrary (nonzero) state of stress. The equivalent stress (Tresca or Mises) will then take the following form

$$\sigma_{eq} = K \ {}^{\circ}\sigma_{eq} \tag{2.33}$$

Substituting Eq. (2.31) into the Prandtl-Reuss relation of Eq. (2.27) gives

$$d\varepsilon_{ij}^{p} = \frac{3}{2}\frac{d\varepsilon_{eq}^{p}}{{}^{\circ}\sigma_{eq}} \ {}^{\circ}S_{ij} \tag{2.34}$$

which upon integration yields the Hencky relation given in Eq. (2.26). This proves the equivalence of the two theories for proportional stressing.

However, Budiansky (1959) showed that the deformation theory of plasticity may be used for a range of loading paths other than proportional loading without violating the general requirements for physical soundness of a plasticity theory. Assuming Drucker's (1951) basic postulates as criteria for physical soundness of a plasticity theory, Budiansky showed that deformation theory is consistent with these requirements for a range of loading paths that are close to proportional loading. Drucker's postulates (Drucker, 1951) on the theory of plasticity are based on thermodynamic principles and result in two inequalities related to the rate of plastic work increment and the maximum plastic work. Budiansky rearranged Drucker's inequalities using deformation plasticity for a situation in which a corner is formed in the yield locus at the current stress point during plastic deformation. The Tresca yield surface (hexagon in Fig. 2.3) is an example of a yield surface with discontinuous corners. Drucker's inequalities then reduce to (Chakrabarty, 1987)

$$(d\sigma_1 - d\sigma_2)^2 + (d\sigma_2 - d\sigma_3)^2 + (d\sigma_3 - d\sigma_1)^2 < 2(1+m)d\sigma_{eq}^2 \tag{2.35}$$

where m is the exponent for the stress-strain curve represented by the Ramberg-Osgood equation. Also, $d\sigma_1$, $d\sigma_2$, and $d\sigma_3$ are the principal stress increments and $d\sigma_{eq}$ is the increment of equivalent stress. For a hardening material, this inequality will be satisfied in a large number of practical problems where the stress ratios vary during the deformation (Chakrabarty, 1987).

Due to the mathematical complexity arising from the incremental formulation, a deformation plasticity solution is preferred for many applications. Most finite element packages, such as ABAQUS, offer a deformation plasticity option as well as an incremental plasticity option. For many problems where monotonic loading is of concern, deformation plasticity not only gives an answer with reasonable accuracy but takes less computational time. A comparison of the two theories on the basis of computational time and accuracy for a nonproportionally loaded thick-walled cylinder is given in chapter five. Similar comparisons can be found in different areas of solid mechanics, for example, Chen (1996) in fracture mechanics. Deformation plasticity has been extensively used for cyclic plasticity (Dowling, 1993) and notch analysis (Seegar 1985, Moftakhar 1994).

While Hencky's theory is valid for monotonic loading only, with modifications it may be applied to unloading as well. This has been done widely for cyclic plasticity (Dowling, 1993) and residual stress field prediction (Jahed and Dubey, 1996 and 1997).

Even though deformation plasticity is utilized for proportional loading, the possibility of using a total deformation formulation for nonproportional loading which can be defined as a sequence of linear loading steps has not been addressed in the literature. Such a loading is shown in Fig. 2.4 (loading paths $OP`A$, or $OT`A$). In chapter five, this possibility is examined and it is shown that, for deformations where stresses are known a priori, such a relationship gives the same results as incremental plasticity. Furthermore, for situations where stresses are not known a priori in a nonproportional loading of a linear hardening material, a total deformation method is proposed for strain field calculation.

2.4 HARDENING RULES

Hardening rules describe how the yielding criterion changes during the course of plastic deformation. For unloading situations, they also describe the onset of reversed yielding. There are two widely used hardening rules: 1) isotropic hardening and 2) kinematic hardening. Both rules preserve the shape and orientation of the yield surface. Note, however, that some research (Phillips and Lee, 1979) suggests a distortion of the surface.

Despite the fact that it is necessary to work with a hardening rule for complex loading such as cyclic plasticity, neither of these rules are able to capture all features of material behavior. Figure 2.5 shows an experimentally obtained stress-strain curve. The hardening rule approximations (both are the same in this case) are also shown. The material (AISI 4333) has a perfectly plastic loading behavior while showing a hardening effect upon unloading. Even the Bauschinger effect (early yielding behavior on unloading, e.g., prior to reaching the yield strength under monotonic loading) is not captured by the kinematic hardening rule because of the nonhardening response in loading. Unlike during loading, the material transition from elastic unloading to reversed yielding is smooth. These points show the importance of utilizing the actual material curve, where applicable.

2.4.1 Isotropic hardening

The isotropic hardening rule (Hill, 1950) states that the yield surface grows during plastic deformation, effectively changing the yield stress as the material becomes elastic-plastic. The center of the yield surface, however, remains fixed. Such behavior is shown in deviatoric stress space (two dimensional case) in Fig. 2.6. Adopting the von Mises yield criterion, the yield surface is described by

$$\sigma_{eq}^2 - \frac{3}{2} S_{ij} S_{ij} = 0 \tag{2.36}$$

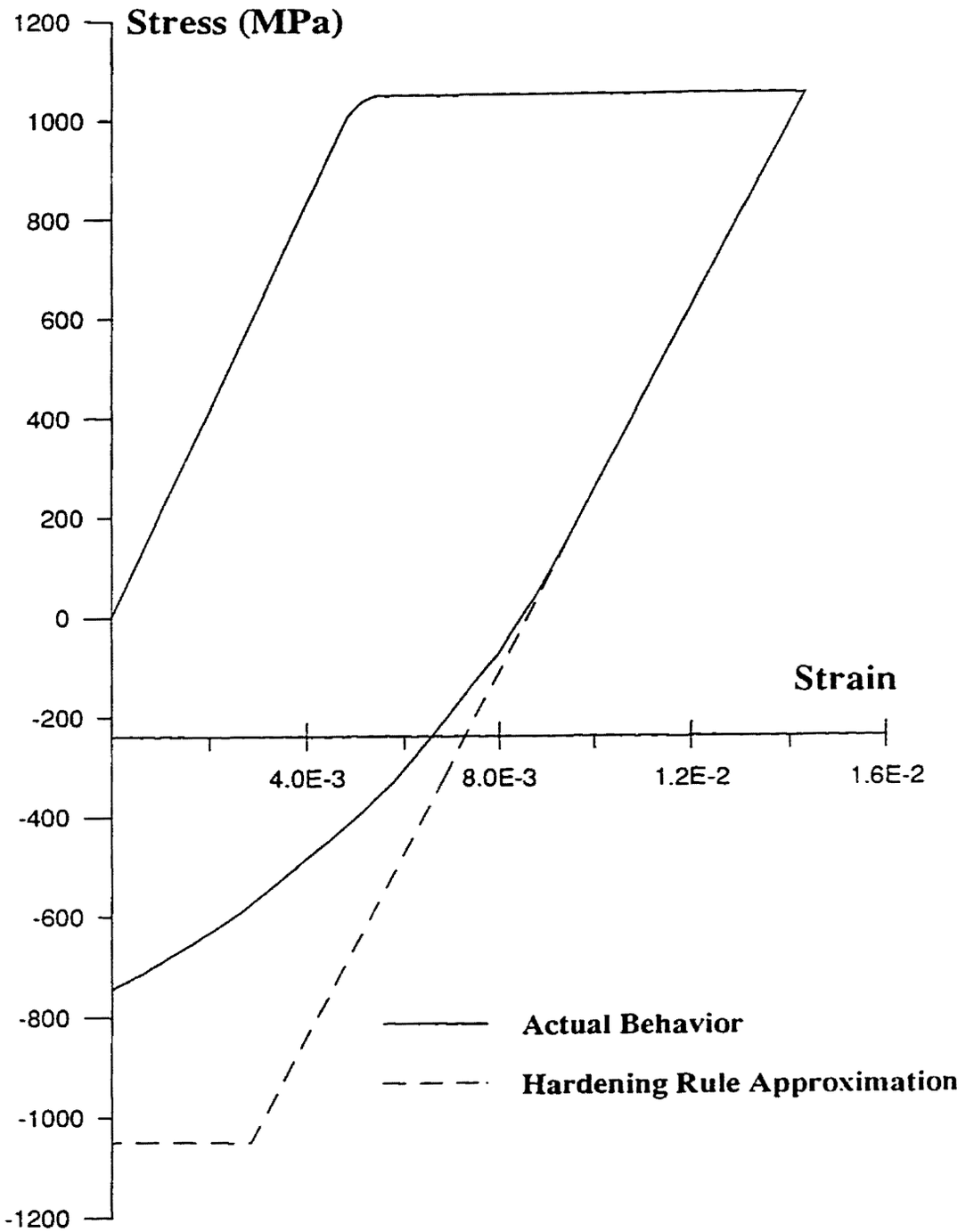


Figure 2.5: AISI 4333 M4 loading-unloading curve
(Stacey and Webster, 1988)

where σ_{eq}, the Mises equivalent stress, attains its largest value during loading.

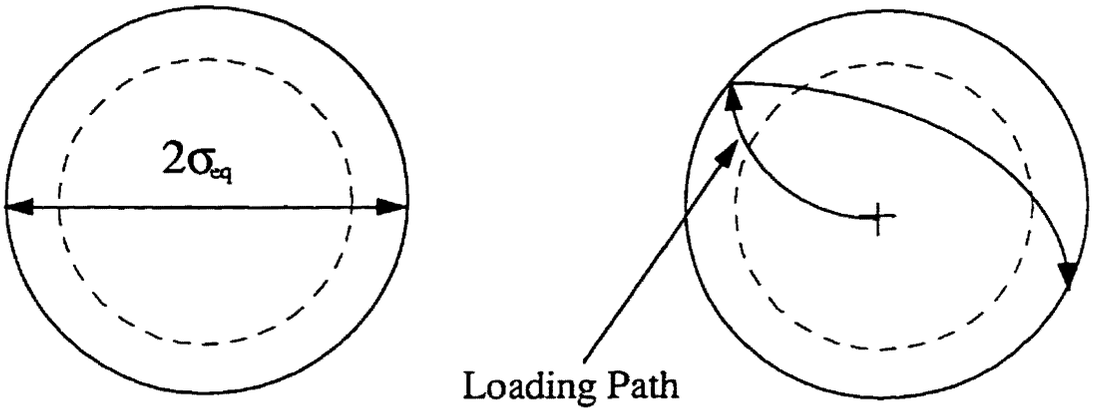


Figure 2.6: Isotropic hardening

Isotropic hardening cannot account for the Bauschinger effect which is experimentally observed for many metals (Milligan et. al. 1966). In terms of uniaxial behavior, the isotropic hardening predicts reversed yielding at $-2\sigma_{eq}$, where σ_{eq} is the maximum stress reached during loading. Figure 2.7 shows possible unloading paths on the uniaxial stress-strain curve.

Isotropic hardening is thought to best describe material behavior for large strains. For this reason, this rule is used more in metal forming problems.

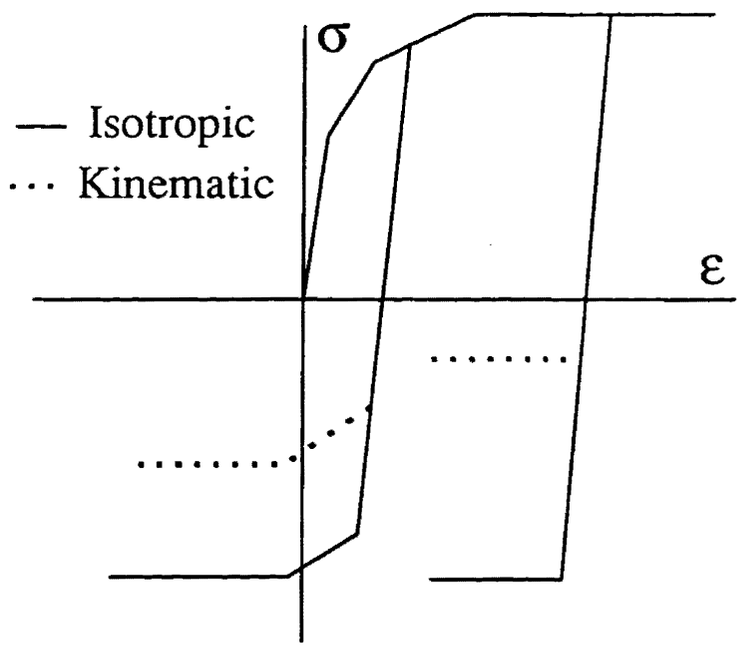


Figure 2.7: Isotropic and kinematic hardening

2.4.2 Kinematic hardening

Kinematic hardening model was first proposed by Prager (1956) as a way to model the Bauschinger effect. The yield surface in kinematic hardening is allowed to translate in stress space. Figure 2.8 shows the yield surface movement in deviatoric stress space based on Prager's kinematic hardening rule. The yield surface equation for the von Mises criterion is

$$\sigma_e^2 - \frac{3}{2}\left(S_{ij} - \alpha_{ij}\right)\left(S_{ij} - \alpha_{ij}\right) = 0 \tag{2.37}$$

where α_{ij} is the shift tensor which accommodates translation. Different relations for the shift tensor increment have been proposed. Ziegler (1959) modified Prager's rule by proposing the following evolution form for the shift tensor

$$d\alpha_{ij} = d\mu\left(S_{ij} - \alpha_{ij}\right) \tag{2.38}$$

Some finite element programs, e.g., ABAQUS, utilize Prager's kinematic hardening rule with Ziegler's modification. Kinematic hardening is used mostly in fatigue analysis and cyclic plasticity.

2.5 Boundary Value Problem

A boundary value problem is formulated when the solution to a particular problem is of interest. A boundary value formulation requires consideration of: 1) the equilibrium equation, 2) the compatibility condition, and 3) the constitutive relation.

In analytical or numerical formulations of solid mechanics, such as the finite element method, it is very important to understand and enforce these considerations. A complete,

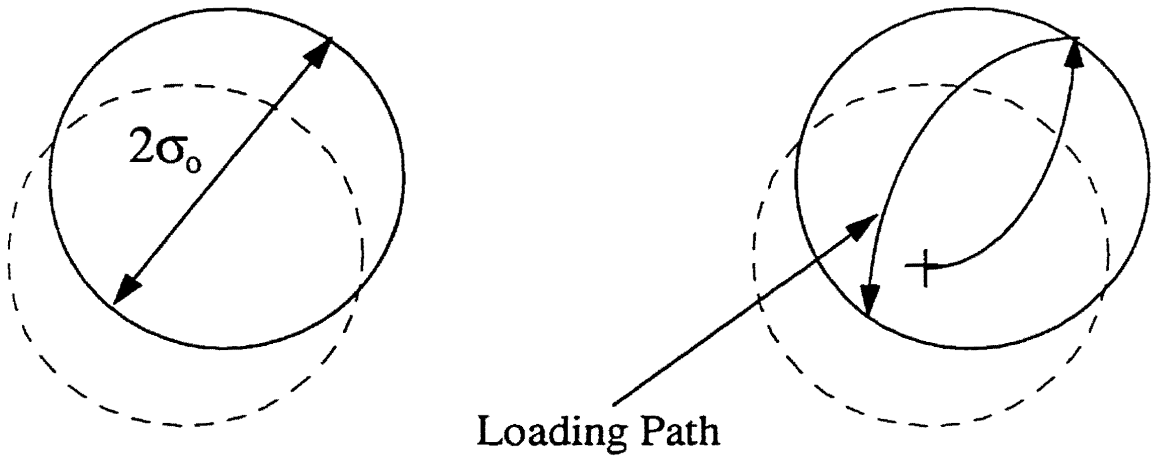


Figure 2.8: Kinematic hardening

reliable solution is achieved only if equilibrium and compatibility are maintained, and the correct constitutive model is employed.

2.5.1 Equilibrium

Forces acting on a body give rise to stresses. Through a static (or dynamic) analysis of forces involved in a deformation, a set of equations restricting the stress distribution in a body are formed.

Consider a body of volume Ω enclosed within surface Γ. In the absence of body forces, the body is in equilibrium if the stress tensor, σ_{ij}, satisfies the following equation

$$\sigma_{ij,j} = 0 \tag{2.39}$$

where the comma followed by a suffix denotes partial differentiation. This ensures the equilibrium of points interior to Γ. In addition, equilibrium of the points on the boundary Γ should be satisfied. If the boundary condition consists of prescribed tractions, t_i^*, and/or displacements, u_i^*, then the following two conditions must be satisfied to ensure equilibrium and compatibility of points on the boundary:

- traction t_i^* over the boundary Γ_1

$$\sigma_{ij} n_j = t_i^* \big|_{\Gamma_1} \tag{2.40}$$

- displacement u_i^* over the boundary Γ_2

$$u_i = u_i^* \big|_{\Gamma_2} \tag{2.41}$$

where the union of the two parts of the boundary give the entire boundary

$$\Gamma = \Gamma_1 + \Gamma_2 \tag{2.42}$$

and n_j is the unit outward normal to the surface Γ_1.

2.5.2 Compatibility

Displacements give rise to strains. A kinematic analysis of the deformation leads to certain restrictions on the strain tensor. Here and throughout this work, only small strain theory is considered. Therefore, the displacements and strains are related by the following equation

$$\varepsilon_{ij} = \frac{1}{2}\left(u_{i,j} + u_{j,i}\right) \tag{2.43}$$

where u_i is the displacement vector. While the physical meaning of the equilibrium equation is fairly straightforward, it is not as easy to physically understand the

compatibility equation. Mathematically, the strains are compatible when they are definable in terms of a single valued, continuously differentiable displacement. Also, a compatible strain field ensures: 1) all of that part of space which is specified by the body configuration is being occupied by the body (i.e. no vacancies or overlaps), and 2) there is a one-to-one correspondence between particles of the body and points in this part of space. However, a more physical interpretation of compatibility is that the separate particles of the body must deform in such a way that they fit together after deformation. This requirement is essential in finite element calculations to satisfy compatibility.

2.5.3 Constitutive relations

Equilibrium equations which involve only stresses are independent of the compatibility equations which involve only strains. Constitutive equations are necessary to relate stresses to strains through the material properties. For this reason, knowledge of the material behavior is necessary. Here, only isotropic materials are considered. A material is said to be isotropic if it possess the same behavior in all directions. The number of independent material constants for linear elastic behavior of this class of material reduces to two (Barber 1992) as given by Eq. (2.21). Hencky's relation and Prandtl-Reuss equation are also examples of constitutive equations.

In chapter three, a set of constitutive relations analogous to Hooke's Law, but describing elastic-plastic behavior, is derived.

2.6 Elastic-Plastic Method of Solution Based on Elastic Solution

Linear elastic behavior of materials is a well established branch of solid mechanics. There exists a unified understanding of the linear elastic response of materials. Also, linear elastic formulations of problems are mathematically simple and their solution are readily attainable. Most practical problems in this field have either analytical or numerical solutions which are in good agreement with experimental observation.

Plasticity, however, is much more complex. Although a unified theory of plasticity began to emerge about 1945, even today there is not a unified understanding of plastic behavior of materials. On one hand, theoretical plasticity with complex mathematics is a matter of debate and research. On the other hand, practical plasticity (e.g., metal forming) has deviated from pure theoretical plasticity and is based more on experimental results and related empirical formulas. Because of its mathematical complexity, many theoretical works find a narrow range of application, and for this reason simpler methods of elastic-plastic analysis have attracted attention amongst researchers in the practical field of plasticity.

The simplicity of linear elasticity and difficulties with nonlinear plasticity have made way for researchers to attempt solving elastic-plastic problems by adapting a modified form of available elastic solutions. The idea of estimating the elastic-plastic behavior by using elastic analysis is not new, and can be traced back to Nadai (1931) who discussed some of his earlier work such as the plastic analysis of a pressurized cylinder using an elastic solution.

2.6.1 Modified elastic solution in elastic-plastic notch analysis

The earliest work dealing with elastic-plastic behavior at a stress concentration was based on elasticity (Nadai, 1930). Nadai studied the maximum shear stress around a circular hole in a thin wide plate using the elasticity equation and Mohr's circle to describe the progression of yielding.

Stowell (1950) employed a modified form of the elastic notch solution to come up with a formula for stress and strain concentration factors for plastic loading. By assuming that the effect of plasticity of the material was to lower the stress concentration factor obtained from elasticity, he argued that the complete stress field in an infinite plate with a central circular hole may be found by modifying its elastic stress field. Stowell separated the terms in the elastic solution of the circular notch problem to terms due to the far field stress and terms due to the local concentration. He then scaled down the terms due to the presence of the hole by the ratios of the local secant modulus and the far

field secant modulus. In this manner he simulated the plasticity effect by lowering the elastic modulus. Based on this, he proposed the following modification to the elastic stress concentration factor

$$K_s = 1 + 2\frac{E_s}{E_\infty} \tag{2.44}$$

where K_f is the elastic-plastic stress concentration factor, E_s and E_∞ are the secant moduli at the notch root and away from the notch, respectively. This equation, which has to be solved by trial and error, gave good stress concentration factors when compared to experimental results. However, based on the same analogy, the strain concentration factor, K_ε, defined by

$$K_\varepsilon = \frac{K_s}{\frac{E_s}{E_\infty}} \tag{2.45}$$

failed to give satisfactory results at relatively high loads. In a similar manner, Budiansky and Vidensek (1953) obtained the elastic-plastic stress field in a plate with a circular hole by adding a correction to the corresponding elastic solution.

Neuber (1961) used the notch tip stress and strain components obtained for a linear elastic body to estimate the elastic-plastic strain and stress components in a geometrically identical elastic-plastic body. He originally proposed the following relation

$$S^2 \frac{K_t^2}{E} = \sigma\varepsilon \tag{2.46}$$

where S is the remote stress and K_t is the elastic stress concentration factor. He assumed that the actual total strain energy density (the sum of strain energy density and the complementary strain energy density) at the notch tip is equal to that which would be obtained if the material were to remain linearly elastic.

Walker (1977) and Dowling (1977) extended Neuber's rule for different types of loading. This method of analysis has been used widely in design codes and has proven to be a good approximation (Conle and Nowack 1977, and Sharp and Wang 1991).

Subsequently, Hoffmann and Seeger (1985) generalized Neuber's method for estimating multiaxial elastic-plastic notch stresses and strains based on the corresponding elastic solution. This method, which is based on proportional loading, utilizes Hencky's deformation theory and provides the following general Hooke's Law formulation

$$\varepsilon_i = \frac{\varepsilon_{eq}}{\sigma_{eq}}\left(\sigma_i - \nu'\left(3\sigma_m - \sigma_i\right)\right) \tag{2.47}$$

where ε_i and σ_i denote the principal strains and stresses, respectively, and

$$\begin{aligned} \sigma_m &= \frac{\sigma_1 + \sigma_2 + \sigma_3}{3} \\ \nu' &= \frac{1}{2} - \left(\frac{1}{2} - \nu\right)\frac{\sigma_{eq}}{E\varepsilon_{eq}} \end{aligned} \tag{2.48}$$

and σ_{eq} is calculated from a hypothetical linear elastic solution by adopting a yield criterion such as von Mises. The corresponding equivalent notch strain, ε_{eq}, is then calculated through a relationship (like Neuber's rule for equivalent stress and strain) involving the modulus of elasticity. Including von Mises yield criterion, Eq. (2.47) provides four equations for the five unknown stresses and strains (in a plane stress problem one of the principal stress is zero which makes the number of unknowns five).

By making the extra assumption that the ratio of elastic strains remain the same in elastic-plastic behavior, principal stresses and strains at the notch tip can be obtained. Later, Hoffmann et al. (1991) extended their method to nonproportional loading.

In a similar correlation, Molski and Glinka (1981) used the elastic strain energy density, instead of total energy density, to calculate the corresponding elastic-plastic stress and strain components at the notch tip. This assumption was motivated by Hutchinson (1968) who found that the strain energy density at a crack tip in a bilinear material is the same as that computed from a purely elastic solution. This method has been extended to multiaxial proportional loading (Moftakhar, 1994) and nonproportional loading (Chu and Conle, 1994). Sharp et al. (1992) modified Glinka's method to account for notches where the initial elastic state is neither plane stress nor plane strain.

2.6.2 Method of successive elastic solution

Ilyushin (1946) used a method of successive elastic solutions to solve the problem of a plastically deformed thin shell. This method is based on Picard's method (Ince, 1944) of successive approximations to nonlinear equations. Later, in a more general sense, this method was proposed by Mendelson and Manson (1959) as a practical solution for plastic deformation. This method uses the following constitutive relation

$$\varepsilon_{ij} = \frac{1}{2G}\sigma_{ij} - \frac{\nu}{E}\sigma_{kk}\delta_{ij} + \varepsilon_{ij}^{\,p} + \Delta\varepsilon_{ij}^{\,p} \tag{2.49}$$

where $\varepsilon_{ij}^{\,p}$ is the total accumulated plastic strain up to, but not including, the current increment of loading $\Delta\varepsilon_{ij}^{\,p}$. The method allows the plastic strain increment to be related to the stresses through any yield criterion and the associated flow rule, but the Prandtl-Ruess relations (Mendelson, 1968) are preferred. In this method, the loading path is divided into a number of increments. For the first increment of load, a distribution is assumed for the components of plastic strain increments $\Delta\varepsilon_{ij}^{\,p}$. The components of total

plastic strain ε_{ij}^{p} are zero. Therefore, the boundary value problem formed by the above constitutive equation can be solved as for any elastic problem to give a first approximation for the stresses and total strains. The assumed values for $\Delta\varepsilon_{ij}^{p}$ give an equivalent plastic increment $\Delta\varepsilon^{p}$ based on Eq. (2.30). From the uniaxial stress-strain curve, the corresponding value of equivalent stress is obtained and new sets of $\Delta\varepsilon_{ij}^{p}$ are calculated from the Prandtl-Reuss equation. Using the new plastic strain increments, the boundary value problem is solved again as a new elastic problem. This process is continued until convergence is obtained, i.e., the differences between two successive sets of strain increments are less than some prescribed values. Mendelson (1968) records a collection of work on different plastic problems using this method. Davis (1964) and Tuba (1966) extended this method to two dimensional problems and provided the solution to a plate with a central hole.

2.6.3 Reduced modulus method

Structural limit loads can be calculated by a number of analysis techniques, the state of art being incremental finite element analysis by specialist nonlinear programs such as ABAQUS. However, calculation of limit loads by detailed inelastic analysis can be difficult and computationally expensive. In practice, limit load analysis for design considerations is often performed using simplified methods, most commonly based on the limit load boundary theorem of plasticity (Mackenzie et al., 1994). Such simplified methods are based on elastic analysis. The basis of this method was proposed by Jones and Dhalla (1981). In their method, rather than performing an inelastic analysis, the inelastic response was investigated by iterative linear elastic analyses in which highly stressed regions of the structure were systematically weakened by reduction of the local modulus of elasticity in order to simulate the effect of local inelasticity. First an elastic analysis is performed and the equivalent stress and strain at the most highly loaded location noted. A rough estimate of the inelastic strain corresponding to the elastically calculated stress is then made. The minimum secant modulus is defined as the ratio of the effective elastic stress to the estimated inelastic strain:

$$E_s^{min} = \frac{\sigma_A}{\varepsilon^P} \tag{2.50}$$

where A is the most highly loaded location. Once the minimum secant modulus is defined, three values of reduced moduli between the minimum secant modulus and Young's modulus are defined. Next, an elastic analysis is performed in which these reduced modulus values are assigned to the most highly stressed local regions of the component. This procedure was used for partitioning the stress at A into primary and secondary components.

A modified version of Dhalla's method was presented later by Marriott (1988). Marriott's procedure is a truly iterative elastic procedure. An initial elastic analysis is performed and all elements with a maximum difference in principal stress greater than some stress S_m (to be defined by pressure vessel design code) are identified. The elastic moduli of these elements are then individually reduced on an element by element basis, according to the equation

$$E_R = E_o \frac{S_m}{SI} \tag{2.51}$$

where E_R and E_o are the reduced and previous values of modulus, respectively, S_m is the code allowable and SI is the element stress (i.e., the maximum difference in the principal stresses). The analysis is then rerun to obtain a reduced modulus analysis solution. The modulus reduction procedure is then repeated in an iterative manner until the maximum element stress, SI, is less than S_m or convergence to some other value occurs.

Seshadri (1990 and 1991) incorporated aspects of the Dhalla and Marriott procedure in estimating creep damage in pressurized components. Seshadri, like Dhalla used equivalent elastic stress but, like Marriott's method, the reduced modulus is calculated on an element-by-element basis. He applied the modulus reduction method to deformation

control and elastic-perfectly plastic material. The reduced modulus required for perfectly plastic behavior is calculated by the following equation:

$$E_R = E_\circ \frac{\sigma_\bullet}{\sigma_{eq}} \tag{2.52}$$

Mackenzie and Boyle (1993) have developed an elastic compensation method which uses conventional elastic finite element analysis to derive suitable stress and strain fields for bounding theorems of classical plasticity. The elastic compensation method requires only a few linear elastic finite element analyses of a structure. After each iteration, the elastic modulus of each element is modified according to the equation

$$E_i = E_{(i-1)} \frac{\sigma_n}{\sigma_{(i-1)}} \tag{2.53}$$

where subscript i is the present iteration number, σ_n is a nominal stress value and $\sigma_{(i-1)}$ is the maximum nodal equivalent stress associated with the element from the previous solution. After a few iterations, an estimate of the limit load is calculated. This method has been applied to a number of different problems (Nadarajah et al., 1993 and Shi et al. 1993).

In a different approach, Seshadri and Marriott (1992) and Seshadri and Fernando (1992) laid out a procedure based on two elastic analyses. This method is based on Schulte's (1960) discovery of points in the cross section of a structure at which the stress did not change as the solution progressed from the initial elastic solution to the final stationary solution. The aim of this method, known as GLOSS, is to find these points called redistribution nodes or R-nodes. In this method, a linear elastic solution is first obtained. A location j is arbitrarily chosen. The elastic moduli of all other elements are then modified according to the following equation:

$$E_R = E\frac{(\sigma_{eq})_j}{\sigma_{ei}} \tag{2.54}$$

where σ_{ei} is the equivalent stress in the *i*th element. Based on the two linear elastic analyses the R-node element is identified and by interpolation the exact location of the R-node is obtained. Having found the R-node, an estimate of the limit load is obtained. This method has been applied to different structures by Seshadri et al. (1992).

3. VARIABLE MATERIAL PROPERTY METHOD

The variable material property method for the solution of nonlinear plasticity uses linear elastic results to model nonlinear plastic response. The constitutive equation relates total strains to the current value of stresses in a linear fashion. However, the material parameters are treated as field variables. For isotropic materials, the number of these independent parameters is limited to two. The distribution of these variable parameters are obtained as a part of the solution in an iterative manner. This method is also capable of predicting the load induced residual stress field.

First the constitutive equation is derived. The functional form of the parameters for elastic-perfectly plastic materials, elastic-linear hardening materials and materials characterized by the Ramberg-Osgood relation are then derived. A method for numerical implementation is also discussed. Five different schemes to evaluate the material parameters are also presented in this chapter. Finally, a method for the prediction of residual stress fields is introduced and implemented.

An axisymmetric elastic-plastic analysis based on the proposed method is presented in this chapter. While the axisymmetric method is applicable to a number of problems, the main focus here is on cylindrical tubes. Equations for different end conditions and loadings are also derived. A comparison of the different schemes of parameter evaluation is made at the end of this chapter.

3.1 FORMULATION

The total strain tensor, ε_{ij}, is assumed to be the sum of an elastic part ε_{ij}^{e} and a plastic part ε_{ij}^{p}:

$$\varepsilon_{ij} = \varepsilon_{ij}^{e} + \varepsilon_{ij}^{p} \tag{3.1}$$

The elastic part is given by Hooke's Law (Eq. 2.21), which may be represented in the form:

$$\varepsilon_{ij}^{e} = \frac{1+\nu}{E}\sigma_{ij} - \frac{\nu}{E}\sigma_{kk}\delta_{ij} \tag{3.2}$$

where ν and E are Poisson's ratio and Young's modulus. The plastic component of strain is given by Hencky's total deformation relation (Eq. 2.23). Substituting the elastic and plastic components of strain into Eq. (3.1), the total strain is then related to the current stress through

$$\varepsilon_{ij} = \left(\frac{1+\nu}{E} + \phi\right)\sigma_{ij} - \left(\frac{\nu}{E} + \frac{1}{3}\phi\right)\sigma_{kk}\delta_{ij} \tag{3.3}$$

where the function ϕ is defined in Eq. (2.25). The quantities inside parentheses in Eq. (3.3) are all functions of the material properties and hence could be represented in the following alternative form

$$\varepsilon_{ij} = \frac{1+\nu_{eff}}{E_{eff}}\sigma_{ij} - \frac{\nu_{eff}}{E_{eff}}\sigma_{kk}\delta_{ij} \tag{3.4}$$

which is similar to the linear elastic constitutive relation. The effective Young's modulus, E_{eff}, and the effective Poisson's ratio, ν_{eff}, are defined as follows:

$$E_{eff} = \frac{3E}{3+2E\phi}$$
$$\nu_{eff} = \frac{3\nu + E\phi}{3+2E\phi} \tag{3.5}$$

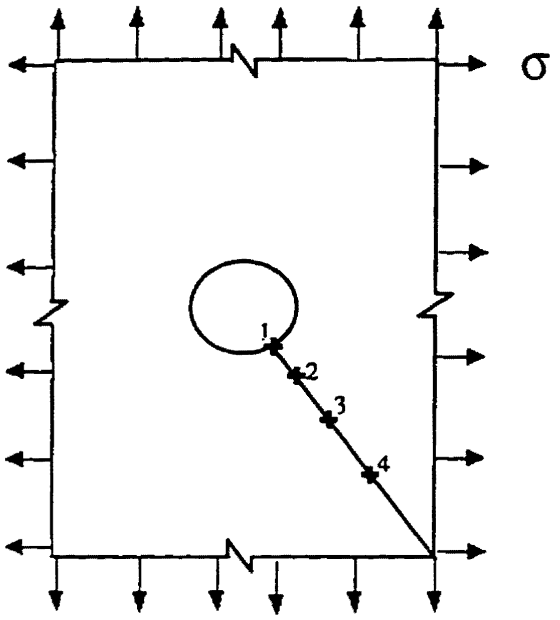
These effective values depend on ν , E and the current stress and/or strain.

3.1.1 Pseudo linear elastic points

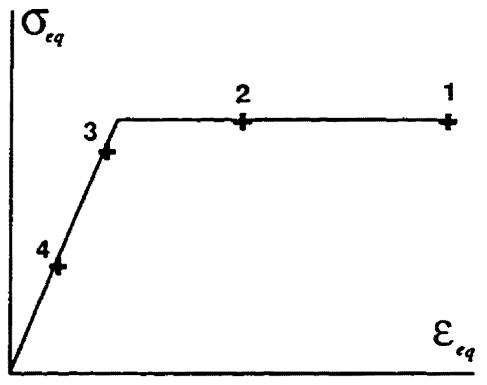
Stress and strain are intrinsically point functions; they are always defined at a material point inside a body. A constitutive equation which relates these two is also a point function. It is a material point rather than a collection of points (i.e., a body) which behaves elastically or inelastically. If a body possesses homogeneity, then the same constitutive relation is applicable throughout the body. For a body under load, a linear elastic relation may be applicable to some material points while a nonlinear stress-strain relation may be applicable to others (Fig. 3.1). Truesdell and Noll (1965) defined elastic points as material points which obey a constitutive relation of the form

$$\underline{T} = \underline{H}(\underline{G}) \tag{3.6}$$

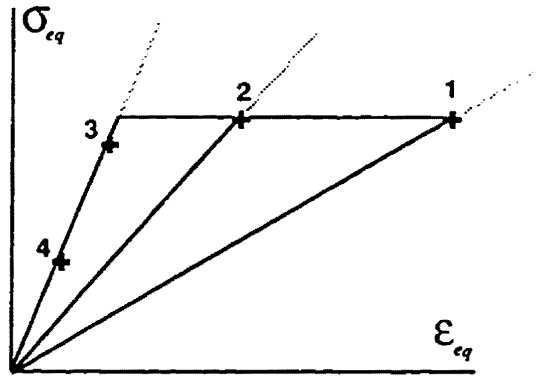
where $\underline{T}$ and $\underline{G}$ are measures of stress and strain, respectively, and $\underline{H}$ is a response function. Equation (3.4) is an example of a generalization of Eq. (3.6), where stress and strain measures are σ_{ij} and ε_{ij}, respectively. The response function, Eq. (3.4), is homogeneous of order one in stresses and strains and depends on corresponding values of E_{eff} and ν_{eff} at each point. The variability of parameters E_{eff} and ν_{eff} are with respect to their position in the body. Therefore, once the load is applied and is fixed, E_{eff} and ν_{eff} will have different values at different points which means that Eq. (3.4) will take a different linear form at each point.



(a)



(b)



(c)

Figure 3.1: Pseudo linear elastic points

Material points obeying the constitutive relation of Eq. (3.4) are called *pseudo linear elastic points.*

Figure 3.1 shows how the parameters E_{eff} and ν_{eff} are treated in a typical body obeying the constitutive relation given by Eq. (3.4). For simplicity, it is assumed that the body behaves in an elastic-perfectly plastic manner. Assume that the stress and strain at each point is known and some of the material points *1, 2, 3* etc. shown in Fig. 3.1a are experiencing plastic deformation. They can be identified by the same numbers *1, 2, 3* etc. on the stress-strain curves in Fig. 3.1b and c. In this example, it is assumed that the total load has been applied and that the differences in strain states of the points are due to the different positions they occupy within the body. In other words, the changing variable is attributed to position and not to load (also sometimes referred to as time). To identify point *1*, for example, on the stress-strain curve, one may follow the nonlinear stress-strain path (Fig. 3.1b) or alternatively take linear paths as shown in Fig. 3.1c. In this manner the corresponding stresses and strains at material point *1* are related by a linear equation. In a similar way, stresses and strains at other material points, e.g., *2,3* etc., are also linearly related (Fig. 3.1c). The corresponding parameters in the linear relations at each material point are E_{eff} and ν_{eff} at that point.

3.1.2 Effective moduli forms

The stress-strain relation under uniaxial loading for elastic-perfectly plastic materials is given in Eq. (2.8). The effective moduli for these materials are of the following form

$$\frac{1}{E_{eff}} = \frac{1}{E} + \frac{\varepsilon^p}{\sigma_o}$$

$$\nu_{eff} = \frac{2\nu\frac{\sigma_o}{E} + \varepsilon^p}{2\frac{\sigma_o}{E} + 2\varepsilon^p} \qquad (3.7)$$

For linear hardening materials, the stress-strain relation under uniaxial loading is given by Eq. (2.9). The effective moduli are then of the from:

$$\frac{1}{E_{eff}} = \frac{1}{E_t} - \frac{\sigma}{\sigma_*}\frac{1}{E_p}$$

$$\nu_{eff} = \frac{2\nu E_p + E\left(1-\frac{\sigma}{\sigma_*}\right)}{2E_p + 2E\left(1-\frac{\sigma}{\sigma_*}\right)} \tag{3.8}$$

where the relation between elastic, plastic and tangent moduli given by Eq. (2.6) has been used.

For materials obeying the Ramberg-Osgood equation given in Eq. (2.10), the effective moduli are defined as

$$\frac{1}{E_{eff}} = \frac{1}{E} + \frac{\alpha}{E}\left(\frac{\sigma}{\sigma_*}\right)^{m-1}$$

$$\nu_{eff} = \frac{2\nu + \alpha\left(\frac{\sigma}{\sigma_*}\right)^{m-1}}{2 + 2\alpha\left(\frac{\sigma}{\sigma_*}\right)^{m-1}} \tag{3.9}$$

The distribution of these moduli throughout the body is obtained as part of the solution.

3.1.3 Implementation

In order to solve a boundary value problem utilizing the constitutive relation given by Eq. (3.4), it is necessary to know the complete spatial distribution of ν_{eff} and E_{eff}. This has

to be found as part of the solution. For this reason, the following procedure is used for determination of ν_{eff} and E_{eff}.

First, a purely elastic solution of the problem is obtained. It is therefore assumed that the effective moduli at all points in the body equal their elastic values, E and ν. Assuming the loading is sufficient to cause plasticity at some points in the body, this will be called a hypothetical or pseudo-elastic solution. Based on this solution, the equivalent stress (von Mises or Tresca equivalent stress) is calculated at all points. Then the points with the same equivalent stress are connected to construct σ_{eq}=*constant* curves. It is assumed that, for each iteration, all of the points lying on the same σ_{eq}=*constant* curve are represented by a single point on the uniaxial stress-strain curve, i.e., they have the same values for ν_{eff} and E_{eff}. That is, material points at the same stress level can be identified by the same set of material properties values.

Now suppose that σ_{eq} remains constant over a small strip of thickness *ds*. As a consequence ν_{eff} and E_{eff} remain constant throughout this strip. Next the strip is isolated and its boundary value problem is defined. Each strip is subjected to compatible tractions and displacements on its boundaries with neighboring strips. The solution of this boundary value problem is obtained so that the behavior of points within the strip is ascertained. In this manner, the original problem is discretized into several infinitesimal strips. The material properties remain constant for points within a particular strip. Hence, an inelastic solution for each strip can be obtained from the elastic solution.

The solution for each strip is reconstituted once the values of the corresponding moduli have been updated. To implement this procedure a scheme is needed for updating the effective material properties. Three general methods are discussed here: projection, arc-length and energy methods (including methods based on Neuber's approach, Glinka's approach and a combination of these two approaches).

3.1.4 Moduli evaluation

Once the strips are formed, the new values of effective moduli will be assigned to each strip based on the results of the previous solution using one of the three general methods described below.

3.1.4.1 Projection method

This method is based on the assumption that the total strain predicted by a hypothetical elastic solution is always less than or equal to the strain calculated from an actual elastic-plastic analysis. Hence, the updated value of E_{eff} is always less than the previous value, which results in a monotonic convergence to the solution.

To implement this scheme, first a hypothetical elastic solution based on the elastic modulus and Poisson's ratio is obtained. The state of stress in each strip is defined through an equivalent stress. Each strip is then identified by a point on the hypothetical straight line which is the extension of the elastic line on the stress-strain curve (Fig. 3.2). Points a, b, and c shown in Fig. 3.2, correspond to material points a, b, and c defined for a particular problem (like points *1,2,3 etc.* shown in Fig. 3.1a). To update the values of the moduli, a point on the real stress-strain curve is defined for each strip which possess the same strain as that predicted by the pseudo-elastic solution. For example point a' from point **a** in Fig. 3.2. The updated value of E_{eff} for the strip including **a**, is then obtained by taking the ratio of the stress and strain at **a'**

$$E_{eff} = \left.\frac{\sigma}{\varepsilon}\right|_{a'} \tag{3.10}$$

The corresponding updated value of ν_{eff} is then calculated using Eq. (3.5) in general, or Eq. (3.7),Eq. (3.8) or Eq. (3.9) for the corresponding material behavior. Next, an inelastic solution is obtained based on the updated values for the moduli. Since it is assumed that the corresponding values of effective moduli remain constant in each strip,

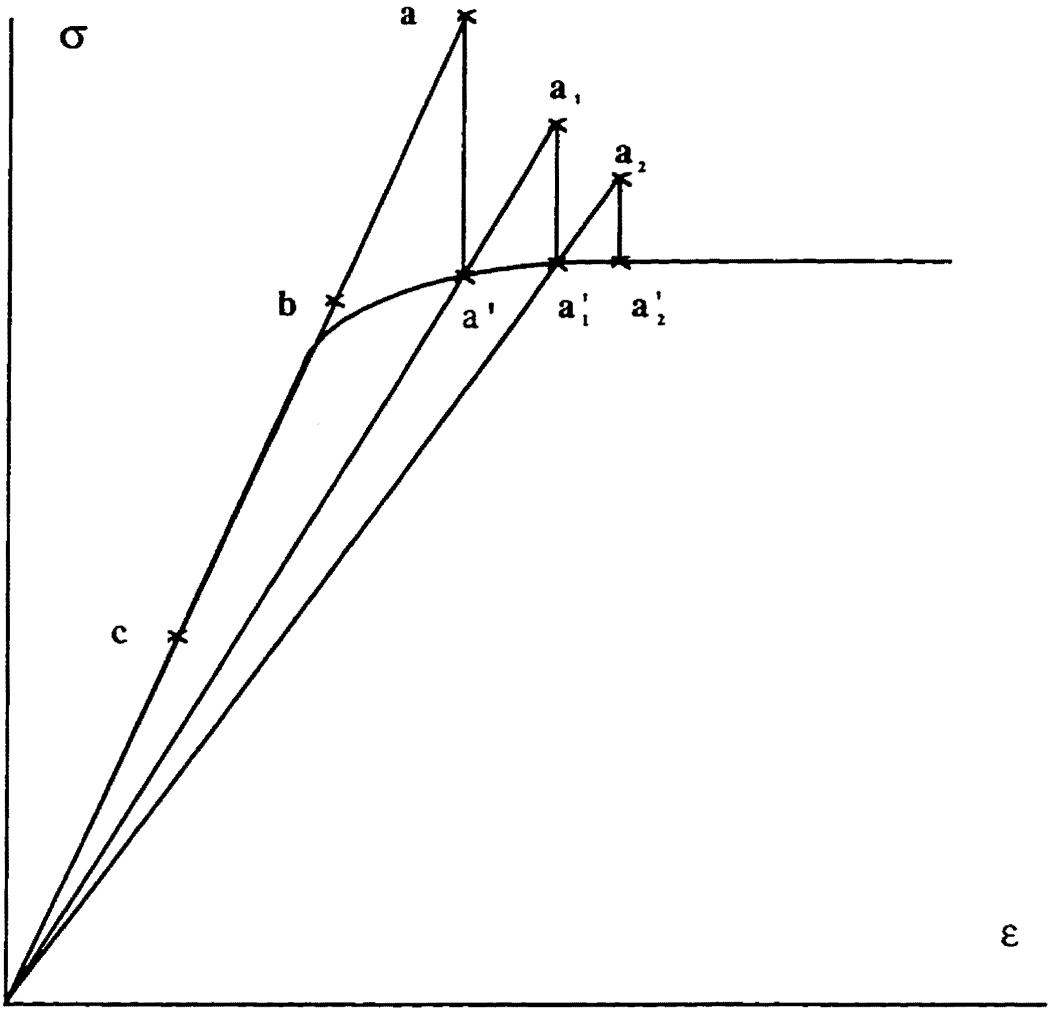


Figure 3.2: Projection method

the solution for each strip can be obtained from an elastic solution. This next solution will provide new stress and strain values for each strip. The stress and strain at the strip including a will now be defined by a_1 in Fig. 3.2. Equation (3.10) is now used at point a_1'.

The effective values for moduli obtained in this manner are updated in each iteration until the σ_{eq} vs. σ_{eq}/E_{eff} curve obtained from the calculation coincides with the experimentally obtained uniaxial stress-strain curve to within an acceptable tolerance.

3.1.4.2 Arc-length method

In this method, it is more convenient to work with a dimensionless uniaxial stress-strain curve. Each strip is identified by a point on the hypothetical straight line which is the extension of the elastic line on the dimensionless stress-strain curve (Fig. 3.3). Next a radius r is defined:

$$r = \sqrt{\left(\frac{\sigma_{eq}}{\sigma_o}\right)^2 + \left(\frac{\sigma_{eq}}{E\varepsilon_o}\right)^2}. \tag{3.11}$$

An arc of radius $r=oa$ from the origin of the dimensionless uniaxial stress-strain curve intersects the actual uniaxial curve at the point $\mathbf{a}'$ (Fig. 3.3). Equation (3.10) gives the new value for E_{eff}. The corresponding updated value of ν_{eff} is then calculated using Eq. (3.5) in general, or Eq. (3.7) ,Eq. (3.8) or Eq. (3.9) for any corresponding material behavior. Next, an inelastic solution is obtained based on the updated values for the moduli. Since it is assumed that the corresponding values of effective moduli remain constant in each strip, the solution for each strip remains identical in form to the elastic solution. As shown in Fig. 3.3, the next solution shows the stress and strain at the strip including $\mathbf{a}$ to be that corresponding to point $\mathbf{a}_1$ on the dimensionless uniaxial stress-strain curve. Equation (3.10) is now used at point $\mathbf{a}_1'$.

The effective moduli values obtained in this manner are updated in each iteration until the σ_{eq} vs. σ_{eq}/E_{eff} curve obtained coincides with the experimentally obtained uniaxial stress-strain curve to within an acceptable tolerance.

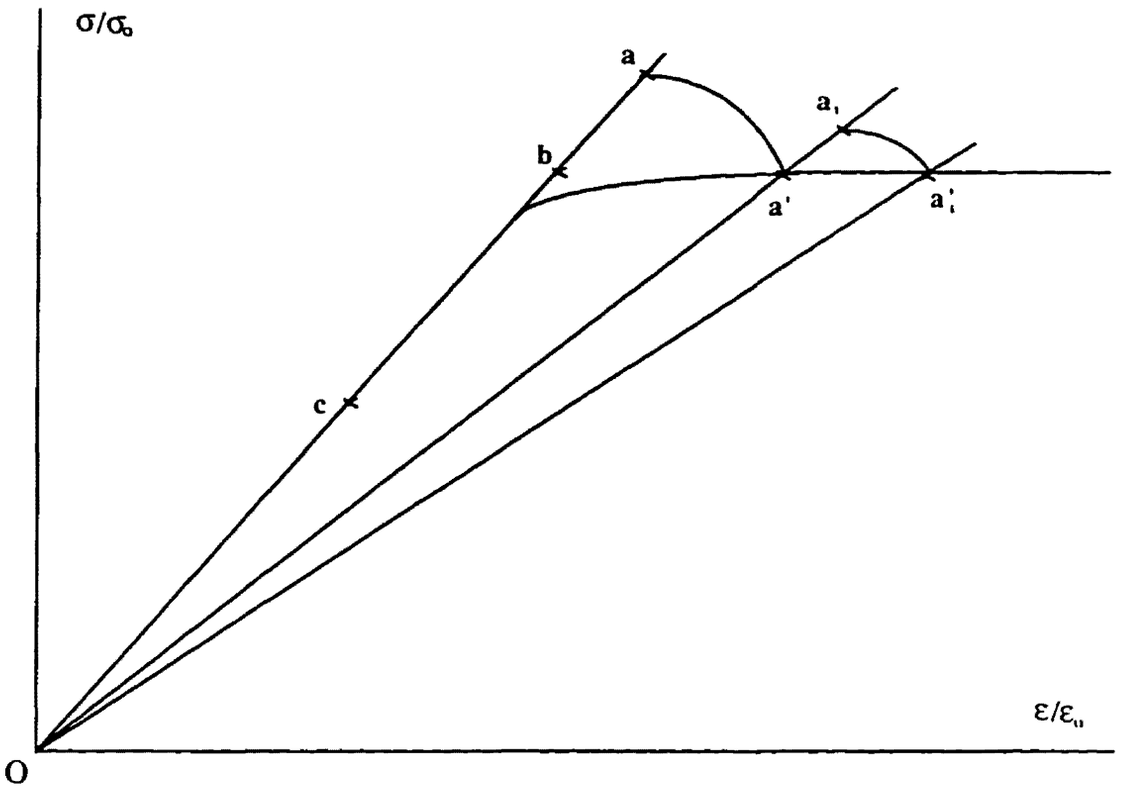


Figure 3.3: Arc-length method

3.1.4.3 Energy methods

There are three different energy based methods for updating the effective moduli values: Neuber's rule for elastic-plastic total strain energy, Glinka-Molski's method for strain energy density, and a combination of the these two. All three are discussed below.

3.1.4.3.1 Neuber's method

As mentioned in section 2.6.1, Neuber (1961) suggested that the total strain energy density (the sum of strain energy and the complementary strain energy density) at the notch tip in elastic-plastic materials is equal to that of a hypothetical elastic solution. While Neuber's calculation was for shear loading, he argued that the assumption can be extended to other modes. Walker (1977) showed the validity of this approximation for other loads.

Although this method was intended for localized plasticity and more specifically for notches, it may also be taken as a scheme for updating the effective moduli. To implement this method, each strip is first assigned an equivalent stress value calculated from a hypothetical elastic solution. An equivalent total strain energy density is calculated for each strip using the following equation,

$$W^{TE} = \frac{\sigma_{eq}^2}{E_{eff}} \tag{3.12}$$

where W^{TE} is the total strain energy density. Next, a point (with strain ε^{TE}) on the actual stress-strain curve is selected such that it gives the same W^{TE} (Fig. 3.4). The corresponding value of stress at that point yields the updated value for E_{eff} from Eq. (3.10). The corresponding updated value for ν_{eff} is then calculated using Eq. (3.5) in general, or Eq. (3.7), Eq. (3.8) or Eq. (3.9) for any corresponding material behavior. Next, an inelastic solution is obtained based on the updated moduli values.

The effective moduli values obtained in this manner are updated in each iteration until the σ_{eq} vs. σ_{eq}/E_{eff} curve obtained coincides with the experimentally obtained uniaxial stress-strain curve to within an acceptable tolerance.

3.1.4.3.2 Glinka's Method

Hutchinson (1968) showed that, for a material with a bilinear stress-strain curve, the strain energy density (rather than the total energy density) at the crack tip is independent of material hardening, and hence is exactly the same as that predicted using a purely elastic analysis. Motivated by this observation, Molski and Glinka (1981) and Glinka (1985) proposed that, instead of the total strain energy density used by Neuber, one should use the strain energy density. They argued that the strain energy density at the notch root does not change significantly if the localized plasticity is surrounded by predominately elastic material.

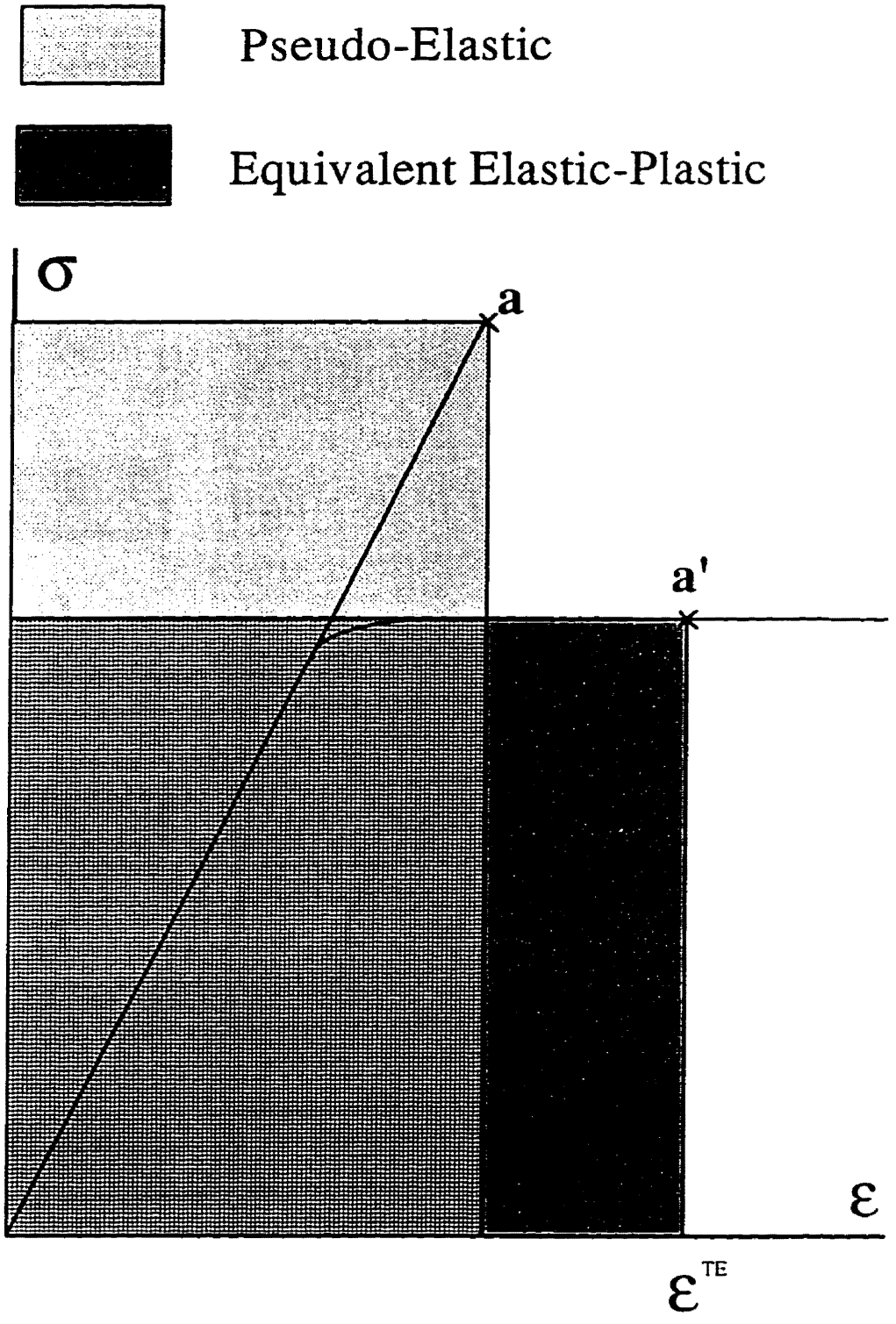


Figure 3.4: Neuber's method

To implement this method, each strip is first assigned an equivalent stress value obtained from a hypothetical elastic solution. An equivalent strain energy density is calculated for each strip using the following equation,

$$W^{SE} = \frac{\sigma_{eq}^2}{2E_{eff}} \tag{3.13}$$

where W^{SE} is the strain energy density. Next, a point (with strain ε^{SE}) on the actual stress-strain curve is selected such that it gives the same W^{SE} (Fig. 3.5). The corresponding value of stress at that point yields the updated value for E_{eff} from Eq. (3.10). The corresponding updated value for ν_{eff} is then calculated using Eq. (3.5) in general, or Eq. (3.7), Eq. (3.8) or Eq. (3.9) for any corresponding material behavior. Next, an inelastic solution is obtained based on the updated moduli values.

The effective moduli values obtained in this manner are updated in each iteration until the σ_{eq} vs. σ_{eq}/E_{eff} curve obtained coincides with the experimentally obtained uniaxial stress-strain curve to within an acceptable tolerance.

3.1.4.3.3 Combined method

Moftakhar et al. (1995) compared the results based on Nueber's and Glinka's assumptions to experimental and numerical results and concluded that Neuber's method serves as an upper bound, and Glinka's method serves as a lower bound to many elastic-plastic solutions. That is, the actual values of elastic-plastic stresses and strains at the notch tip are less than that predicted by Neuber and greater than that calculated by Glinka. For this reason, the following method of updating effective moduli is proposed. After calculating ε^{TE} and ε^{SE} from the hypothetical elastic solution, the updated value of effective moduli are defined as the geometric mean value of Neuber's and Glinka's estimates,

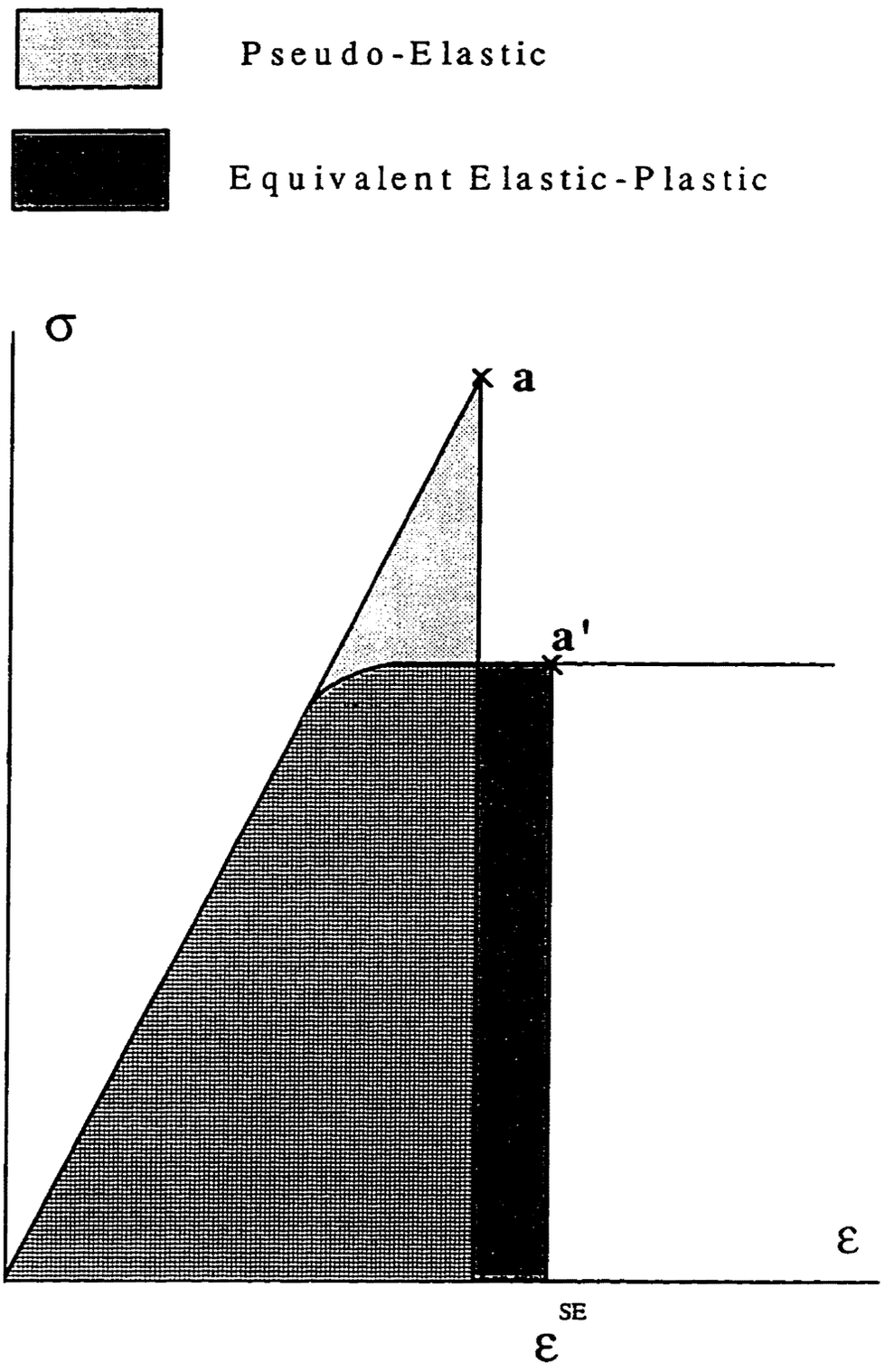


Figure 3.5: Glinka's method

$$\varepsilon = \sqrt{\varepsilon^{TE}\varepsilon^{SE}} \tag{3.14}$$

and its corresponding stress, σ, from the actual uniaxial stress-strain curve. The updated value for E_{eff} is defined using Eq. (3.10).The corresponding updated value for ν_{eff} is then calculated using Eq. (3.5) in general, or Eq. (3.7), Eq. (3.8) or Eq. (3.9) for any corresponding material behavior. Next, an inelastic solution is obtained based on the updated moduli values.

The effective moduli values obtained in this manner are updated in each iteration until the σ_{eq} vs. σ_{eq}/E_{eff} curve obtained coincides with the experimentally obtained uniaxial stress-strain curve to within an acceptable tolerance.

3.1.5 Unloading and reversed yielding

At the end of loading, the unloading stress-strain curve for each material point (i.e., each strip) is defined using the current value of yield stress at the end of loading for each strip within the plastic zone, the loading curve, and the material hardening rule. This is discussed below.

If the actual unloading curve is known, then this would be employed instead of adapting a hardening model. Otherwise, two different material hardening models, isotropic and kinematic hardening, may be considered. If the unloading is fully elastic then the corresponding stresses and strains due to unloading can be calculated simply with one totally elastic analysis. However, in cases of reversed yielding, the prediction based on each hardening rule is different. In the case of isotropic hardening, reverse yielding is controlled by

$$\sigma_{\bullet}^{\alpha} = 2\sigma_{Y} \tag{3.15}$$

where σ_o^u is the difference of the stress at the end of loading and the reversed yield. In the case of kinematic hardening, reverse yielding is assumed to occur according to the following general relationship

$$\sigma_o^u = (1 + BEF)\sigma_o \tag{3.16}$$

where the Bauschinger effect factor, BEF, is defined as the ratio of the initial yield stress in tension to the yield stress in compression (Walter 1948). For a case where the Bauschinger effect factor is one, i.e. BEF=1, Eq. (3.16) yields $\sigma_o^u = 2\sigma_o$.

For each material point, the starting point for the unloading curve is the final yield stress at the end of loading. From this point, the unloading is linear over a stress difference of σ_o^u after this, hardening begins, following the same hardening curve as for loading from the point of take off (Fig. 2.7).

Having defined the unloading curve, a second proportional loading, which in this case is unloading, is considered. The method of analysis is the same as described above for loading. However, in this case each strip has to follow its own unloading curve.

Results from the second analysis are subtracted from those from loading to obtain the corresponding residual stress or strain fields,

$$\begin{aligned} \sigma_{ij}^R &= \sigma_{ij} - \sigma_{ij}^u \\ \varepsilon_{ij}^R &= \varepsilon_{ij} - \varepsilon_{ij}^u \end{aligned} \tag{3.17}$$

where superscripts R and u stand for residual and unloading, respectively.

3.2 AN AXISYMMETRIC METHOD OF ELASTIC-PLASTIC ANALYSIS

In this section, the proposed method is used to develop a general method for analyzing elastic-plastic axisymmetric problems. While this method is applicable to all axisymmetric problem (thick-walled tubes, fastener holes, spherical vessels, rotating disks etc.), attention is focused herein on the analysis of thick-walled tubes and related problems.

Figure 3.6 shows a typical thick tube under pressure. In this figure, p_i and p_o are inside and outside pressures, and r_i and r_o are inside and outside radii of the cylinder, respectively.

The σ_{eq}=*constant* curves for this problem are concentric circles. Moreover, the σ_{eq}=*constant* curves defined by the first pseudo elastic solution remain σ_{eq}=*constant*

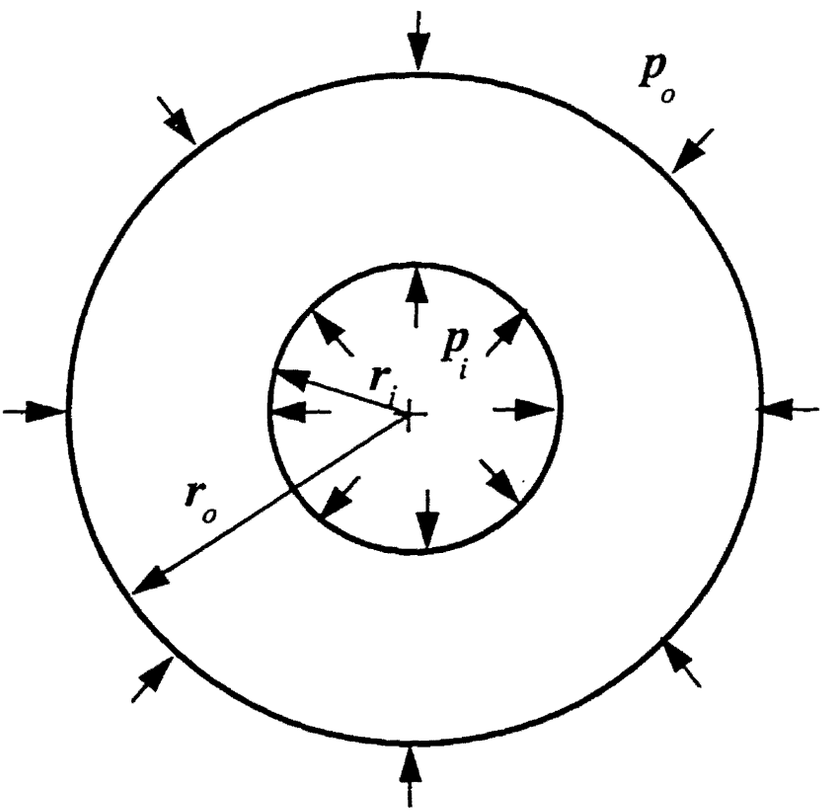


Figure 3.6: Thick-walled cylinder

curves in the final elastic-plastic solution due to the axisymmetric nature of this problem. Assuming that the value of equivalent stress remains constant within a small radius, *ds*, the strips for this problem are annular, as shown in Fig. 3.7. The boundary value problem defined by each strip is that of a cylinder under internal and external pressure. The elastic solution to this problem is the well known Lamé solution which is reviewed briefly below. Since the effective moduli values are assumed to remain constant within each strip, Lamé's solution is applicable to all strips.

3.2.1 Lamé solution

Consider a thick-walled cylinder under external and internal pressure (Fig. 3.6). It is convenient to use cylindrical coordinates (r, θ, z), where θ is the angle between a radius vector and a fixed axis, and z is taken along the axis of the cylinder. By virtue of symmetry the stresses at any given point are a function of r only, and the equilibrium equation may be written as

$$\frac{\partial \sigma_r}{\partial r} = \frac{\sigma_\theta - \sigma_r}{r} \tag{3.18}$$

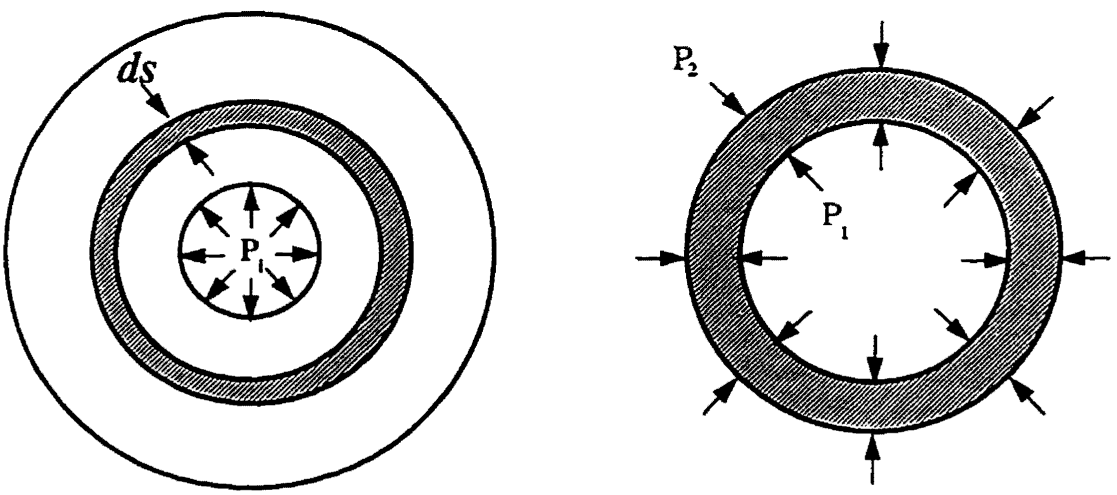


Figure 3.7: Strip in a thick-walled cylinder

where σ_r and σ_θ are radial and tangential (or hoop) stresses, respectively.

The radial strain, ε_r, and the hoop strain, ε_θ, may be written as

$$\begin{aligned} \varepsilon_r &= \frac{\partial u}{\partial r} = -\nu\varepsilon_z + \frac{1+\nu}{E}\left[(1-\nu)\sigma_r - \nu\sigma_\theta\right] \\ \varepsilon_\theta &= \frac{u}{r} = -\nu\varepsilon_z + \frac{1+\nu}{E}\left[(1-\nu)\sigma_\theta - \nu\sigma_r\right] \end{aligned} \tag{3.19}$$

where u denotes the radial displacement.

Since ε_z is independent of r, elimination of u from the above equations and the substitution for $(\sigma_\theta-\sigma_r)$ from Eq. (3.18) leads to the compatibility equation:

$$\frac{\partial}{\partial r}(\sigma_r + \sigma_\theta) = 0 \tag{3.20}$$

It follows that $(\sigma_\theta+\sigma_r)$ and σ_z have constant values at each point in an elastic deformation. Writing $\sigma_\theta+\sigma_r=2A$, the equilibrium equation can be integrated to obtain Lamé's solution:

$$\begin{aligned} \sigma_r &= A_1 - \frac{A_2}{r^2} \\ \sigma_\theta &= A_1 + \frac{A_2}{r^2} \end{aligned} \tag{3.21}$$

where r is the mean radius of each strip, and A_1 and A_2 are constants obtained by applying the boundary condition $\sigma_r=-p_o$ at $r=r_o$ and $\sigma_r=-p_i$ at $r=r_i$. These constants take the following form:

$$A_1 = \frac{p_i r_i^2 - p_o r_o^2}{r_o^2 - r_i^2}$$
$$A_2 = \frac{(p_i - p_o) r_i^2 r_o^2}{r_o^2 - r_i^2}. \tag{3.22}$$

In addition, the strain displacement relations Eq. (3.19) may be solved in terms of the displacements. For the plane strain case ($\varepsilon_z=0$),

$$\sigma_r = \frac{E}{(1+\nu)(1-2\nu)}\left[(1-\nu)\frac{\partial u}{\partial r} + \nu\frac{u}{r}\right]$$
$$\sigma_\theta = \frac{E}{(1+\nu)(1-2\nu)}\left[\nu\frac{\partial u}{\partial r} + (1-\nu)\frac{u}{r}\right] \tag{3.23}$$

Substituting this into the equilibrium relation Eq. (3.18) yields the following differential equation after some manipulation:

$$\frac{\partial^2 u}{\partial r^2} + \frac{1}{r}\frac{\partial u}{\partial r} - \frac{u}{r} = 0 \tag{3.24}$$

Therefore, the radial displacement has the following form:

$$u = C_1 r + \frac{C_2}{r} \tag{3.25}$$

where C_1 and C_2 are found by applying the boundary conditions:

$$C_1 = \frac{(1+\nu)(1-2\nu)}{E}\frac{p_i r_i^2 - p_o r_o^2}{r_o^2 - r_i^2}$$
$$C_2 = \frac{(1+\nu)}{E}\frac{(p_i - p_o) r_i^2 r_o^2}{r_o^2 - r_i^2} \qquad (3.26)$$

Different end conditions (closed, open or plane strain) result in different values for σ_z and ε_z. If the resultant longitudinal load is denoted by P, the axial stress, σ_z, is $P/[\pi(r_o^2-r_i^2)]$, since this stress is constant over the cross section. In particular, $P=0$ for an open-ended cylinder and $P=\pi r_i^2 p_i$ for a closed-ended internally pressurized cylinder away from the ends. The plane strain condition, sometimes considered for simplicity, gives

$$\sigma_z = \nu(\sigma_r + \sigma_\theta) \qquad (3.27)$$

Hence, for an internally loaded cylinder

$$\sigma_z = \begin{cases} \dfrac{p_i}{\dfrac{r_o^2}{r_i^2}-1} & \text{closed end} \\ 0 & \text{open end} \\ \dfrac{2\nu p_i}{\dfrac{r_o^2}{r_i^2}-1} & \text{plane strain} \end{cases} \qquad (3.28)$$

Similarly, the axial strain is

$$\varepsilon_z = \begin{cases} \dfrac{1}{E}\dfrac{(1-2\nu)p_i}{\dfrac{r_o^2}{r_i^2}-1} & \text{closed end} \\ 0 & \text{open end (long cylinder)} \\ -\dfrac{1}{E}\dfrac{2\nu p_i}{\dfrac{r_o^2}{r_i^2}-1} & \text{plane strain} \end{cases} \tag{3.29}$$

3.2.2 Implementation for elastic-plastic analysis

As shown in Fig. 3.7, an annular strip in the cylinder forms a boundary value problem which admits the Lamé solution. However, a modification needs to be made in Lamé's solution to make it suitable for the proposed elastic-plastic analysis. The modification concerns replacing the elastic modulus and Poisson's ratio with effective moduli values. Hence, the constants in Eq. (3.25) are now of the following form:

- for plane strain

$$\begin{aligned} C_1 &= \frac{(1+\nu_{eff})(1-2\nu_{eff})}{E_{eff}}\frac{p_1 r_1^2 - p_2 r_2^2}{r_2^2 - r_1^2} \\ C_2 &= \frac{(1+\nu_{eff})}{E_{eff}}\frac{(p_1 - p_2) r_1^2 r_2^2}{r_2^2 - r_1^2} \end{aligned} \tag{3.30}$$

- for plane stress

$$C_1 = \frac{(1-\nu_{eff})}{E_{eff}} \frac{p_1 r_1^2 - p_2 r_2^2}{r_2^2 - r_1^2}$$
$$C_2 = \frac{(1+\nu_{eff})}{E_{eff}} \frac{(p_1 - p_2) r_1^2 r_2^2}{r_2^2 - r_1^2} \tag{3.31}$$

Here, r_1, r_2 are the inner and outer radii, p_1, and p_2, internal pressure, and external pressure on each strip, respectively. It should be noted that for other axisymmetric problems, e.g., thick spherical vessels where the strips take the form of a spherical shell, the form of the displacement function (Eq. 3.25) must be modified accordingly. However, the analysis is identical to the one described here.

The inside and outside displacements of the strip can be related to its inside and outside pressures in the following form

$$\begin{bmatrix} C_{11} & C_{12} \\ C_{21} & C_{22} \end{bmatrix}^{-1} \begin{Bmatrix} u_1 \\ u_2 \end{Bmatrix} = \begin{Bmatrix} p_1 \\ p_2 \end{Bmatrix} \tag{3.32}$$

The components of coefficient matrix $[C]^{-1}$ in the case of plane strain are as follows:

$$C_{11} = \frac{1+\nu_{eff}}{E_{eff}} \frac{r_1^3}{r_2^2 - r_1^2} \left(1 - 2\nu_{eff} + \frac{r_2^2}{r_1^2}\right)$$
$$C_{12} = -2 \frac{\left(1-\nu_{eff}^2\right)}{E_{eff}} \frac{r_1 r_2^2}{r_2^2 - r_1^2}$$
$$C_{21} = 2 \frac{\left(1-\nu_{eff}^2\right)}{E_{eff}} \frac{r_1^2 r_2}{r_2^2 - r_1^2} \tag{3.33}$$
$$C_{22} = -\frac{1+\nu_{eff}}{E_{eff}} \frac{r_2^3}{r_2^2 - r_1^2} \left(1 - 2\nu_{eff} + \frac{r_1^2}{r_2^2}\right)$$

In the case of plane stress, the components take the following form

$$
\begin{aligned}
C_{11} &= \frac{1+\nu_{eff}}{E_{eff}} \frac{r_1^3}{r_2^2 - r_1^2}\left(\frac{1-\nu_{eff}}{1+\nu_{eff}} + \frac{r_2^2}{r_1^2}\right) \\
C_{12} &= -\frac{2}{E_{eff}} \frac{r_1 r_2^2}{r_2^2 - r_1^2} \\
C_{21} &= \frac{2}{E_{eff}} \frac{r_1^2 r_2}{r_2^2 - r_1^2} \\
C_{22} &= -\frac{1+\nu_{eff}}{E_{eff}} \frac{r_2^3}{r_2^2 - r_1^2}\left(\frac{1-\nu_{eff}}{1+\nu_{eff}} + \frac{r_1^2}{r_2^2}\right)
\end{aligned}
\tag{3.34}
$$

After assembling all strips together, a system of linear equations of the form

$$[C'][U] = \{P\} \tag{3.35}$$

is obtained and solved for $\{U\}$. Then p_1 and p_2 are calculated from Eq. (3.32) for each strip. The hoop stress, σ_θ, radial stress, σ_r, and axial stress, σ_z, for plane strain or plane stress analyses are determined from Eq. (3.21). The axial stress, which is zero for plane stress, may be obtained from the following equation for plane strain:

$$\sigma_z = 2\nu_{eff} A_1 \tag{3.36}$$

where A_1 is given by

$$A_1 = \frac{p_1 r_1^2 - p_2 r_2^2}{r_2^2 - r_1^2} \tag{3.37}$$

3.2.2.1 Residual stresses calculation

The pressure is removed entirely once the loading is completed. Analysis for unloading is carried out by first employing a hardening rule. Accordingly, the unloading curves are defined. In the case where the actual unloading curve is available, this is used. The method described (in section 3.1.5) above is then used to find the stresses due to unloading. In the unloading analysis, each strip is forced to follow its own unloading curve. The residual stress field is then calculated from the following equations:

$$\begin{aligned} \sigma_\theta^{\,R} &= \sigma_\theta - \sigma_\theta^{\,u} \\ \sigma_r^{\,R} &= \sigma_r - \sigma_r^{\,u} \\ \sigma_z^{\,R} &= \sigma_z - \sigma_z^{\,u}. \end{aligned} \tag{3.38}$$

where $\sigma_\theta^{\,u}$, $\sigma_r^{\,u}$, and $\sigma_z^{\,u}$, are the hoop, radial, and axial stresses due to unloading, and $\sigma_\theta^{\,R}$, $\sigma_r^{\,R}$, and $\sigma_z^{\,R}$ are the corresponding values of the residual stresses. The unloading analysis is capable of handling elastic unloading as well as reversed yielding.

3.3 Convergence Comparison

A FORTRAN code based on the proposed method of axisymmetric elastic-plastic analysis was developed. This code (see Appendix A), utilizes all five methods of moduli evaluation outlined in section 3.1.4. The code is also capable of calculating residual stress, strain and displacement fields. It can also handle different stress-strain curve idealizations as well as actual loading and unloading curves. The code was used for different applications which are given in the next chapter.

An equilibrium iteration criterion is used in this code. Stress values for each strip are compared to their previous values in each iteration. A mean value of the stress difference over all strips is compared to the tolerance.

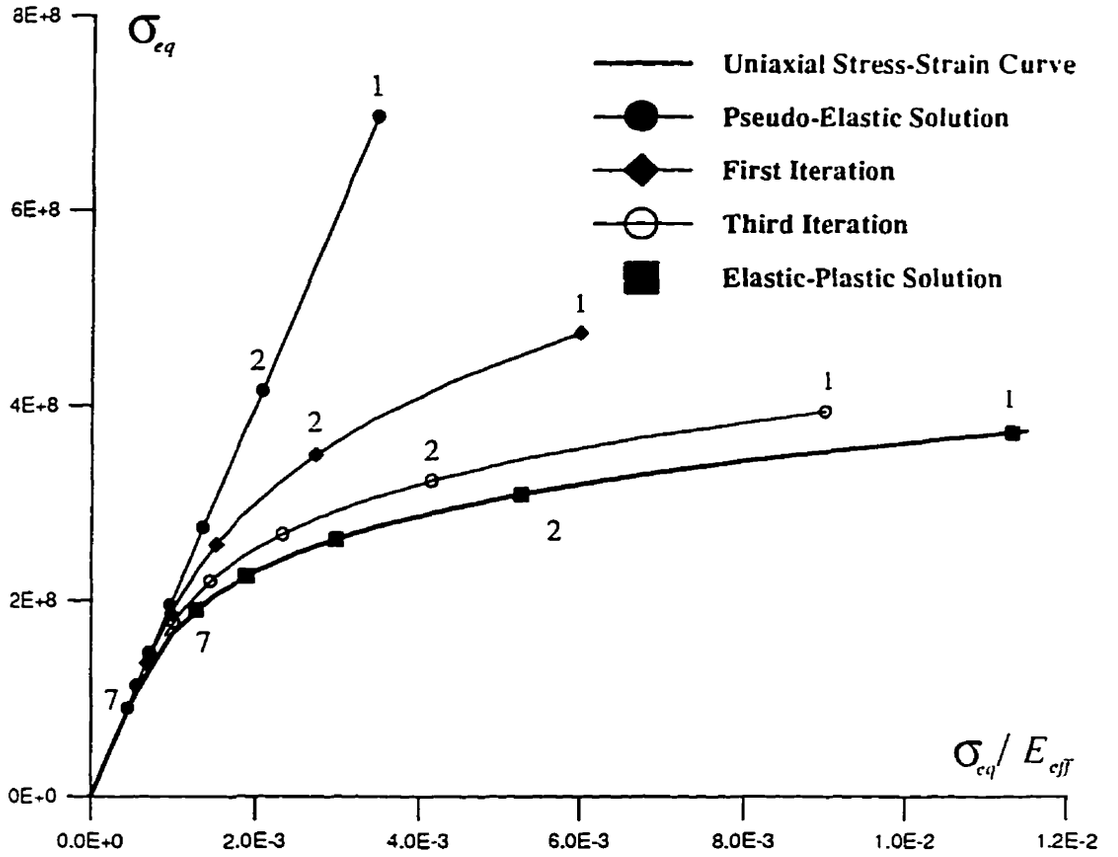


Figure 3.8: Convergence of the pseudo elastic solution to the elastic plastic solution

3.3.1 Evaluation of methods for updating the moduli

When any of the five discussed methods of moduli evaluation is used, the first hypothetical elastic solution gradually (within a couple of iterations) converges to the elastic-plastic solution. Figure 3.8 compares pseudo elastic solutions to the elastic solution for points along the radius.

Point *1* corresponds to the first strip at the bore of a thick-walled cylinder. Other points correspond to strips near the bore. It can be seen from this figure that the elastic-plastic solution obtained by the proposed method (dark squares in the figure) matches the uniaxial stress-strain curve. The figure also shows that for each modification of the moduli (iteration), the solution gets closer to the true elastic-plastic solution.

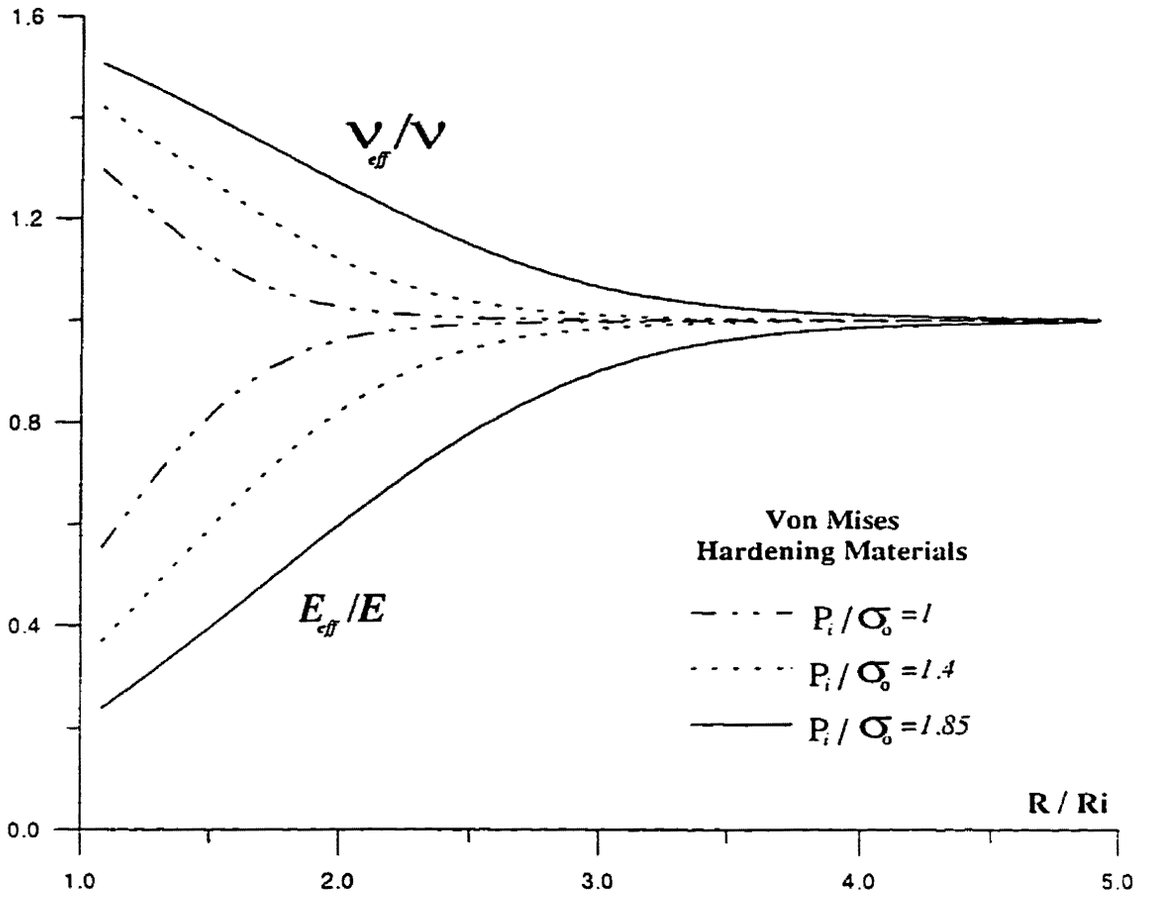


Figure 3.9: Effective moduli variation

A typical moduli distribution through the wall thickness of a cylinder is shown in Fig. 3.9. This variation depends on the level of loading. In Fig. 3.9, three different ratios of the internal pressure to the yield stress are considered; the material is assumed to obey the Ramberg-Osgood equation with $\alpha=3/7$ and $m=5$; the ratio of the outside to inside radius is *5*; Poisson's ratio is *0.3*; the ratio of the elastic modulus to the yield stress is 1000 and the von Mises yield criterion is used.

The following tube is considered for comparing the five different methods of evaluating the effective moduli: inside radius of *22 mm*, outside radius of *66 mm*, nonhardening behavior, yield stress of *1000 MPa*, modulus of elasticity of *180 GPa*, Poisson's ratio of *0.3*, obeying the Tresca yield criterion. The first comparison is based on the number of iterations required for convergence to the elastic-plastic solution. Table 3.1 records the

results for a cylinder in the plane stress situation. In this table, the number of iterations is compared as the plastic zone size increases with increasing load. Neuber's method and the combined method give the fastest convergence rates.

	Number of Iterations					
Plastic Penetration r_p/r_o	Load p_i/σ_o	Projection Method	Arc-Length Method	Neuber's Method	Glinka's Method	Combined Method
0.17	0.7	10	7	8	10	7
0.27	0.8	14	10	8	13	9
0.40	0.9	18	14	10	18	12
0.57	1.0	25	21	13	24	16
0.68	1.05	32	27	16	31	21
0.76	1.07	37	32	18	36	24
0.87	1.09	49	42	24	48	32

Table 3.1: Convergence comparison (plane stress)

Table 3.2 shows the results for a cylinder in the plane strain situation. The combined method and Glinka's method give the best convergence rates. The arc-length method gives better convergence rates than the remaining methods.

Sharpe (1995), in an experimental evaluation of the Neuber's and Glinka's methods in predicting local plastic strains and stresses, concluded that "Neuber's model works best

when the local region is in a state of plane stress and the Glinka's model is best for plane strain". Results tabulated in Table 3.1 and 3.2 show that, in a plane stress case, solutions based on Neuber's method are the fastest. In a plane strain case, Glinka's method gives much faster convergence rates than Neuber's method.

	Number of Iterations					
Plastic Penetration r_p/r_o	Load p_i/σ_o	Projection Method	Arc-Length Method	Neuber's Method	Glinka's Method	Combined Method
0.18	0.7	9	6	16	9	6
0.28	0.8	12	8	20	11	8
0.38	0.9	15	11	27	14	10
0.56	1.0	21	16	37	20	14
0.68	1.05	27	21	46	26	18
0.75	1.07	32	26	51	31	21
0.86	1.09	44	36	59	43	29

Table 3.2: Convergence comparison (plane strain)

The convergence behavior at a given material point on the above cylinder has also been compared. The projection method result is compared to energy methods in Figure 3.10 for the first strip (at the bore). Since all three energy methods show the same type of behavior, only the results of the one which gave the fastest convergence (i.e., Neuber's method) is shown in this figure. The projection method shows a more stable (i.e.,

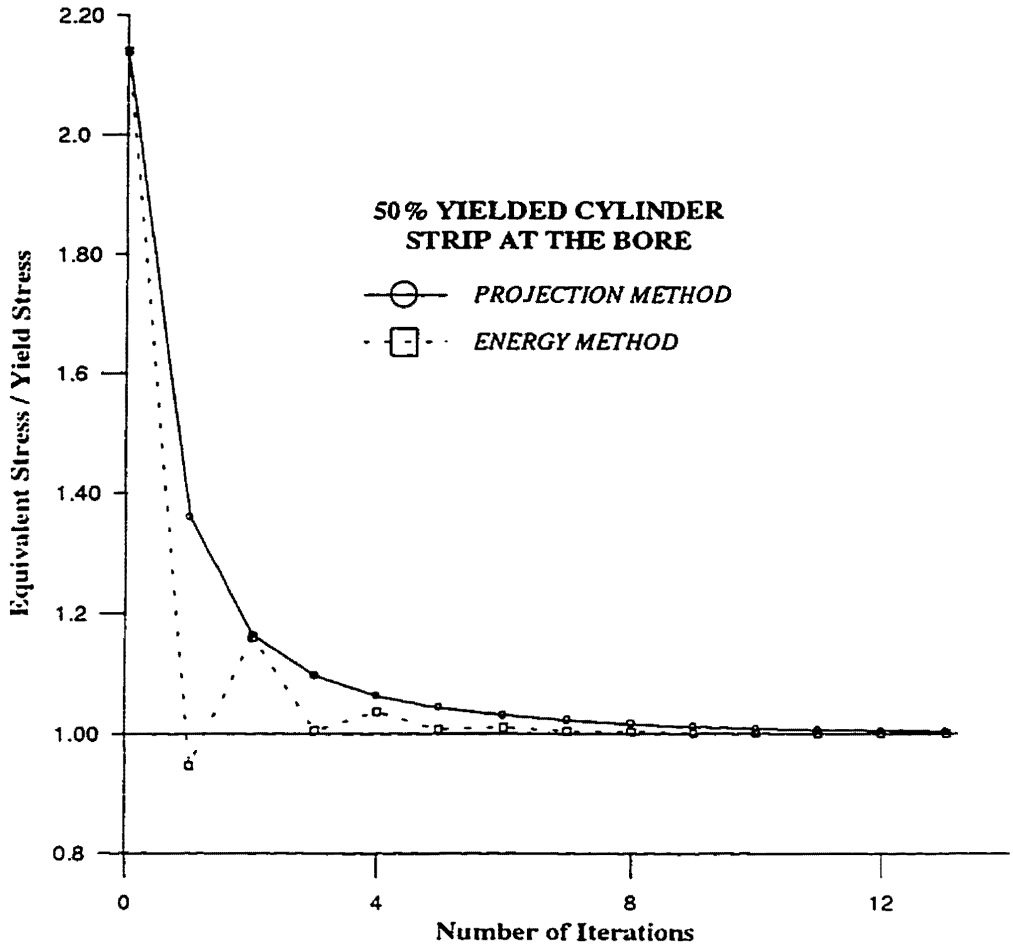


Figure 3.10: Convergence behavior at the bore

monotonic) convergence than the energy method. As shown in tables 3.1 and 3.2, the rate of convergence is 35% faster when the energy method is used.

3.3.2 Number of strips

A convergence study on the number of strips has shown that around 30 strips are enough for a reliable solution, based on studies for different loadings, cylinder sizes and plastic zone sizes.

Increasing the number of strips beyond 30 will not alter the results. Except for the displacements, all calculations are done at the mid radius of each strip. The radial displacements at the inside and outside radii of each strip are calculated assuming

constant moduli values across the strip. This is the value obtained at the mid radius of each strip.

For this study a nonhardening cylinder with an outside-to-inside diameter ratio of 4 was used. The cylinder was internally loaded such that half of the wall thickness yielded. It was assumed that the cylinder is in plane strain state.

Figures 3.11-3.16, show the results for this study. Figure 3.11- 3.13 show the results for the hoop, radial and axial stress based on 30, 90 and 270 strips. Figures 3.14 and. 3.15 compare the strain results while Fig. 3.16 shows the results for radial displacements. It should be noted that the displacements calculated based on 30, 90 and 270 strips are in close agreement, even though they are calculated at the inside and outside radius of each strip, and not at the mid radius where the moduli are calculated. This comparison shows that 30 strips is sufficient and that an increase beyond this does not alter the solution.

However, in this research, 99 strips were used in general to provide a more detailed solution (i.e., more data points), especially near the bore, where the residual stresses are of interest.

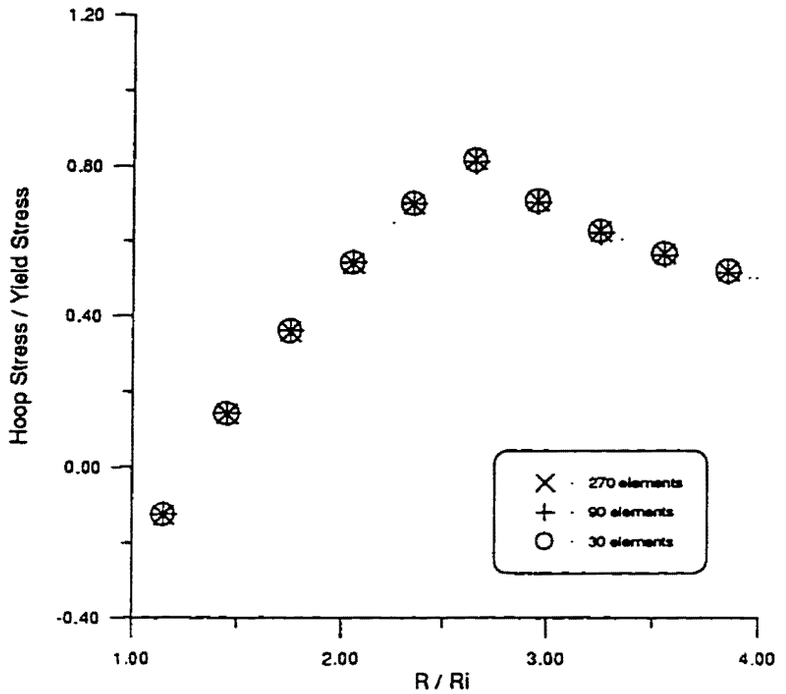


Figure 3.11: Effect of number of elements (hoop stress)

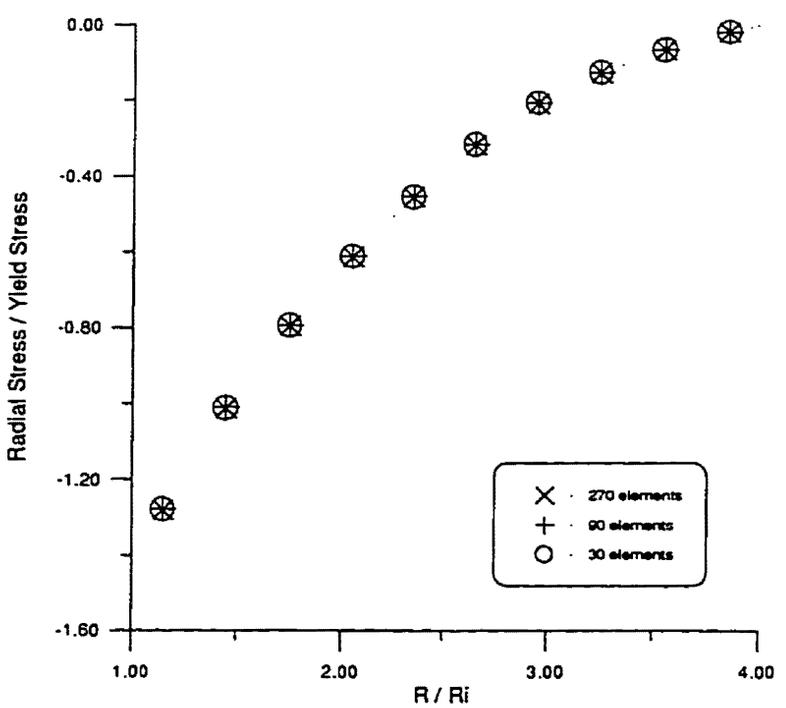


Figure 3.12: Effect of number of elements (radial stress)

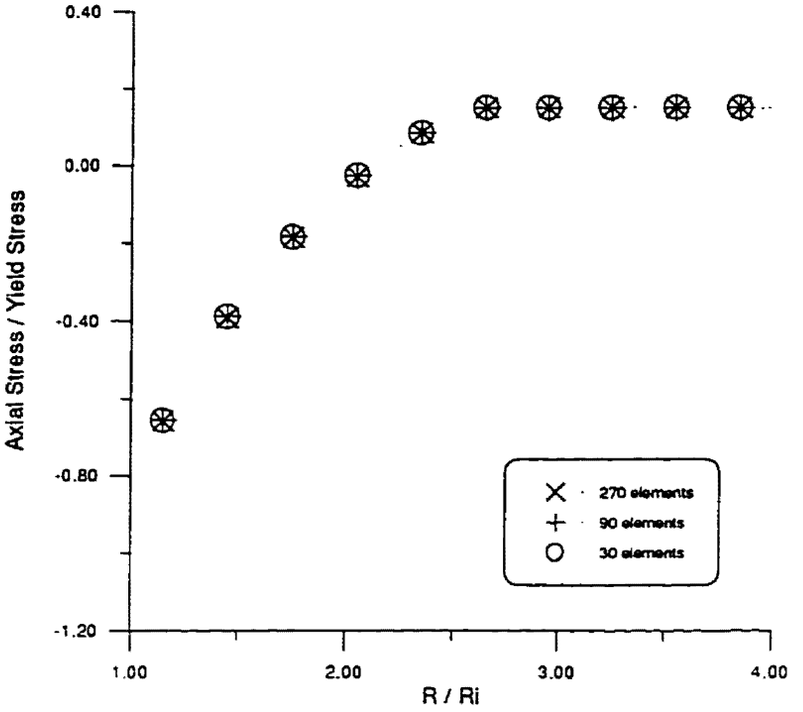


Figure 3.13: Effect of number of elements (axial stress)

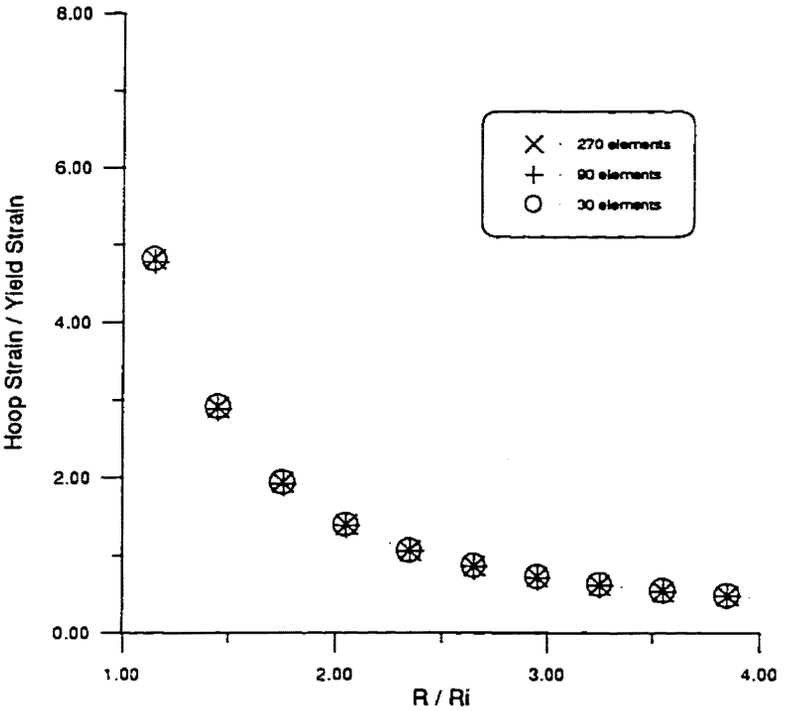


Figure 3.14: Effect of number of elements (hoop strain)

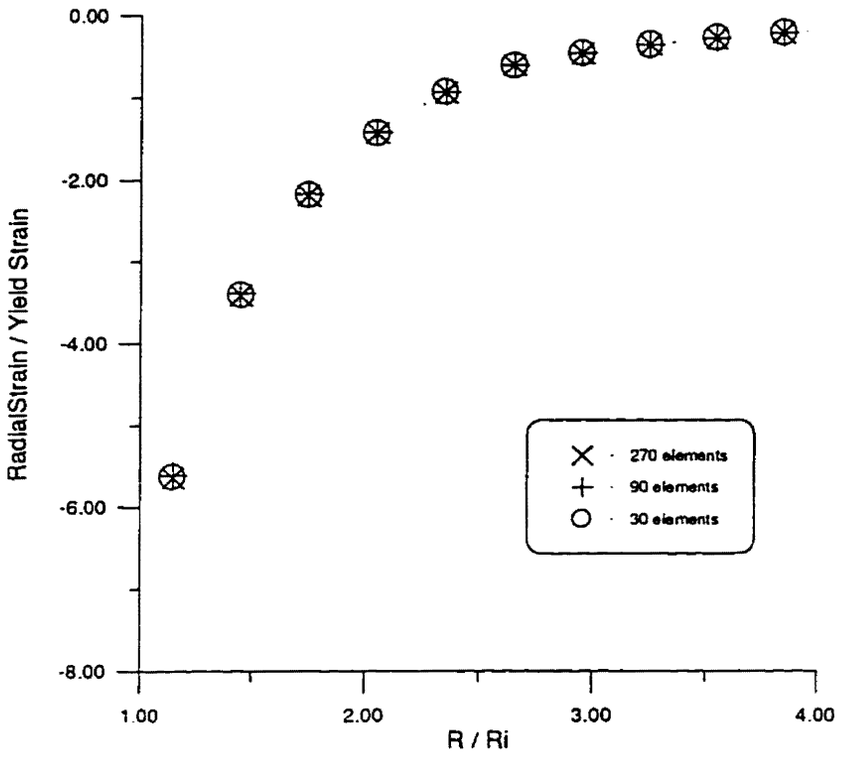


Figure 3.15: Effect of number of elements (radial strain)

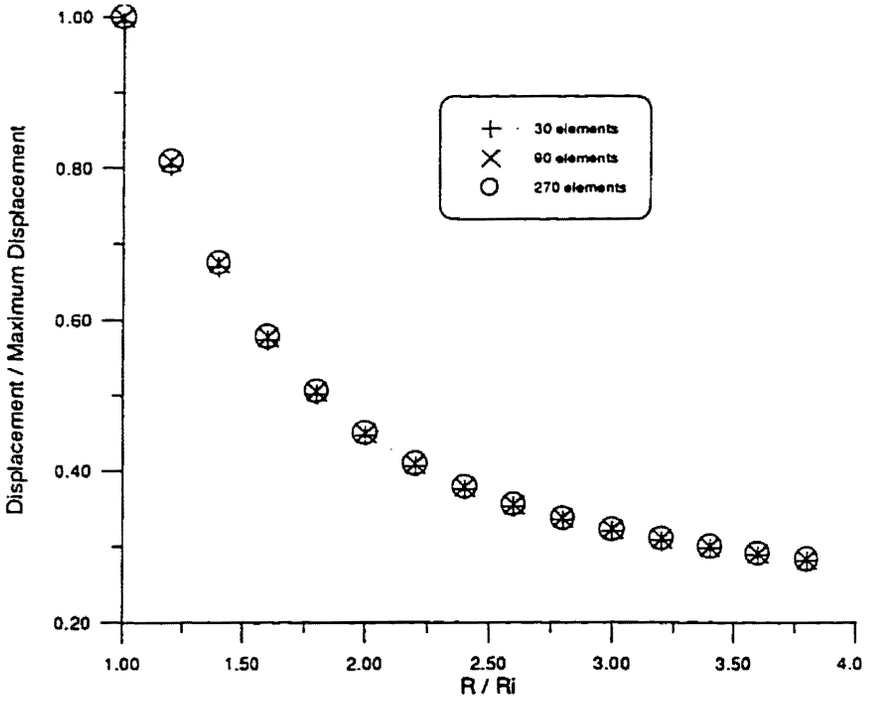


Figure 3.16: Effect of number of elements (displacement)

4. APPLICATIONS

The variable material property approach proposed in chapter 3 is used herein for the analysis of thick-walled cylinders and fastener holes. Both loading and unloading are considered. Results obtained from the present method are compared to other analytical solutions (where applicable), finite element solutions and/or experimental solutions (where applicable).

The plastic loading of hardening and nonhardeninig thick tubes is considered first. Autofrettage is discussed next, followed by loading and residual stress calculation for fastener holes. Multiaxial loading of thick-walled cylinders is considered at the end of this chapter.

4.1 LOADING OF THICK-WALLED CYLINDERS

Pressurized tubes have a very wide range of applications. Their elastic-plastic behavior is of interest to achieve optimum design in, for instance, pressure vessels, nuclear reactors, rocket boosters and containment shells for nuclear generating facilities. The inelastic behavior of thick-walled cylinders, therefore, is of considerable technological importance.

4.1.1 Literature Review

Due to the wide range of applications and technological importance, elastic-plastic deformation of thick-walled tubes has been treated at great length. Literature includes experimental investigations (Roach and Priddy, 1994); finite difference (Chen, 1980), finite element (Chen, 1972), boundary element (Yong and Naijie 1991) solutions and analytical solutions.

There have been several analytical solutions obtained in closed form or with numerical implementations. These solutions differ in their assumptions of the type of material response, yield criterion, plasticity theory, compressibility of the material, manner of loading, end conditions and the completeness of the solution. Table 4.1 summarizes and compares several methods for elastic-plastic analysis of thick-walled cylinders.

4.1.1.1 Elastic-perfectly plastic Tresca cylinder

The problem of a nonhardening thick-walled cylinder obeying Tresca's yield criterion under internal pressure is statically determinate. It has an exact stress field solution (Prager and Hodge, 1951), which is reviewed here.

Let the thick-walled cylinder shown in Fig. 3.6 be made of elastic-perfectly plastic material obeying Tresca's yield criterion. The equilibrium of an differential element on the wall is given by Eq. (3.18). The yield condition based on Eq. (2.15) is

$$\sigma_\theta - \sigma_r = \sigma_\bullet \tag{4.1}$$

This implies that σ_z has an intermediate value between σ_θ and σ_r. This is valid in the plastic range if the ratio of the outer to inner radius, r_o/r_i, is less than a certain value which depends on the value of Poisson's ratio (Koiter, 1953). For example, this value for $\nu=0.3$, is 5.75. By combining Eq. (3.18) and Eq. (4.1), the corresponding differential equation has the following general solution

$$\sigma_r = \sigma_\bullet \ln r + C \tag{4.2}$$

Method	Nadai	Cook	Sokolovsky	Hill, Lee and Tupper
Year	1931	1934	1946	1947
Yield Criterion	von Mises	Tresca	von Mises	Tresca
Plasticity model	Hencky	Hencky	Hencky	Prandtl-Reuss
Material Behavior	Linear hardening	Nonhardening	Linear hardening	Nonhardening
End conditions	Plane strain	Plane strain	Plane strain	Plane strain
Loading	Internal pressure	Internal pressure	Internal pressure	Internal pressure
Dilatation	No	No	Yes	Yes
Type of Solution	Closed form	Closed form	Numerical	Numerical
Capabilities	Stress strain	Stress strain	Stress strain	Stress strain

Table 4.1: Comparison of several theories for plastic analysis of thick cylinders

Method	MacGregor, Coffin and Fisher	Hodge and White	Hill, Lee and Tupper
Year	1948	1950	1951
Yield Criterion	von Mises	von Mises	Tresca
Plasticity model	Hencky	Hencky	Prandtl-Reuss
Material Behavior	Nonhardening	Nonhardening	Nonhardening
End conditions	Open ends	Plane strain	Closed ends
Loading	Internal pressure	Internal pressure	Internal pressure
Dilatation	Yes	Yes	Yes
Type of Solution	Numerical	Numerical	Numerical
Capabilities	Stress and strain	Stress and strain	Stress and strain

Table 4.1 (cont.): Comparison of several theories for plastic analysis of thick cylinders

Method	Allen and Sopwith	Steele	Koiter
Year	1951	1952	1953
Yield Criterion	Tresca	Tresca	Tresca
Plasticity model	Hencky	Hencky	Incremental
Material Behavior	Nonhardening	Linear hardening	Nonhardening
End conditions	Plane strain opened and closed end	Opened and closed ends	closed ends
Loading	Internal pressure and end load	Internal pressure	Internal pressure
Dilatation	Yes	No	Yes
Type of Solution	Closed form	Closed form	Closed form
Capabilities	Stress and strain	Stress and strain	Stress and strain

Table 4.1 (cont.): Comparison of several theories for plastic analysis of thick cylinders

Method	Bland	Smith and Sidebottom	Mendelson
Year	1956	1965	1968
Yield Criterion	Tresca	von Mises	von Mises or Tresca
Plasticity model	Incremental	Deformation theory	Incremental & Hencky
Material Behavior	Linear hardening	Linear hardening	Actual material loading curve
End conditions	closed ends	Plane strain opened and closed ends	Generalized plane strain with unloaded ends
Loading	Internal pressure and temperature	Internal pressure	Internal, pressure thermal
Dilatation	No	No	Yes
Type of Solution	Closed form	Closed form	Numerical
Capabilities	Stress, strain displacement and temperature	Stress and strain	Stress, strain and temperature

Table 4.1 (cont.): Comparison of several theories for plastic analysis of thick cylinders

Method	Shih-Chi Chu	Chen	Shih-Chi Chu and Vasilakis
Year	1972	1973	1973
Yield Criterion	von Mises	von Mises	von Mises
Plasticity model	Incremental	Incremental & Deformation	Incremental
Material Behavior	Linear hardening	Nonhardening	Linear hardening
End conditions	Plane strain opened and closed end	Plane stress	Plane strain opened and closed end
Loading	Internal, external pressure and end load	Internal pressure	Internal, external pressure nonproportional pressure-tension
Dilatation	Yes	Yes	Yes
Type of Solution	Numerical	Numerical	Numerical
Capabilities	Stress and strain	Stress, strain and displacement	Stress and strain

Table 4.1 (cont.): Comparison of several theories for plastic analysis of thick cylinders

Method	Sidebottom and Chu	Durban	Chen	Durban and Kubi
Year	1975	1979	1980	1992
Yield Criterion	von Mises	von Mises	von Mises	Tresca
Plasticity model	Deformation theory	Deformation theory	Incremental	Deformation theory
Material Behavior	Actual stress-strain curve	Romberg-Osgood with no elastic part	Nonhardening and hardening	Romberg-Osgood and nonhardening
End conditions	Plane strain closed end	Plane strain	Generalized plane strain	Plane strain
Loading	internal, external pressure, tension and torsion	Internal pressure	Internal, external, end force	Internal pressure
Dilatation	No	No	Yes	Yes
Type of Solution	Numerical	closed form	Numerical	closed form
Capabilities	Strain, finite deformation	Burst pressure	Stress, strain displacement	stress strain displacement

Table 4.1 (cont.): Comparison of several theories for plastic analysis of thick cylinders

Method	Chen	Loghman and Wahab	Present method
Year	1992	1994	1996
Yield Criterion	Tresca	von Mises	von Mises or Tresca or any other yield criterion
Plasticity model	Deformation theory	Incremental	Deformation theory
Material Behavior	Linear hardening	Hardening with temperature effect	Actual stress-strain curve or Ramberg-Osgood model
End conditions	Plane stress	Generalized plane strain	Plane stress or Plane strain
Loading	Internal pressure	Internal pressure	Internal, external pressure and torsion
Dilatation	Yes	No	Yes
Type of Solution	Numerical	Numerical	Numerical
Capabilities	Stress strain displacement	Stress strain	Stress, strain displacement nonproportional loading

Table 4.1 (cont.): Comparison of several theories for plastic analysis of thick cylinders

where C is an integration constant. For any value of internal pressure p_i less than the ultimate pressure and greater than the pressure for first yield, the cross section of the cylinder between the inner radius, r_i, and an intermediate radius, r_p, is fully plastic, whereas that between r_p and outer radius, r_o, is in the elastic domain. At the elastic-plastic boundary ($r=c$), the yield condition is just satisfied, and the corresponding radial stress can be computed:

$$\sigma_r\Big|_{r=c} = -\frac{\sigma_o}{2}\frac{r_o^2 - r_i^2}{r_o^2} \tag{4.3}$$

This equation along with Eq. (4.2) gives the integration constant

$$C = -\frac{\sigma_o}{2}\frac{r_o^2 - r_i^2}{r_o^2} - \sigma_o \ln r_p \tag{4.4}$$

If this constant is substituted into Eq. (4.2), then at $r=r_i$ where $\sigma_r=p_i$

$$\frac{p_i}{\sigma_o} = \ln\frac{r_p}{r_i} + \frac{1}{2}\left(1 - \frac{r_p^2}{r_o^2}\right) \tag{4.5}$$

which can be solved for the elastic-plastic boundary. The stress distribution in the plastic zone is of the following form:

$$\begin{aligned} \sigma_r &= \sigma_o \ln\frac{r_p}{r_i} + \frac{\sigma_o}{2}\left(1 - \frac{r_p^2}{r_o^2}\right) \\ \sigma_\theta &= \sigma_o + \sigma_r \end{aligned} \tag{4.6}$$

and the stress in the elastic zone can be obtained by Lame's solution (Eq. 3.21).

4.1.2 Elastic-plastic behavior of nonhardening materials

The nonhardening response of a thick-walled cylinder obtained using the proposed method of solution is considered here. Numerical results have been obtained for a cylinder with $r_o/r_i=5$, $\nu=0.3$, and $E/\sigma_o=1000$. The first example is a Tresca cylinder under internal pressure. The above cylinder is loaded such that half the wall becomes plastic. The stress field due to this internal pressure, obtained by using present method, is compared to the analytical solution given by Eq. (4.6). In Fig. 4.1 the two solutions match extremely well.

The stress field for a cylinder of the same dimensions and under the same pressure but obeying the von Mises yield criterion is shown in Fig. 4. 2.

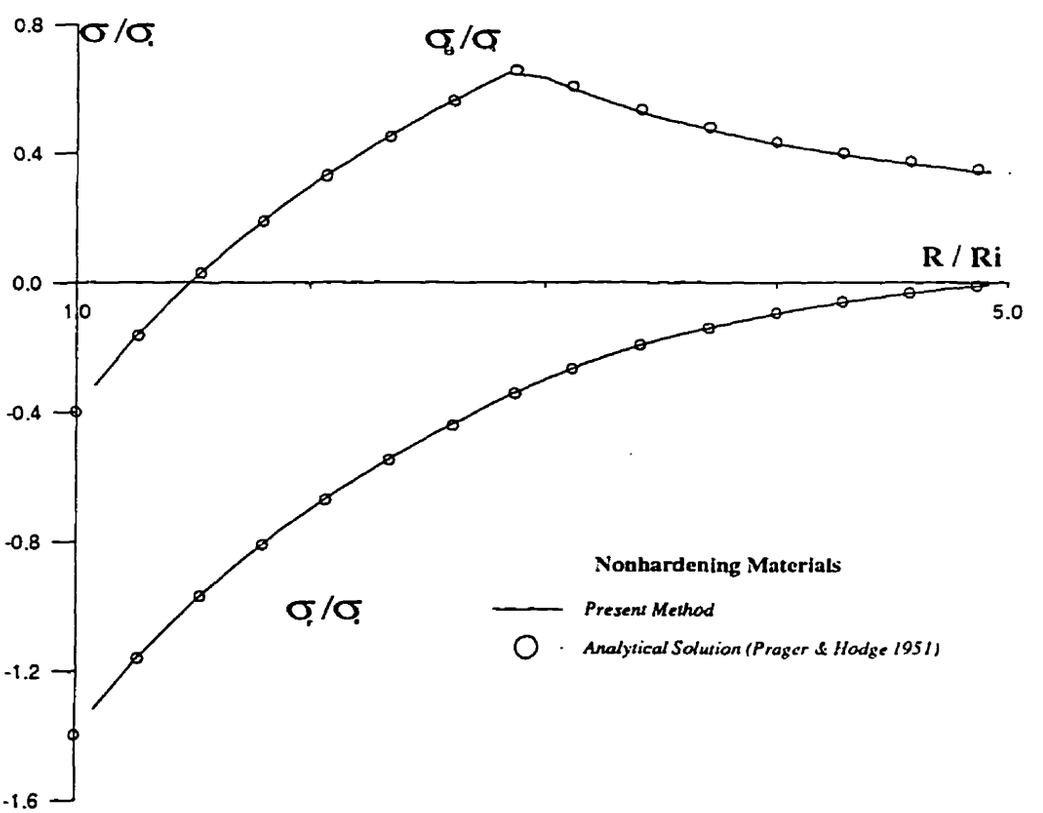


Figure 4.1: Comparison of present method and analytical solution

A finite element solution of the problem using ABAQUS (Hibbit, Karlsson & Sorensen, 1996), was obtained by the author for comparison purposes. The stress field obtained by the finite element solution is compared to the present method in Fig. 4.2. The two solutions are in excellent agreement.

The changes in the stress distribution for the above cylinder in a plane stress situation as the internal pressure increases has also been studied. These stress distributions are shown in Fig. 4.3. As has been noticed by MacGregor et al. (1948), and more recently by Bon and Haupt (1995), the circumferential stress changes from tension to compression even for partially yielded cylinders. Moreover, for a nonhardening material the cylinder reaches its limiting pressure very quickly. The corresponding strain field is shown in Fig. 4.4.

The behavior of an externally loaded thick cylinder was also studied. The geometry of the cylinder was the same and it was assumed to be in plane strain. The distribution of

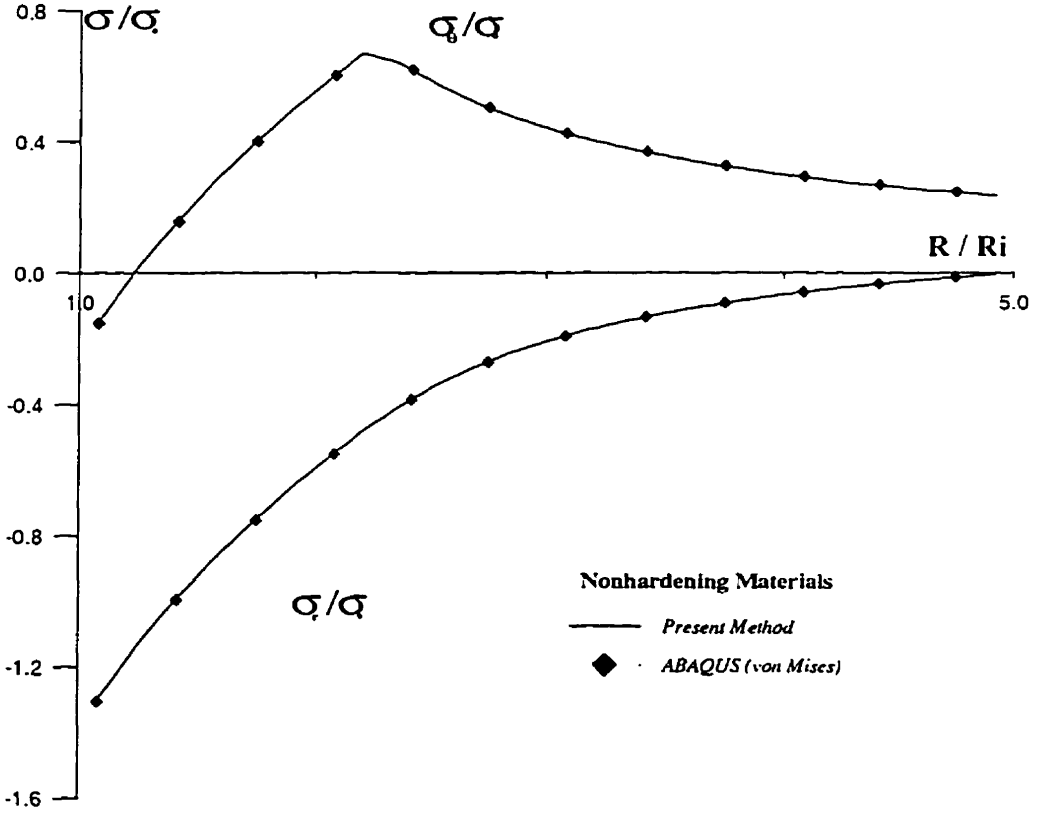


Figure 4.2: Comparison of present method and finite element solution

hoop and axial stresses for various load ratios are shown in Figs. 4.5 and 4.6. In this case, the maximum hoop stress, unlike for elastic behavior, is not at the bore. The maximum value is at the elastic-plastic boundary and is compressive. In this case, the ultimate pressure is lower than for an internally loaded cylinder. The axial stress, which is also compressive, increases from the bore toward the elastic-plastic boundary and remains constant in the elastic region.

4.1.3 Elastic-plastic behavior of hardening materials

The plastic response of a thick-walled cylinder obeying the Ramberg-Osgood equation was obtained using the proposed method of solution. Numerical results have been obtained for a cylinder with $r_o/r_i=5$, $\nu=0.3$, $E/\sigma_o=1000$, $\alpha=3/7$ and $m=5$. The first example is a von Mises cylinder under internal pressure and plane strain conditions. The above cylinder is loaded until it is partially plastic. Since there is no exact solution for this situation, ABAQUS has been used for comparison purposes. The finite element analysis was performed using the deformation plasticity option of ABAQUS. This option is based on total deformation plasticity and employs the Ramberg-Osgood formula. Fig. 4.7 shows the hoop, axial and radial stress distribution for this cylinder from the present analysis and as predicted by the finite element method. The agreement is excellent. The corresponding strain field for the same cylinder is compared in Fig. 4.8. The agreement between the two solutions is again excellent.

The change in hoop and radial stresses due to changes in the internal pressure was also studied. Results are shown in Fig. 4.9. Unlike nonhardening materials, the hoop stress remains tensile even for high values of pressure. Only close to the ultimate pressure does the hoop stress becomes compressive. Also, as expected, the ultimate pressure is much higher in this case as compared to the nonhardening case. The corresponding change in the strain field is shown in Fig. 4.10. Not only are the strain values in this case much lower than the corresponding nonhardening case, but also the changes in the strain field

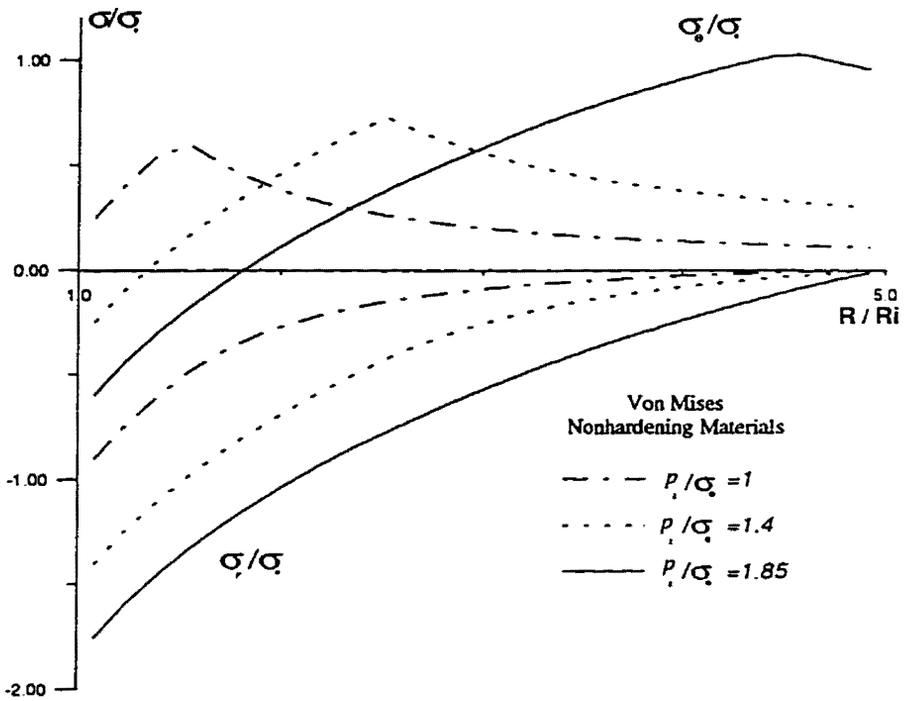


Figure 4.3: Stress variation in internally loaded cylinder

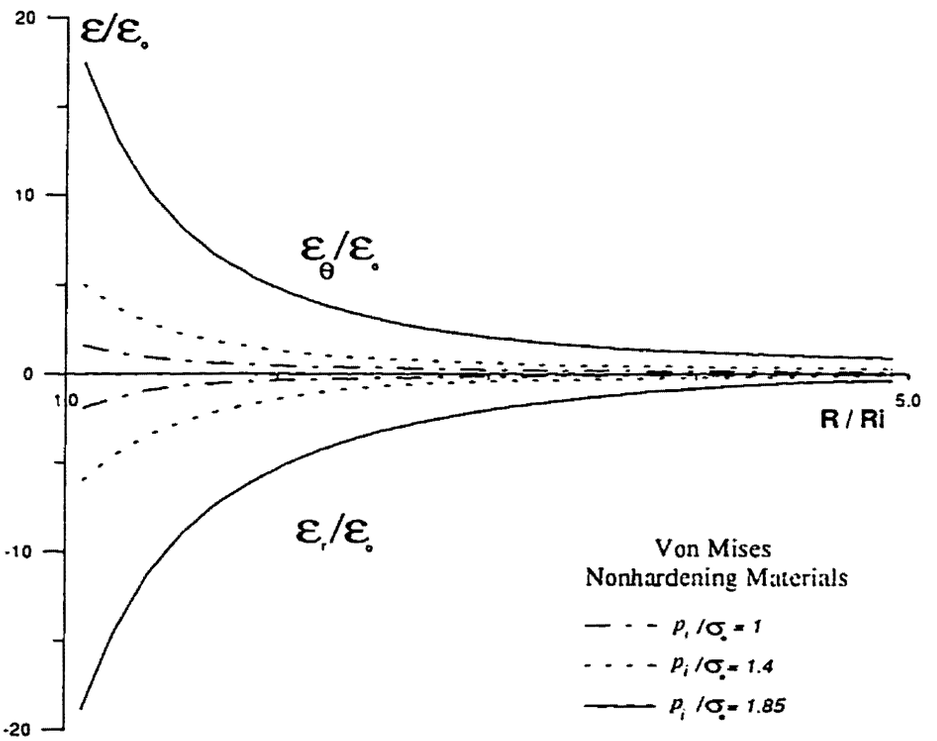


Figure 4.4: Strain variation in internally loaded cylinder

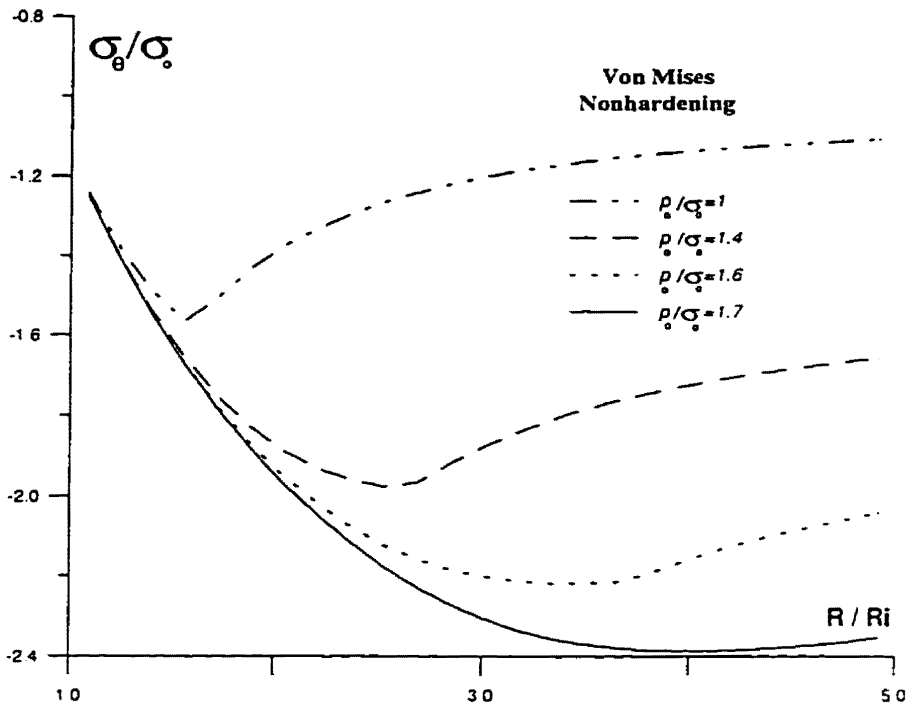


Figure 4.5: Hoop stress variation in externally loaded cylinder

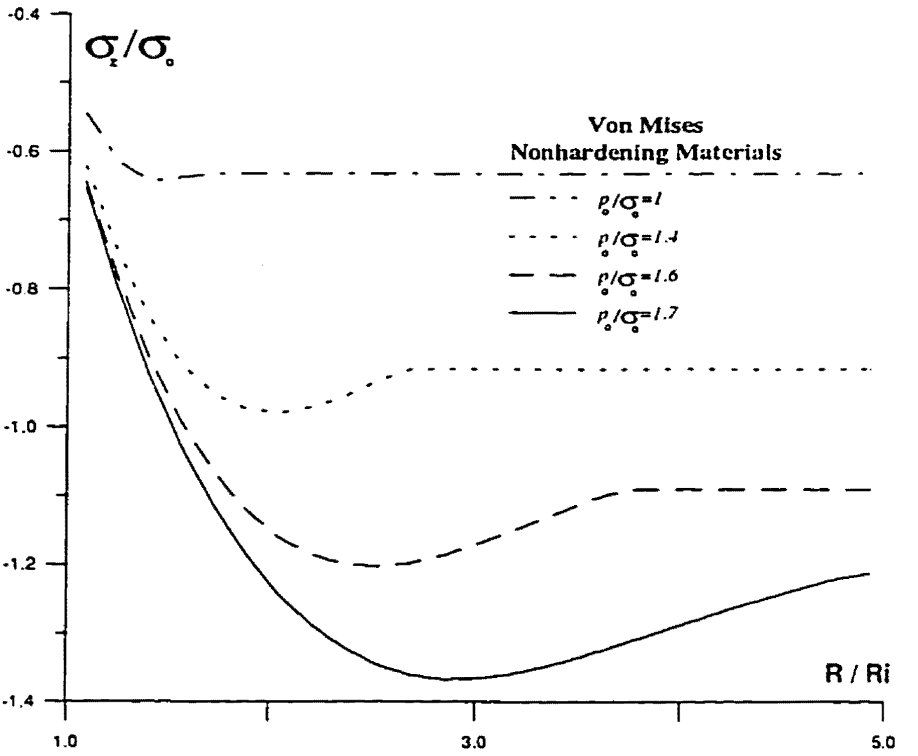


Figure 4.6: Axial stress variation in externally loaded cylinder

due to changes in the pressure is much more gradual. Note that the loading for both the nonhardening and hardening cylinders is the same (Fig. 4.4).

To study the effect of plane strain or plane stress assumptions on the stress field, the hoop stresses resulting from plane strain or plane stress analysis are compared in Fig. 4.11. The difference is not very appreciable. In the plane stress cylinder, the stresses tend to be higher in the plastic zone. However, in the elastic region, the stress calculated using plane strain is higher.

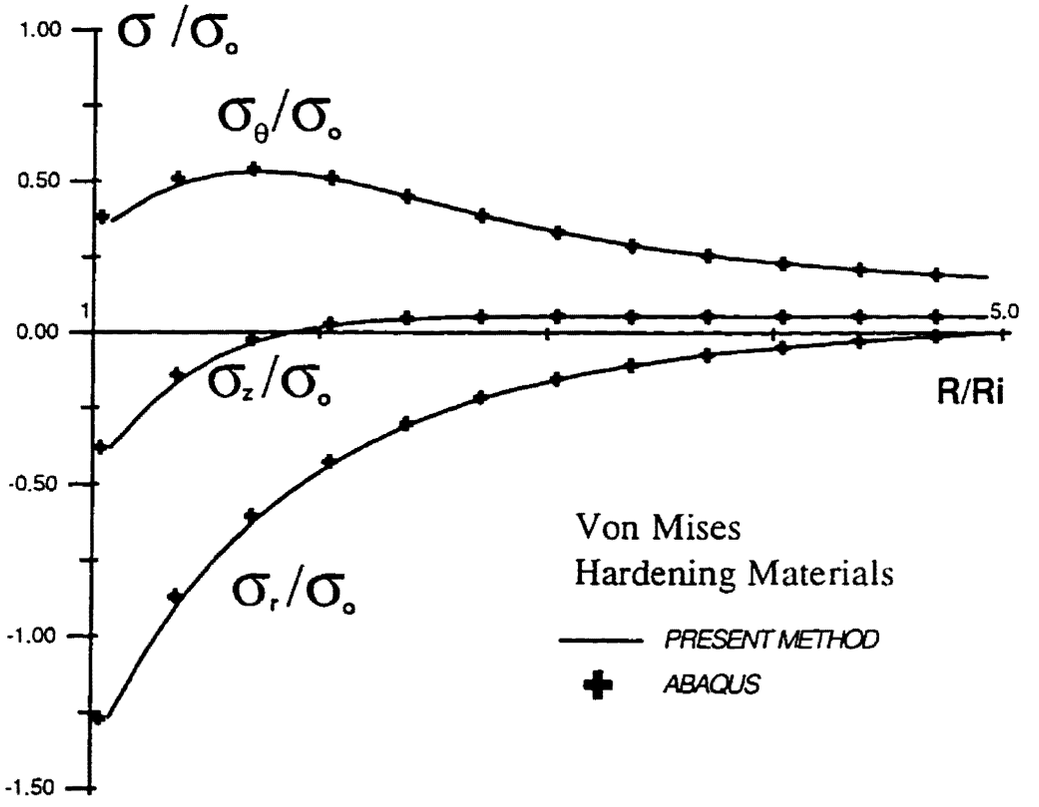


Figure 4.7: Comparison of present method and finite element solution (stress field)

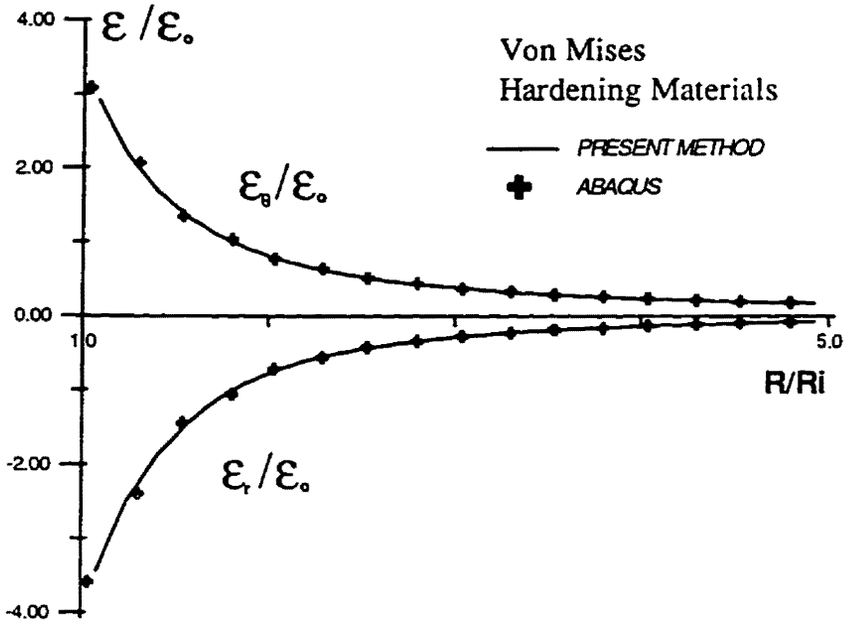


Figure 4.8: Comparison of present method and finite element solution (strain field)

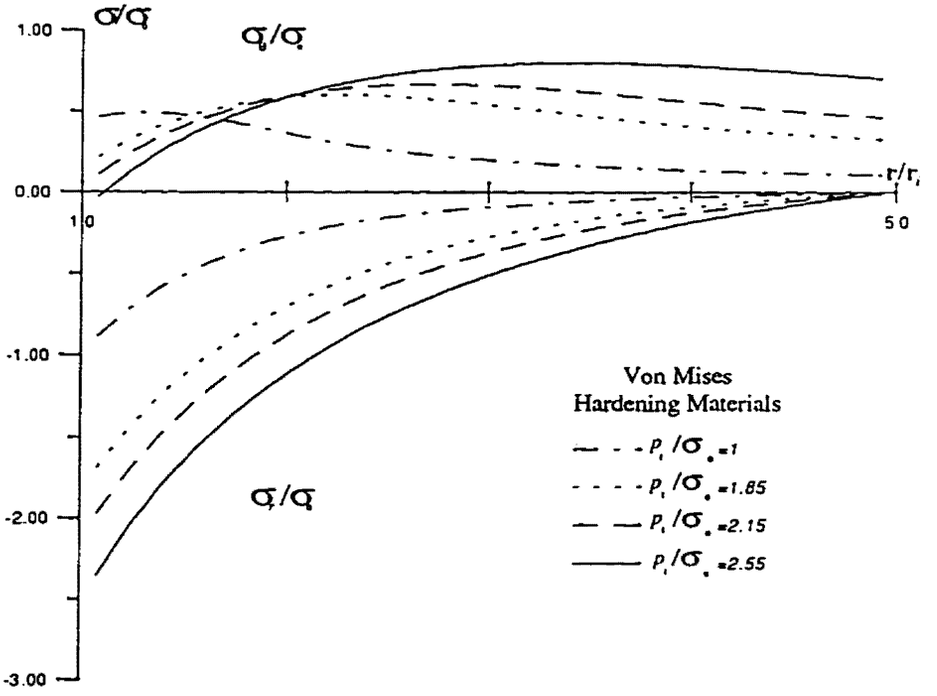


Figure 4.9: Stress variation in internally loaded cylinder

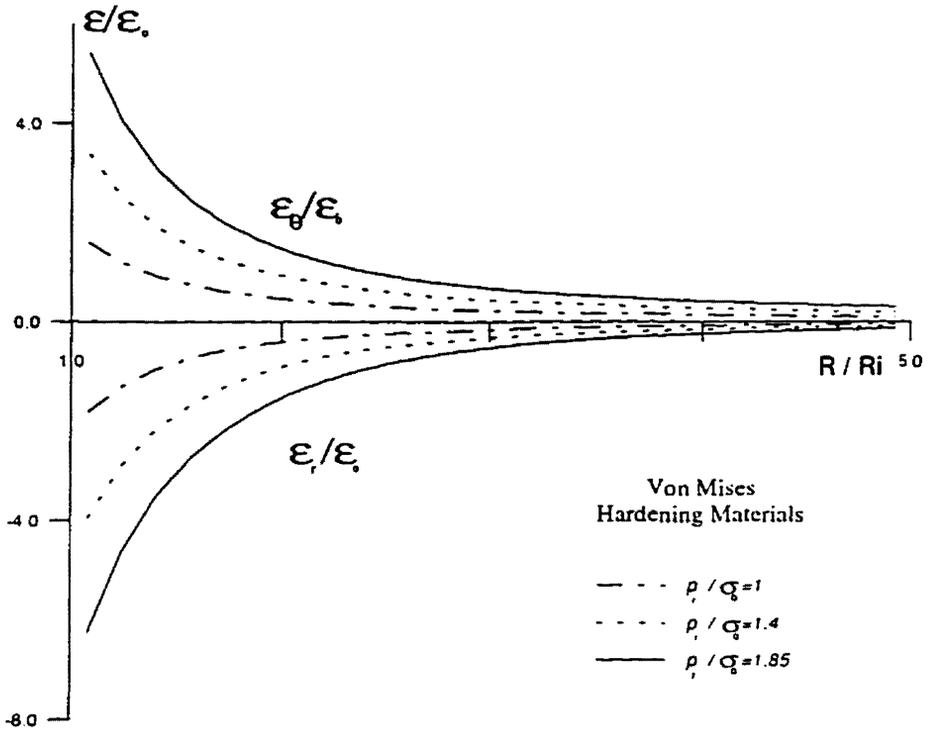


Figure 4.10: Strain variation in internally loaded cylinder

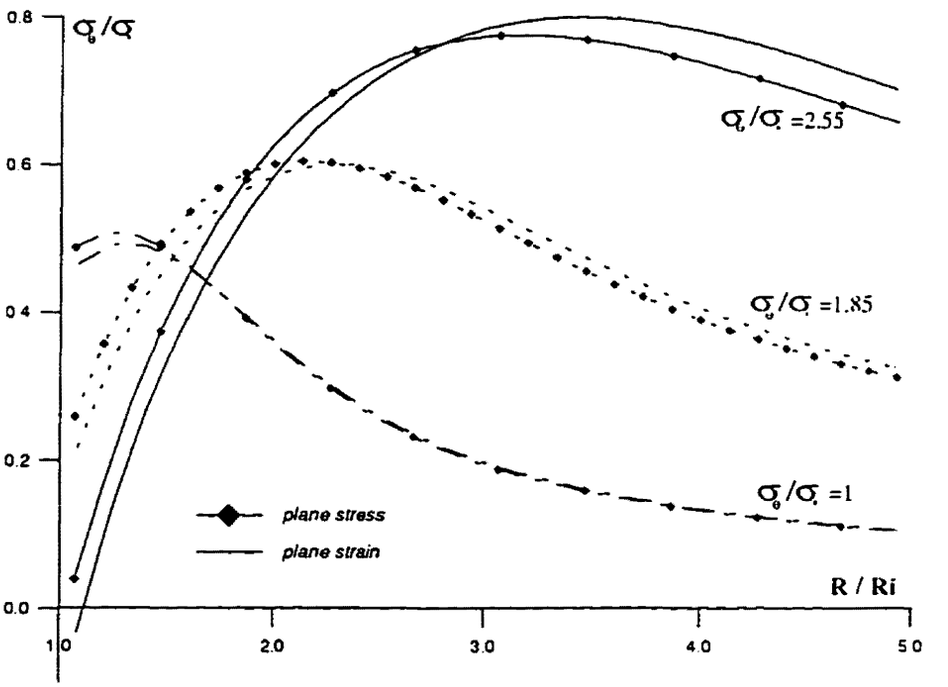


Figure 4.11: Comparison of plane strain and plane stress results

4.2 AUTOFRETTAGE

The concept of introducing compressive residual hoop stresses at the inner portion of a cylindrical pressure vessel as a means of increasing the maximum allowable pressure that the vessel can withstand originates in the gun barrel industry of the nineteenth century (Perl and Arone, 1994). Various techniques and processes to attain these favorable residual stresses were developed, e.g., casting hollow iron guns while cooling them from within, winding sheet iron around wrought iron gun tubes, or using hoops welded from coils and shrunk together. When it became apparent that a further increase in barrel strength could not be obtained using these techniques, designers turned to built-up guns which were composed of several concentric tubes shrunk onto each other, thus creating pre-stressing. At the turn of the century, a French artillery officer (Jacob, 1907) suggested an alternative process for pre-stressing monobloc gun barrels, now known as autofrettage, from the French word for "self-hooping". In this process, the cylinder is subjected to an internal pressure with an intensity sufficient to produce yielding through a part of or the entire cylinder wall. This process is carried out either by hydraulic pressurization or by pushing an oversized mandrel or swage through the forging. Once the required permanent deformation is reached, the pressure is released. While the outer layers tend to return to their original dimensions, the inner layers, having been considerably expanded due to plastic deformation, tend to maintain their enlarged diameter. Thus, a residual stress field is introduced in the cylinder's wall. This residual stress is compressive at inner layers and tensile at outer ones. The process of autofrettage has become common practice since about 1930. The application of autofrettage is not limited to the armament industry, but is widely used in industries utilizing very high pressure cylindrical vessels, such as chemical reactors and hydrostatic extrusion chambers.

Apart from increasing the pressure bearing capacity of the vessel, the residual stress induced by autofrettage enhances the vessel's fatigue life. The presence of compressive stresses at the bore reduces the probability of crack initiation and slows the growth of fatigue cracks (Parker and Farrow, 1981; Stacey and Webster, 1988). This enhancement

may result in an extension of fatigue life by a factor of up to three (Perl and Arone, 1988).

A reliable prediction of the influence of autofrettage on the critical crack length and fatigue life of a thick-walled pressurized cylinder requires an accurate prediction of the actual residual stress field prevailing in the cylinder wall. It is therefore essential to develop accurate and reliable methods to calculate the residual stress field induced by autofrettage.

The variable material property approach for axisymmetric problems is capable of accurately predicting mechanically induced residual stress fields. This method employs the actual loading and unloading stress-strain curve to give a close estimate of the actual residual stress field.

The application of this method to residual stress prediction in autofrettage is presented in this section. Three major capabilities of this method are: 1) employment of the actual unloading material curve, 2) employment of different hardening models, and 3) consideration of variability in the Bauschinger effect factor (BEF).

A review of different methods of calculating residual stress induced by autofrettage is discussed first. Results obtained by the present method are presented and compared with different experimental, finite element and analytical results later.

4.2.1 Literature Review

There have been many solutions proposed for the calculation of residual stress fields induced by autofrettage. Most of them consider only elastic unloading (Hill, 1950; Steel, 1952). However, there are a number of solution which take into account reversed yielding. These solutions differ due to their assumptions on loading behavior (hardening or nonhardening), unloading behavior (hardening or nonhardening), yield criterion (Mises or Tresca), hardening rules (kinematic or isotropic hardening), dilatation assumption, end conditions, and Bauschinger effect factor (constant or variable).

Manning (1945) provided a method of calculating residual stress fields which employs the actual loading and unloading curve. Adapting the assumption previously employed by Nadai (1931) and Nacrae (1930), that the shear strain is inversely proportional to the square of the cylinder radius, he was able to predict the residual stress field. Later, Franklin and Morrison (1960), using the same assumption, proposed and validated a method of residual stress calculation. Their method requires full knowledge of the shear stress-strain properties of the material in pure torsion. In their two-step method, the cylinder is first divided into an even number of equal (maximum of eight) layers and successive values of strain at the external boundary are assumed. By using the basic assumption that the total shear strain is inversely proportional to the square of the cylinder radius in the form

$$\gamma = \frac{(\varepsilon_\theta + \nu\varepsilon_z)_o}{(1-\nu)}\left(\frac{r_o}{r_i}\right)^2 \tag{4.7}$$

the shear strain in different layers is calculated. Based on this calculation and using the shear stress-strain curve, the corresponding stress value is read from the torsion curve. Clearly, the Tresca yield criterion is embedded in this procedure. Using equilibrium and Simpson's rule of integration, the internal pressure causing this strain and stress field is calculated. This method, which assumes plane strain, gave reasonable estimates to the residual hoop stress field when compared with experimental measurements of residual stress (Franklin and Morrison, 1960). However, the axial strain predicted from this method did not agree with experimental results, especially in the proximity of the bore. Ideally, the torsion data needed in this method should be obtained from a cylinder with an identical shear stress gradient.

Kendall (1970 and 1986) proposed a correction factor to the elastic unloading results to compensate for the Bauschinger effect during unloading. This correction factor was based on extensive experimental study conducted by Kendall (1970) to determine the pressure at which the material of a previously autofrettaged cylinder first undergoes

additional plastic deformation. In his method, Kandell (1986) assumed that for the points inside the plastic zone of the cylinder, the difference between the tangential and radial residual stresses was a linear function of the radius between the inside radius and the radius at a point, r_z, at which this stress difference is zero. Using the Tresca yield criterion and a method similar to linear elastic unloading, he introduced equations for the calculation of hoop and radial stresses within the plastic zone. The linear elastic unloading method was used to estimate the residual hoop and radial stresses in the elastic zone of the cylinder. However, to ensure continuity of stresses at r_z, the linear unloading stresses were multiplied by a correction factor. This factor was determined by calculating the radial stress at r_z, by using the equation introduced for the plastic zone, and dividing the radial stress by the corresponding stress calculated for assuming a linear elastic unloading. Comparing his predictions with the published experimental results, he concluded that there was general agreement between his predictions and experimental results but that there were significant differences in the value of the residual hoop stress at the bore. This method lacked a procedure to calculate the axial stress.

Chen (1986), proposed a different method which incorporated both the Bauschinger effect and the hardening effect due to unloading. Based on experimental observations of high strength steel behavior, the Bauschinger effect factor is very important in determining the range of elastic unloading. After reversed yielding occurs, a very large degree of strain hardening will develop, even when the initial tensile test exhibits very little strain hardening. Chen argued that any discrepancy between the different solutions and the experimental results was due to two factors: 1) the Bauschinger effect factor dependency on the value of reversed yielding, and 2) the linear hardening response during elastic-plastic unloading. He then proposed a bilinear stress-strain unloading curve to model the behavior of the high strength steel usually used in autofrettage. Chen's solution is a two step closed form solution. The first step involves loading of the cylinder. During loading the material is assumed to be elastic-perfectly plastic, obeying Tresca's yield criterion and associated flow theory. Chen employed Koitter's (1953) closed form solution for loading. In the second step, if the pressure is not sufficient to cause reversed yielding, the unloading is purely elastic. However, if the pressure is high

enough to cause reversed yielding, by introducing a BEF factor and a hardening factor, elastic-plastic unloading is analyzed. Bland's (1956) closed form solution for linear hardening material's obeying Tresca's yield criterion was used. This method is capable of using a better model of the unloading curve, once the BEF and the hardening parameter are selected. For such a selection the actual unloading curve is needed. Also, this method is restricted to the elastic-perfectly plastic behavior and the Tresca's yield criterion.

The three methods discussed above are the methods that are used most. A comparison of the different methods for residual stress field calculation is given in Table 4.2. This comparison is limited to those methods that consider reversed yielding. Methods with elastic unloading are not discussed here.

4.2.2 Actual Stress-Strain Unloading Curve

The material chosen for the numerical simulation was a high strength steel (AISI 4333 M4). The actual material behavior is shown in Fig. 4.12 . This figure is a reproduction of the experimentally obtained stress-strain curve for AISI 4333 steel recorded by Stacey and Webster (1988, Fig. 2). For comparison, some of the material models used in the residual stress calculations are also shown in the same figure. In this analysis, it was assumed that the unloading curve was independent of the level of over-strain.

In accordance with the specimen used in experiments performed by Stacey et al. (1985), a tube with a nominal bore diameter of 30 mm and outside diameter of 62 mm was considered. It was assumed that the tube is in a plane stress situation and has been internally pressurized to 662 MPa and subsequently fully unloaded.

Since the stress distribution in the autofrettaged tubing is a result of a combination of the initial manufacturing (known as as-received residual stress) and the autofrettage process, Stacey et al. (1985) measured the as-received residual stress distribution of the tube used in their experiment. This stress distribution is shown in Fig. 4.13 .

Methods/Year	Manning (1945)	Franklin & Morrison (1960)	Kendall (1970, 1986)
Yield Criterion	Tresca	Tresca	Tresca
Model	Total Deformation	Total Deformation	Total Deformation
Basic Assumption	$\gamma \propto \frac{1}{r^2}$	$\gamma \propto \frac{1}{r^2}$	$\tau_{max} \propto \frac{1}{r\|_{\tau_{max}=0} - r_i}$
Loading Behavior	Actual Curve	Actual Behavior in Torsion	Elastic- Perfectly plastic
Unloading Behavior	Actual Curve	Actual Behavior in Torsion	Elastic with correction factor
End Conditions	Plane Strain	Plane Strain	-
Compressibility	Yes	Yes	-
BEF	Yes	Yes	As a Correction
Variable BEF	No	No	No
Generality	Residual Hoop & Radial Stresses	Residual Hoop, Axial & Radial Stresses	Residual Hoop & Radial stresses
Solution	Numerical	Numerical	Analytical

Table 4.2: Comparison of several autofrettage theories

Methods/Year	Chen (1986)	Rees (1990)
Yield Criterion	Tresca	Tresca & von Mises
Model	Total Deformation	Incremental Plasticity
Loading Behavior	Elastic- Perfectly plastic	Elastic- Perfectly Plastic
Unloading Behavior	Elastic- Linear Hardening	Kinematic & Isotropic Models
End Conditions	Plane Strain & stress	Open end with nonzero axial strain
Compressibility	Yes	Yes
BEF	Yes	No
Variable BEF	No	No
Generality	Residual Hoop, axial & Radial Stresses and Displacement	Residual Hoop, Axial & Radial Stresses and Strains
Solution	Closed Form(Two Step)	Numerical

Table 4.2(cont.): Comparison of several autofrettage theories

Methods/Year	Meghahed & Abbas (1991)	Present Method
Yield Criterion	Tresca	Tresca & von Mises or any Yield Criterion
Model	Total Deformation	Total Deformation
Loading Behavior	Power Law Hardening	Actual curve, Nonhardening, Linear hardening and the Ramberg-Osgood model
Unloading Behavior	Power Law Hardening and Kinematic & Isotropic Models	Actual curve, Kinematic & Isotropic Models
End Conditions	Plane Strain	Plane Strain & Stress
Compressibility	Yes	Yes
BEF	Yes	Yes
Variable BEF	Yes (BEF dependency is defined by an exponential equation)	Yes (Actual BEF dependency on over strain / any representation of BEF dependency)
Generality	Residual Hoop, & Radial Stresses and Displacement	Residual Hoop, Axial & Radial Stresses and Strains, and Displacement
Solution	Analytical (Two Step)	Numerical

Table 4.2(cont.): Comparison of several autofrettage theories

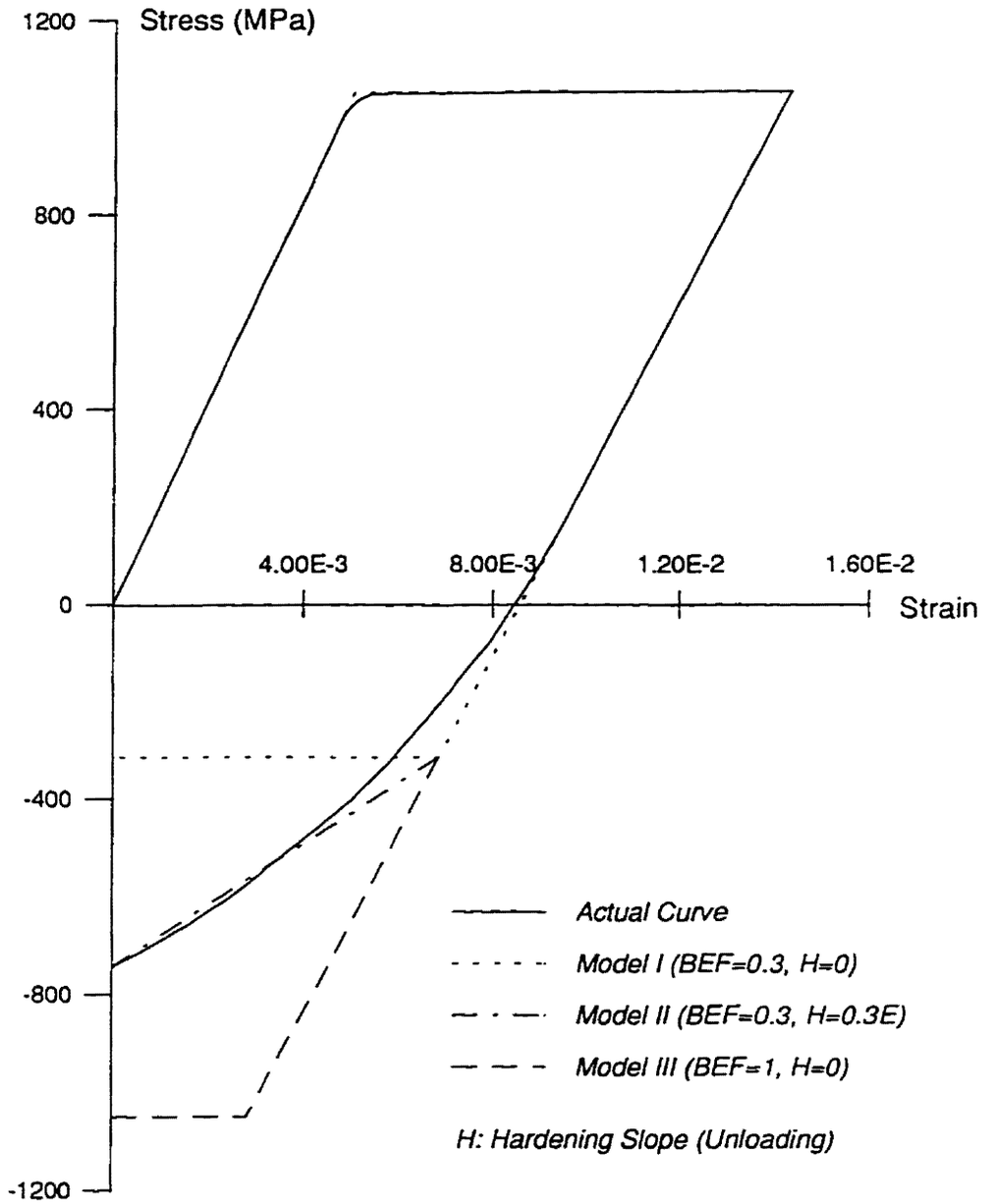


Figure 4.12: AISI 4333 M4 Material curve
(Fig. 2, Stacey & Webster, 1988)

The present analysis of the same tube was carried out assuming that the cylinder was pre-stressed prior to application of the autofrettage pressure. Hence, the results obtained include the as-received stress field. When the von Mises yield criterion was used, more than 1/3 of the wall thickness was found to be plastic at the end of loading. Also, there were no indication of reversed yielding upon unloading. Figure 4.14 compares the

present results with experimental measurements of Stacey et al. (1985) who used neutron diffraction method to determine residual stresses for autofrettage samples of 5 mm and 10 mm thickness. There is very good agreement between the present results and their measurements, especially near the bore. This good agreement signifies the importance of employing the actual unloading behavior of material in residual stress calculations.

The residual stress fields calculated using the different material models shown in Fig. 4.12 are shown in Fig. 4.15. The results shown in this figure were all obtained using the present method, which is capable of employing any unloading model. Stacey and Webster (1988), following the method proposed by Chen (1986), suggested a Bauschinger factor of *0.3* and a linear hardening factor equal to *0.3E* for an accurate model of the unloading behavior.

Since the actual loading-unloading behavior was employed, the choice of yield criterion had the main influence over the results. Results using different yield conditions were obtained and are compared with the experimental results in Fig. 4.16.

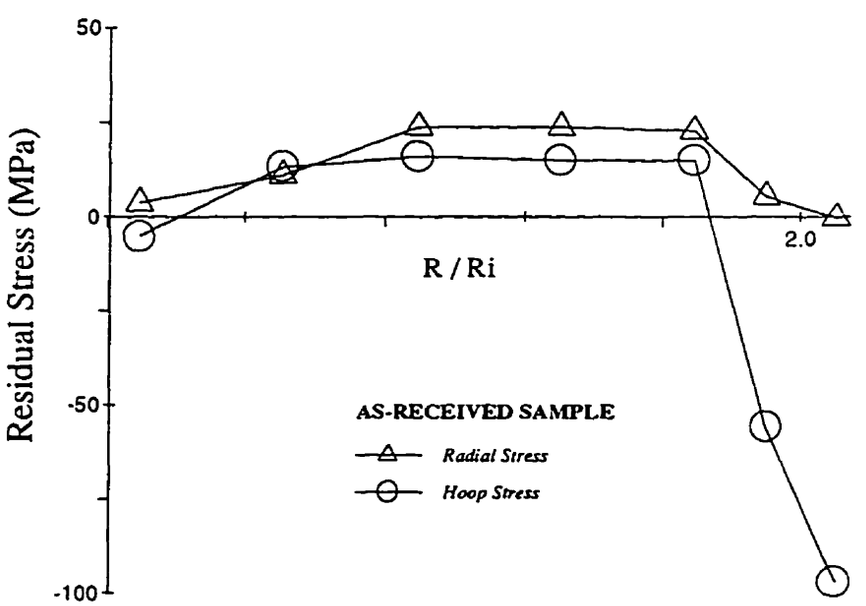


Figure 4.13: Residual stress field induced by manufacturing

(Fig. 7, Stacey et al., 1985)

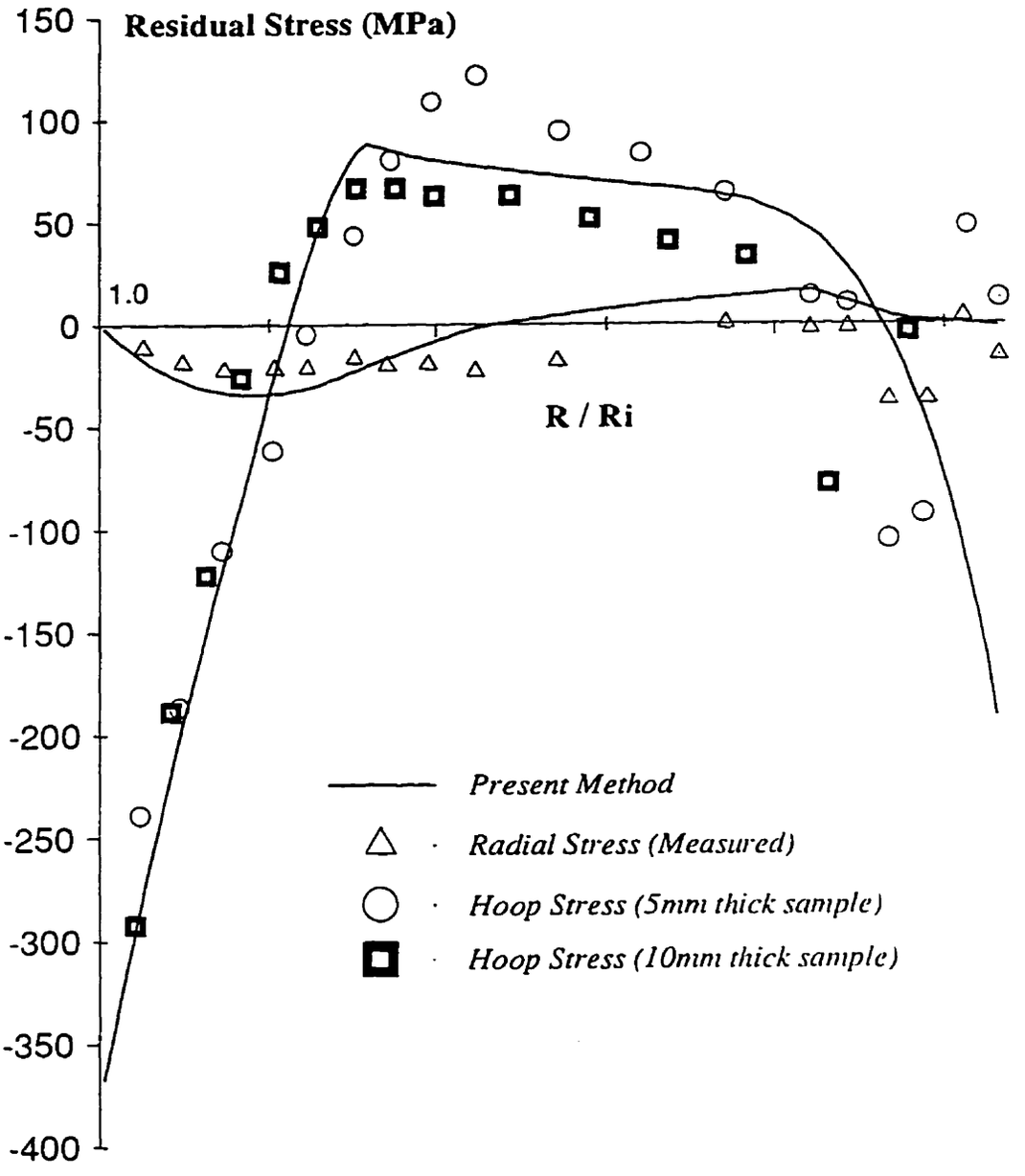


Figure 4.14: Residual stress comparison

(Experimental data from Stacey et al., 1985)

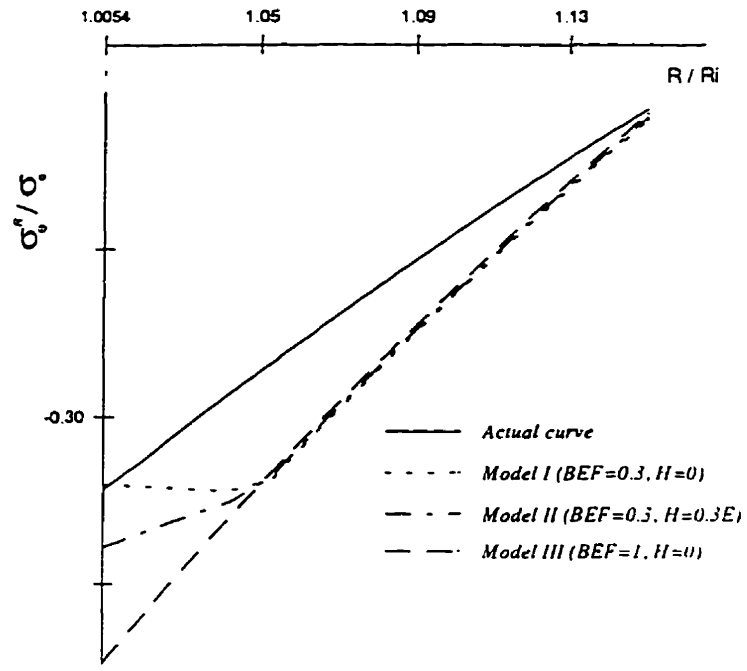


Figure 4.15: Comparison of different material models

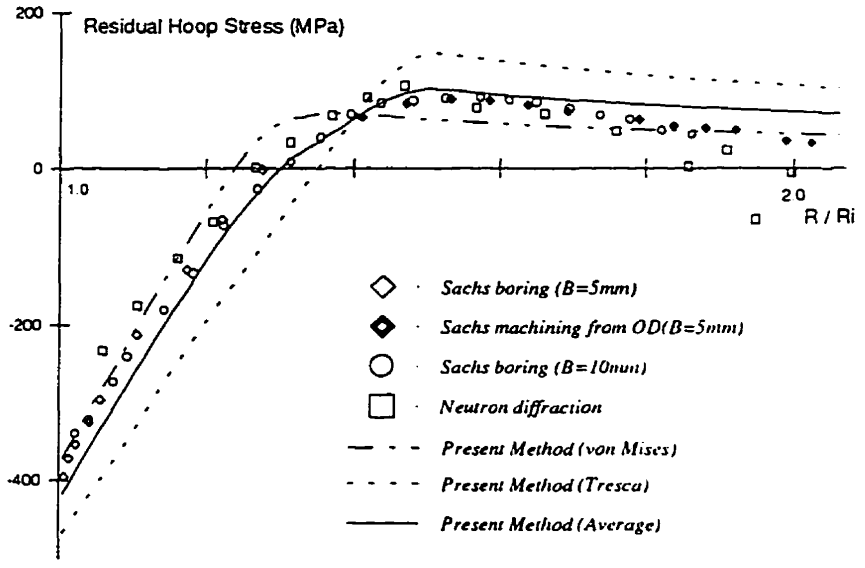


Figure 4.16: Comparison of different yield criteria
(Experimental data from Stacey & Webster, 1988)

The Tresca criterion, the von criterion Mises and an average value of hoop stress as predicted by the two criteria were used in the analysis. Results are compared with experimental results obtained from neutron diffraction, the Sach boring out technique and the Sach machining from outside technique, provided by Stacey and Webster (1988). The measured values are due to autofrettage only. That is, the as-received residual field has been subtracted from the measured value to show the effect of autofrettage (Stacey and Webster, 1988). The solution based on the Tresca yield criterion clearly over-predicts the experimental results, while that based on the von Mises criterion shows the best prediction near the bore. The average of the two criteria's best predicts the intermediate transition between the plastic and elastic zones. In general, it seems that the experimental results obtained using the different techniques lie between the prediction based on the von Mises and the average of prediction based on the von Mises and the Tresca criteria.

4.2.3 Isotropic and Kinematic Hardening Models

Hunsaker et al. (1976), in an extensive study of hardening rules in plasticity, concluded that isotropic (IH) and kinematic (KH) hardening rules represent the limit of actual reversed yielding behavior and other models usually fall within this limit. Here, both models were used to predict the residual stress field.

Chen and O'Hara (1984) presented a comprehensive study of the two models by using ADINA finite element software. To compare the present analysis with their finite element results, the same cylinder dimensions and loading were considered. In the present study, a closed ended cylinder with a outside-to-inside radii ratio of 4.63, internal radius of 0.865 inches (=2.2 cm), and external radius of 4.005 inches (=10.17 cm) was pressurized to 250 Ksi (=1720 MPa) in ten steps and then unloaded in five subsequent steps. Chen and O'Hara (1984) used a multilinear (6 point) representation of the stress-strain curve. These data points are tabulated in Table 4.3. The stress-strain curve and unloading curve is shown in Fig. 4.17. Based on the results obtained by the present method, at the end of loading, 43% of the cylinder had yielded. As expected, each model

predicted a different residual stress field. When the load was fully removed, 8.3% of the wall thickness near the bore experienced reversed yielding according to the kinematic hardening model, whereas for isotropic hardening the percentage decreased to 3.3%. The results are compared with the results obtained by Chen and O'Hara (1984) using ADINA finite element code in Fig. 4.18. In this figure, *a* and b are the inside and outside radii of the cylinder. The agreement is excellent. Figure 4.19 shows the residual radial and axial stresses. Again the agreement is very good. The differences between the residual axial stress from the present method and that of ADINA are due to compressibility assumptions. The present solution assumes the material to be compressible. The radial displacement at inner and outer radii from the two solutions are also compared in Fig. 4.20 and 4.21 for isotropic and kinematic hardening, respectively. The agreement is very good.

Stress : Ksi	MPa	Strain
155	1066	0.0060
167	1150	0.0085
172	1183	0.0125
177	1218	0.0300
181	1245	0.0500
181	1245	0.1500

Table 4.3: Uniaxial stress-strain data (Chen & O'Hara, 1984)

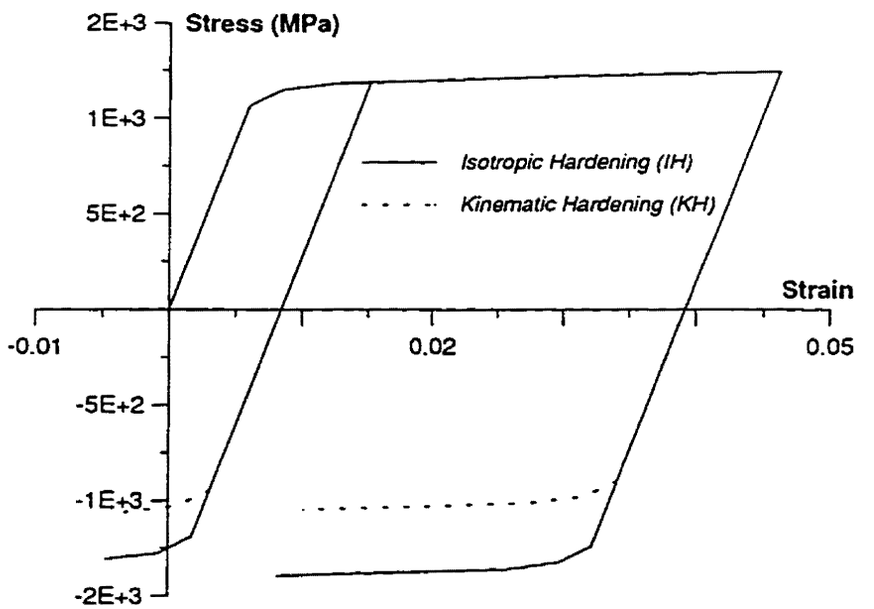


Figure 4.17: Stress-strain curve used in the analysis

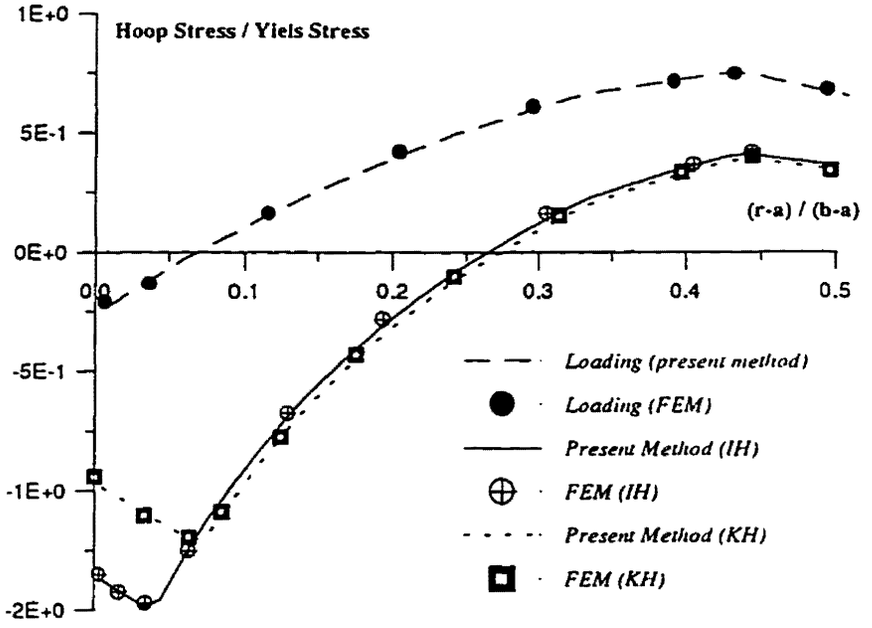


Figure 4.18: Residual hoop stress comparison
(FEM result from Chen & O'Hara, 1984)

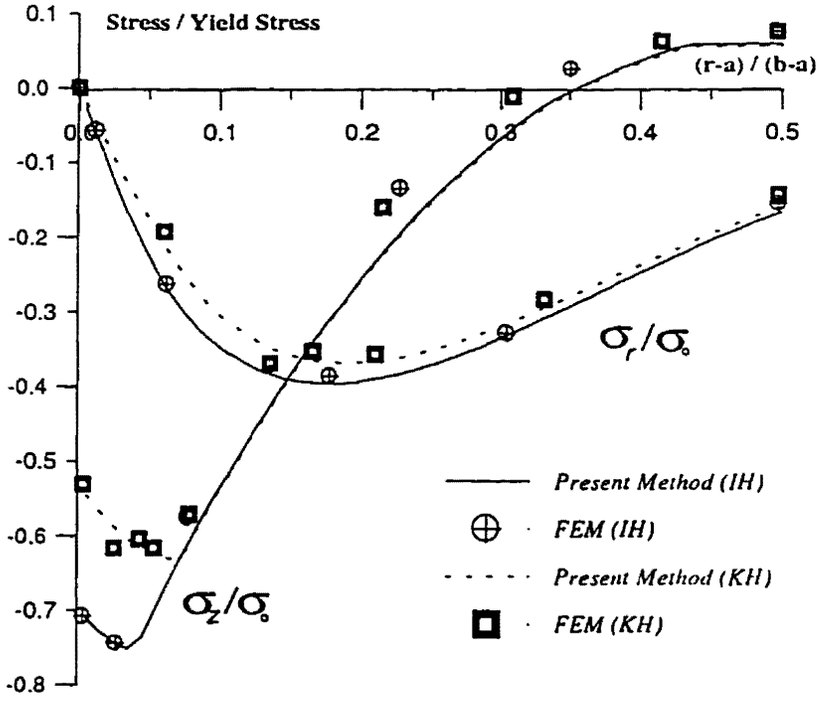


Figure 4.19: Residual radial and axial stresses comparison
(FEM result from Chen & O'Hara, 1984)

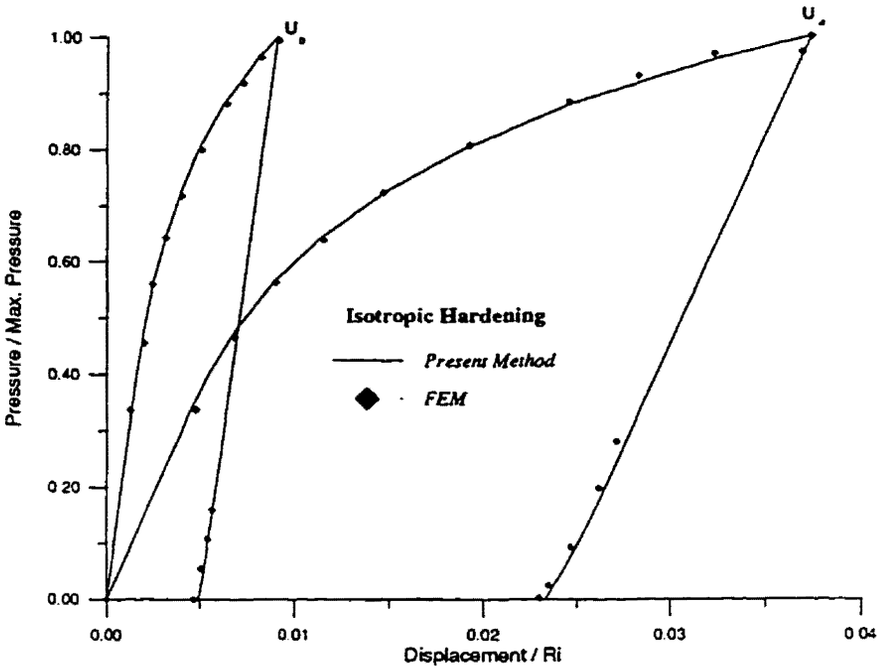


Figure 4.20: Comparison of the boundary displacements (IH)
(FEM results from Chen & O'Hara, 1984)

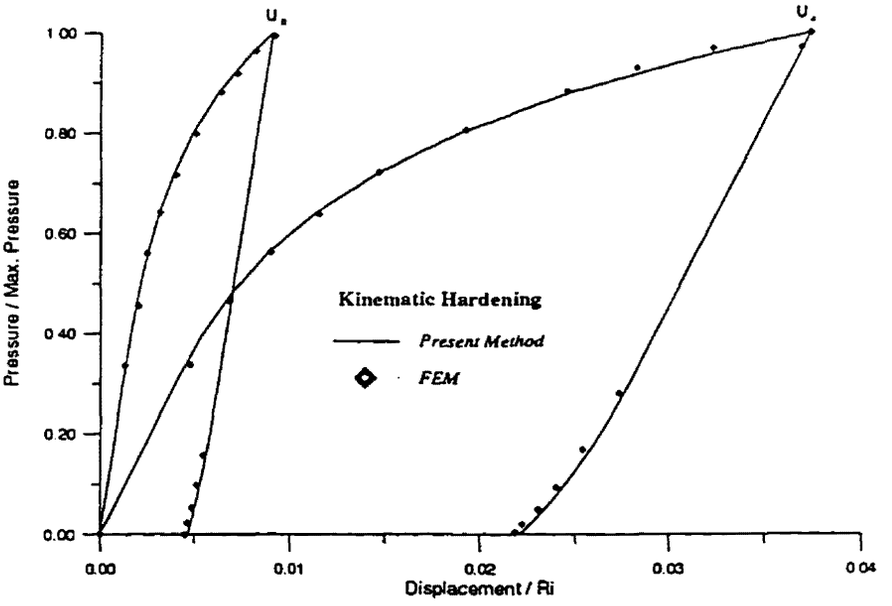


Figure 4.21: Comparison of the boundary displacements (KH)
(FEM results from Chen & O'Hara, 1984)

4.2.4 Variable Bauschinger Effect

Milligan et al. (1966), in an experimental investigation on high strength steel, concluded that the Bauschinger effect factor decreases (Bauschinger effect increases) in magnitude with increasing permanent strain up to approximately 2%. Thereafter, it tends to remain at a fixed value of 0.35. Figure 4.11 is a reproduction of figure 8 in Milligan et al. (1966) for 4330 modified steel. There have been many attempts to develop a method that includes the Bauschinger effect in the calculation of residual stresses induced by autofrettage. As discussed earlier, Franklin and Morrison (1960) provided a method which employed the actual unloading curve and hence considered a BEF. Kendall (1984) proposed a simple (empirical) BEF correction for use when the residual hoop stress has been obtained by assuming elastic unloading. Chen (1986) proposed a closed-form solution for calculating residual stresses in autofrettage using a simple model of the stress-strain curve which included a BEF and a hardening effect upon unloading. These solutions use a fixed value for BEF only and do not allow for changes in the BEF as a function of over-strain.

Other attempts have been made to take into account the changes in the Bauschinger effect factor as a function of plastic strain. Chaaban et al. (1986), in a rather complicated manner, provided a method of generating stress-strain curves as a function of plastic strain by introducing fictitious thermal loads. In their method, which is designed to be used with a finite element package (e.g., ABAQUS), the dependency of the BEF on over-strain was modeled by introducing a fictitious thermal load to develop different stress-strain loading curves. Then, using isotropic hardening, the unloading curves were defined. Each layer of the cylinder would then have a different unloading curve to follow. In this way they simulated the changes in BEF as the plastic strain changes. Megahed and Abbas (1991) proposed a method that employs variable BEF's in the calculation of residual stresses in an autofrettaged cylinder by including an empirical equation describing the BEF dependence on plastic strain. Their solution, as mentioned earlier, is for material whose behavior is modeled by a power law. The present method employs the experimentally obtained BEF-plastic strain curve (e.g., Fig. 4.22) and

automatically generates the unloading curve of each strip based on its plastic strain value at the end of loading. The reversed yield point is defined by the equivalent stress at the end of loading (current yield value for each strip) and the corresponding BEF. The unloading curve resumes its (loading) shape after reversed yield.

The third example discussed here examines the effect of a variable Bauschinger effect on residual stress predictions in autofrettaged tubes. The experimental results of Milligan et al. (1966) were used as the BEF data. A cylinder with inner to outer radii ratio of 3, E/σ_y = 1000, and elastic-perfectly plastic behavior during loading and unloading was considered. The cylinder was assumed to be in plane strain and the plastic deformation was based on the von Mises yield criterion. Four different autofrettage levels were considered. Figures 4.23-4.26 show the results obtained. The highest autofrettage percentage where the unloading was fully elastic was found to be 16%. At this level, not only does a constant BEF=0.35 falsely predict reverse yielding but also underestimates the bore hoop stress by a factor of 1/3 (Fig. 4.23). However, the discrepancy in the axial stress was lower. At higher levels of autofrettage, the differences between the two predictions decreases (Figs. 4.24-4.26), and eventually vanish (Fig. 4.26). Therefore, it can be concluded that including the dependence of BEF on plastic strain for low level autofrettaged analyses is important, especially for the prediction of reverse yielding.

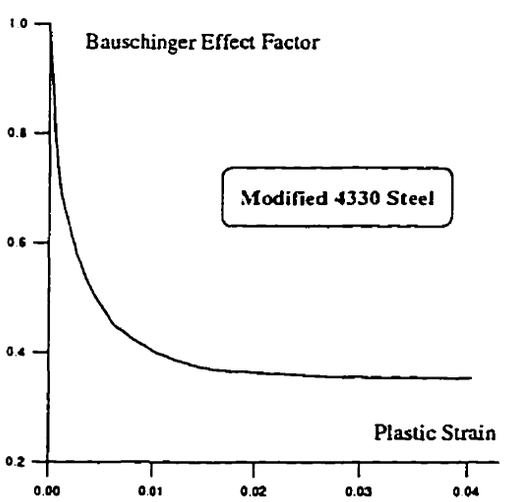


Figure 4.22: BEF in 4330 Steel
(Fig. 8 in Milligan et al., 1966)

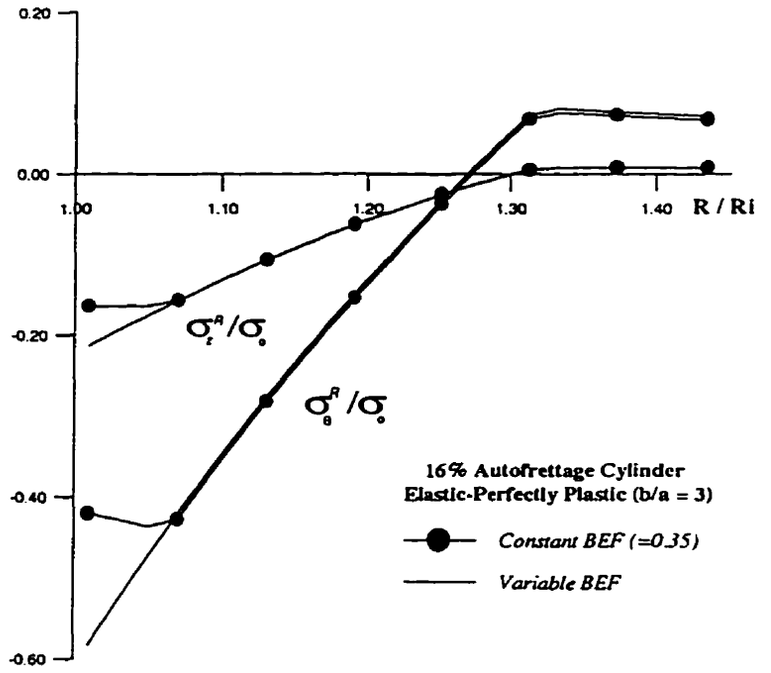


Figure 4.23: Variable BEF vs Constant BEF

(Autofrettage level=16%)

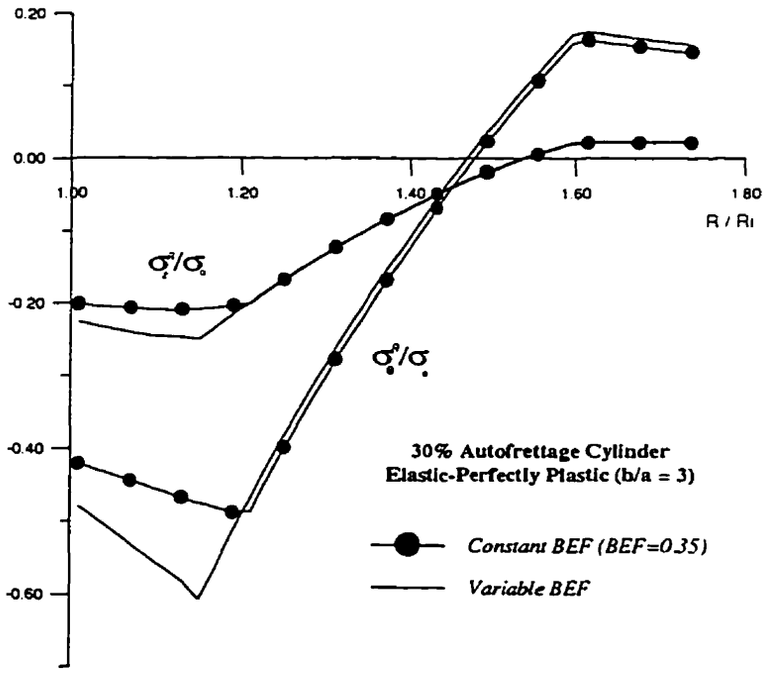


Figure 4.24: Variable BEF vs Constant BEF

(Autofrettage level=30%)

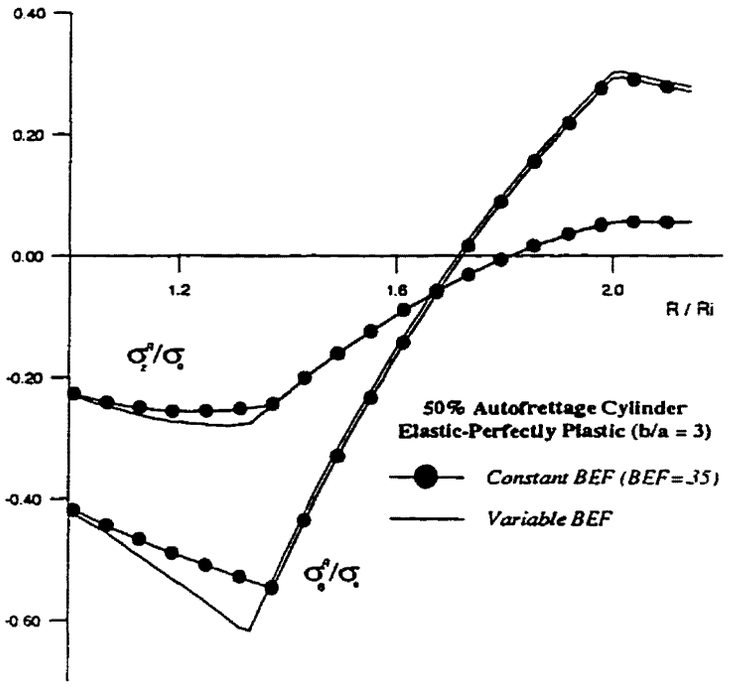


Figure 4.25: Variable BEF vs Constant BEF

(Autofrettage level=50%)

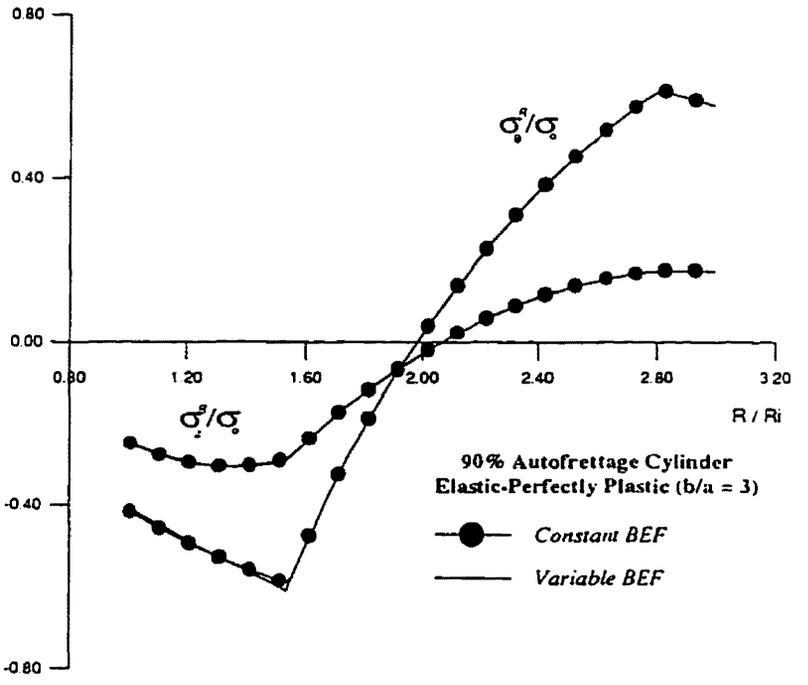


Figure 4.26: Variable BEF vs Constant BEF

(Autofrettage level=90%)

4.3 Loading and Unloading of Fastener Holes

Riveted and bolted joints often appear in built-up, mechanically loaded structures. For a plate containing a hole and subjected to a uniform remote tensile stress load, the hoop stress at the notch surface is roughly three times larger than the remote stress. Such stress concentrations are very important in fatigue life. In an earlier investigation in the aircraft industry, the most important source of failure in sixty-four aircraft incidents was found to be poor quality of the fastener holes. Results of this study (Wood, 1975) are summarized in Fig. 4.27. However, more recent studies of fatigue failure of airplane structures reveal that up to 70% of all fatigue cracks originated from joints hole (Buxbaum and Huth, 1987).

The demand for longer service lives in aircraft is dominated by the limited fatigue performance of critical airframe components. Therefore, it is desirable to reduce the tensile hoop stress at the hole surface. Methods of improving the fatigue performance of fastener holes which are simple, of relatively low cost, and that do not add weight or material to the airframe are particularly desirable. Foremost among such processes, cold expansion of holes has gained particular importance over the past thirty years and a variety of techniques by which expansion may be achieved have been considered (Champoux, 1986). All processes require insertion of a hard tool to deform the periphery of a hole plastically both in the radial and hoop directions. When the tool is removed from the hole, the elastic bulk surrounding the permanently deformed region forces it to spring back so that the vicinity of the

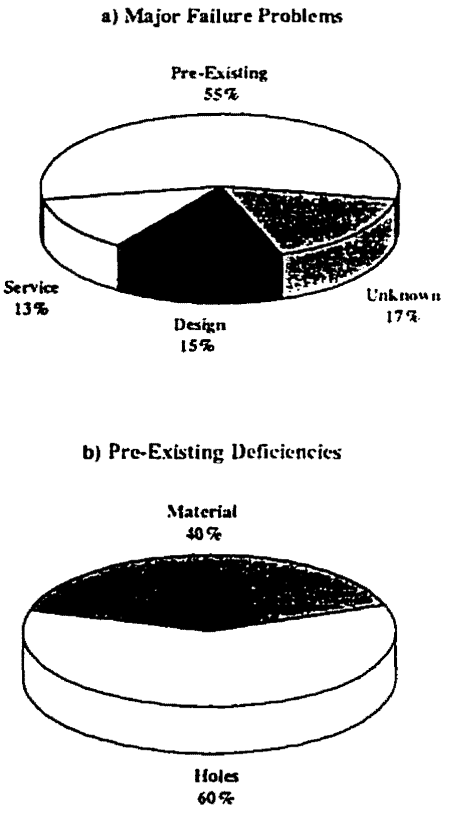


Figure 4.27: Importance of Fastener Holes in Failure of Aircraft (Fig. 1 in Wood, 1975)

hole develops compressive residual stresses. Superposition of these stresses with service loads results in fatigue life improvements by factors of 2-10, either by retarding the crack initiation or, more often, by reducing crack growth rates (Ozelton and Coyle, 1986).

The level of the cold work expansion is usually defined by one of the following. The percentage (or degree) of applied cold work is calculated by dividing the change in the hole diameter due to the insertion of the mandrel by the diameter of the hole before cold working

$$\text{Applied Cold Work}(\%) = \frac{(D+2t)-d}{d} \times 100 \qquad (4.8)$$

where D, t and d are the mandrel diameter, the sleeve thickness and hole diameter, respectively. The percentage (or degree) of residual cold working is defined by the ratio of the increase in the hole radius after removal of the mandrel, u_r, to the radius of the hole, r, prior to cold working

$$\text{Residual Cold Work}\ (\%) = \frac{u_r}{r} \qquad (4.9)$$

In order to take full advantage of cold working at the design stage, it is necessary to quantify the magnitude and distribution of the residual stresses induced by cold work expansion of the fastener holes. The proposed general axisymmetric method of elastic-plastic analysis based on the variable material property approach is capable of predicting residual stress, strain and displacement fields close to a cold worked fastener hole. Due to the flexibility of the present method in employing different yield criteria, loading behavior, unloading behavior, Bauschinger effect factors and hardening rules, application to fastener holes covers a wide range problems. The application of this method to loading and unloading of fastener holes is discussed.

4.3.1 Literature Review

4.3.1.1 Loading

For the loading of a fastener hole, the main concern is the stress concentration factor calculation. Stowell (1950) was the first to present an acceptable approximate formula for the stress concentration factor at a circular hole in an infinite plate. His formula was obtained from an approximate stress distribution which was adjusted by minimizing the mean square of the error in satisfying the equilibrium equations. There was no consideration of the compatibility equations. Hardrath and Ohman (1953) generalized Stowell's formula to include different loadings. Their formula for the case of a balanced biaxial tension plate with a circular hole which obeys the Ramberg-Osgood formula is

$$K_\sigma = 1+\frac{1+\alpha\left(\frac{\sigma_\infty}{\sigma_o}\right)^{m-1}}{1+\alpha\left(\frac{\sigma_\infty}{\sigma_o}\right)^{m-1} K_\sigma^{m-1}} \tag{4.10}$$

where $K_\sigma=[(\sigma_\theta)_{hole}]/\sigma_\infty$ is the stress concentration and σ_∞ is the remote biaxial tension.

Budiansky and Mangasarian (1960) using the Ramberg-Osgood formula and the total deformation theory of plasticity, found a general analytical equation for the stress concentration factor in a uniformly all around loaded plate with a circular hole. This equation has a closed form solution only for a material with no elastic response and a plastic response completely defined by a pure power law. A power series solution technique was presented for the general case. They included numerical results with stress concentration factors for different materials.

Neuber (1961), by considering a notched prismatic body obeying an arbitrary nonlinear stress-strain law, derived the following relationship between stress and strain concentration factors:

$$K_\sigma K_\varepsilon = K_\epsilon^2 \tag{4.11}$$

where K_ε is the strain concentration factor and K_ϵ is the elastic stress (or strain) concentration factor. Neuber's rule for the case of a balanced biaxial tension plate with a circular hole for a material obeying the Ramberg-Osgood model is

$$K_\sigma^2 = \frac{4\left[1+\alpha\left(\frac{\sigma_\infty}{\sigma_o}\right)^{m-1}\right]}{1+\alpha\left(\frac{\sigma_\infty}{\sigma_o}\right)^{m-1} K_\sigma^{m-1}} \tag{4.12}$$

Tuba (1965), using the iterative method of Manson and Mendelson (1959) and the stress function method for plane problems, solved for the stress and strain concentration factors at a circular hole in a uniformly stressed infinite plate for a linear hardening material. In this method, the nonhomogeneous biharmonic equation was solved by estimating the plastic strain and successive readjustment by the method of successive elastic solutions (see section 2.6.2). Numerical results for a wide range of strain hardening, from perfectly plastic to purely elastic, were presented.

In an extensive theoretical study of stress concentrations at a circular hole, Huang (1972) solved the problem by a method involving Fourier series and finite differences. The governing equations, based on the J_2 deformation theory of plasticity and the Ramberg-Osgood stress-strain relation, were formulated in terms of a stress function for both plane stress and plane strain (under the restriction of no unloading). The solution was expanded into a Fourier series in the circumferential direction and the Fourier coefficients, which

are a function of radial coordinate only, were determined by a finite difference method. Numerical results, including that for equal biaxial loading of a plate was presented.

In a different approach, Gao et al. (1991), using a method of solving plane stress problems for power law materials with a complex pseudo stress function, gave a closed form equation for the stress distribution around a hole in an infinite plate under uniform all-around tension. This solution, which is based on the total deformation theory of plasticity, and does not consider compressibility of the material, is given in the following form

$$\sigma_\theta = 2^{(1-n)} p \left[\left(1 + \frac{R^2}{r^2} \right) \left(4 + \frac{12R^4}{r^4} \right)^{\left(\frac{n-1}{2}\right)} \right] \qquad (4.13)$$

where n is the hardening power in the power law relation: $\sigma_{eq} = A\varepsilon_{eq}^{n}$.

4.3.1.2 Residual stress calculations

There have been many investigations regarding the calculation of residual stress fields in a cold worked fastener hole. Most of the analytical work in this area follows one of the three most prominent theories proposed by Nadai (1943), Hsu and Forman (1975) and Rich and Impellizzeri (1977). One of the main subjects of these theories is the calculation of the elastic-plastic radius, r_p, upon removal of the mandrel. At this location, the maximum residual tensile stress occurs, which is very important in design and specification of hole location. The maximum compressive stress is also of interest. This maximum value may occur at the bore (for elastic unloading) or close to the bore (for reverse yielding). Hence, calculation of stresses within the residual compressive plastic zone due to reversed yielding is also of interest. Not all of the above theories give relations for the calculation of the above mentioned points of interest. A summary of the analytical work in predicting the residual stress field in fastener holes follows.

Nadai (1943) published a theory of plastic expansion of tubes fitted into boiler heads. In the manufacturing process these tubes were expanded by a roller device to insure a leak-free fit. He considered both the plastic deformation of the plate and the tubes. First, he solved the plate problem which is of interest here. His main assumptions were: 1) a perfectly plastic material, i.e., neglecting elastic response, 2) a linear approximation to the von Mises yield criterion, 3) elastic unloading, 4) deformation theory and 5) plane stress. He developed a simple closed form expression for the stresses and displacements in the plastic zone as well as for the location of the elastic-plastic interface. These expressions for stresses and displacements are as follows:

$$\sigma_r = \frac{\sigma_o}{\sqrt{3}}\left[-1+2\ln\frac{r}{r_p}\right],\ \sigma_\theta = \frac{\sigma_o}{\sqrt{3}}\left[1+2\ln\frac{r}{r_p}\right]$$
$$u_r = u_{aE}\frac{r}{a}\left[1+\frac{2}{3}\ln\frac{r}{r_p}\right]^{1/3} \tag{4.14}$$

where r_p is the radius of the elastic-plastic boundary, a is the initial radius of the hole and r is the radius of interest. The maximum elastic displacement at the hole, u_{aE}, is

$$u_{aE} = \frac{(1+\nu)\sigma_o a}{E\sqrt{3}} \tag{4.15}$$

The simplicity of these formulas makes this theory very easy to use.

Carter and Hanagud (1974) performed an experimental investigation of the stress corrosion susceptibility of cold worked fastener holes since the residual tensile stresses surrounding the hole could be greater than the threshold for stress corrosion cracking. They developed their own theory, which was similar to an earlier theory by Taylor (1947), to calculate loading and unloading stresses. Their main assumptions were: 1) the Tresca yield criterion was valid, 2) the radial displacement at the edge of the hole was

known, 3) the material was responding in an elastic-plastic manner, i.e., elastic response was included, and 4) the plate was in a state of plane stress. Based on these assumptions they developed an equation for the elastic-plastic radius r_p when the hole edge displacement was known.

Hsu and Forman (1975) proposed a theory which was basically the Nadai theory extended to account for hardening response. They utilized a solution technique developed by Budiansky (1971) for elastic-plastic stress concentrations. Their main assumptions were: 1) the material behavior was represented by the Ramberg-Osgood formulation, 2) the von Mises yield criterion was applicable, 3) the unloading was elastic, 4) deformation theory was valid and 5) the plate was in a plane stress state. Their solution in the plastic region was developed in terms of a parameter α varying between 90° (corresponding to initial yield) and α_a (corresponding to final expansion). The solution was in a closed form, and the equations are easily programmable.

Chang (1975) used the elastic-plastic solution of Hoffman and Sachs (1953) for thick-walled tubes to compute the residual stress distribution adjacent to an open hole in a thick plate and then used it for the analytical prediction of fatigue crack growth for cold worked holes. The assumptions of this theory were: 1) perfectly plastic behavior of the material, 2) the von Mises yield criterion, 3) plane strain conditions under uniform pressure at the hole edge, and 4) deformation theory. He then gave a relation between the elastic-plastic radius and the hole edge displacement.

Rich and Impellizzeri (1977), proposed an approximate closed form solution for residual stresses surrounding cold worked holes. Their assumptions were: 1) the material behavior was elastic-perfectly plastic, 2) the thick-walled cylinder solution was valid, 3) the von Mises yield criterion was applicable, 3) deformation theory was applicable, 4) the hole was in a state of plane strain, and 5) the material was plastically incompressible. They basically modified the elastic unloading solution of Hoffman and Sachs (1953) to predict an approximate compressive yield zone, r_c, upon removal of the mandrel:

$$r_c = \sqrt{\frac{a^2}{2\left(1-\left(\frac{a}{b}\right)^2\right)}\left(2\ln\frac{r_p}{a}+1-\left(\frac{r_p}{b}\right)^2\right)} \tag{4.16}$$

where a is the internal radius, b is the distance from the hole center to the edge of the plate, and r_p is the radius of plastic zone. They further developed a relation for predicting the circumferential residual stress at the hole wall

$$(\sigma_\theta)_{RES} = \frac{4\sigma_o}{\sqrt{3}}\left[-\gamma+\left(\frac{a}{b}\right)^2 e^{\gamma}\right] \tag{4.17}$$

where

$$\gamma = \left[\frac{1}{2}-\left(\frac{a}{b}\right)^2+\frac{1}{2}\left(\frac{r_p}{b}\right)^2\right] \tag{4.18}$$

and the radius of the plastic zone is calculated from

$$\frac{u_a}{a} = \frac{\sigma_o}{\sqrt{3}E_B}\left[0.52\left(2\ln\frac{r_p}{a}+1-\frac{r_p^2}{b^2}\right)+1.5\frac{r_p^2}{a^2}\frac{E_B}{E_P}\right] \tag{4.19}$$

In this equation, E_B and E_p are the moduli of elasticity of the mandrel and the plate, respectively. This equation relating the plastic radius, r_p, and the hole displacement, u_a, was introduced by setting the radial interference fit equal to the sum of radial displacements of the mandrel and the plate.

Potter et al. (1978), developed expressions for the residual stress field at fastener holes. Their assumptions were: 1) elastic-perfectly plastic material response, 2) the von Mises yield criterion, 3) an incompressible plastic zone, 4) plastic unloading, and 5) a plane stress state. The expressions for stresses and strains were in closed form and are function of the plastic re-yield zones. However, the size of these zones can only be obtained with knowledge of the applied expansion and are found by numerically solving nonlinear equations.

Clark (1982 and 1991), provided an approximation for the residual stress field in fastener holes. His assumptions were: 1) elastic-perfectly plastic material behavior, 2) modified Tresca yield criterion (based on Hill (1950) and Warren (1947) modified yield stress), 3) the plane stress condition, and 4) reversed yielding upon unloading.

Mann and Jost (1983), by an extensive study of different theories, showed the influence of different assumptions on residual stresses field predictions. The effect of different conditions considered by different theories were studied. These conditions included: 1) yield criteria (Mises, Tresca or others), 2) stress state (plane stress for thin plate, or plane strain for thick plate), 3) deformation (elastic, elastic-perfectly plastic or elastic-plastic), 4) unloading (elastic or embodying reverse yielding), 5) displacement (small or large), 6) plate width (infinite, semi-infinite or infinite), and 7) mandrel and fastener properties (rigid or deformable). Their study showed how each of these conditions change the residual stress field. They concluded that there were significant shortcomings in some of the models that have been used to predict the residual stress fields (particularly in assumptions regarding elastic-plastic behavior of the plate material and the relevance of reverse yielding) and there is very little evidence that experimentally verifies the predicted stress distributions.

Jost (1988), developed relations for the residual stress of an annulus of finite dimensions. His assumptions were: 1) elastic-perfectly plastic material response, 2) then von Mises yield criterion, 3) an incompressible plastic zone, 4) plastic unloading, and 5) the plane strain state. His method is similar to Potter et al. (1978) but is for plane strain.

Wang (1988) presented a closed form residual stresses solution for a circular hole under uniform pressure. His assumptions were 1) a modified Ramberg-Osgood model, where the elastic response is separated from its plastic response (given by a power law), was applicable, 2) the J_2 deformation theory was applicable, 3) plastic unloading was allowed, 4) a constant Bauschinger effect factor defined the reversed yield stress value, and 5) the hole expanded in a plane strain state. His solution was based on Nadai's technique and was an extension to Nadai (1943) and Hsu and Forman (1975).

Wanlin (1993), extended the work of Hsu and Forman (1975) to include not only the elastic plastic response during unloading but also the effects of a finite size plate. He considered the dependency of the compressive yield stress value on a constant Bauschinger effect.

Ball (1995) followed the solution technique of Budiansky (1971) for both loading and unloading. This solution is also an extension to Hsu and Forman (1975). He assumed further that the radial expansion of the hole was affected by an elastic insert and the required relationships among interference ratio, applied expansion, interface pressure and retained expansion (after removal of the insert) were given. His solution was for a plane stress state.

Beside these analytical approaches, there have been many experimental measurements and finite element analyses of the cold worked fastener holes. It is very interesting to note that there has been very little agreement between the proposed methods and experimental results (Poolsuk and Sharpe, 1978; Mann and Jost, 1983; Forgues et al., 1993; Priest et al., 1995, Poussard et al., 1995). There are a number of reasons provided for such discrepancies and some are discussed here. There have been some studies regarding the three dimensional nature of the fastener hole problem. Poussard et al. (1994) simulated the cold work process using finite elements. He studied the change in stress distribution at the entrance face of the mandrel, mid-thickness plane and exit face. The changes were appreciable. Forgues et al. (1995), through a three dimensional axisymmetric numerical study, concluded that the residual stress distribution through the thickness of plate was different. However, three dimensional residual stress

measurements (Ozdemir and Edwards, 1996) show some changes through the thickness near the hole but very little away from the hole. Also, the 3-D analysis results do not agree with experimental results (Forgues et al., 1995). Another reason is the modeling of the material behavior. It is amazing to note that, among many experimental studies on the fastener hole problem, there are very few that provide the actual loading-unloading curves of the material used in the experiment. It looks as if the unique unloading behavior of high strength aluminum (such as Al 7050), usually used in aircraft industries, has not been taken into consideration. Poussard et al.(1995), one of the few who noticed this point, noted that the observed material behavior under compression does not initially agree with either kinematic or isotropic hardening models for reversed yielding. They further suggest that a material model allowing the compressive material behavior to be closely approximated would be extremely beneficial. None of the present methods of solution is capable of including the actual material behavior in compression.

Another reason provided for such disagreement is that the plate does not remain axisymmetric in the industrial process of hole expansion. Even though this point is valid to some extent, adding to the complexity of the analysis is something one would like to avoid. Moreover, further away from the hole, the material responds as if the expansion had been uniform. Therefore, this has only a local influence and it should not effect the position of the elastic-plastic boundary as calculated by the axisymmetric analysis.

The proposed method of axisymmetric elastic-plastic analysis is capable of predicting the residual stress field induced by the fastener hole expansion. The capabilities embedded in this method are far more than each single method described above. This method is able to consider: 1) either elastic-perfectly-plastic behavior, behavior based on the Ramberg-Osgood formula (and not only the modified form of it) or the actual material behavior during loading and unloading; 2) the von Mises, Tresca or any other yield criteria; 3) plastic unloading with kinematic or isotropic hardening rules; 4) the Bauschinger effect and its changes as a function of plastic strain induced during loading; 5) a pre-stressed hole in cold work expansion, and 6) material compressibility. All of these features are included in a single simple FORTRAN code (see appendix A) which performs the

analysis in few seconds on a personal computer. Desired options are chosen from an input file. Some of the results obtained by this program are discussed in this chapter.

4.3.2 Loading of a Fastener hole

The variable material property approach has been applied to the problem of an infinite plate with a circular hole under an all-around tensile field. The schematic for this problem is shown in Fig. 4.28 . The strips have the shape of annular rings under tension. The elastic solution is given by the Lame solution where the usual external and internal pressures are replaced by a tensile stress. Stress and strain concentration factors at the notch tip are calculated for different nonhardening or hardening materials. Figure 4.29 shows the results for nonhardening materials. The stress and strain concentration factors for a wide range of loading from elastic to full plastic load is shown. The values of stress concentration factors are compared with the analytical solution of Budiansky and Mangasarian (1960), and the strain concentration factors are compared with the results obtained by Tuba (1965). The agreement is very good.

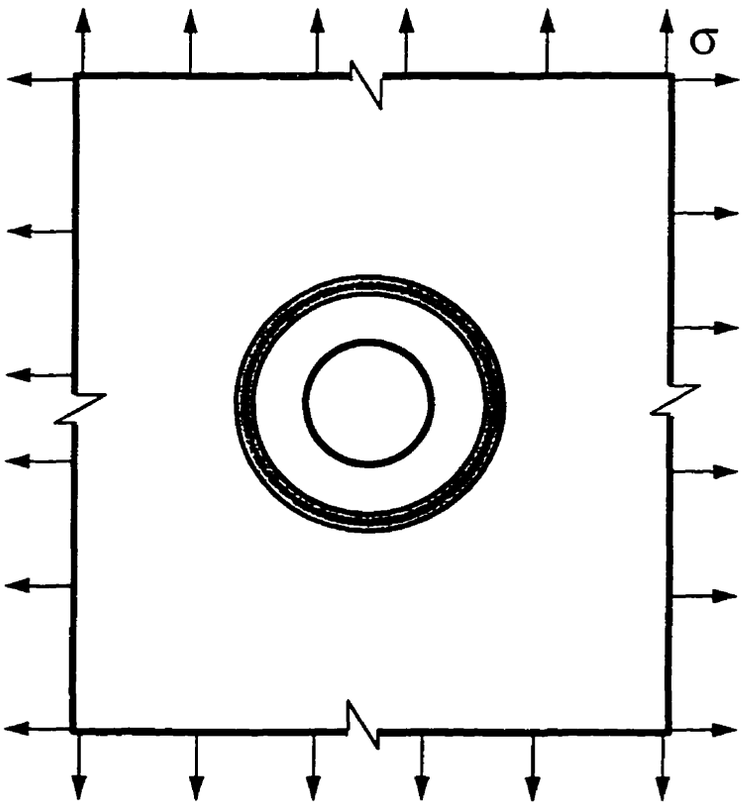


Figure 4.28: Circular hole under uniform tension

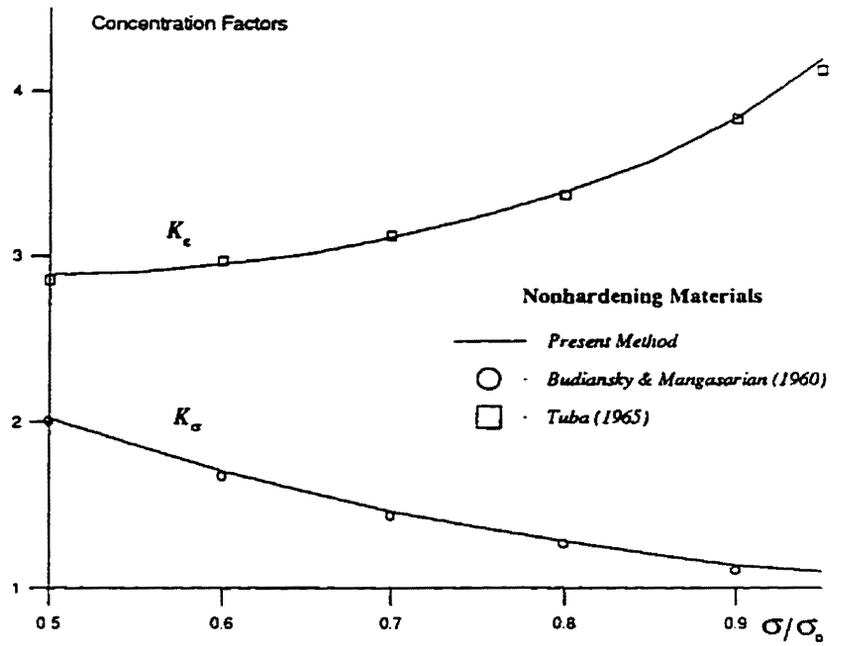


Figure 4.29: Comparison of concentration factors (nonhardening materials)

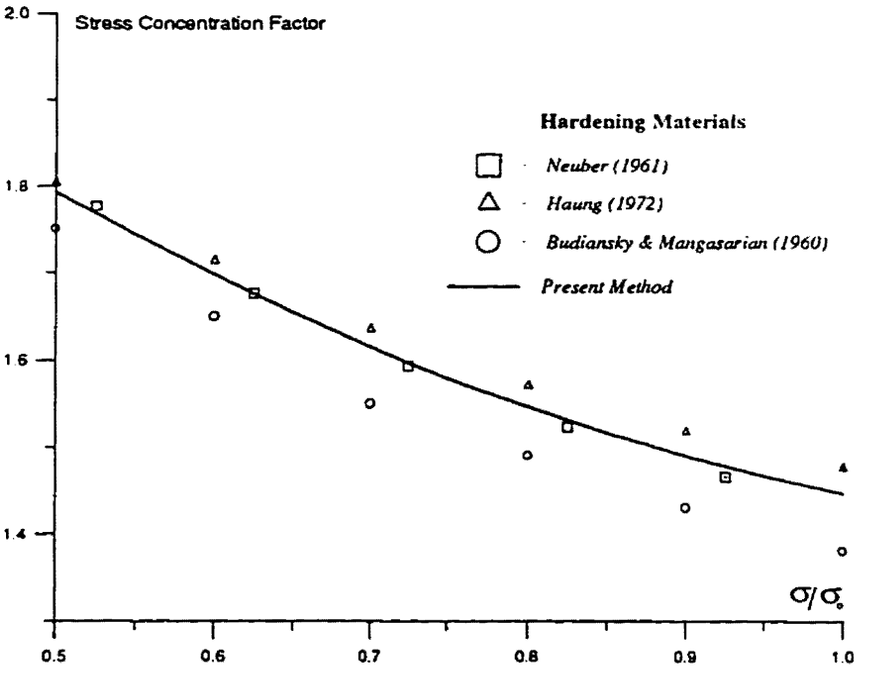


Figure 4.30: Comparison of concentration factors (hardening materials)

The results for stress concentration factors for a hardening material are shown in Fig. 4.30. The results of the present method are compared to concentration factors obtained from Neuber's rule, Haung (1972) solution and the Budiansky and Mangasarian (1961) series solution. The present method agrees very well with Nueber's rule, which has proven to be an acceptable approximation of stress concentration. The results of Haung (1972) and Budiansky and Mangasarian (1961), which are Fourier series solutions, deviate from the present method.

Figure 4.31 shows a summary of concentration factors obtained using the present method and other methods, including results obtained using ABAQUS. The ABAQUS results were obtained by the author. The agreement is very good.

The hoop and radial stress distributions around the hole are shown in Fig. 4.32. The results are compared with the closed form solution of Gao et al. (1991) for a material obeying a power law σ-ε behavior and the agreement is found to be excellent.

To examine the changes in stress response for different materials, a study on hoop and equivalent stress changes of different materials was conducted using the present method. The materials considered in this study include nonhardening and hardening materials obeying the Ramberg-Osgood formula with different hardening exponents. The stress distributions along the horizontal line from the hole edge are shown in Figs. 4.33. and 4.34. The stress concentration factor decreases as the hardening exponent increases. This drop for a nonhardening material is about 70% as compared to a material with hardening exponent equal to 3.

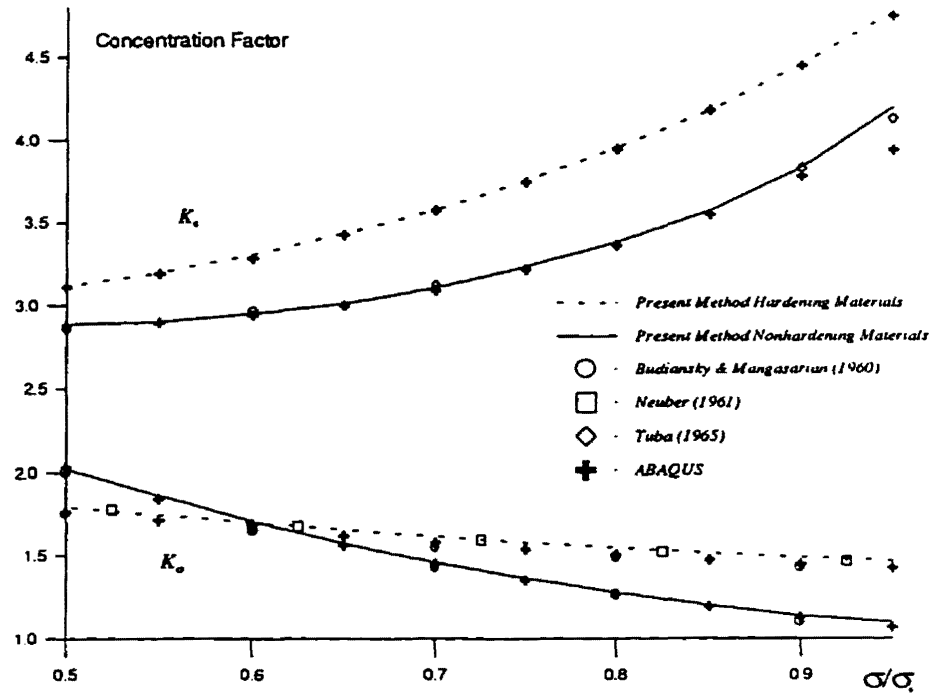


Figure 4.31: Stress and strain concentration factors

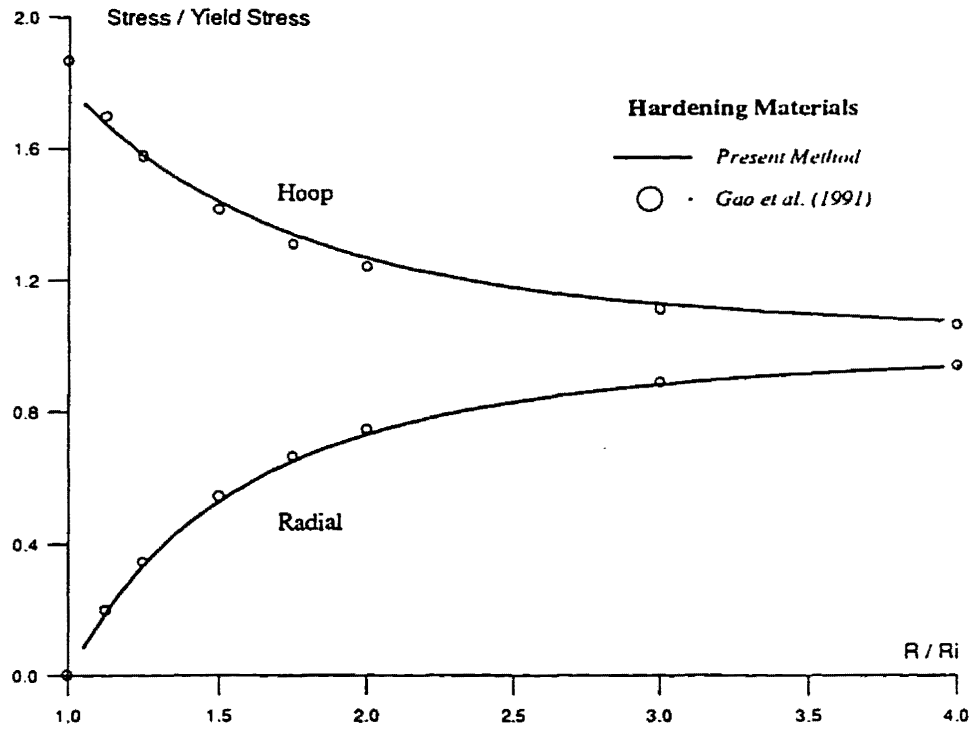


Figure 4.32: Hoop and radial stress distributions

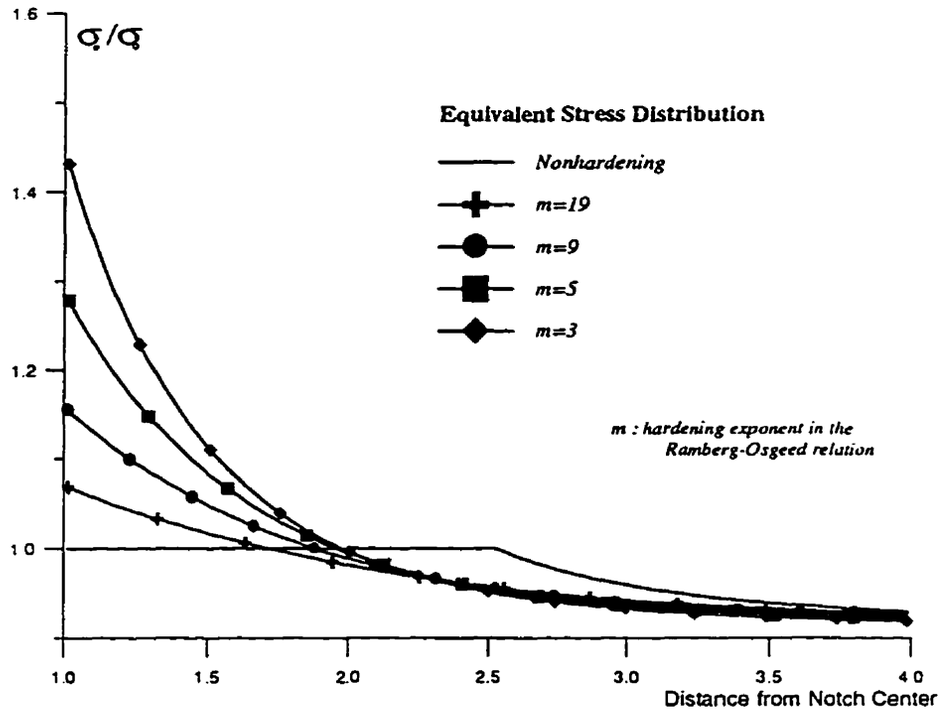


Figure 4.33: Equivalent stress distribution near the notch

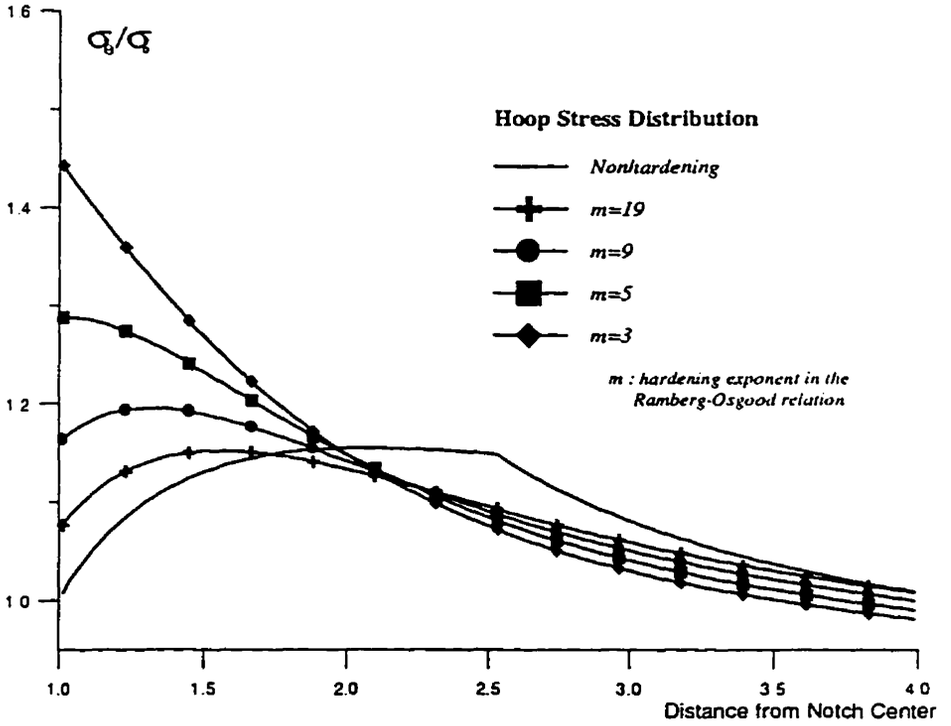


Figure 4.34: Hoop stress distribution near the notch

4.3.3 Residual stresses in Cold worked Fastener Holes

The variable material property method was used here for the analysis of the unloading behavior of fastener holes. This study includes: 1) residual stress predictions based on consideration of the actual loading-unloading behavior and 2) prediction of the elastic-plastic boundary. Results are compared to available experimental measurements and finite element calculations.

4.3.3.1 Actual Stress-Strain Unloading Curve

There have been many experimental measurements of the residual stress in fastener holes. With the exception of a few, none of these recorded the actual loading-unloading behavior of the material used. In many of these investigations the uniaxial stress-strain curve (for monotonic loading) was obtained to find the values of the modulus of elasticity, Poisson's ratio and yield strength. To the authors knowledge, there have been no analyses based on the actual unloading behavior of material. None of the methods mentioned in literature review is capable of employing the actual material curve. Commercial finite element packages are not designed to follow the exact unloading curve either.

Poussard et al. (1995) are among the few to record the actual unloading curve. They used 2024 T351 aluminum alloy in their finite element analysis. Figure 4.35 is a reproduction of Fig. 1 from Poussard et al. (1995). Two commonly used approximations of the behavior are also shown in the same figure. None of these models can represent the unloading behavior precisely. There exists a pronounced Bauschinger effect in this aluminum alloy. While the monotonic loading curve represents a linear hardening behavior, with a slope of $0.022E$, the reversed yield stress (based on 0.1% proof stress) remains at a constant value of -110 MPa for unloading from different plastic strain states. This suggest that the BEF is a function of plastic strain.

The experimental measurements of the residual stresses in the same Al 2024-T351 were recorded by Priest et. al. (1995). The results are very scattered and unreliable. For

example, the measured hoop residual stress in a 4% cold worked plate is compressive even far away from the hole edge. Priest et al. (1995) suggest that the measured values are highly influenced by the stresses existing in the plate prior to cold working. However, They did not record the as-received residual stress field.

In earlier independent work, Mann and Jost (1983) also recorded results of experimental measurements on aluminum 2024. The experimental results, based on the work of Lowak (1981), are for a 4.5% cold worked fastener hole with an initial hole radius of 8 mm.

The present method of analysis was used to predict the residual stress field for a 4.5% cold worked plate. The actual unloading behavior of 2024 aluminum alloy shown in Fig. 4.35 was used. The changes in the BEF were accounted for in the analysis. This was done by setting the compressive yield at *-110* MPa as observed from the uniaxial curve.

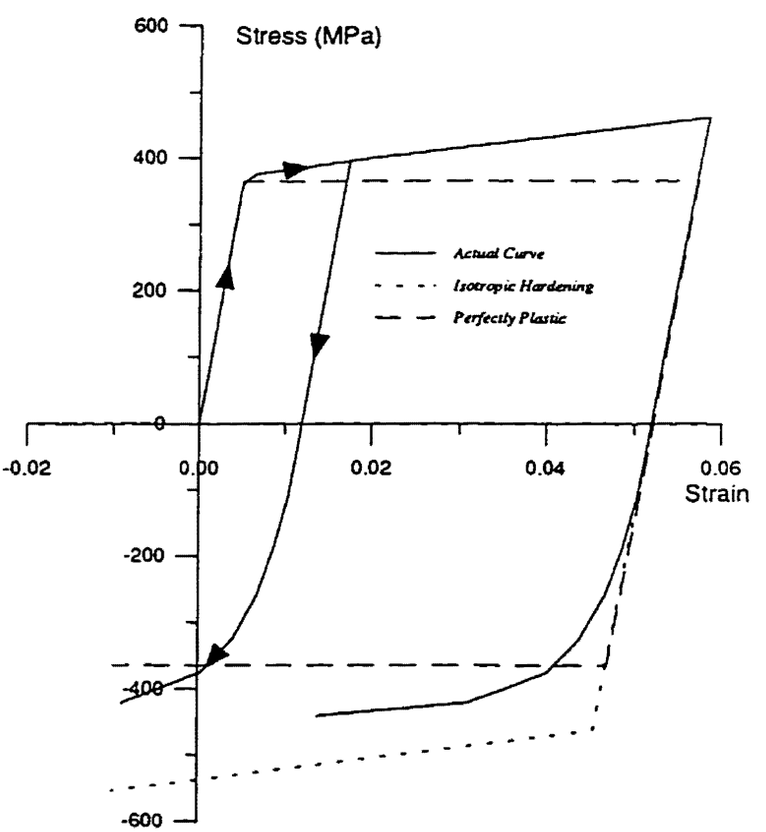


Figure 4.35: Uniaxial loading-unloading response of Al 2024 T351

(Poussard et al., 1995, Fig. 1)

An infinite plate with a hole of 8 mm initial radius was considered. The residual stress field due to 4.5% expansion of the hole was obtained and the results are shown in Fig. 4.36. The shape of the curve near and at the hole edge indicate a possibility of reversed yield. However, the experimental results do not show any reversed yielding and show only elastic unloading. This may be due to size of the plate used in the experiment which

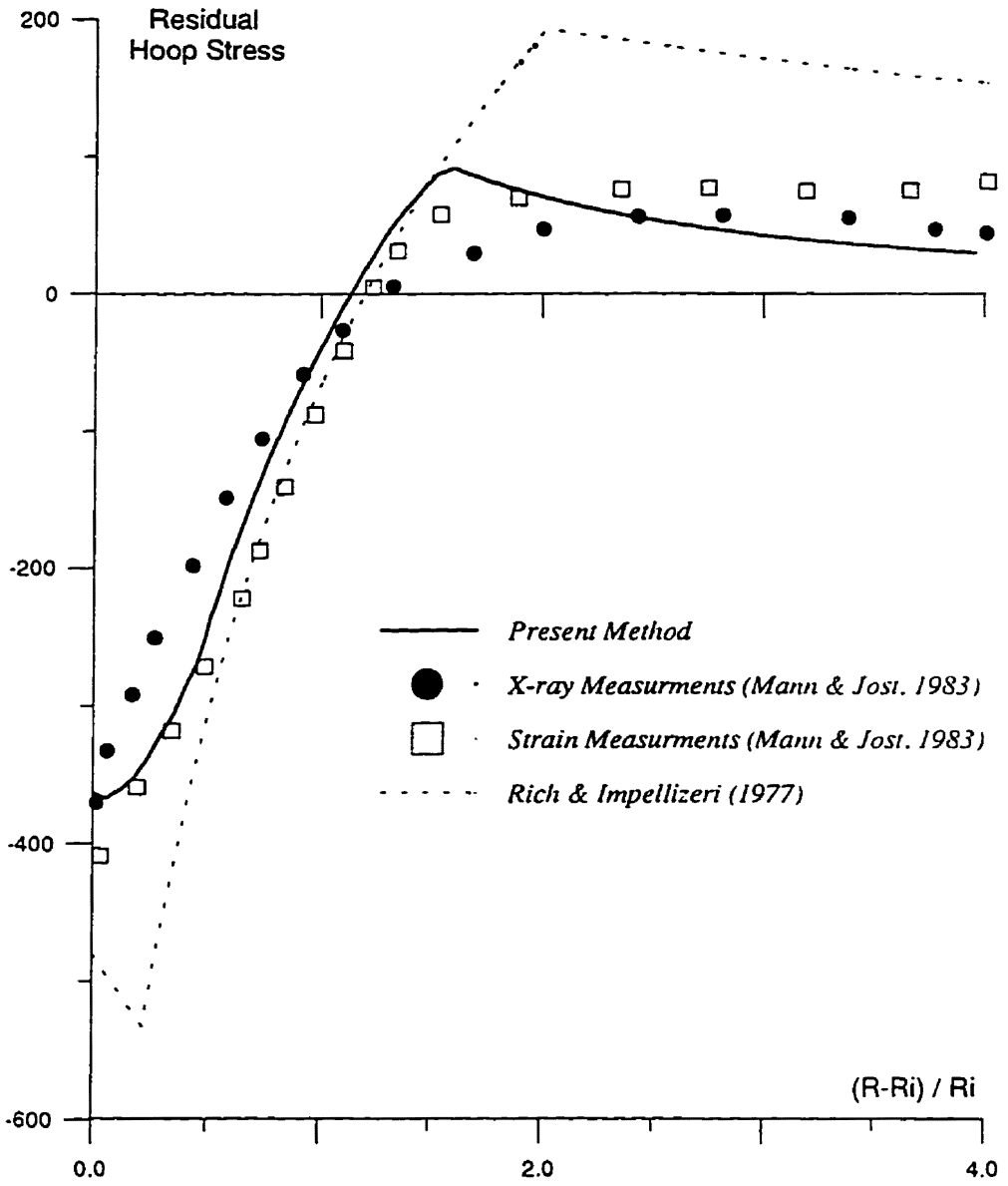


Figure 4.36: Comparison of calculated and measured residual stress distribution for 4.5% cold expanded hole in Al 2024 alloy plate (Experimental results from Mann & Jost, 1983)

is of finite size (80 mm). The general agreement between the present method and the experimental values is good. The prediction by Rich and Implizzerri (1977), which is one of the few methods which accounts for reversed yielding is also shown in the figure. It is quite obvious that consideration of the actual unloading curve is very important.

Poussard et al. (1995), have employed the actual loading behavior of Al 2024 with the ABAQUS finite element package to predict the residual stress field. Different hardening models provided by ABAQUS (isotropic and kinematic hardening rules) were used. Their finite element analysis was on a plate with an initial hole radius of 3.175 mm and width of 200 mm. The hole was assumed to be 4% cold expanded. The same dimensions were employed by the author to obtain the residual stress field using the variable material property method. The results are shown in Fig. 4.37. While the kinematic hardening model underestimates the compressive stress at the hole edge by 20%, the isotropic model shows a uniform compressive field near the hole. Both model predictions away

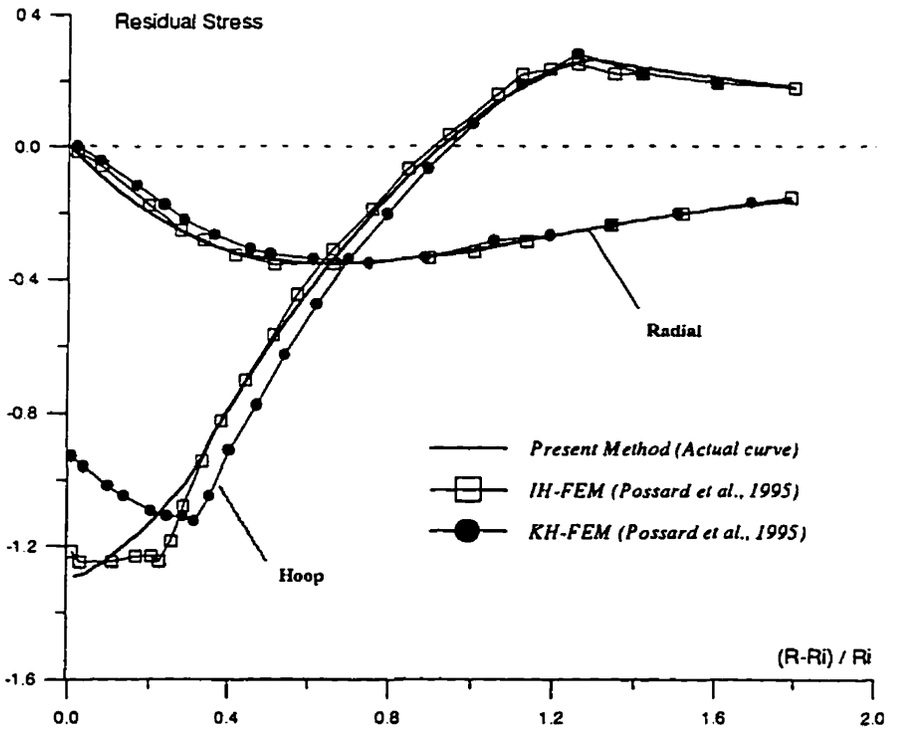


Figure 4.37: Comparison of residual stress distribution for 4% cold expanded hole in Al 2024 alloy plate
(FEM results from Poussard et al., 1995)

from the hole are very close to the present analysis based on the actual unloading behavior. The isotropic hardening model stays closer to the present analysis away from the hole. The difference in radial residual stress is not significant.

4.3.3.2 Elastic-Plastic Boundary Prediction

Knowledge of the size of the plastic zone in a fastener hole is very important because a larger plastic zone will delay crack propagation emerging from the hole edge (Bernard et al., 1995). It is also very important in design and spacing of hole locations. Some theoretical studies have been based entirely on predicting the size of the plastic zone (e.g., Carter and Hanagud, 1947). A comparison of the prediction from different theories with the prediction from present method for the plastic zone radius is given herein.

Poolsuk and Sharpe (1978) conducted a series of experiment to measure the exact size of the plastic zone and to examine the validity of different theories in this regard. They argued that it was easier to measure the location of the elastic-plastic boundary, rather than the complete residual stress field. Since most of the experimental results for stress field have been found to be in poor agreement with the values predicted by different theories, Poolsuk and Sharpe (1978) suggested that the theories could be evaluated based on their capabilities of predicting the elastic plastic boundaries. The experiment was conducted on a plate with a central hole of 3.3 mm radius made of 7075 T6 aluminum alloy. They used four different levels of cold work and compared their measurements with different theories.

The loading-unloading behavior of Al 7075-T6 was given by Endo and Morrow (1969) and Landgraf et al. (1969). The data points for the monotonic loading curve are given in Table 4.4. The yield stress and modulus of elasticity for this curve matches the specifications of one of the samples used with Poolsuk and Sharpe's (1978) experiments. The behavior of this aluminum alloy can not be modeled precisely by any of the available hardening models. However, consideration of the actual unloading curve will only influence the prediction of residual stresses near the hole edge and will have very little effect on the prediction of the elastic-plastic boundary location.

Strain	Elastic Strain	Plastic Strain	Stress (psi)	Stress (MPa)
0.0057	0.0057	0.0000	60.92	420
0.0063	0.0063	0.0000	65.41	451
0.0079	0.0079	0.0000	72.95	503
0.0121	0.0114	0.0007	77.89	537
0.0185	0.0145	0.0040	87.89	606
0.0290	0.0090	0.0200	95.87	661
0.0450	0.0095	0.0355	99.93	689

Table 4.4: Data for loading behavior of Al 7075 T6
(From Endo and Morrow, 1969)

The elastic plastic radius results obtained from the present method are shown in Table 4.5. The value of $u_{a\varepsilon}$ in this table is given by Eq. (4.15).

Figure 4.38 shows the comparison of the results obtained by the present method and the experimental measurements. The agreement is very good. The prediction from some other theories are also shown in the same figure. As can be seen from Fig. 4.38, some of these predictions are far from the experimental results (Potter & Grandt, 1978; and Carter & Hanagud, 1975). Nadai (1943) and Hsu & Forman (1975) show the same trend as the experimental results. However, the plastic radius predicted by these two methods are not accurate. Rich & Impellizzei's (1977) solution is the best among the different theories compared here. Nevertheless, the trend shown by Rich & Implezzeri (1977) is different from that shown by the experiment. It appears that this solution will deviate

very much from the experimental results for higher values of u_a/u_{aE}. Chang's (1974) solution is very close to the Rich and Impellizerri (1977) solution.

Expansion	u_a (mm)	u_a / u_{aE}	r_p / a
1.15%	0.038	2	1.550
1.73%	0.057	3	1.816
2.3%	0.076	4	1.970
3.0%	0.102	5.368	2.180
3.85%	0.127	6.68	2.288
4.60%	0.152	8	2.394

Table 4.5: Present method results of elastic-plastic boundary location

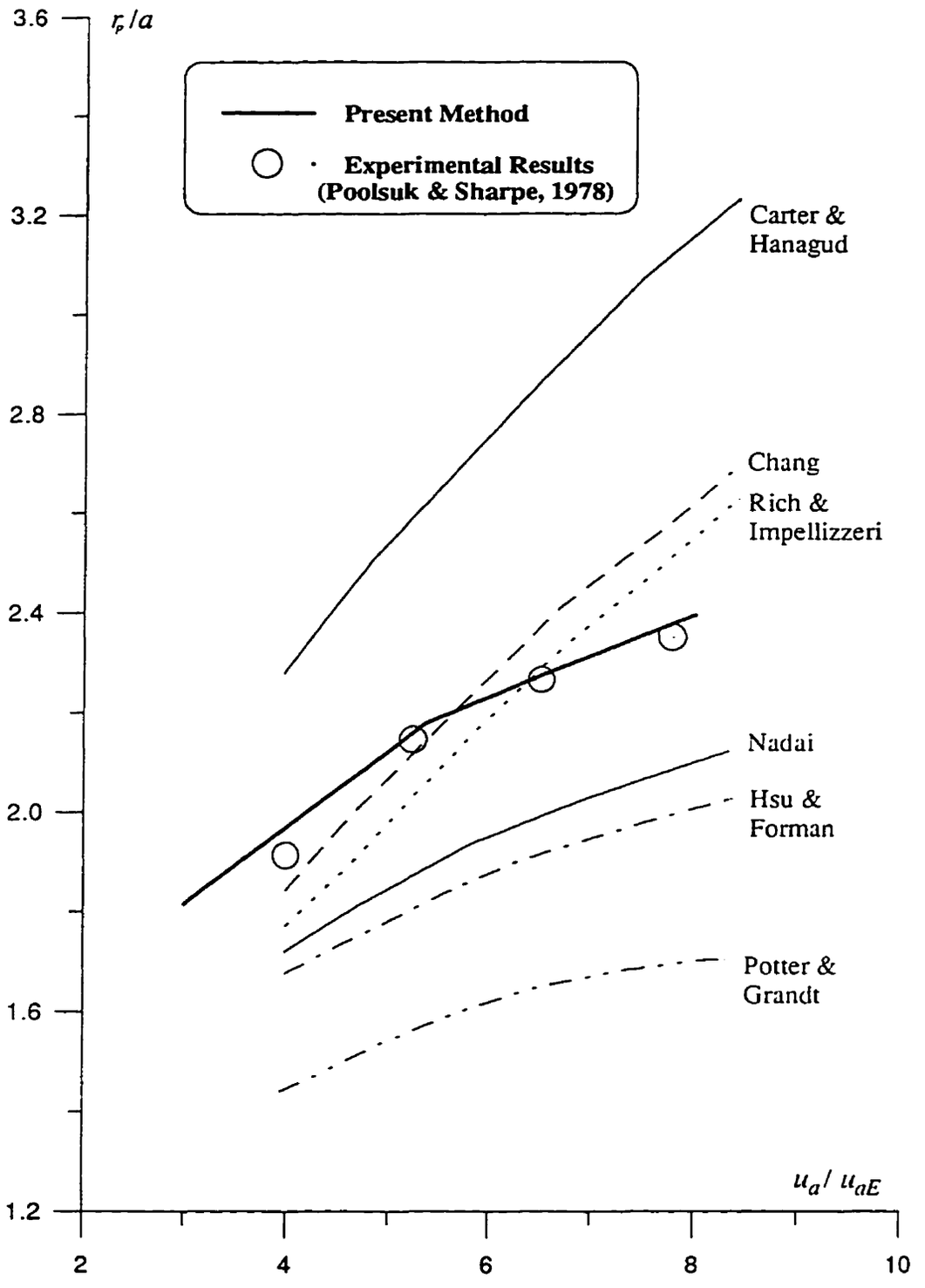


Figure 4.38: Comparison of predicted elastic-plastic boundaries with measurements for 7075 T6 Aluminum

(Experimental results from Poolsuk and Sharpe, 1987)

4.4 Multiaxial Loading of a Thick-Walled Cylinder

The problem of a thick-walled cylinder under proportional pressure and torsion is considered here. It is assumed that an internal torque, T, is applied at the cylinder bore (Fig. 4.39) while its outer surface is kept fixed. The stress in any strip of mean radius r can be obtained directly from the equilibrium equation. Assuming a uniform shear stress distribution at r, the shear stress is related to the torque by:

$$\tau_{r\theta} = \frac{T}{2\pi r^2} \tag{4.20}$$

The constitutive equation proposed in chapter three (Eq. 3.4) relates shear stress and shear strain, $\gamma_{r\theta}$, in the following way

$$\tau_{r\theta} = G_{eff}\gamma_{r\theta} \tag{4.21}$$

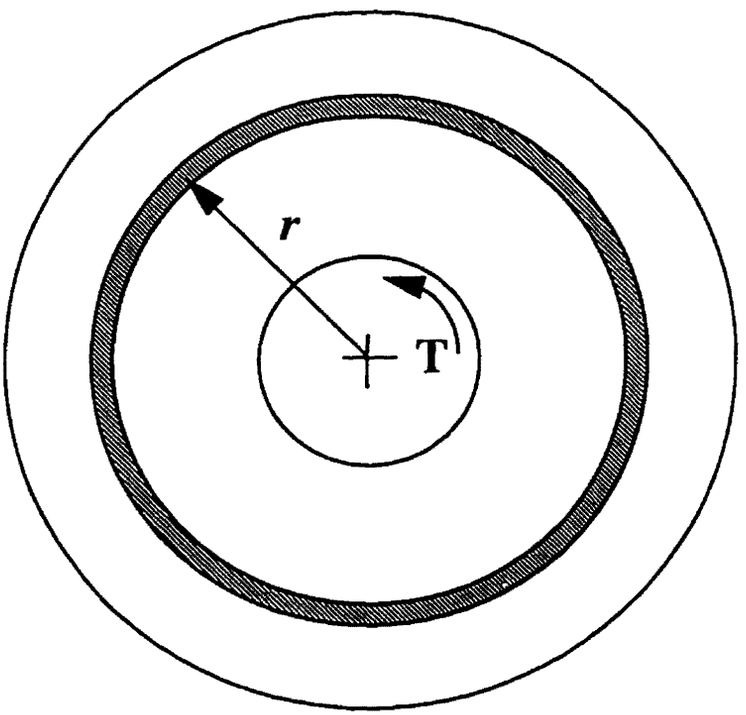


Figure 4.39: Internal moment in a thick-walled cylinder

where G_{eff}, the effective modulus of rigidity, is defined as

$$G_{eff} = \frac{E_{eff}}{2(1+\nu_{eff})} \tag{4.22}$$

This set of equations, along with equations for a pressurized cylinder (discussed in chapter 3), were used for the analysis of torsion-pressure loading of a thick walled cylinder. The cylinder dimensions and loading in this study were: internal radius of 22 mm, external radius of 66 mm, modulus of elasticity of 180 GPa, Poisson's ratio of 0.3, yield strength of 1070 MPa, α=3/7, m=5, internal pressure of 1000 MPa and internal torque of 4 MN-m. The results obtained from the present method were compared with results obtained by the author using ABAQUS. The deformation plasticity option in ABAQUS, which is based on Hencky's total deformation, was used for the finite element analysis. As mentioned before, this option in ABAQUS only allows for a Ramberg-Osgood model of material behavior. The stress and strain distribution through the wall thickness were obtained and are shown in Fig. 4.40 -4.48.

The general agreement is very good except for points close to the bore. ABAQUS does not allow for tangential distributed forces on the edge of elements. Therefore, to model the torque at the inner surface of the cylinder, appropriate concentrated forces were applied to the nodes at the bore. The application of these concentrated forces have local effects which are clearly seen, for example, in Fig. 4.41. An increase in the number of elements does not eliminate such local effects; however, it will reduce the scatter in the results since this effect is restricted to the first one or two elements at the bore. Hence, the results of the present solution, which uses the exact form for the displacement, stress and strain functions are believed to be more accurate at the bore.

An important application of multiaxial loading is nonproportional loading which is discussed in the next chapter.

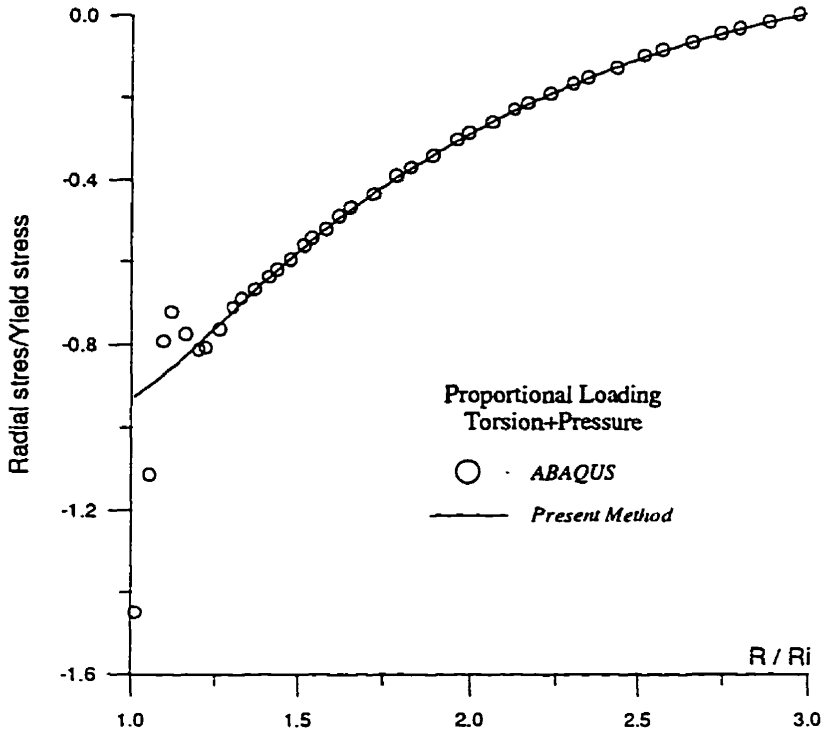


Figure 4.40: Comparison of radial stresses in multiaxial loading of cylinder

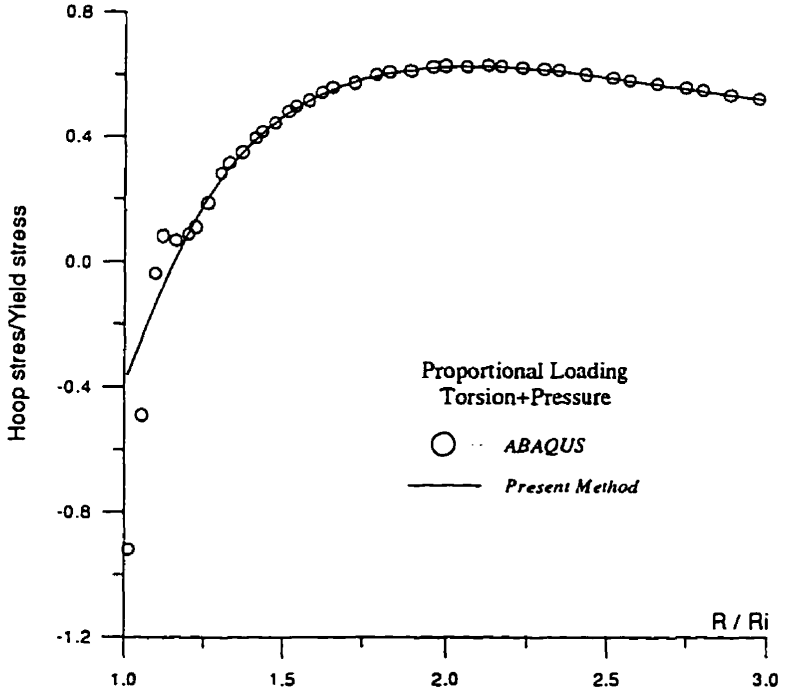


Figure 4.41: Comparison of hoop stresses in multiaxial loading of cylinder

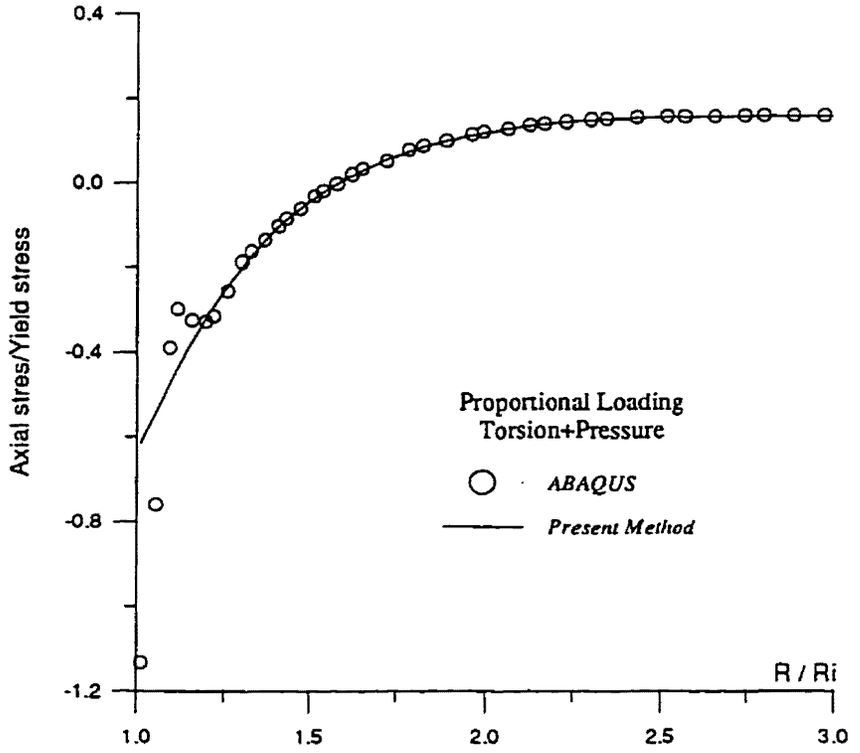


Figure 4.42: Comparison of axial stresses in multiaxial loading of cylinder

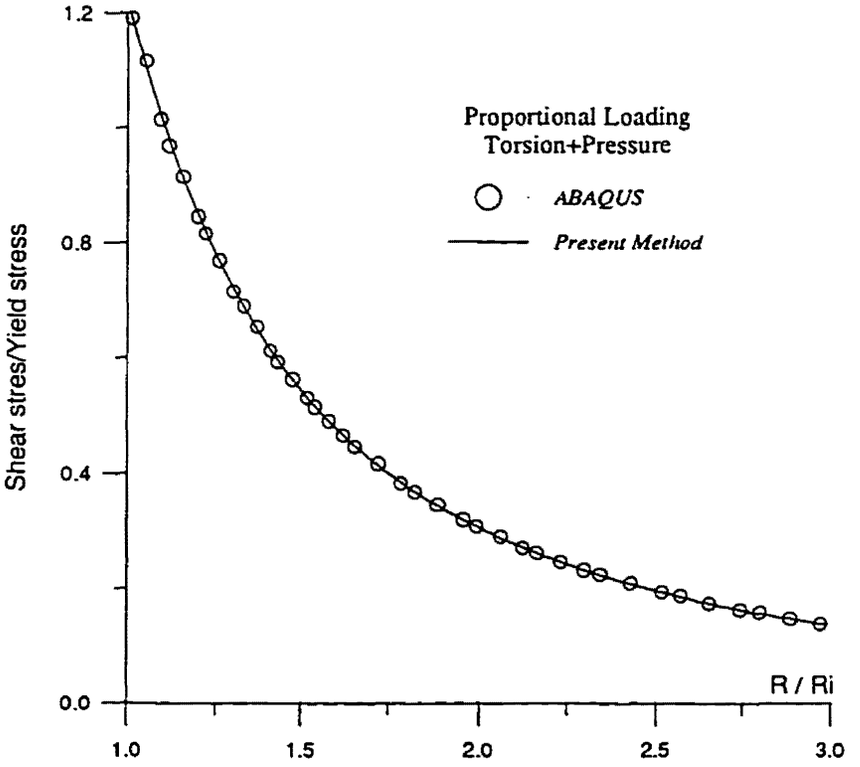


Figure 4.43: Comparison of shear stresses in multiaxial loading of cylinder

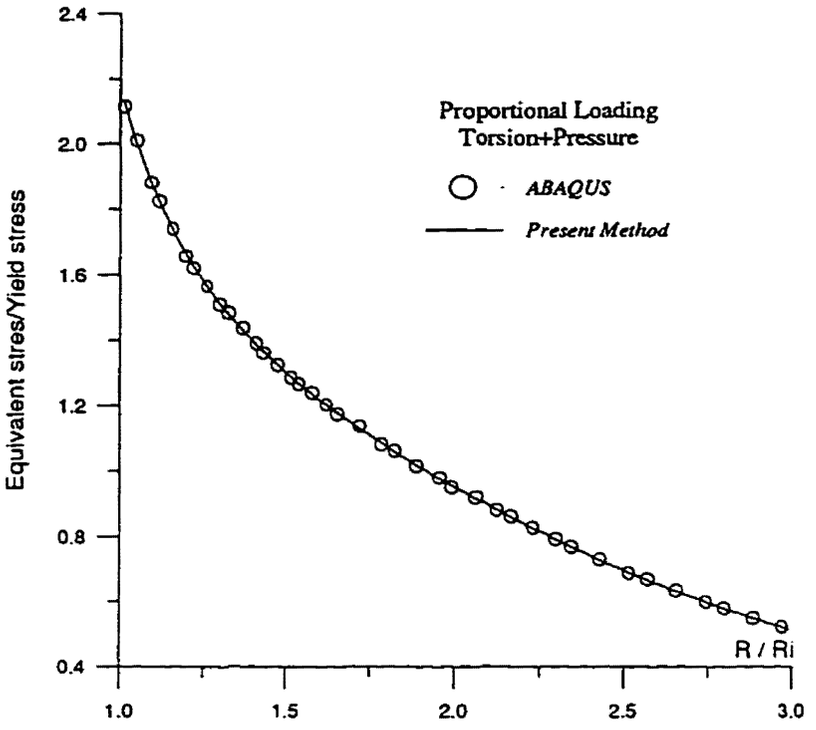


Figure 4.44: Comparison of equivalent stresses in multiaxial loading of cylinder

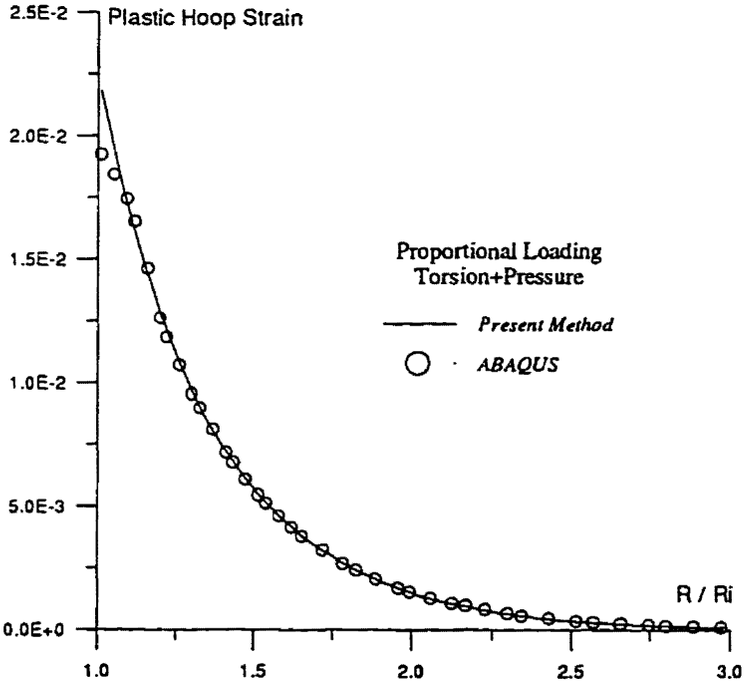


Figure 4.45: Comparison of plastic hoop strain in multiaxial loading of cylinder

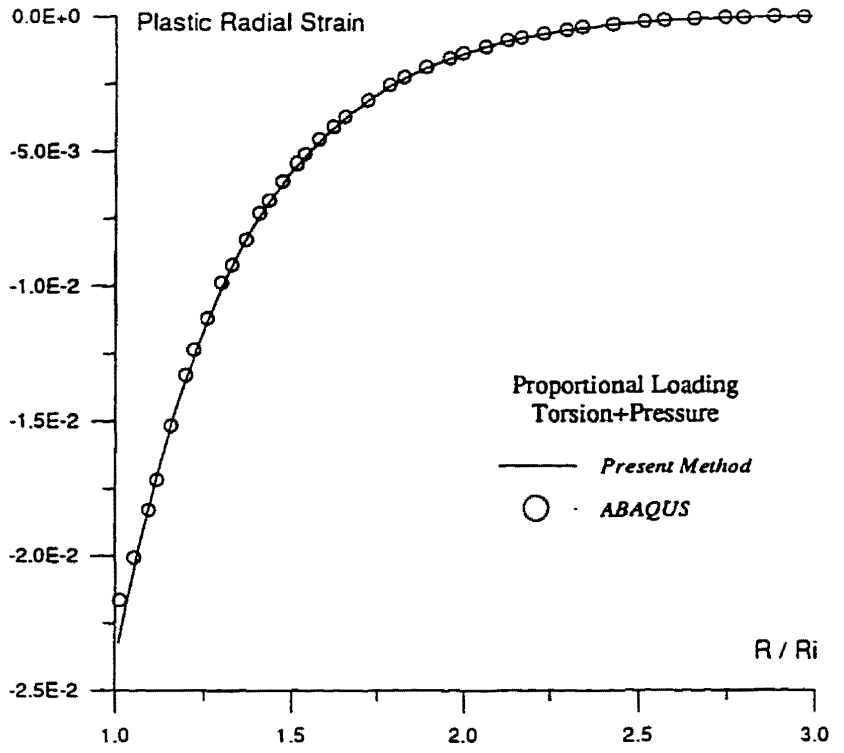


Figure 4.46: Comparison of plastic radial strain in multiaxial loading of cylinder

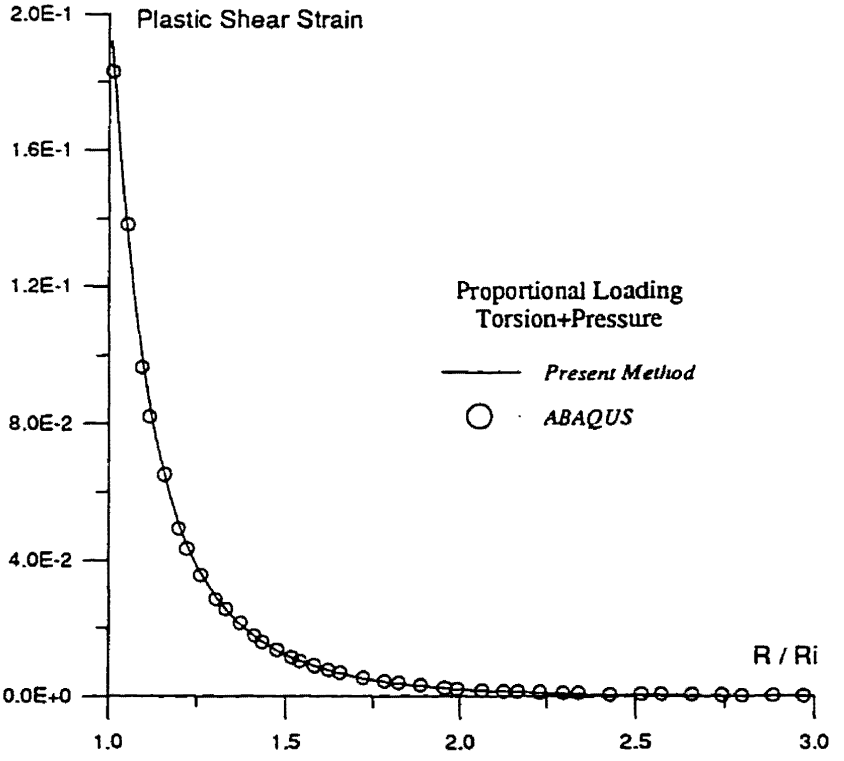


Figure 4.47: Comparison of plastic shear strain in multiaxial loading of cylinder

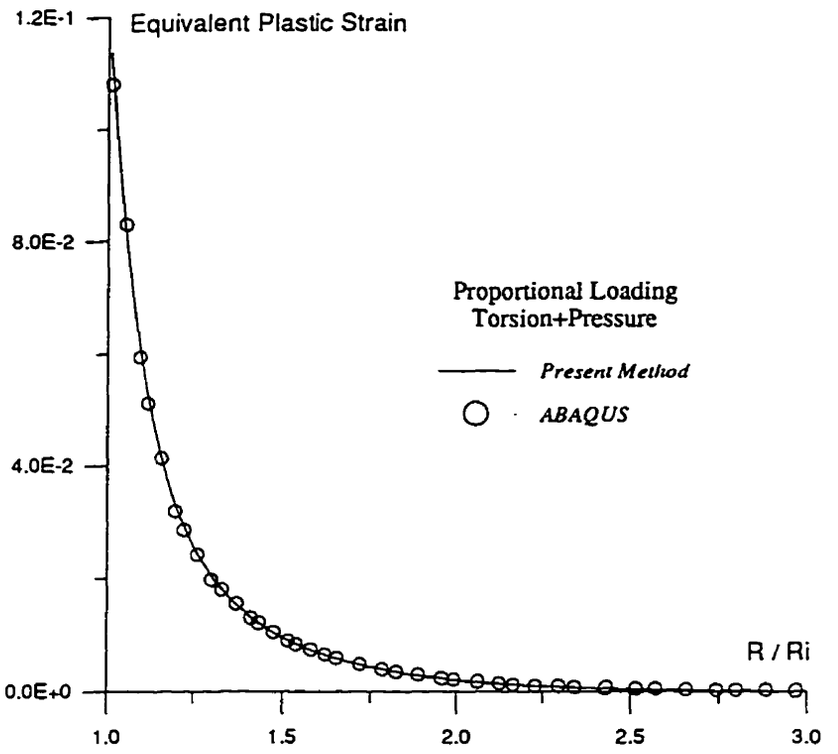


Figure 4.48: Comparison of equivalent plastic strain in multiaxial loading of cylinder

5. TOTAL DEFORMATION FORMULATION FOR NONPROPORTIONAL LOADING

5.1. INTRODUCTION

As pointed out in chapter 2 (sections 2.3.2-2.3.4), two main methods of elastic-plastic analysis are deformation plasticity and incremental plasticity. Total deformation plasticity (Eq. 2.23), which was postulated by H. Hencky (1924), presumes a one-to-one correspondence between stress and strain. Thus, the components of total plastic strain are taken to be proportional to the corresponding deviatoric stresses (see Eq. 2.23). Incremental plasticity (Eq. 2.27), which was proposed by L. Prandtl (1924) and A. Reuss (1930), sets a one-to-one correspondence between the increment of strain and the total stress. Thus, the components of the plastic strain increments are taken to be proportional to the corresponding deviatoric stresses (see Eq. 2.27). Although the Prandtl-Reuss relation provides the most satisfactory basis for treating plasticity problems, the theory is incremental and generally leads to mathematical and computational complexities. Considerable simplifications are often achieved by using deformation plasticity. However, as discussed in chapter 2, experimental results indicate that plastic strains depend not only on the current value of the stresses but also on the stress history. Hence, total deformation plasticity gives inaccurate strain fields for situations with nonproportional loading. Although the validity of total deformation theory can be proven mathematically for proportional loading (R. Hill, 1950) and its validity for limited degrees of nonproportional loading has been shown by B. Budiansky (1959), the validity of deformation theory for nonproportional loading, which can be represented as a sequence of linear loadings (one linear loading followed by a different linear loading), has not been adequately addressed in general.

In the following, a total deformation formulation is derived from the Prandtl-Ruess equation for a sequence of proportional loadings. The validity of the formulation is examined by applying it to thin-walled and thick-walled tubes under combined loading.

5.2. FORMULATION

It has been shown in section 2.3.4 that if all loads are applied so that their magnitudes are proportional, and if no unloading occurs, then incremental plasticity theory gives the same results as deformation theory. For a given point in a deforming solid, proportional stressing describes a condition where the stresses maintain a constant ratio as their values increase. This may be represented by the stress tensor, σ_{ij},

$$\sigma_{ij} = K^{\circ}\sigma_{ij} \tag{5.1}$$

or in terms of deviatoric stress tensor (Eq. 2.18), S_{ij},

$$S_{ij} = K^{\circ}S_{ij} \tag{5.2}$$

where ${}^{\circ}\sigma_{ij}$ or ${}^{\circ}S_{ij}$ is an arbitrary (nonzero) state of stress and K, the proportionality function, is a monotonically increasing function of time.

A typical nonproportional loading which is of interest here is shown in Fig. 5.1. The loading is a sequence of two linear loadings, i.e., linear loading OA and linear loading AB. Conventionally, a load path such as OA which passes through the origin of the principal stress space is considered a proportional loading. However, a loading path such as AB, even though it is still linear, is not considered proportional loading. It simply does not go through origin O.

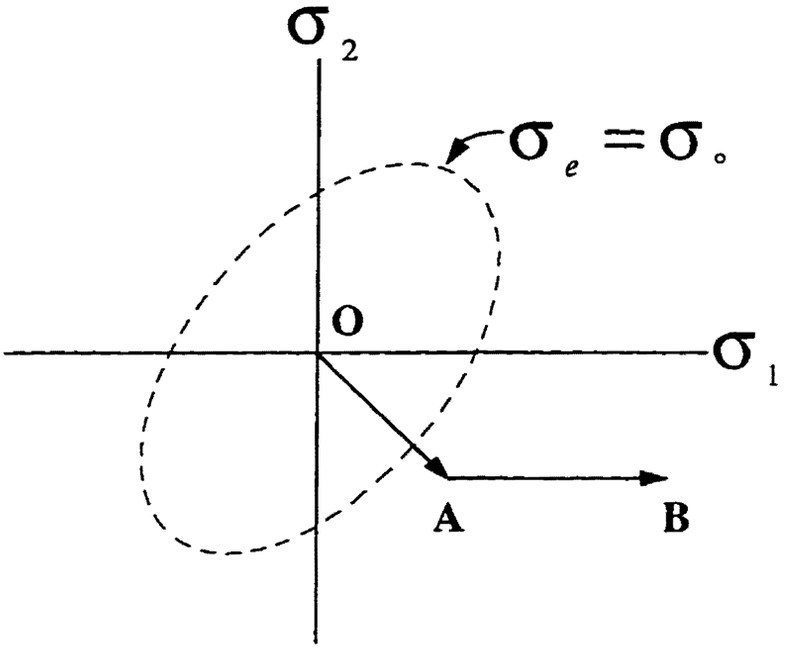


Figure 5.1: A typical sequence of proportional loading

The primary aim here is to define the second linear loading, AB, in a manner similar to proportional loadings. It is shown in this section that, if the second linear loading, AB, is taken with reference to point A rather than origin O, then it can be defined as a proportional loading.

The deviatoric stresses during the second linear loading AB (Fig. 5.1) may be written as

$$\begin{aligned} S_{ij} &= {}^{A}S_{ij} + K\Delta S_{ij} \\ \Delta S_{ij} &= {}^{B}S_{ij} - {}^{A}S_{ij} \end{aligned} \tag{5.3}$$

where ${}^{A}S_{ij}$ and ${}^{B}S_{ij}$ are the deviatoric components of the stress states at the end of loading state **A** and **B**, respectively. Further, the Mises equivalent stress

$$\sigma_e = \sqrt{\frac{3}{2} S_{ij} S_{ij}} \tag{5.4}$$

during the second loading will be

$$\sigma_e^{\,2} = K^2 \Delta\sigma_e^{\,2} - K\left(\Delta\sigma_e^{\,2} + {}^{A}\sigma_e^{\,2} - {}^{B}\sigma_e^{\,2}\right) + {}^{A}\sigma_e^{\,2} \tag{5.5}$$

where the change in equivalent stress, $\Delta\sigma_e$, is defined as

$$\Delta\sigma_e^{\,2} = \frac{3}{2} \Delta S_{ij} \Delta S_{ij} \tag{5.6}$$

Differentiating Eq. (5.5) with respect to K

$$\frac{d\sigma_e}{\sigma_e} = \frac{1}{2} \left\{ \frac{(2K-1)\Delta\sigma_e^{\,2} - {}^{A}\sigma_e^{\,2} + {}^{B}\sigma_e^{\,2}}{K^2 \Delta\sigma_e^{\,2} - K\left(\Delta\sigma_e^{\,2} + {}^{A}\sigma_e^{\,2} - {}^{B}\sigma_e^{\,2}\right) + {}^{A}\sigma_e^{\,2}} \right\} dK \tag{5.7}$$

and substituting in the Prandtl-Reuss equation

$$d\varepsilon_{ij} = \frac{3}{2} \frac{1}{E_p} \frac{d\sigma_e}{\sigma_e} S_{ij} \tag{5.8}$$

yields

$$d\varepsilon_{ij} = \frac{3}{4} \frac{1}{E_p} \left[\frac{(2K-1)\Delta\sigma_e^{\,2} - {}^{A}\sigma_e^{\,2} + {}^{B}\sigma_e^{\,2}}{K^2 \Delta\sigma_e^{\,2} - K\left(\Delta\sigma_e^{\,2} + {}^{A}\sigma_e^{\,2} - {}^{B}\sigma_e^{\,2}\right) + {}^{A}\sigma_e^{\,2}} \right] \left({}^{A}S_{ij} + K\Delta S_{ij} \right) dK \tag{5.9}$$

where $E_p = \frac{d\sigma_e}{d\varepsilon_e^{\,p}}$ is the plastic modulus. The change in plastic strain during the second loading can now be obtained by integrating the above equation

$$\Delta\varepsilon_{ij} = \int_0^1 \frac{3}{4}\frac{1}{E_p}\left[\frac{(2K-1)\Delta\sigma_e^{\,2} - {}^{A}\sigma_e^{\,2} + {}^{B}\sigma_e^{\,2}}{K^2\Delta\sigma_e^{\,2} - K\left(\Delta\sigma_e^{\,2} + {}^{A}\sigma_e^{\,2} - {}^{B}\sigma_e^{\,2}\right) + {}^{A}\sigma_e^{\,2}}\right]\left({}^{A}S_{ij} + K\Delta S_{ij}\right)dK \qquad (5.10)$$

where

$$\Delta\varepsilon_{ij} = {}^{B}\varepsilon_{ij} - {}^{A}\varepsilon_{ij} \qquad (5.11)$$

and the plastic strain at the end of the second loading, ${}^{B}\varepsilon_{ij}$, is of interest. The integrated form of Eq. (5.10) for two classes of material is obtained next.

5.2.1 Linear hardening materials

For linear hardening materials

$$\frac{1}{E_p} = \frac{1}{E_t} - \frac{1}{E} \qquad (5.12)$$

where E_t and E are the tangent and elastic moduli, respectively. Integration of Eq. (5.10) yields

$$\Delta\varepsilon_{ij} = \Delta\phi\left\{\left\{1 + \frac{(1+A)}{2}\ln C - \frac{B}{2}\left[\tan^{-1}\left(\frac{1-A}{B}\right) + \tan^{-1}\left(\frac{1+A}{B}\right)\right]\right\}\Delta S_{ij} + (\ln C)\,{}^{A}S_{ij}\right\} \qquad (5.13)$$

where

$$\Delta\phi = \frac{3}{2}\left(\frac{1}{E_t} - \frac{1}{E}\right) \tag{5.14}$$

and

$$A = \frac{{}^{A}\sigma_e{}^2 - {}^{B}\sigma_e{}^2}{\Delta\sigma_e{}^2}$$

$$B = \sqrt{4\frac{{}^{B}\sigma_e{}^2}{\Delta\sigma_e{}^2} - (1-A)^2} \tag{5.15}$$

$$C = \frac{{}^{B}\sigma_e}{{}^{A}\sigma_e}$$

the coefficients A, B and C depend on the end stress values only. This integration, performed using Maple, is given in Appendix B. The first term in Eq. (5.13), $\Delta\phi\ \Delta S_{ij}$, is a direct application of Hencky's equation for the second linear loading. Other terms are correction terms which account for the coupling effect of the two linear loadings. In other words, the remaining terms account for the path of stress. Application of this relation (Eq. 5.13) to a thin tube under tension and torsion, and a thick-walled cylinder under pressure and torsion are presented in section 5.5.

5.2.2 Hardening materials obeying Ramberg-Osgood equation

As mentioned in chapter 2, Ramberg and Osgood (1943) recommended the following power law

$$\varepsilon_e = \alpha \frac{\sigma_e}{E}\left(\frac{\sigma_e}{\sigma_\circ}\right)^{m-1} \tag{5.16}$$

for plastic strain dependency on equivalent stress in a uniaxial stress-strain curve. The plastic modulus therefore is given by

$$\frac{1}{E_p} = \frac{\alpha m}{E}\left(\frac{\sigma_e}{\sigma_\circ}\right)^{m-1} \tag{5.17}$$

The change in plastic strain can now be obtained from the following general equation

$$\begin{aligned}\Delta\varepsilon_{ij} = \int_0 \frac{3}{4}\frac{\alpha\ m}{E\sigma_Y^{m-1}}\left[K^2\Delta\sigma_e^{\,2} - K\left(\Delta\sigma_e^{\,2} + {}^A\sigma_e^{\,2} - {}^B\sigma_e^{\,2}\right) + {}^A\sigma_e^{\,2}\right]^{\left(\frac{m-3}{2}\right)} \\ \cdot \left[(2K-1)\Delta\sigma_e^{\,2} - {}^A\sigma_e^{\,2} + {}^B\sigma_e^{\,2}\right]\left({}^AS_{ij} + K\Delta S_{ij}\right)dK\end{aligned} \tag{5.18}$$

which can be integrated for any given value of m. For example, for a material with m=3, Eq. (5.18) reduces to

$$\Delta\varepsilon_{ij} = \frac{1}{4}\Delta\phi\Delta S_{ij} - \frac{3}{4}\Delta\phi\,(\Delta S_{ij} + 2\,{}^AS_{ij})\,A \tag{5.19}$$

where $\Delta\phi$ and A are defined in Eq. (5.15). For m=5, the form becomes

$$\Delta\varepsilon_{ij} = \frac{-1}{24}\Delta\phi\Delta S_{ij} + \frac{5}{24}\Delta\phi\left[(A^2 + D)\Delta S_{ij} - 3AD(\Delta S_{ij} + 2\,{}^AS_{ij})\right] \tag{5.20}$$

with

$$D = \frac{{}^{A}\sigma_e{}^2 + {}^{B}\sigma_e{}^2}{\Delta\sigma_e{}^2} \tag{5.21}$$

where $\Delta\phi$ is defined in Eq. (5.14) and A is defined in Eq. (5.15).

5.3. APPLICATION

The application of the above total deformation formulation will now be examined. A thin tube made of linear hardening material is considered first. The same tube, made of a material modeled by the Ramberg-Osgood equation, is examined next. The loading for both cases is combined tension and torsion. In the above cases, the proposed method is exact since the final stress state is known a priori. These thin tube results are compared with analytical solutions.

Linear hardening thick walled vessels under combined pressure and torsion are then discussed. For this problem, the final stress state is not known and an approximate method for plastic strain field calculation is proposed. This method estimates the strain field induced by a nonproportional loading using a number of proportional analyses along with the derived total deformation formulation. The thick walled tube results are compared to incremental finite element solutions produced by the author using ABAQUS.

5.3.1 Thin tubes under tension and torsion

First, the incremental plasticity solution to combined loading of a thin tube is discussed briefly. Results of this solution will be used later for comparison with the proposed method. Figure 5.2 shows a thin tube under tension and torsion. Two possible loading paths are shown in Fig. 5.3. The tube may be loaded first in tension (OC) and then in torsion (CB), or first in torsion (OA) and then in tension (AB).

The increment of plastic strain is related to the deviatoric stresses by

$$d\varepsilon_{ij} = d\lambda\, S_{ij} \tag{5.22}$$

where for a linear hardening material with tangent modulus E_p

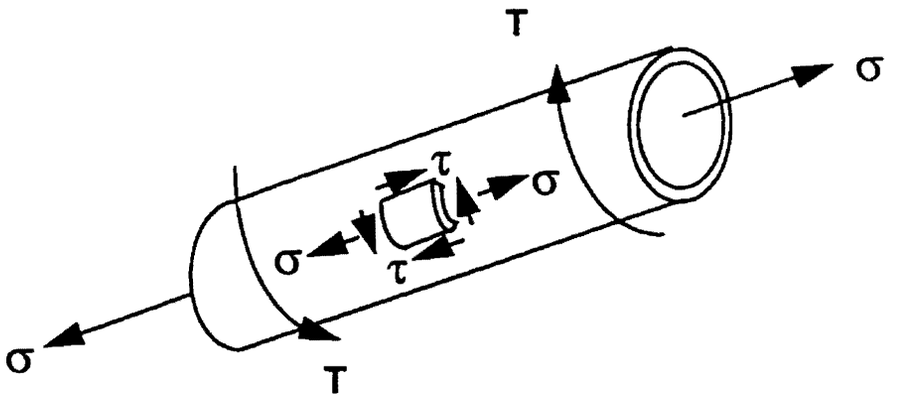


Figure 5.2: Thin tube under tension and torsion

$$d\lambda = \frac{3}{2}\frac{1}{E_p}\frac{d\sigma_e}{\sigma_e}. \tag{5.23}$$

For the present case

$$\sigma_e^{\,2} = \sigma^2 + 3\tau^2 \tag{5.24}$$

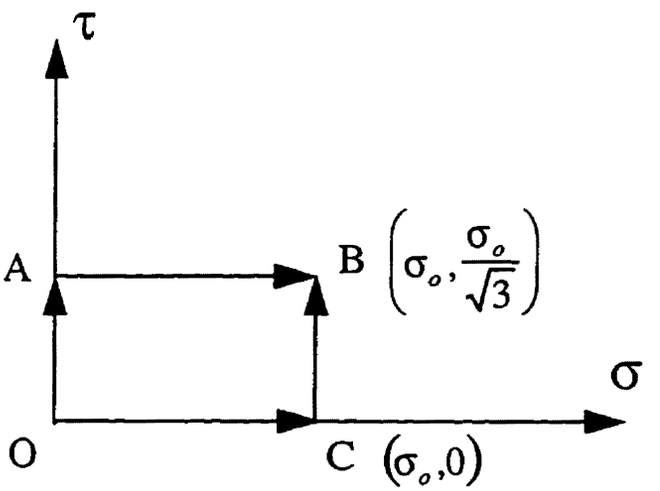


Figure 5.3: Different loading paths

where σ and τ are the axial and torsional stresses, respectively. Also,

$$\frac{d\sigma_{eq}}{\sigma_{eq}} = \frac{\sigma d\sigma + 3\tau d\tau}{\sigma^2 + 3\tau^2} \tag{5.25}$$

and noting that

$$S_{11} = \frac{2}{3}\sigma, \quad S_{12} = \tau \tag{5.26}$$

then from Eq. (5.22)

$$d\varepsilon^p = \frac{1}{E_p}\frac{\sigma^2 d\sigma + 3\tau\sigma d\tau}{\sigma^2 + 3\tau^2} \tag{5.27}$$

and

$$d\gamma^p = \frac{1}{E_p}\frac{3\sigma\tau d\sigma + 9\tau^2 d\tau}{\sigma^2 + 3\tau^2} \tag{5.28}$$

where $d\varepsilon^p$ and $d\gamma^p$ are the increments of plastic axial and shear strains, respectively. Each of the Eqs. (5.27) and (5.28) should be integrated along loading paths to give the value of the strains. For example, integration along path CB where

$$d\sigma = 0, \quad \sigma = \sigma_o, \quad \tau_C = 0, \quad \tau_B = \frac{\sigma_o}{\sqrt{3}} \tag{5.29}$$

yields

$$\varepsilon^p = \left(\frac{1}{E_t} - \frac{1}{E}\right) \ln(\sqrt{2})\, \sigma_o$$
$$\gamma = \sqrt{3}\left(\frac{1}{E_t} - \frac{1}{E}\right)\left(1 - \frac{\pi}{4}\right)\sigma_o \tag{5.30}$$

Similarly integration along path AB where

$$d\tau = 0, \quad \tau = \frac{\sigma_o}{\sqrt{3}}, \quad \sigma_A = 0, \quad \sigma_B = \sigma_o \tag{5.31}$$

yields

$$\varepsilon^p = \left(\frac{1}{E_t} - \frac{1}{E}\right)\left(1 - \frac{\pi}{4}\right)\sigma_o$$
$$\gamma = \sqrt{3}\left(\frac{1}{E_t} - \frac{1}{E}\right) \ln(\sqrt{2})\, \sigma_o \tag{5.32}$$

For a material obeying the Ramberg-Osgood formula where the plastic modulus is given by Eq. (5.17), the increment of plastic strains are

$$d\varepsilon^p = \frac{\alpha m}{E}\left(\frac{\sigma_e}{\sigma_o}\right)^{m-1} \frac{\sigma^2 d\sigma + 3\tau\sigma d\tau}{\sigma^2 + 3\tau^2}$$
$$d\gamma^p = \frac{\alpha m}{E}\left(\frac{\sigma_e}{\sigma_o}\right)^{m-1} \frac{3\sigma\tau d\sigma + 9\tau^2 d\tau}{\sigma^2 + 3\tau^2} \tag{5.33}$$

These equation should be integrated along the path of loading. For example, for a material with $\alpha=3/7$ and m=5, the integration along path CB yields

$$\varepsilon^{p}=\frac{45}{28E}\sigma_{\bullet}$$
$$\gamma^{p}=\frac{8\sqrt{3}}{7E}\sigma_{\bullet} \tag{5.34}$$

Likewise, integration along path AB gives

$$\varepsilon^{p}=\frac{8}{7E}\sigma_{\bullet}$$
$$\gamma^{p}=\frac{45\sqrt{3}}{28E}\sigma_{\bullet} \tag{5.35}$$

5.3.1.1 Linear hardening materials

Figure 5.4 shows a linear hardening material characterized by E and E_t, the elastic and tangent moduli, respectively. The stress-strain relationship for these materials is given by

$$\varepsilon=\begin{cases}\dfrac{\sigma}{\varepsilon} & \sigma \le \sigma_0 \\ \dfrac{\sigma_o}{E}+\dfrac{\sigma-\sigma_0}{E_t} & \sigma \ge \sigma_o\end{cases} \tag{5.36}$$

where σ_o is the yield stress.

Let the loading paths be described as shown in Fig. 5.3 . Two different routes for arriving at B, OCB and OAB, are considered next. Note that in each case, the first loading path just produces yielding.

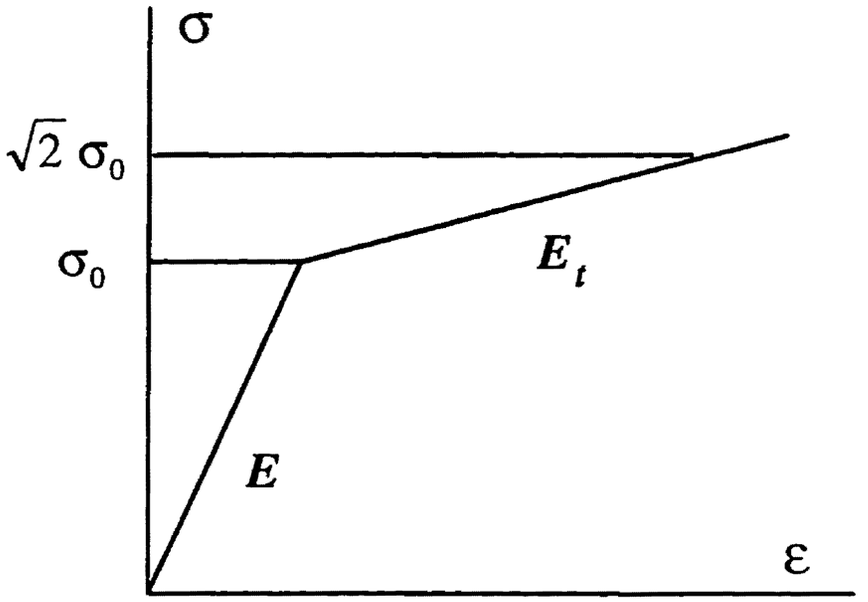


Figure 5.4: Linear hardening material

5.3.1.1.1 Tension-torsion (path OCB)

Figure 5.5 shows the loading paths based on the von Mises yield criterion in stress space. No plastic strain is induced from O to C, since C corresponds to the onset of yielding, as illustrated in Fig. 5.5. From C to B, Eq. (5.13) can be used to obtain the plastic strain at B. For this linear loading the equivalent stresses are

$$ {}^{C}\sigma_e = \sigma_0 \qquad {}^{B}\sigma_e = \sqrt{2}\,\sigma_0 \qquad \Delta\sigma_e = \sigma_o \tag{5.37} $$

and the deviatoric stresses at the end of each loading stage are

$$ {}^{C}S_{ij} = \begin{bmatrix} \frac{2}{3}\sigma_o & 0 \\ 0 & \frac{-1}{3}\sigma_o \end{bmatrix} \qquad {}^{B}S_{ij} = \begin{bmatrix} \frac{2}{3}\sigma_o & \frac{1}{\sqrt{3}}\sigma_o \\ \frac{1}{\sqrt{3}}\sigma_o & \frac{-1}{3}\sigma_o \end{bmatrix} \tag{5.38} $$

so that the change in deviatoric stress is

$$\Delta S_{ij} = \begin{bmatrix} 0 & \frac{1}{\sqrt{3}}\sigma_o \\ \frac{1}{\sqrt{3}}\sigma_o & 0 \end{bmatrix}. \tag{5.39}$$

Also, the coefficients in Eq. (5.13) are

$$\begin{aligned} A &= \frac{{}^{A}\sigma_e{}^2 - {}^{B}\sigma_e{}^2}{\Delta\sigma_e{}^2} = -1 \\ B &= \sqrt{4\frac{{}^{B}\sigma_e{}^2}{\Delta\sigma_e{}^2} - (1-A)^2} = 2 \\ C &= \frac{{}^{B}\sigma_e}{{}^{A}\sigma_e} = \sqrt{2} \end{aligned} \tag{5.40}$$

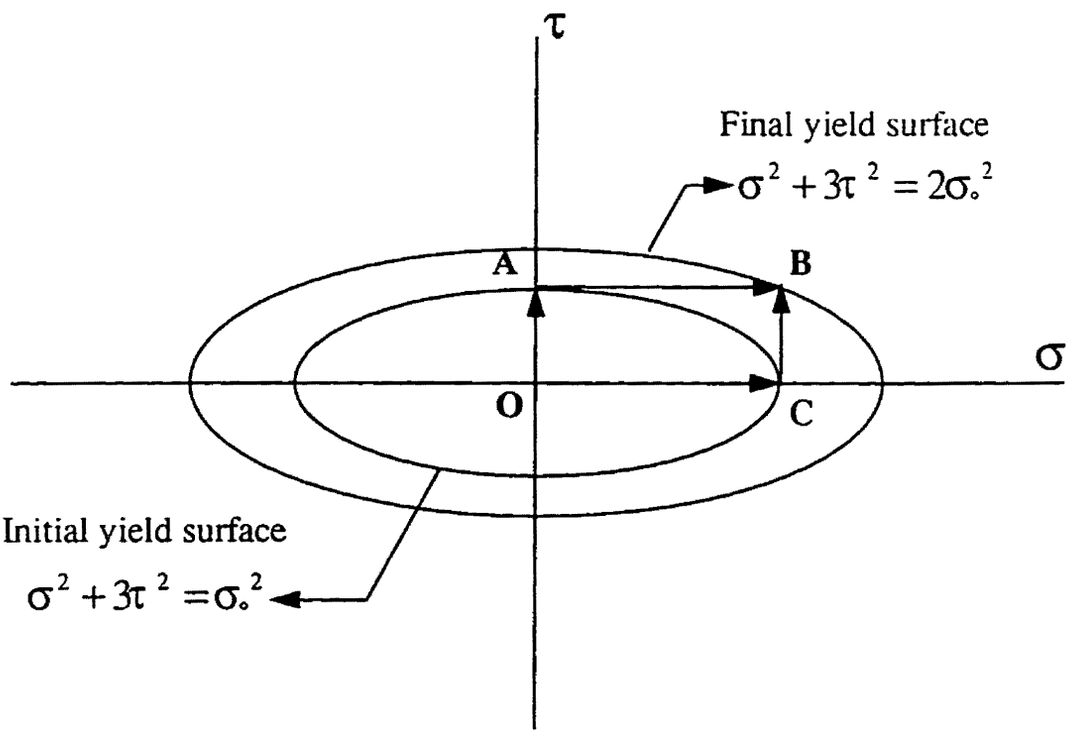


Figure 5.5: Loading path for von Mises isotropic material under consideration

and substitution into Eq. (5.13) yields

$$\Delta\varepsilon_{ij}{}^{P} = \frac{3}{2}\left(\frac{1}{E_t}-\frac{1}{E}\right)\left\{\left(1-\frac{\pi}{4}\right)\begin{bmatrix} 0 & \sigma_o/\sqrt{3} \\ \sigma_o/\sqrt{3} & 0 \end{bmatrix}+\ln(\sqrt{2})\begin{bmatrix} \frac{2}{3}\sigma_o & 0 \\ 0 & \frac{-1}{3}\sigma_o \end{bmatrix}\right\} \tag{5.41}$$

which gives the following values for strain at the end of loading

$$\begin{aligned} \Delta\varepsilon_{11}{}^{P} &= \left(\frac{1}{E_t}-\frac{1}{E}\right)\ln(\sqrt{2})\,\sigma_o \\ \Delta\varepsilon_{22}{}^{P} = \Delta\varepsilon_{33}{}^{P} &= \frac{-1}{2}\left(\frac{1}{E_t}-\frac{1}{E}\right)\ln(\sqrt{2})\,\sigma_o \\ \Delta\gamma &= \sqrt{3}\left(\frac{1}{E_t}-\frac{1}{E}\right)\left(1-\frac{\pi}{4}\right)\sigma_o \end{aligned} \tag{5.42}$$

These results agree with the incremental solution given by Eq. (5.30).

5.3.1.1.2 Torsion-tension (path OAB)

No plastic strain is induced from O to A, since A corresponds to the onset of yielding (Fig. 5.5). From A to B, Eq. (5.13) can be used to obtain plastic strain at B. For this proportional loading the equivalent stresses are

$$^{A}\sigma_e = \sigma_0 \qquad {}^{B}\sigma_e = \sqrt{2}\,\sigma_0 \qquad \Delta\sigma_e = \sigma_o \tag{5.43}$$

and the deviatoric stresses at the end of each proportional loading are

$$ {}^{A}S_{ij} = \begin{bmatrix} 0 & \frac{1}{\sqrt{3}}\sigma_o \\ \frac{1}{\sqrt{3}}\sigma_o & 0 \end{bmatrix} \qquad {}^{B}S_{ij} = \begin{bmatrix} \frac{2}{3}\sigma_o & \frac{1}{\sqrt{3}}\sigma_o \\ \frac{1}{\sqrt{3}}\sigma_o & \frac{-1}{3}\sigma_o \end{bmatrix} \tag{5.44} $$

and the change in stress is

$$ \Delta S_{ij} = \begin{bmatrix} \frac{2}{3}\sigma_o & 0 \\ 0 & \frac{-1}{3}\sigma_o \end{bmatrix}. \tag{5.45} $$

Substitution into Eq. (5.13) results in

$$ \Delta\varepsilon_{ij}{}^{p} = \frac{3}{2}\left(\frac{1}{E_t}-\frac{1}{E}\right)\left\{\left(1-\frac{\pi}{4}\right)\begin{bmatrix} \frac{2}{3}\sigma_o & 0 \\ 0 & \frac{-1}{3}\sigma_o \end{bmatrix} + \ln\left(\sqrt{2}\right)\begin{bmatrix} 0 & \sigma_o/\sqrt{3} \\ \sigma_o/\sqrt{3} & 0 \end{bmatrix}\right\} \tag{5.46} $$

which gives the following strain values

$$ \begin{aligned} \Delta\varepsilon_{11}{}^{p} &= \left(\frac{1}{E_t}-\frac{1}{E}\right)\left(1-\frac{\pi}{4}\right)\sigma_o \\ \Delta\varepsilon_{22}{}^{p} = \Delta\varepsilon_{33}{}^{p} &= \frac{-1}{2}\left(\frac{1}{E_t}-\frac{1}{E}\right)\left(1-\frac{\pi}{4}\right)\sigma_o \\ \Delta\gamma &= \sqrt{3}\left(\frac{1}{E_t}-\frac{1}{E}\right)\ln\left(\sqrt{2}\right)\sigma_o \end{aligned} \tag{5.47} $$

These results agree with the incremental solution given by Eq. (5.32).

5.3.1.2 Materials obeying the Ramberg-Osgood relation

In this section, materials obeying the Ramberg-Osgood relation are examined. To simplify mathematical manipulation, it is assumed that $\alpha=3/7$ and $m=5$. However, it will be shown later that this is not necessary.

In this case, equivalent plastic strain is related to equivalent stress through Eq. (5.16). The loading path is the same as shown in Fig. 5.3 andFig. 5.5. using Eq. (5.17), the plastic modulus takes the following form:

$$\frac{1}{E_p}=\frac{15}{7E}\left(\frac{\sigma_e}{\sigma_*}\right)^4. \tag{5.48}$$

Plastic strains for the two load paths, OCB and OAB, are obtained below.

5.3.1.2.1 Tension-torsion (path OCB)

The equivalent stresses, the deviatoric stress tensors at the end of each loading, and the change in the deviatoric stress tensor are the same as in Eqs. (5.37), (5.38) and (5.39), respectively. Therefore, the two coefficients in Eq. (5.20) are

$$\begin{aligned} A&=\frac{{}^{A}\sigma_e{}^2-{}^{B}\sigma_e{}^2}{\Delta\sigma_e{}^2}=-1\\ D&=\frac{{}^{A}\sigma_e{}^2+{}^{B}\sigma_e{}^2}{\Delta\sigma_e{}^2}=3. \end{aligned} \tag{5.49}$$

Substitution in Eq. (5.20) yields

$$\Delta\varepsilon_{ij} = \frac{15}{112}\frac{1}{E}\left\{\frac{64}{5}\begin{bmatrix} 0 & \frac{1}{\sqrt{3}}\sigma_o \\ \frac{1}{\sqrt{3}}\sigma_o & 0 \end{bmatrix} + 18\begin{bmatrix} \frac{2}{3}\sigma_o & 0 \\ 0 & \frac{-1}{3}\sigma_o \end{bmatrix}\right\} \tag{5.50}$$

which gives the following strains:

$$\begin{aligned} \varepsilon_{11}{}^{P} &= \frac{45}{28E}\sigma_o \\ \gamma^{P} &= \frac{8\sqrt{3}}{7E}\sigma_o \end{aligned} \tag{5.51}$$

These results agree with the incremental solution given by Eq. (5.34).

5.3.1.2.2 Torsion-tension (path OAB)

The equivalent stresses, the deviatoric stress tensors at the end of each loading, and the change in the deviatoric stress tensor are the same as in Eqs. (5.43), (5.44) and (5.45), respectively. Therefore, the two coefficient obtained from Eq. (5.20) are the same as given in Eq. (5.49). Substitution in Eq. (5.20) yields

$$\Delta\varepsilon_{ij} = \frac{15}{112}\frac{1}{E}\left\{\frac{64}{5}\begin{bmatrix} \frac{2}{3}\sigma_o & 0 \\ 0 & \frac{-1}{3}\sigma_o \end{bmatrix} + 18\begin{bmatrix} 0 & \frac{1}{\sqrt{3}}\sigma_o \\ \frac{1}{\sqrt{3}}\sigma_o & 0 \end{bmatrix}\right\} \tag{5.52}$$

which gives the following strains:

$$\varepsilon_{11}^{\ p} = \frac{8}{7E}\sigma_{\bullet}$$
$$\gamma^{p} = \frac{45\sqrt{3}}{28E}\sigma_{\bullet}\,. \tag{5.53}$$

These results agree with the incremental solution given by Eq. (5.35).

In conclusion, for situations where stresses are known a priori such as the examples considered in this section, the derived formulation and the incremental plasticity are the same.

5.3.2 Nonproportional loading of thick walled cylinders

The method of elastic-plastic analysis proposed in chapter 3 and applied in chapter 4 is based on total deformation plasticity. Although it has been modified to handle unloading, it cannot handle nonproportional loading. One natural extension of the proposed method is to nonproportional loading.

The formulation derived in section 5.1 gives answers similar to incremental plasticity provided the exact stress field is known. In other words, it works very well for cases with a known stress field. However, in situations where stresses are not known, such as a thick-walled vessel under pressure sufficient to produce plasticity, the applied pressure is known but not the stress. The application of torsion following an applied pressure not only produces shear strains and stresses but also changes the normal stresses and strains.

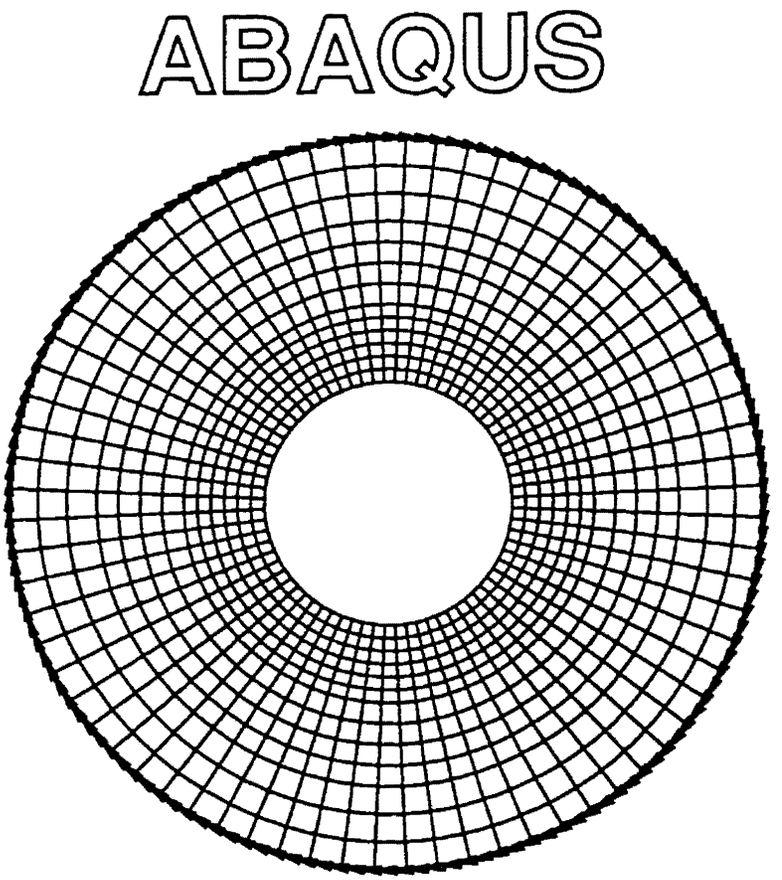


Figure 5.6: Finite element mesh (undeformed configuration)

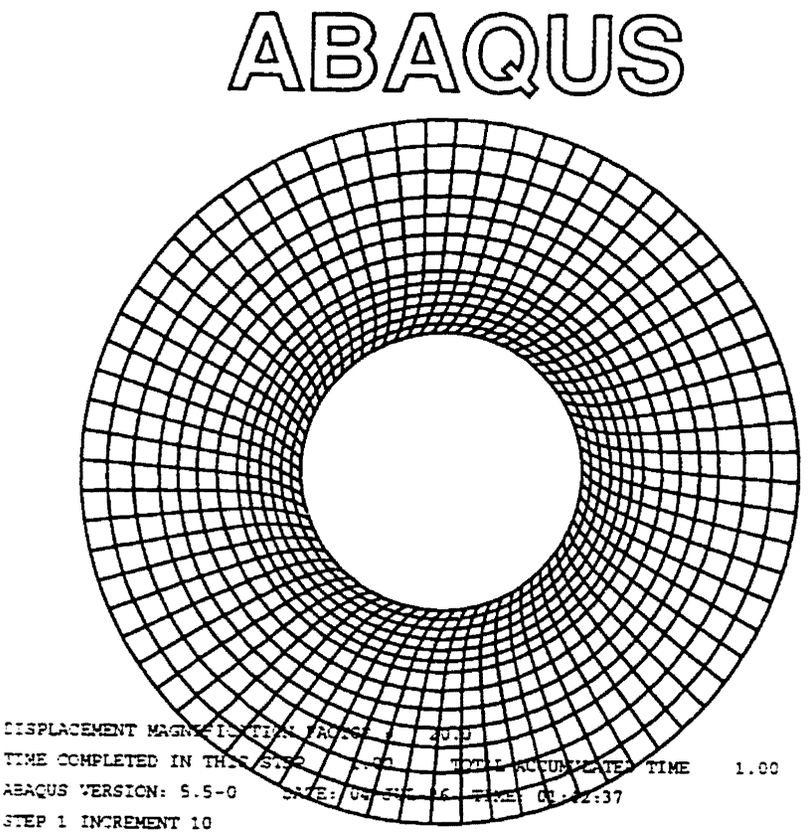


Figure 5.7: Finite element mesh (deformed configuration)

This makes the process much more complex and requires long computational times for a conventional incremental solution. To use the proposed formulation for nonproportional loading of a thick walled cylinder, the stress field at the end of each loading is needed. To obtain the proper stress field it is necessary to consider different factors such as computation time, complexity, and accuracy.

First, a conventional incremental solution for a thick walled cylinder under nonproportional pressure and torsion was obtained using ABAQUS version 5.6 (Hibbit, Karlsson & Sorensen, 1996). As shown in Fig. 5.6, the mesh was generated for the whole cylinder. The applied pressure was assumed to be uniformly distributed on the internal surface. The internal torque was simulated by applying proper tangential concentrated forces at the nodes of the internal surface. The nodes at the outer surface were fixed. Figure 5.7 shows the deformed shape of the finite element model.

ABAQUS offers two plasticity options: incremental plasticity (Prandtl-Reuss equation) and deformation plasticity (Hencky's equation). The deformation plasticity option is based on isotropic hardening and the von Mises yield criterion. This option describes the equivalent stress and equivalent plastic strain relationship using the Ramberg-Osgood relation. The incremental plasticity option uses the same hardening and yield criterion. However, this option uses a multi-linear equivalent stress-equivalent plastic strain relationship. The elastic analysis in this option is entirely linear and is based on the elastic modulus and the yield stress.

There have been a number of comparisons of the two plasticity theories for thick walled cylinders under internal pressure (for example, Hodge et al., 1950 and Chen, 1973). However, none have considered nonproportional loading as a basis for comparison. In this study, the two plasticity theories were compared for a thick cylinder under a sequence of linear loadings. Attention was focused on computational time vs stress field results. It was observed that when deformation plasticity option (Hencky's equation) is used, the CPU time is less than 40% of that in incremental plasticity.

The strain fields predicted by the two theories, as expected, are quite different. A typical plastic hoop strain distribution, as predicted by the two theories, is shown in Fig. 5.8. The total deformation prediction of the plastic hoop strain at the bore is two times that predicted by incremental plasticity. However, the stress field predicted by the two analyses remain reasonably close, especially for cases with larger plastic zones.

Figures 5.9 -5.13 show a comparison of the stress fields from the two analyses for two nonproportional loading path in linear hardening materials. In one case, pressure is applied first followed by torsion, whereas in the second case, torsion is applied first. It is evident from these graphs that the stresses remain reasonably close when different plasticity theories are used. This suggests that for this case at least, one could use the stress field predicted by proportional loading. Therefore, this stress field can be employed in the total deformation formulation presented here in. In this manner, instead of a lengthy incremental solution, a proportional loading solution can be used.

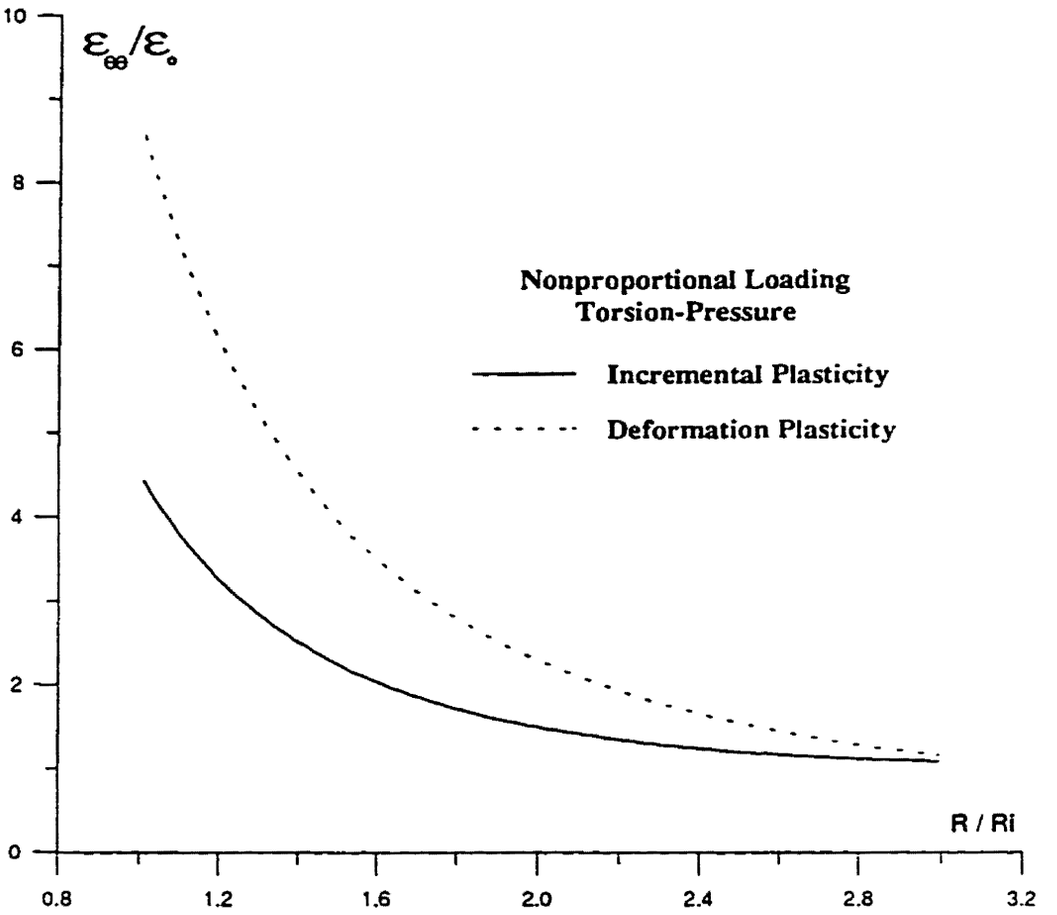


Figure 5.8: Comparison of plastic hoop strain predictions of the two plasticity theories (deformation and incremental) for a nonproportional loading

The total deformation theory proposed here (Eq. 5.13) requires the end values of stress for each linear loading. For a nonproportional loading, such as thick cylinder under torsion and tension, these stresses may be obtained by a proportional analysis. In this way significant CPU time is saved. These stresses, obtained from Eq. (5.13), will then give the plastic strain field for the corresponding nonproportional loading. That is, the stress field due to the application of pressure only, along with the stress field due to the application of proportional pressure and torsion may be used in Eq. (5.13) to estimate the plastic strain field for a corresponding nonproportional loading.

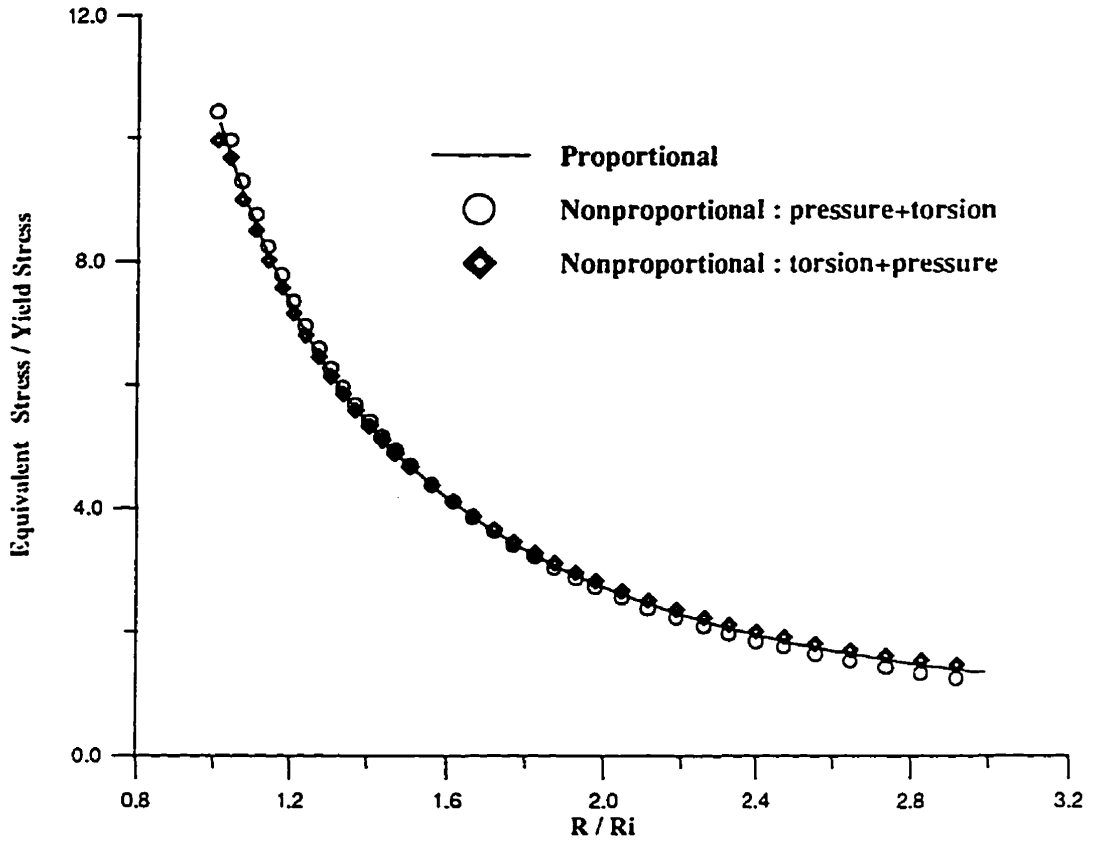


Figure 5.9: Stress comparison (proportional vs nonproportional), equivalent stress

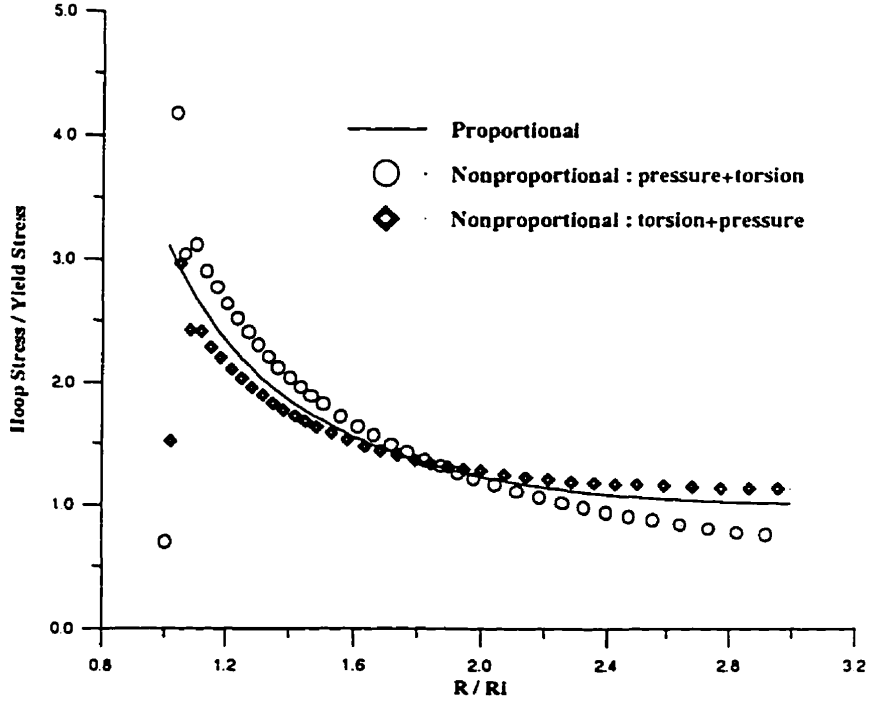


Figure 5.10: Stress comparison (proportional vs nonproportional), hoop stress

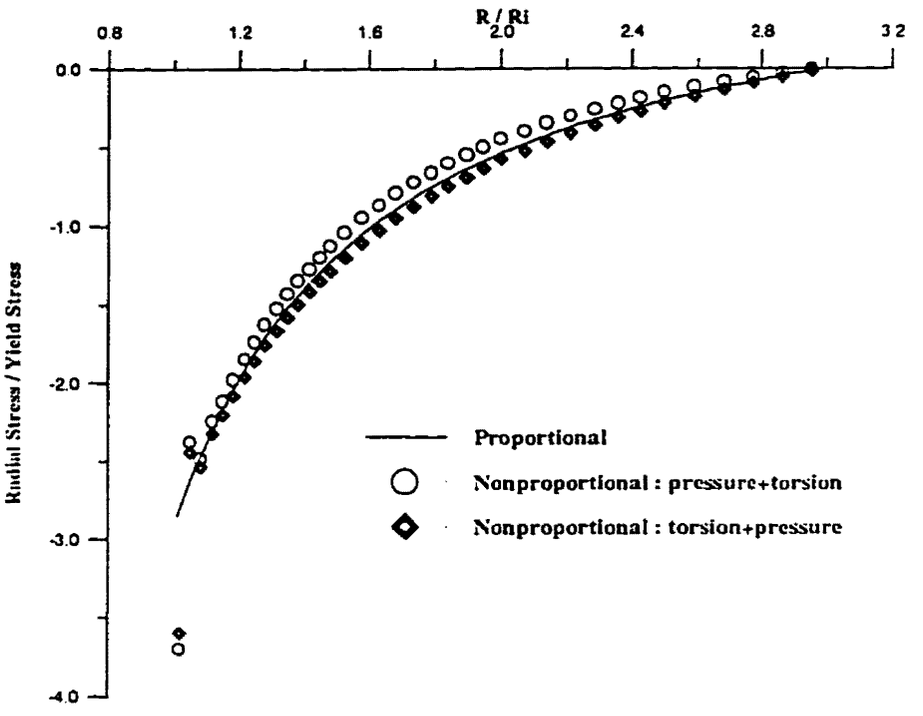


Figure 5.11: Stress comparison (proportional vs nonproportional), radial stress

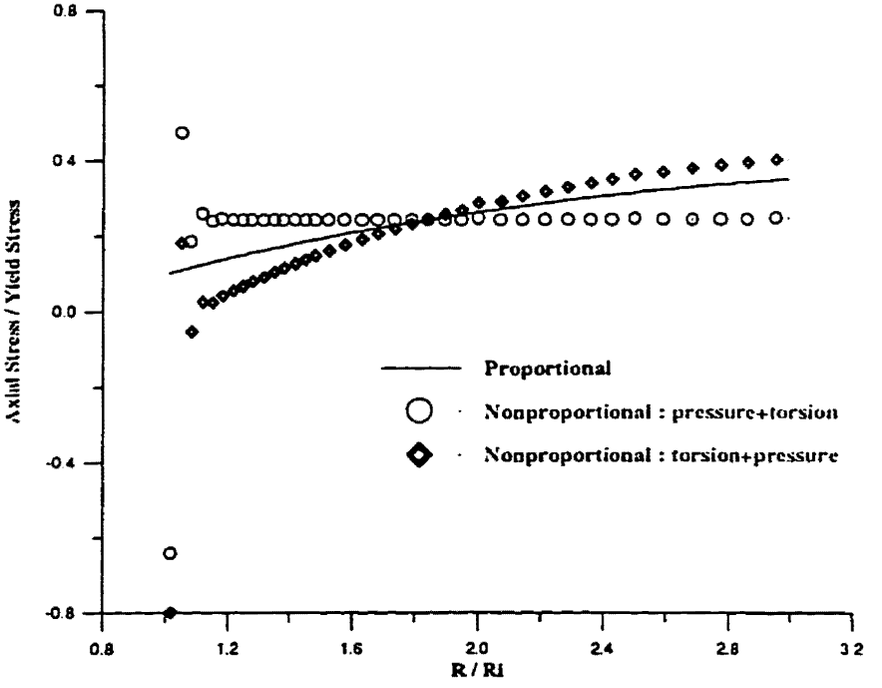


Figure 5.12: Stress comparison (proportional vs nonproportional), axial stress

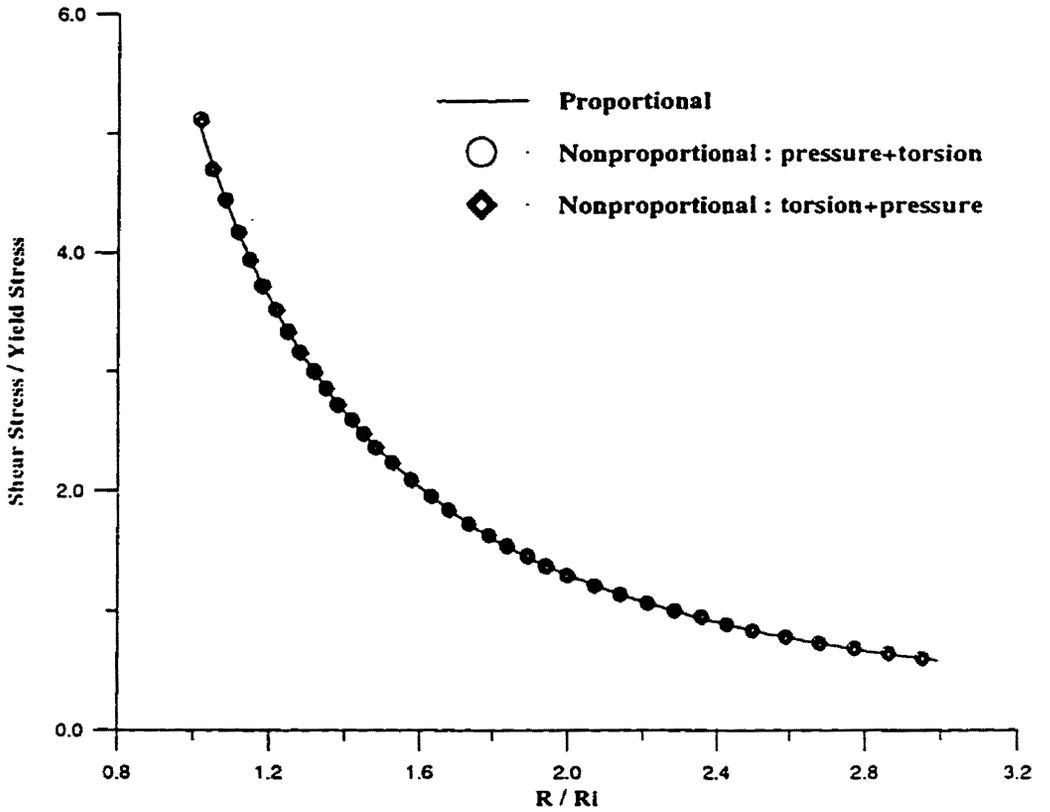


Figure 5.13: Stress comparison (proportional vs nonproportional), shear stress

5.3.2.1 Plastic strain field

To estimate the strain field of a thick walled cylinder under nonproportional loading, the stress field of two proportional loadings were used in Eq. (5.13). These stress fields can be easily obtained from the proposed method in chapter 3. Since the stress field obtained in this manner is close to that of the incremental solution for a linear hardening thick walled cylinder, one would expect the strain field also to be close. Appendix C shows the subroutine that was added to the main program (see Appendix A) for axisymmetric elastic-plastic analysis. Note that this subroutine, for the Ramberg-Osgood relation with different hardening exponents, is automatically generated by MAPLE V (Waterloo Maple Inc., 1996) once the integration is performed.

5.3.2.1.1 Torsion-pressure

The stress field resulting from the application of torsion alone, along with the stress field resulting from the application of torsion and pressure together were used in Eq. (5.13) to estimate the changes in the plastic strain field during the application of pressure. This value was then added to the plastic strain at the end of the first loading (application of torsion) to give the total plastic strain field. The resulting strain field is compared with the strain field obtained from a nonproportional loading, incremental plasticity solution using ABAQUS. These results, which are shown in Figures 5.14 -5.16 , show a very close agreement with the incremental solution. The strain field predicted by the conventional deformation theory of plasticity is also shown. As discussed in section 4.4 the scatter in FEM results at the bore is due to local effect of tangential concentrated forces on the node at the bore. Both the deformation plasticity and proposed method solutions in these graphs were obtained from the axisymmetric elastic-plastic analysis proposed in chapter 3. The computational time for the proposed method solution in these examples were a few (15-25) seconds on a 100 MHz, 486 personal computer.

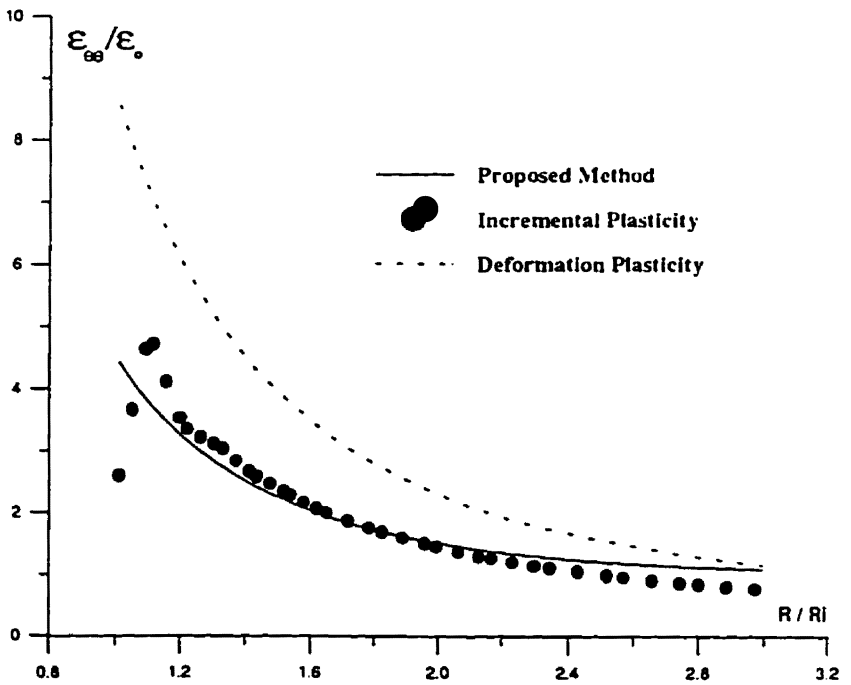


Figure 5.14: Strain comparison (incremental vs present method), hoop strain

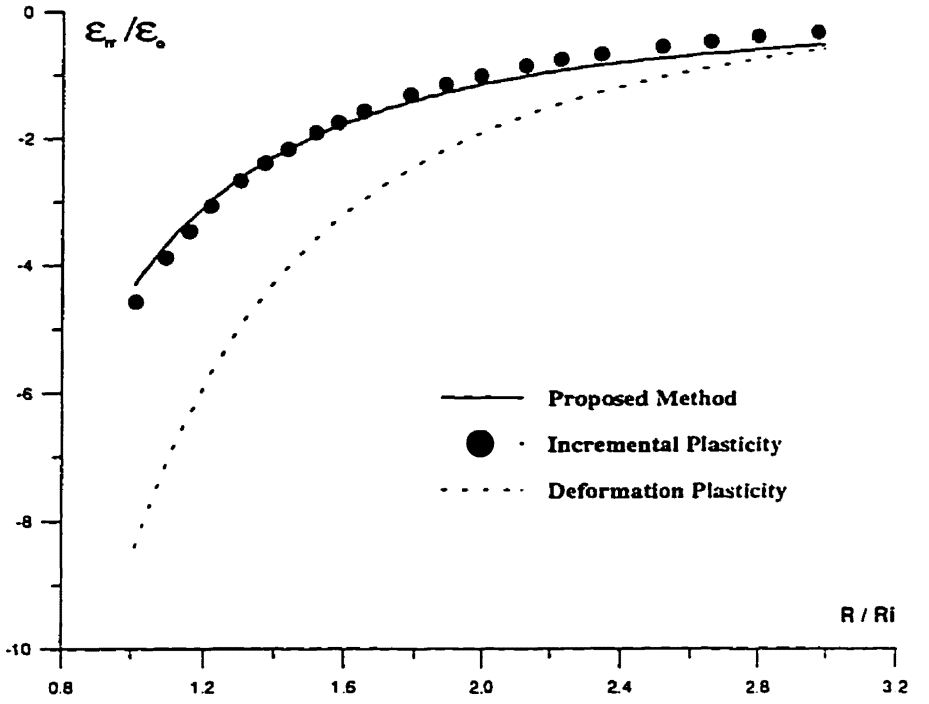


Figure 5.15: Strain comparison (incremental vs present method), radial strain

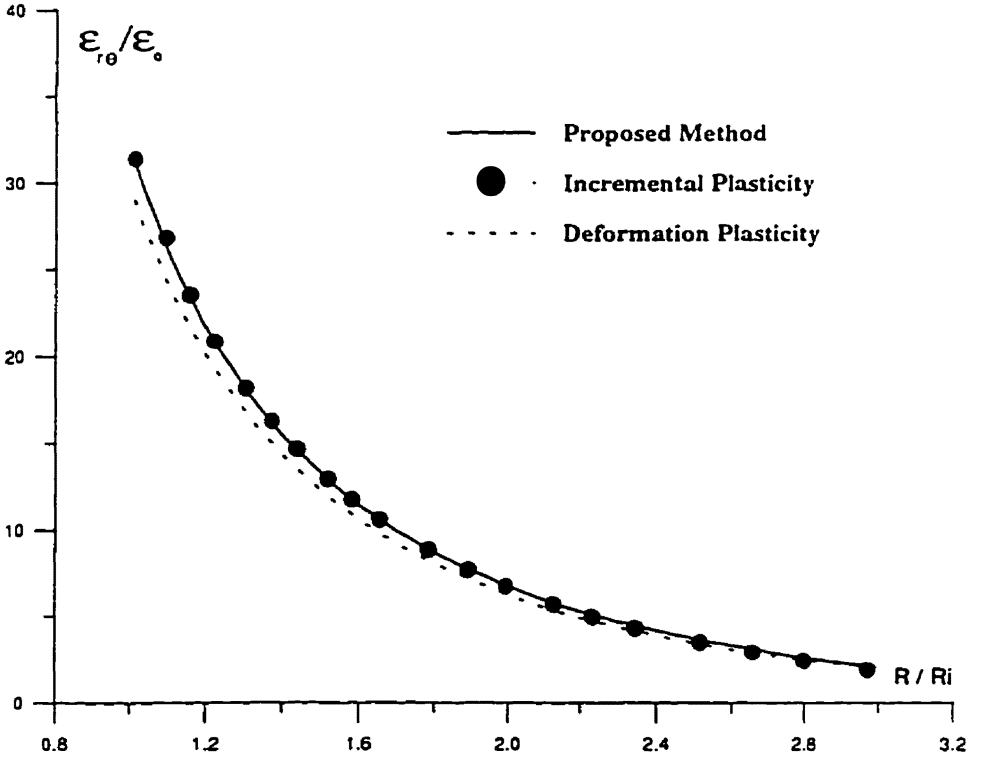


Figure 5.16: Strain comparison (incremental vs present method), shear strain

5.3.2.1.2 Pressure-torsion

The same procedures were used to consider the alternative loading: pressure, followed by torsion. The stress field resulting from the application of pressure alone, with the stress field resulting from the application of pressure and torsion together were used in Eq. (5.13) to find the changes in the plastic strain during the application of torsion. This value was then added to the plastic strain at the end of the first loading (application of pressure) to give the total plastic strain. The resulting strain field was compared with the strain field resulting from a nonproportional loading, incremental plasticity solution using ABAQUS. These results are shown in figures 5.17 -5.19. They also show a very close agreement.

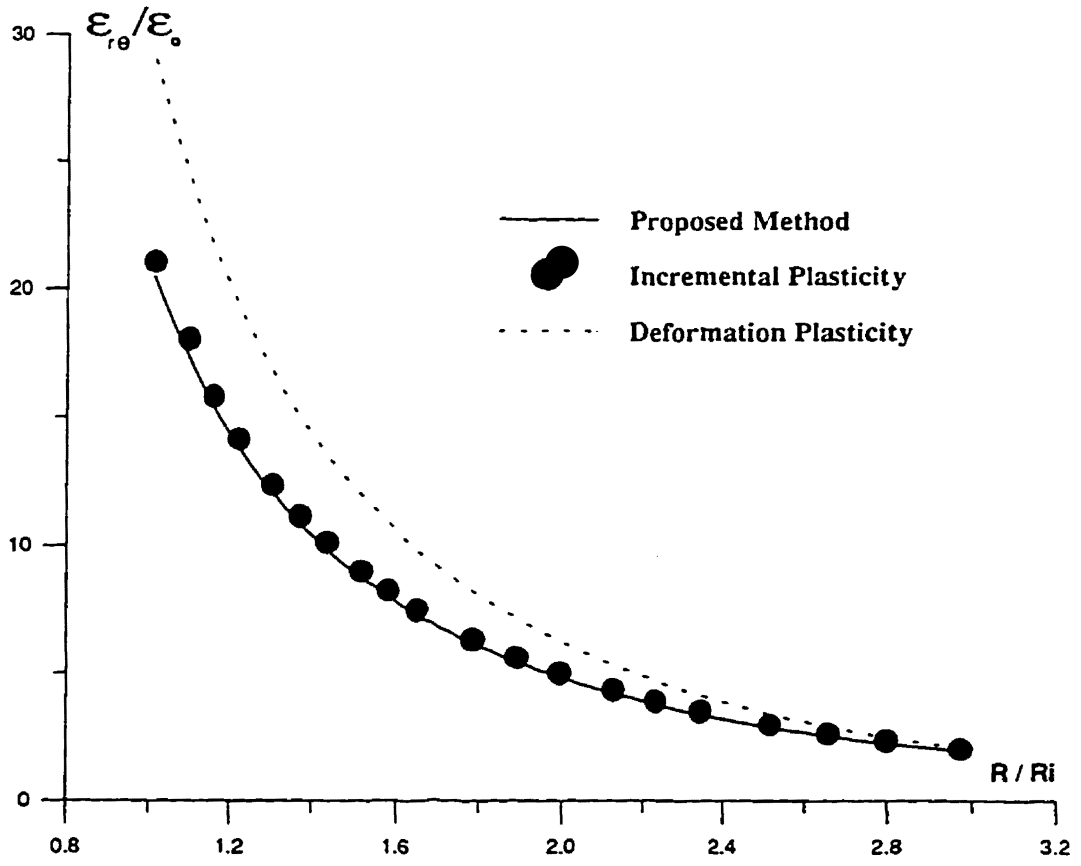


Figure 5.17: Strain comparison (incremental vs present method), shear strain

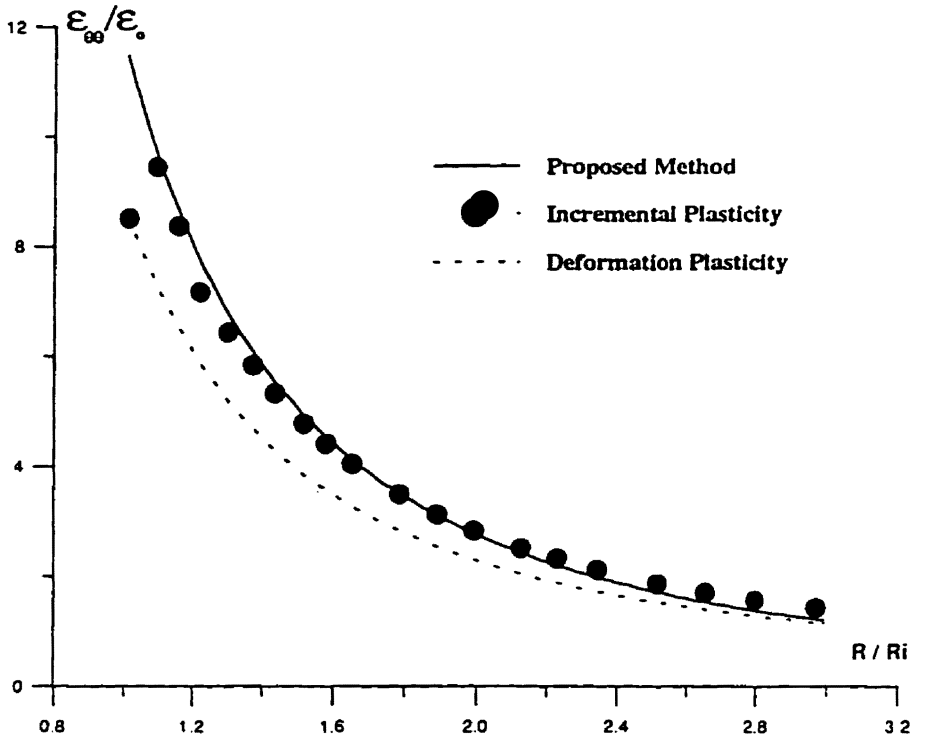


Figure 5.18: Strain comparison (incremental vs present method), hoop strain

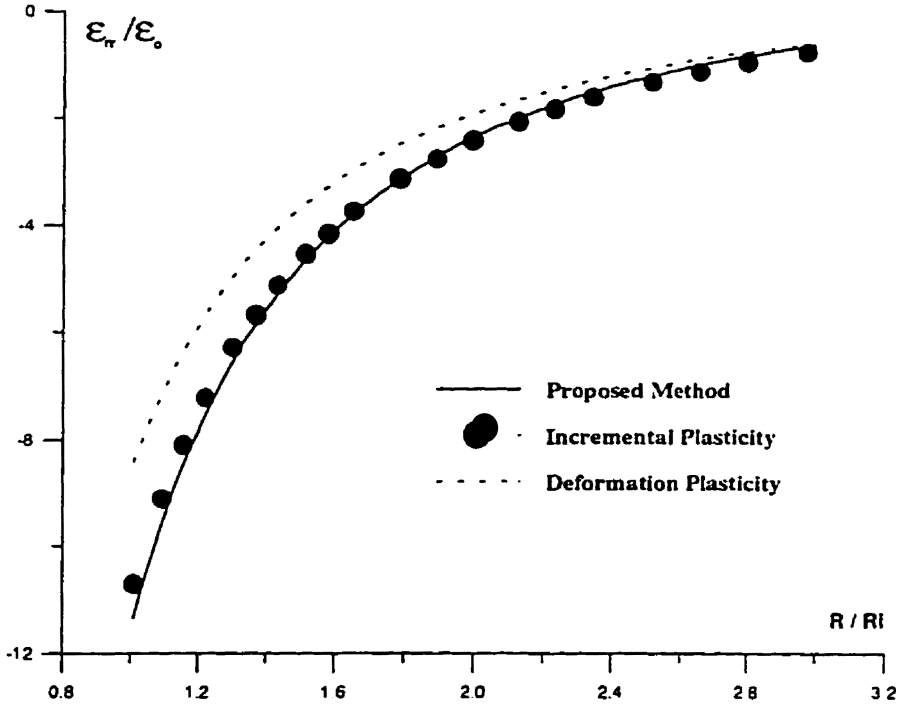


Figure 5.19: Strain comparison (incremental vs present method), radial strain

6. CONCLUSIONS AND RECOMMENDATIONS

6.1 CONCLUSIONS

The aims of this work were to: 1) establish a method of elastic-plastic analysis based on linear elastic solutions capable of predicting mechanically induced residual stress fields, and 2) develop a total deformation theory applicable to a sequence of linear nonproportional loadings.

The results presented here lead to the following conclusions:

A) The variable material property approach

I. A method of elastic-plastic analysis based on linear elastic solutions has been presented. This method uses the concept of pseudo linear elastic points treating material properties as field variables.

II. A general axisymmetric method of elastic-plastic analysis has been proposed. This method provides a complete elastic-plastic solution for axisymmetric problems.

III. Five different schemes for evaluating material moduli have been presented. It has been shown that iteration methods based on a strain energy density concept, i.e., Neuber's or Glinka's interpretation of strain energy equivalence in elastic and elastic-plastic behaviors, are most useful for updating the material properties. While the projection method guarantees a monotonic convergence, energy methods give faster convergence rates.

IV. The axisymmetric method has been successfully applied to the analyses of autofrettaged thick-walled cylinders and cold worked fastener holes. In these applications the analyses are based on Lame's linear elastic solution. This method

employs the actual material unloading curve and is capable of modeling reversed yielding using isotropic and/or kinematic hardening, as well as a variable Bauschinger effect factor. The capabilities of this method in predicting autofrettage residual stress field and residual stress field around a fastener holes have been compared to other theories. It has been concluded that this method provides a more comprehensive and a more accurate method than other available methods.

V. It has been shown that consideration of a variable Bauschinger effect factor during unloading has a significant effect on reversed yield prediction in low-level autofrettage.

B) Total deformation theory for nonproportional loading

VI. A total deformation theory has been presented and successfully applied to nonproportional loading. In this mathematical model, a proper way of representing a sequence of linear loadings, analogous to proportional loading, has been proposed. It has been proven that with this representation a total deformation formulation may be used for calculation of plastic strain even for nonproportional loading. This method, unlike conventional plasticity, defines loadings with reference to previous loadings. This allows for a representation similar to proportional loading.

VII. It has been shown for situations where stresses are known a priori that the proposed method gives the same results as incremental plasticity.

VIII. For situations where stresses are not known a priori a method for estimating the plastic strain field for linear hardening materials has been proposed. This method calculates the necessary stress fields using conventional deformation theory. The results for plastic strain field estimation in a nonproportional load controlled situation has been compared to plastic strain field estimates using incremental plasticity. The results are in very good agreement.

IX. The proposed method for estimating the plastic strain field significantly reduces computation time as compared to an incremental plasticity solution.

6.2 RECOMMENDATIONS

The variable material property approach in elastic-plastic analysis for proportional and nonproportional loading has been developed herein. The results give rise to many ideas which could be explored in future research:

a) The total deformation theory presented here should be extended to nonproportional problems involving strain and displacement controlled deformation processes.

b) The proposed total deformation theory, which has been applied to the situation involving loading only, should be extended for nonproportional unloading situations as well.

c) The proposed total deformation theory should be extended to cyclic plasticity. A method to determine whether the stressing (or straining) is elastic, elastic-plastic, or unloading during each linear loading, along with a memory model for material cyclic behavior, is necessary for such a task.

d) Different problems should be studied to generalize the applications of the proposed total deformation theory.

e) The general axisymmetric method proposed here should be extended to 3-D axisymmetric problems, such as the fastener hole problem.

f) A study on the effective moduli distribution in different applications should be conducted. This may lead to a generalized form for these moduli distributions in terms of load, elastic properties and body dimensions. These could give a good approximation to the actual axisymmetric stress, strain and displacement fields, without iteration.

APPENDIX A

This appendix includes the FORTRAN code for the axisymmetric elastic-plastic problem using the variable material property method. The code is based on Lame linear elastic solution for thick-walled tubes.

```
C       PROGRAM MAIN
*********************************************************
*  ELASTIC-PLASTIC ANALYSIS OF AXISYMMETRIC PROBLEM
*  USING VARIABLE MATERIAL PROPERTY METHOD
*  PROPORTIONAL & NONPROPORTIONAL LOADING
*********************************************************
*       H. JAHED
*       Dept. of Mechanical Eng.
*       University of Waterloo
*
*       Ver.1 : JUNE  1995      THICK-WALLED CYLINDERS
*       Ver.2 : SEPT. 1995      AUTOFRETTAGE
*       Ver.3 : OCT.  1995      FASTENER HOLES
*       Ver.4 : JUNE  1996      MULTIAXIAL LOADING
*       Ver.5 : DEC.  1996      NONPROPORTIONAL LOADING
*********************************************************

C.PROGRAM VARIABLE MAXIMUM DIMENSIONS
        IMPLICIT DOUBLE PRECISION (A-H,K,O-Z)
        PARAMETER (PAI=3.141592654)
........COMMON/BLK0/R(500),AR(500),MXITER,NELM,N,NITER,IUNLD,PII,POO,T
     .   ,MXITR,ITER,IDUM,IADJST,IBOUND
        COMMON/BLK1/K(2,2)
        COMMON/BLK2/A,B,AI,BO,YSTRES(500),SY,ERROR,ICURVE,ALPHA,M
        COMMON/BLK3/AA(500),BB(500),CC(500),U(500),P(500),UT(500)
        COMMON/BLK4/SZZ(500),SRR(500),STT(500),SRT(500),SEQ(500)
        COMMON/BLK5/E(500),ANU(500),EELAS,ANUE,IPLANE,IYCRT
        COMMON/BLK6/SZZIN,SRRIN,STTIN,SRROUT
     .    ,STTOUT,ERRIN,ERROUT,ETTIN,ETTOUT
```

```
      COMMON/BLK7/EL(500),STTL(500),SRRL(500),SZZL(500),ETTL(500)
     .  ,ERRL(500)
     .  ,EZZL(500),UL(500),SEQL(500),SRRLIN,STTLIN,ERRLIN,ETTLIN,SRRLOT
     .  ,STTLOT,ERRLOT,ETTLOT,EEQL(500),SZZLIN,SRTL(500),ERTL(500)
      COMMON/BLK8/ERR(500),ETT(500),EZZ(500),ERT(500)
      COMMON/BLK9/NDAT,SIGDAT(20),ESTDAT(20),SYL(500),SLOPE(20)
      COMMON/BLK10/DESTDT(20)
      COMMON/BLK11/PERR(500),EERR(500),PETT(500),EETT(500)
     .  ,PERT(500),EERT(500)
      COMMON/BLK12/METHOD

C.OPEN INPUT FILE AND CREATE OUTPUT FILES
      OPEN(3,FILE='INPUT')
      OPEN(4,FILE='K',FORM='UNFORMATTED')
      OPEN(5,FILE='OUTPUT')
      OPEN(6,FILE='STRESS.DAT')
      OPEN(7,FILE='STRAIN.DAT')
      OPEN(8,FILE='DISPLAC.DAT')
      OPEN(9,FILE='ST-ES.DAT')


      REWIND(4)

C.CALL INPUT FILE AND READ DIMENSIONS, MATERIAL PROPERTIES, LOAD
C.READ THE SPECIFIED METHOD OF MODULI UPDATING
C.DEFINE STRIPS
      CALL INPUT
C.START ITERATION
C.LOADIN
      IUNLD=0
      NITER=0
      IADJST=0
 7    NITER=NITER+1
      REWIND(4)
      ERROR=0.D0
C.CALL KMATRIX TO RELATE LOAD AND DISPLACEMENT USING LAME SOLUTION
C.UPDATE THE EFFECTIVE MODULI VALUES
      CALL KMATX(I)
C.GET THE AVERAGE VALUE OF STRESS DIFFERENCE OVER ALL STRIPS
      ERROR=DSQRT(ERROR)/FLOAT(NELM)
C.SOLVE THE SYSTEM OF LINEAR EQUATION
      CALL TRIDAG(N)
```

```
C.CALL POST
C.FIND RADIAL, HOOP, AND EFFECTIVE IN EACH STRIP
        CALL POST(U,UT)
C.CALL PRINT
C.PRINT 1ST (ELASTIC SOLUTION) & LAST (ELASTIC-PLASTIC SOLUTION)
        IF(NITER.EQ.1.OR.ERROR.LT.1.D-6.OR.
     .   NITER.EQ.MXITER) CALL PRINT
C.UNLOADING
        IF(NITER.GT.1.AND.ERROR.LT.1.D-6.AND.IUNLD.EQ.0) CALL UNLOAD
        IF(NITER.GT.1.AND.ERROR.LT.1.D-6.AND.IUNLD.EQ.1) CALL ADJUST
        IF(NITER.EQ.MXITER) GO TO 9
        GO TO 7
 9      CLOSE(3,STATUS='KEEP')
        CLOSE(5,STATUS='KEEP')
        CLOSE(6,STATUS='KEEP')
        CLOSE(7,STATUS='KEEP')
        CLOSE(8,STATUS='KEEP')
        STOP
        END

*************************************************************************
C                                INPUT SUBROUTINE
*************************************************************************

        SUBROUTINE INPUT
        IMPLICIT DOUBLE PRECISION (A-H,K,O-Z)
        COMMON/BLK0/R(500),AR(500),MXITER,NELM,N,NITER,IUNLD,PII,POO,T
     .  ,MXITR,ITER,IDUM,IADJST,IBOUND
        COMMON/BLK2/A,B,AI,BO,YSTRES(500),SY,ERROR,ICURVE,ALPHA,M
        COMMON/BLK3/AA(500),BB(500),CC(500),U(500),P(500),UT(500)
        COMMON/BLK5/E(500),ANU(500),EELAS,ANUE,IPLANE,IYCRT
        COMMON/BLK7/EL(500),STTL(500),SRRL(500),SZZL(500),ETTL(500)
     .   ,ERRL(500)
     .  ,EZZL(500),UL(500),SEQL(500),SRRLIN,STTLIN,ERRLIN,ETTLIN,SRRLOT
     .  ,STTLOT,ERRLOT,ETTLOT,EEQL(500),SZZLIN,SRTL(500),ERTL(500)
        COMMON/BLK9/NDAT,SIGDAT(20),ESTDAT(20),SYL(500),SLOPE(20)
        COMMON/BLK10/DESTDT(20)
        COMMON/BLK12/METHOD

C.CHOOSE THE UPDATING METHOD
        READ(3,11)
        READ(3,111)METHOD
```

```
      READ(3,11)
C.READ INTERNAL AND EXTERNAL RADIUS
      READ(3,*)AI,BO
      A=AI
      B=BO
      READ(3,11)
C.NUMBER OF STRIPS AND DEFINE THE STRIPS
      READ(3,111)NELM
      DR=(B-A)/FLOAT(NELM)
      N=1
      R(1)=AI
      DO 10 I=1,NELM
      N=N+1
 10   R(N)=R(N-1)+DR
C.FOR MORE DETAILS NEAR THE BORE USE THE FOLLOWING
      DR=(3.D0*AI)/(1.D0*(NELM-2))
      READ(3,11)
      DO 10 I=1,NELM-2
      N=N+1
 100  R(N)=R(N-1)+DR
      N=N+1
      R(N)=R(N-1)+INT((B-R(N-1))/2.)
      N=N+1
      R(N)=B
C.READ THE ELASTIC PROPERTIES AND STRESS STATE
      READ(3,*)EELAS,ANUE,IPLANE
      READ(3,11)
C.READ YIELD STRESS VALUE AND TYPE OF UNIAXIAL CURVE MODEL
      READ(3,*)SY,IYCRT
      READ(3,11)
C. FOR RAMBERG-OSGOOD GET THE COEFFICIENTS
      READ(3,*)M,ALPHA,ICURVE
C.ASSIGN INITIAL PROPERTIES TO ALL STRIPS
      DO 5 I=1,NELM
      E(I)=EELAS
      ANU(I)=ANUE
      YSTRES(I)=SY
 5    CONTINUE
C.INITIALIZATION OF STRESS FIELD
      DO 103 I=1,NELM
      STTL(I)=0.
      SRRL(I)=0.
```

```
          SZZL(I)=0.
          SRTL(I)=0.
          UL(I)=0.
  103      CONTINUE
          UL(I)=0.
          SRRLIN=0.
          STTLIN=0.
          SZZLIN=0.
          SRRLOT=0.
          STTLOT=0.
C.BOUNDARY CONDITION
          READ(3,11)
C.READ THE INTERNAL AND EXTERNAL PRESSURES AND INTERNAL TORQUE
          READ(3,*)PII,POO,T
          P(1)=PII
          P(N)=POO
          DO 80 I=2,N-1
 80       P(I)=0.D0
          READ(3,11)
C.MAXIMUM NUMBER OF ITERATION
          READ(3,111)MXITER
          READ(3,11)
C.READ THE STRESS-STRAIN CURVE DATA (LOADING)
          READ(3,11)
          READ(3,*)NDATL
          DO 81 I=1,NDATL
 81       READ(3,*)ESTDL(I),SIGDL(I)
          DO 83 J=1,NDATL-1
 83       SLOPEL(J)=(SIGDL(J+1)-SIGDL(J))/(ESTDL(J+1)-ESTDL(J))
C.READ THE STRESS-STRAIN CURVE DATA (UNLOADING)
          READ(3,11)
          READ(3,*)NDAT
          DO 85 I=1,NDAT
 85       READ(3,*)ESTDAT(I),SIGDAT(I)
          DO 87 J=1,NDAT-1
 87       SLOPE(J)=(SIGDAT(J+1)-SIGDAT(J))/(ESTDAT(J+1)-ESTDAT(J))
C.BAUSCHINGER FACTOR VALUES
          READ(3,11)
          READ(3,*)LDAT
          DO 93 L=1,LDAT
 93       READ(3,*)EP(L),BE(L)
          DO 95 L=1,LDAT-1
```

```
 95      SLLOP(L)=(BE(L+1)-BE(L))/(EP(L+1)-EP(L))
 11      FORMAT(2D10.5)
 111     FORMAT(I4)
         RETURN
         END

*************************************************************************
C                                SUBROUTINE
C              FOR CALCULATIONS OF MATRIX "K" AND ITS INVERSE
*************************************************************************

         SUBROUTINE  KMATX(I)
         IMPLICIT DOUBLE PRECISION (A-H,K,O-Z)
         COMMON/BLK0/R(500),AR(500),MXITER,NELM,N,NITER,IUNLD,PII,POO,T
     .   ,MXITR,ITER,IDUM,IADJST,IBOUND
         COMMON/BLK1/K(2,2)
         COMMON/BLK2/A,B,AI,BO,YSTRES(500),SY,ERROR,ICURVE,ALPHA,M
         COMMON/BLK3/AA(500),BB(500),CC(500),U(500),P(500),,UT(500)
         COMMON/BLK4/SZZ(500),SRR(500),STT(500),SRT(500),SEQ(500)
         COMMON/BLK5/E(500),ANU(500),EELAS,ANUE,IPLANE,IYCRT
         COMMON/BLK9/NDAT,SIGDAT(20),ESTDAT(20),SYL(500),SLOPE(20)
         COMMON/BLK12/METHOD

C.INITIALIZATION OF THE COEFFICIENT MATRIX
         DO 100 I=1,N
         AA(I)=0.D0
         BB(I)=0.D0
         CC(I)=0.D0
 100     CONTINUE
         DO 50 I=1,NELM
         A=R(I)
         B=R(I+1)
         IF(NITER.GT.1.OR.IUNLD.EQ.1) CALL MATRPR(I)
         IF(IPLANE.EQ.0) THEN
         K11=((1.D0+ANU(I))/E(I))*(A**3/(B**2-A**2))
     .    *(1.D0-2.D0*ANU(I)+B**2/A**2)
         K22=(-(1.D0+ANU(I))/E(I))*(B**3/(B**2-A**2))
     .    *(1.D0-2.D0*ANU(I)+A**2/B**2)
         K12=-2.D0*((1.D0-ANU(I)**2)/E(I))*B**2*A/(B**2-A**2)
         K21=2.D0*((1.D0-ANU(I)**2)/E(I))*A**2*B/(B**2-A**2)
         ELSE
         K11=((1.D0+ANU(I))/E(I))*(A**3/(B**2-A**2))
```

```
     .   *(((1.D0-ANU(I))/(1.D0+ANU(I)))+B**2/A**2)
         K22=(-(1.D0+ANU(I))/E(I))*(B**3/(B**2-A**2))
     .   *(((1.D0-ANU(I))/(1.D0+ANU(I)))+A**2/B**2)
         K12=(-2.D0/E(I))*B**2*A/(B**2-A**2)
         K21=(2.D0/E(I))*A**2*B/(B**2-A**2)
         ENDIF
         DETK=K11*K22-K12*K21
         IF(DETK.EQ.0) THEN
         PRINT*,'ERROR DETK=0'
         WRITE(7,*)    'ERROR DETK=0'
         STOP
         ELSE
         DETK=1.D0/DETK
         ENDIF
C.FIND THE INVERSE OF "K"
         IF(I.EQ.1) THEN
         K(1,1)=DETK*K22
         K(1,2)=-DETK*K12
         ELSE
         K(1,1)=-DETK*K22
         K(1,2)=DETK*K12
         ENDIF
         K(2,2)=DETK*K11
         K(2,1)=-DETK*K21
         BB(I)=BB(I)+K(1,1)
         CC(I)=CC(I)+K(1,2)
         AA(I+1)=AA(I+1)+K(2,1)
         BB(I+1)=BB(I+1)+K(2,2)
         WRITE(4)K
 50      CONTINUE
         IF(IADJST.EQ.1)  BB(IBOUND)=BB(IBOUND)*1.D20
         IF(IADJST.EQ.1)  P(IBOUND)=BB(IBOUND)*U(IBOUND)
         RETURN
         END

*************************************************************************
*                                SUBROUTINE
*                             MATERIAL PROPERTIES
*************************************************************************

         SUBROUTINE MATRPR(I)
         IMPLICIT DOUBLE PRECISION (A-H,K,O-Z)
```

```
      COMMON/BLK0/R(500),AR(500),MXITER,NELM,N,NITER,IUNLD,PII,POO,T
     .  ,MXITR,ITER,IDUM,IADJST,IBOUND
      COMMON/BLK2/A,B,AI,BO,YSTRES(500),SY,ERROR,ICURVE,ALPHA,M
      COMMON/BLK4/SZZ(500),SRR(500),STT(500),SRT(500),SEQ(500)
      COMMON/BLK5/E(500),ANU(500),EELAS,ANUE,IPLANE,IYCRT
      COMMON/BLK9/NDAT,SIGDAT(20),ESTDAT(20),SYL(500),SLOPE(20)
      COMMON/BLK10/DESTDT(20)
      COMMON/BLK12/METHOD

C.CHOOSE THE METHOD FOR UPDATING MODULI
C.LOADING
      IF(METHOD.EQ.1.AND.ICURVE.NE.0.AND UNLOAD.EQ.0)THEN
C.ELASTIC-PERFECTLY PLASTIC
C.PROJECTION METHOD
        IF(SEQ(I).LT.YSTRES(I)) RETURN
         EE1=(YSTRES(I)/SEQ(I))*E(I)
          ETOT=YSTRES(I)/EE1
           E(I)=EE1
            EPLAS=ETOT-YSTRES(I)/EELAS
            ERROR=ERROR+(ABS(SEQ(I)-YSTRES(I)))**2
           ANUEE=(2.D0*ANUE*YSTRES(I)/EELAS+EPLAS)/
     .     (2.D0*YSTRES(I)/EELAS+2.D0*EPLAS)
         ANU(I)=ANUEE
      ELSEIF(METHOD.EQ.2) THEN
C.NEUBER'S RULE
        AREA=(SEQ(I)/E(I))*SEQ(I)
        IF(AREA.LT.YSTRES(I)**2/(EELAS)) RETURN
         ETOT=AREA/YSTRES(I)
          EE1=YSTRES(I)/ETOT
           E(I)=EE1
            EPLAS=ETOT-YSTRES(I)/EELAS
           ERROR=ERROR+(ABS(SEQ(I)-YSTRES(I)))**2
          ANUEE=(2.D0*ANUE*YSTRES(I)/EELAS+EPLAS)/
     .    (2.D0*YSTRES(I)/EELAS+2.D0*EPLAS)
         ANU(I)=ANUEE
      ELSEIF(METHOD.EQ.3) THEN
C.GLINKA & MOLSKI
       IF(SEQ(I).LT.YSTRES(I)) RETURN
        ETOT=(SEQ(I)**2+YSTRES(I)**2)/(2.D0*E(I)*YSTRES(I))
         E(I)=YSTRES(I)/ETOT
          EPLAS=ETOT-YSTRES(I)/EELAS
           ERROR=ERROR+(ABS(SEQ(I)-YSTRES(I)))**2
```

```
            ANUEE=(2.D0*ANUE*YSTRES(I)/EELAS+EPLAS)/
     .     (2.D0*YSTRES(I)/EELAS+2.D0*EPLAS)
           ANU(I)=ANUEE
          ELSEIF(METHOD.EQ.4)  THEN
C.AVERAGE
           IF((SEQ(I)**2/E(I)).LT.YSTRES(I)**2/(EELAS)) RETURN
            ETOTN=((SEQ(I)/E(I))*SEQ(I))/YSTRES(I)
             ETOTG=(SEQ(I)**2+YSTRES(I)**2)/(2.D0*E(I)*YSTRES(I))
              ETOT=ABS(DSQRT(ETOTN*ETOTG))
               E(I)=YSTRES(I)/ETOT
                EPLAS=ETOT-YSTRES(I)/EELAS
               ERROR=ERROR+(ABS(SEQ(I)-YSTRES(I)))**2
              ANUEE=(2.D0*ANUE*YSTRES(I)/EELAS+EPLAS)/
     .     (2.D0*YSTRES(I)/EELAS+2.D0*EPLAS)
           ANU(I)=ANUEE
          ELSE
C.ARC-LENGTH

          IF(SEQ(I).LT.YSTRES(I)) RETURN
           C1=YSTRES(I)
            C2=C1/EELAS
             ETOT=SEQ(I)/E(I)
              ARCR=ABS(DSQRT((ETOT/C2)**2+(SEQ(I)/C1)**2))
               ETOT=ABS(DSQRT(ARCR**2-1.D0))*C2
               EE1=YSTRES(I)/ETOT
                E(I)=EE1
                EPLAS=ETOT-YSTRES(I)/EELAS
               ERROR=ERROR+(ABS(SEQ(I)-YSTRES(I)))**2
              ANUEE=(2.D0*ANUE*YSTRES(I)/EELAS+EPLAS)/
     .     (2.D0*YSTRES(I)/EELAS+2.D0*EPLAS)
           ANU(I)=ANUEE
          ENDIF
C.FOR RAMBERG-OSGOOD MODEL USE THE FOLLOWING
C.PROJECTION METHOD
          IF(ICURVE.EQ.0)THEN
           IF(I.EQ.1.AND.NITER.EQ.2) SSS=SEQ(I)/SY
            ETOT=SEQ(I)/E(I)
             IITER=100
              IIET=0
               ICON=0
 1              IIET=IIET+1
                FUNC= SSS+ALPHA*(SSS**M)-(EELAS*ETOT/SY)
```

```
                DFUNC=1.D0+M*ALPHA*(SSS**(M-1))
                 Z1=SSS-FUNC/DFUNC
                 IF(ABS((Z1-SSS)/SSS).LT.1.D-6) ICON=1
                 SSS=Z1
                 IF(ICON.EQ.0.AND.IIET.LT.IITER) GO TO 1
                EE1=(SSS*SY)/ETOT
               E(I)=EE1
              YSTRES(I)=SSS*SY
             EPLAS=ETOT-(SSS*SY)/EELAS
            ANUEE=(2.D0*ANUE*(SSS*SY)/EELAS+EPLAS)/
     1     (2.D0*(SSS*SY)/EELAS+2.D0*EPLAS)
          ANU(I)=ANUEE
         ERROR=ERROR+(ABS(SEQ(I)-SSS*SY))**2
C.OTHERWISE USE THE STRESS-STRAIN CURVE DATA
       ELSE
        ETOT=SEQ(I)/E(I)
         DO 13 M=2,NDAT
          IF (ETOT.LT.ESTDAT(M)) GO TO 7
 13        CONTINUE
            M=M-1
 7           YSTRES(I)=SLOPE(M-1)*(ETOT-ESTDAT(M-1))+SIGDAT(M-1)
             EE1=(YSTRES(I)/SEQ(I))*E(I)
            ETOT=YSTRES(I)/EE1
           E(I)=EE1
          EPLAS=ETOT-YSTRES(I)/EELAS
         ERROR=ERROR+(ABS(SEQ(I)-YSTRES(I)))**2
        ANUEE=(2.D0*ANUE*YSTRES(I)/EELAS+EPLAS)/
     1  (2.D0*YSTRES(I)/EELAS+2.D0*EPLAS)
       ANU(I)=ANUEE
C.UNLOADING
        ELSEIF(IUNLD.EQ.1.AND.NITER.NE.1)THEN
C.GET THE INDIVIDUAL UNLOADING CURVE OF EACH POINT
         ESTDAU(1)=ESTDAT(1)
          SIGDAU(1)=SIGDAT(1)
           ESTDAU(2)=SYL(I)/SLOPE(1)
            SIGDAU(2)=SYL(I)
           SLOPEU(1)=SLOPE(1)
           DO 9 IJ=3,NDAT
 9          IF(EYL(I).LT.ESTDAT(IJ))GO TO 5
             IJ=IJ-1
 5            ESTDAU(3)=ESTDAU(2)+(ESTDAT(IJ)-EYL(I))
             SIGDAU(3)=SIGDAU(2)+SLOPE(IJ-1)*(ESTDAT(IJ)-EYL(I))
```

```
            SLOPEU(2)=SLOPE(IJ-1)
           IJI=IJ
           DO 10 L=4,3+(NDAT-IJ)
            ESTDAU(L)=ESTDAU(L-1)+DESTDT(IJI)
             SIGDAU(L)= SIGDAU(L-1)+SLOPE(IJI)*DESTDT(IJI)
            SLOPEU(L-1)=SLOPE(IJI)
 10         IJI=IJI+1
      ENDIF
      RETURN
      END

*************************************************************************
C                        TRIDIAGONAL SOLVER SUBROUTINE
*************************************************************************

C.SOLVE THE SYSTEM OF LINEAR EQUATION
       SUBROUTINE TRIDAG(N)
        IMPLICIT DOUBLE PRECISION (A-H,O-Z)
        COMMON/BLK3/AA(500),BB(500),CC(500),U(500),P(500),UT(500)
        PARAMETER (NMAX=500)
        DIMENSION GAM(NMAX)
        IF(BB(1).EQ.0.)PAUSE
        BET=BB(1)
        U(1)=P(1)/BET
        DO 11 J=2,N
        GAM(J)=CC(J-1)/BET
        BET=BB(J)-AA(J)*GAM(J)
        IF(BET.EQ.0.)PAUSE
        U(J)=(P(J)-AA(J)*U(J-1))/BET
 11     CONTINUE
        DO 12 J=N-1,1,-1
        U(J)=U(J)-GAM(J+1)*U(J+1)
 12     CONTINUE
        RETURN
        END

*************************************************************************
C                        POST PROCESSING SUBROUTINE
*************************************************************************

        SUBROUTINE POST(U,UT)
        IMPLICIT DOUBLE PRECISION(A-H,K,O-Z)
```

```
      PARAMETER (PAI=3.141592654)
      COMMON/BLK1/K(2,2)
      COMMON/BLK2/A,B,AI,BO,YSTRES(500),SY,ERROR,ICURVE,ALPHA,M
      COMMON/BLK4/SZZ(500),SRR(500),STT(500),SRT(500),SEQ(500)
      COMMON/BLK0/R(500),AR(500),MXITER,NELM,N,NITER,IUNLD,PII,POO,T
     .  ,MXITR,ITER,IDUM,IADJST,IBOUND
      COMMON/BLK6/SZZIN,SRRIN,STTIN,SRROUT
     .   ,STTOUT,ERRIN,ERROUT,ETTIN,ETTOUT
      COMMON/BLK5/E(500),ANU(500),EELAS,ANUE,IPLANE,IYCRT
      COMMON/BLK7/EL(500),STTL(500),SRRL(500),SZZL(500),ETTL(500)
     .   ,ERRL(500)
     .  ,EZZL(500),UL(500),SEQL(500),SRRLIN,STTLIN,ERRLIN,ETTLIN,SRRLOT
     .  ,STTLOT,ERRLOT,ETTLOT,EEQL(500),SZZLIN,SRTL(500),ERTL(500)
      COMMON/BLK8/ERR(500),ETT(500),EZZ(500),ERT(500)
      COMMON/BLK11/PERR(500),EERR(500),PETT(500),EETT(500)
     1   ,PERT(500),EERT(500)
      DIMENSION U(500),UT(500)

      REWIND(4)
C.FIND THE INTERNAL AND EXTERNAL PRESSURES OF EACH STRIP
C.USE LAME SOLUTION
      DO 20 I=1,NELM
      READ(4)K
      IF(I.EQ.1)THEN
       PI=K(1,1)*U(I)+K(1,2)*U(I+1)
       PO=K(2,1)*U(I)+K(2,2)*U(I+1)
      ELSE
       PI=-K(1,1)*U(I)-K(1,2)*U(I+1)
       PO=K(2,1)*U(I)+K(2,2)*U(I+1)
      ENDIF
C.GET THE MID RADIUS OF EACH STRIP
C.FIND THE CORRESPONDING COEFFICIENT MATRIX
      AR(I)=(R(I)+R(I+1))/2.D0
      C0=1.D0/(R(I+1)**2-R(I)**2)
      C1=C0*((PI*R(I)**2)-PO*(R(I+1)**2))
      C2=C0*(PI-PO)*(R(I)**2)*R(I+1)**2
C.FIND THE RADIAL,TANGENTIAL AND SHEAR STRESSES IN EACH STRIP
C.FIND THE RADIAL,TANGENTIAL AND SHEAR STRAINS  IN EACH STRIP
      SRR(I)=C1-C2/(AR(I)**2)
      STT(I)=C1+C2/(AR(I)**2)
      SRT(I)=T/(2.D0*PAI*AR(I)**2)
      ERT(I)=SRT(I)*2.D0*(1+ANU(I))/E(I)
```

```
C.FIND THE VALUE OF AXIAL STRESS AND STRAIN
        IF(IPLANE.EQ.0)THEN
C.PLANE STRAIN
         SZZ(I)=ANU(I)*(STT(I)+SRR(I))
           EZZ(I)=0.D0
            ERR(I)=((1.D0+ANU(I))/E(I))*(SRR(I)-
     .      ANU(I)*(SRR(I)+STT(I)))
           ETT(I)=((1.D0+ANU(I))/E(I))*(STT(I)-
     .     ANU(I)*(SRR(I)+STT(I)))
        ELSE
C.PLANE STRESS
         EZZ(I)=-ANU(I)*(STT(I)+SRR(I))/E(I)
          SZZ(I)=0.D0
          ERR(I)=(1.D0/E(I))*(SRR(I)-ANU(I)*STT(I))
         ETT(I)=(1.D0/E(I))*(STT(I)-ANU(I)*SRR(I))
        ENDIF
C.FIND THE EQUIVALENT STRESS
C.TRESCA CRITERIA
        IF(IYCRT.EQ.0)
     .    SEQ(I)=2.D0*ABS(DSQRT(((SRR(I)-STT(I))/2)**2
     .   +SRT(I)**2))
C.VON MISES CRITERIA
        IF(IYCRT.EQ.1) SEQ(I)=DSQRT(.5D0*((STT(I)-SRR(I))**2
     .   +(STT(I)-SZZ(I))**2+(SRR(I)-SZZ(I))**2+6.D0*SRT(I)**2))
C.FIND THE ELASTIC & PLASTIC STRAIN
        EERR(I)=(1.D0/EELAS)*SRR(I)-(ANUE/EELAS)*(STT(I)+SZZ(I))
        EETT(I)=(1.D0/EELAS)*STT(I)-(ANUE/EELAS)*(SRR(I)+SZZ(I))
        EERT(I)=2.D0*((1.D0+ANUE)/EELAS)*SRT(I)
        PERR(I)=ERR(I)-EERR(I)
        PETT(I)=ETT(I)-EETT(I)
        PERT(I)=ERT(I)-EERT(I)
C.FIND THE STRESSES AT THE BORE
        IF(I.EQ.1)THEN
         SRRIN=C1-C2/(R(I)**2)+SRRLIN
          STTIN=C1+C2/(R(I)**2)+STTLIN
C.PLANE STRAIN
          IF(IPLANE.EQ.0)THEN
            ERRIN=((1.D0+ANU(I))/E(I))*(SRRIN-
     .       ANU(I)*(SRRIN+STTIN))
             ETTIN=((1.D0+ANU(I))/E(I))*(STTIN-
     .       ANU(I)*(SRRIN+STTIN))
            SZZIN=ANU(I)*(SRRIN+STTIN)
```

```
C.PLANE STRESS
          ELSE
           ERRIN=(1.D0/E(I))*(SRRIN-ANU(I)*STTIN)
            ETTIN=(1.D0/E(I))*(STTIN-ANU(I)*SRRIN)
           SZZIN=0.D0
          ENDIF
C.FIND THE STRESSES AT THE EXTERNAL SURFACE
        ELSEIF(I.EQ.NELM)THEN
         SRROUT=C1-C2/(R(I+1)**2)+SRRLOT
          STTOUT=C1+C2/(R(I+1)**2)+STTLOT
C.PLANE STRAIN
           IF(IPLANE.EQ.0)THEN
            ERROUT=((1.D0+ANU(I))/E(I))*(SRROUT-
     .        ANU(I)*(SRROUT+STTOUT))
            ETTOUT=((1.D0+ANU(I))/E(I))*(STTOUT-
     .       ANU(I)*(SRROUT+STTOUT))
           ELSE
            ERROUT=(1.D0/E(I))*(SRROUT-ANU(I)*STTOUT)
            ETTOUT=(1.D0/E(I))*(STTOUT-ANU(I)*SRROUT)
           ENDIF
        ELSE
        ENDIF
 20     CONTINUE
        RETURN
        END

*************************************************************************
C                SUBROUTINE FOR UNLOADING INITIATION
*************************************************************************

        SUBROUTINE UNLOAD
        IMPLICIT DOUBLE PRECISION (A-H,K,O-Z)
        COMMON/BLK0/R(500),AR(500),MXITER,NELM,N,NITER,IUNLD,PII,POO,T
     .  ,MXITR,ITER,IDUM,IADJST,IBOUND
        COMMON/BLK2/A,B,AI,BO,YSTRES(500),SY,ERROR,ICURVE,ALPHA,M
        COMMON/BLK3/AA(500),BB(500),CC(500),U(500),P(500),UT(500)
        COMMON/BLK4/SZZ(500),SRR(500),STT(500),SRT(500),SEQ(500)
        COMMON/BLK5/E(500),ANU(500),EELAS,ANUE,IPLANE,IYCRT
        COMMON/BLK6/SZZIN,SRRIN,STTIN,SRROUT
     .   ,STTOUT,ERRIN,ERROUT,ETTIN,ETTOUT
        COMMON/BLK7/EL(500),STTL(500),SRRL(500),SZZL(500),ETTL(500)
     .   ,ERRL(500)
```

```
     .    ,EZZL(500),UL(500),SEQL(500),SRRLIN,STTLIN,ERRLIN,ETTLIN,SRRLOT
     .    ,STTLOT,ERRLOT,ETTLOT,EEQL(500),SZZLIN,SRTL(500),ERTL(500)
          COMMON/BLK8/ERR(500),ETT(500),EZZ(500),ERT(500)
          COMMON/BLK9/NDAT,SIGDAT(20),ESTDAT(20),SYL(500),SLOPE(20)

C.STORE THE LOADING STRESS FIELD
          DO 10 I=1,NELM
          SEQL(I)=SEQ(I)
          EEQL(I)=SEQ(I)/E(I)
          STTL(I)=STT(I)
          SRRL(I)=SRR(I)
          SZZL(I)=SZZ(I)
          ETTL(I)=ETT(I)
          ERRL(I)=ERR(I)
          ERTL(I)=ERT(I)
          EZZL(I)=EZZ(I)
          SRTL(I)=SRT(I)
          UL(I)=U(I)
          EL(I)=E(I)
C.STORE THE STATE OF STRESS AT THE END OF FIRST LOADING
C.THIS POINT IS THE REFERENCE POINT OF THE UNLOADING
C.IF ISOTROPIC HARDENING
          SYL(I)=2*YSTRES(I)
C.FOR VARIABLE BAUSCHINGER EFFECT FACTOR FIND OVER-STRAIN
          EPLAST=YSTRES(I)*((1./E(I))-(1./EELAS))
          DO 20 J=2,LDAT-1
          IF(EPLAST.LT.EP(J)) GO TO 7
 20       CONTINUE
C.GET THE CORRESPONDING VALUE OF BEF FROM THE DATA
 7        BEF=SLLOP(J-1)*(EPLAST-EP(J-1))+BE(J-1)
C.FIND THE REVERSED YIELD STRSS
          SYL(I)=(1.D0+BEF)*SY
C.NOTE FOR KINEMATIC HARDENING BEF=1 FOR ALL STRIPS
 10       CONTINUE
          UL(I)=U(I)
          IUNLD=1
          NITER=0
          P(1)=0.D0
          PII=P(1)
          P(N)=POO
          T=0.D6
          SRRLIN=SRRIN
```

```
      STTLIN=STTIN
      SZZLIN=SZZIN
      SRRLOT=SRROUT
      STTLOT=STTOUT
      ERRLIN=ERRIN
      ETTLIN=ETTIN
      ERRLOT=ERROUT
      ETTLOT=ETTOUT
      DO 20 I=2,N-1
20    P(I)=0.D0
      RETURN
      END

*************************************************************************
C                    SUBROUTINE FOR PRINTING THE RESULTS
*************************************************************************

      SUBROUTINE PRINT
      IMPLICIT DOUBLE PRECISION(A-H,O-Z)
      COMMON/BLK0/R(500),AR(500),MXITER,NELM,N,NITER,IUNLD,PII,POO,T
     .  ,MXITR,ITER,IDUM,IADJST,IBOUND
      COMMON/BLK2/A,B,AI,BO,YSTRES(500),SY,ERROR,ICURVE,ALPHA,M
      COMMON/BLK3/AA(500),BB(500),CC(500),U(500),P(500),UT(500)
      COMMON/BLK4/SZZ(500),SRR(500),STT(500),SRT(500),SEQ(500)
      COMMON/BLK5/E(500),ANU(500),EELAS,ANUE,IPLANE,IYCRT
      COMMON/BLK6/SZZIN,SRRIN,STTIN,SRROUT
     .  ,STTOUT,ERRIN,ERROUT,ETTIN,ETTOUT
      COMMON/BLK7/EL(500),STTL(500),SRRL(500),SZZL(500),ETTL(500)
     .  ,ERRL(500)
     .  ,EZZL(500),UL(500),SEQL(500),SRRLIN,STTLIN,ERRLIN,ETTLIN,SRRLOT
     .  ,STTLOT,ERRLOT,ETTLOT,EEQL(500),SZZLIN,SRTL(500),ERTL(500)
      COMMON/BLK8/ERR(500),ETT(500),EZZ(500),ERT(500)
      COMMON/BLK11/PERR(500),EERR(500),PETT(500),EETT(500)
     1  ,PERT(500),EERT(500)
      COMMON/BLK11/METHOD
     IF(NITER.GT.1.OR IUNLD.EQ.1) GO TO 5
      WRITE(5,*)
      WRITE(5,*)'              ELASTIC-PLASTIC SOLUTION '
      WRITE(5,*)'                        OF             '
      WRITE(5,*)'               THICK-WALLED CYLINDER   '
      WRITE(5,*)
      WRITE(5,*)
```

```
      WRITE(5,*)
      IF(PII.EQ.0.)WRITE(5,*)
     .            ' PROCESS              : TORSION FOLLOWED BY PRESSURE'
      IF(T.EQ.0)WRITE(5,*)
     .           ' PROCESS               : PRESSURE FOLLOWED BY TORSION'
      WRITE(5,*)
      WRITE(5,*)' NUMBER OF ELEMENTS :',NELM
      WRITE(5,*)' INSIDE RADIUS      :',AI
      WRITE(5,*)' OUTSIDE RADIUS     :',BO
      WRITE(5,*)' INSIDE PRESSURE    :',P(1)
      WRITE(5,*)' OUTSIDE PRESSURE   :',P(N)
      WRITE(5,*)' INSIDE TORQUE      :',T
      WRITE(5,*)' ELASTIC MODULUS    :',EELAS
      WRITE(5,*)' POISSON RATIO      :',ANUE
      WRITE(5,*)' YIELD STRESS       :',SY
      IF(IYCRT.EQ.1) WRITE(5,*)' YIELD CRITERION    :  VON MISES'
      IF(IYCRT.EQ.0) WRITE(5,*)' YIELD CRITERION    :  TRESCA'
      WRITE(5,*)' MAX. # OF ITERATION:',MXITER
      IF(ICURVE.EQ.1)THEN
      WRITE(5,*)' HARDENING RESPONSE : GIVEN STRESS-STRAIN CURVE'
      ELSE
      WRITE(5,*)' RAMBERG-OSGOOD EQUATION'
      WRITE(5,*)'                    :','M=',M,'   ALPHA=',ALPHA
      ENDIF
      IF(IPLANE.EQ.0)WRITE(5,*)' PLANE STRAIN'
      IF(IPLANE.EQ.1)WRITE(5,*)' PLANE STRESS'
      IF(METHOD.EQ.1)WRITE(5,*)' PROJECTION METHOD'
      IF(METHOD.EQ.2)WRITE(5,*)' NEUBER'S METHOD'
      IF(METHOD.EQ.3)WRITE(5,*)' GLINKA'S METHOD'
      IF(METHOD.EQ.4)WRITE(5,*)' AVERAGE ENERGY METHOD'
      IF(METHOD.EQ.5)WRITE(5,*)' ARC-LENGTH METHOD'
      WRITE(5,*)
5     CONTINUE
      EY=SY/EELAS
    IF(NITER.EQ.1) THEN
      WRITE(5,*)
      WRITE(5,*)
      WRITE(5,*)
      IF(IUNLD.EQ.0)
     .  WRITE(5,*)'          PSEUDO ELASTIC SOLUTION (LOADING)'
      IF(IUNLD.EQ.1)
     .  WRITE(5,*)'          PSEUDO ELASTIC SOLUTION (UNLOADING)'
```

```
      WRITE(5,*)
      WRITE(5,*)
     ELSE
      WRITE(5,*)
      WRITE(5,*)
     IF(NITER.EQ.MXITER) WRITE(5,*)' SOLUTION DID NOT CONVERGED'
     IF(NITER.NE.MXITER) WRITE(5,*)' SOLUTION  CONVERGED AFTER',
    .   NITER,'     ITERATION  '
      WRITE(5,*)
      ENDIF
      WRITE(5,*)
      WRITE(5,*)
      WRITE(5,*)' NODE NO.       COORD.        RAD. DISPT.'
      WRITE(5,*)'----------     --------      -------------'
      WRITE(8,*)' NODE NO.       COORD.        RAD. DISPT.'
      WRITE(8,*)'----------     --------      -------------'
      WRITE(5,*)
      DO 10 I=1,N
      IF(NITER.EQ.1) THEN
      WRITE(5,1)I,R(I),U(I),UT(I)
      ELSE
      IF(IUNLD.EQ.1) WRITE(5,1)I,R(I),U(I),UT(I)
      IF(IUNLD.EQ.0) WRITE(5,1)I,R(I),U(I),UT(I)
      IF(IUNLD.EQ.1) WRITE(8,1)I,R(I)/AI,U(I),UT(I)
      IF(IUNLD.EQ.0) WRITE(8,1)I,R(I),U(I),UT(I)
      ENDIF
10    CONTINUE
      WRITE(5,*)
      IF(IPLANE.EQ.0)THEN
      WRITE(5,*)' RAD.        STT             SZZ',
    .  '            SRT,             SEQ,             E'
      ELSE
      WRITE(5,*)' RAD        STT             SZZ',
    .  '            SRT,             SEQ,             E'
      ENDIF
      WRITE(6,*)' RAD        STT             SZZ',
    .  '            SRT             SRR            SEQ'
      WRITE(7,*)' RAD       PERR           PETT',
    .  '          EZZ         PERT          PEEQ'
      DO 20 I=1,NELM
      IF(NITER.EQ.1)THEN
      IF(IPLANE.EQ.0)THEN
```

```
      WRITE(5,2)AR(I),STT(I),SZZ(I),SRT(I),SEQ(I)
      ELSE
      WRITE(5,2)AR(I),STT(I),SZZ(I),SRT(I),SEQ(I)
      ENDIF
      ELSE
      IF(IPLANE.EQ.0)THEN
      IF(IUNLD.EQ.0.) WRITE(5,2)AR(I),STT(I),SZZ(I),SRT(I),SEQ(I),E(I)
      IF(IUNLD.EQ.1) WRITE(5,2)AR(I),STT(I),SZZ(I),SRT(I),SEQ(I),E(I)
      ELSE
      IF(IUNLD.EQ.0) WRITE(5,2)AR(I),STT(I),SZZ(I),SRT(I),SEQ(I),E(I)
      IF(IUNLD.EQ.1) WRITE(5,2)AR(I),STT(I),SZZ(I)
     .  ,SRT(I),SEQ(I),(SEQ(I)/E(I))-(SEQ(I))/EELAS
      ENDIF
      IF(IUNLD.EQ.0) WRITE(6,3)AR(I),STT(I),SZZ(I),SRT(I),SRR(I)
     .  ,SEQ(I)
      IF(IUNLD.EQ.0) WRITE(7,3)AR(I),PERR(I),PETT(I)
     .  ,EZZ(I),PERT(I)
     .  ,(SEQ(I)/E(I)-SEQ(I)/EELAS)
IF(IUNLD.EQ.1) WRITE(6,3)AR(I),STT(I),SZZ(I)
     .  ,SRT(I),
     .  SRR(I),SEQ(I)
IF(IUNLD.EQ.1) WRITE(7,3)AR(I),PERR(I),PETT(I)
     .  ,EZZ(I),PERT(I),
     .  ((SEQ(I)/E(I))-(SEQ(I))/EELAS)
      ENDIF
 20   CONTINUE
      WRITE(5,*)
      WRITE(5,*)
      IF(NITER.EQ.1) RETURN
      IF(IUNLD.EQ.0) THEN
      WRITE(5,*)'HOOP   STRESS AT INSIDE CORE  :',STTIN
      WRITE(5,*)'AXIAL  STRESS AT INSIDE CORE  :',SZZIN
      WRITE(5,*)'RADIAL STRESS AT INSIDE CORE  :',SRRIN
      WRITE(5,*)'HOOP   STRAIN AT INSIDE CORE  :',ETTIN
      WRITE(5,*)'RADIAL STRAIN AT INSIDE CORE  :',ERRIN
      WRITE(5,*)
      WRITE(5,*)'RADIAL STRESS AT OUTSIDE CORE :',SRROUT
      WRITE(5,*)'RADIAL STRAIN AT OUTSIDE CORE :',ERROUT
      WRITE(5,*)'HOOP   STRESS AT OUTSIDE CORE :',STTOUT
      WRITE(5,*)'HOOP   STRAIN AT OUTSIDE CORE :',ETTOUT
      ELSE
      WRITE(5,*)'HOOP   STRESS AT INSIDE CORE  :',STTIN
```

```
      WRITE(5,*)'AXIAL  STRESS AT INSIDE CORE  :',SZZIN
      WRITE(5,*)'RADIAL STRESS AT INSIDE CORE  :',SRRIN
      WRITE(5,*)'AXIAL  STRESS AT INSIDE CORE  :',SZZIN
      WRITE(5,*)'RADIAL STRAIN AT INSIDE CORE  :',ERRIN
      WRITE(5,*)'HOOP   STRAIN AT INSIDE CORE  :',ETTIN
      WRITE(5,*)
      WRITE(5,*)'RADIAL STRESS AT OUTSIDE CORE :',SRROUT
      WRITE(5,*)'RADIAL STRAIN AT OUTSIDE CORE :',ERROUT
      WRITE(5,*)'HOOP   STRESS AT OUTSIDE CORE :',STTOUT
      WRITE(5,*)'HOOP   STRAIN AT OUTSIDE CORE :',ETTOUT
      ENDIF
1     FORMAT(1X,I5,3(8X,E12.6))
2     FORMAT(F5.2,4(3X,E12.5),2X,E12.5)
3     FORMAT(F7.3,5(2X,E12.5),2X,F10.6)
      RETURN
      END
```

APPENDIX B

MAPLE V.4 OUTPUT
TOTAL DEFORMATION THEORY FOR A SEQUENCE OF LINEAR LOADING
(LINEAR HARDENING MATERIALS)

This appendix includes a summary of the integration of Eq. (5.10) based on the output from MAPLE V.4. The result of this integration is given in Eq. (5.13).

```
> restart;
```

DEFINITIONS OF THE PROPORTIONALITY VARIABLES

```
> EQ:=(a+k*b)*((2*k-1)*h^2-(c^2-d^2))/(-k*(1-k)*h^2-k
  *(c^2-d^2)+c^2);
```

(B.1)

$$EQ := \frac{(a+k\,b)\,((2\,k-1)\,h^2-c^2+d^2)}{-k\,(1-k)\,h^2-k\,(c^2-d^2)+c^2}$$

INTEGRATION FROM THE STARTING AND ENDING POINT OF NEXT PROPORTIONAL LOADING

```
> FC:=int(EQ,k=0..1);
```

(B.2)

$$FC := (2\,b\sqrt{\%1}\,h^2 - 2\,\%3\,b\,d^2\,h^2 + 2\,a\sqrt{\%1}\,h^2\ln(d) + \%3\,b\,c^4$$
$$+ b\sqrt{\%1}\,h^2\ln(d) - 2\,\%3\,b\,c^2\,d^2 + b\,c^2\sqrt{\%1}\,\ln(d) + \%3\,b\,d^4$$
$$- b\,d^2\sqrt{\%1}\,\ln(d) - 2\,\%3\,b\,c^2\,h^2 + \%3\,b\,h^4) \Big/ (\sqrt{\%1}\,h^2) - (2\,\%2\,b\,d^2\,h^2$$
$$+ 2\,a\sqrt{\%1}\,h^2\ln(c) - \%2\,b\,c^4 + b\sqrt{\%1}\,h^2\ln(c) + 2\,\%2\,b\,c^2\,d^2$$

$$+ b\,c^2\sqrt{\%1}\,\ln(c) - \%2\,b\,d^4 - b\,d^2\sqrt{\%1}\,\ln(c) + 2\,\%2\,b\,c^2\,h^2 - \%2\,b\,h^4) \Big/ ($$
$$\sqrt{\%1}\,h^2)$$

$$\%1 := 2\,h^2\,c^2 - h^4 + 2\,h^2\,d^2 - c^4 + 2\,c^2\,d^2 - d^4$$

$$\%2 := \arctan\left(\frac{h^2 + c^2 - d^2}{\sqrt{\%1}}\right)$$

$$\%3 := \arctan\left(\frac{h^2 - c^2 + d^2}{\sqrt{\%1}}\right)$$

DEFINITION OF END POINTS STRESS AND STRAIN PARAMETERS

```
> alias(S[A]=a):
> alias(Delta(S)=b):
> alias(sigma[A]=c):
  (B.3)
> alias(sigma[B]=d):
> alias((Delta(epsilon[ij]))=FC1):
> alias((Delta(sigma))=h):
```

SUBSTITUTION

```
> EQ:=EQ;
  (B.4)
```

$$EQ := \frac{(S_A + k\,\Delta(S))\,((2\,k-1)\,\Delta(\sigma)^2 - \sigma_A^{\,2} + \sigma_B^{\,2})}{-k\,(1-k)\,\Delta(\sigma)^2 - k\,(\sigma_A^{\,2} - \sigma_B^{\,2}) + \sigma_A^{\,2}}$$

THE CHANGE IN PLASTIC STRAIN

```
> FC1:=FC;
  (B.5)
```

$$\Delta(\varepsilon_{ij}) := (2\,\Delta(S)\sqrt{\%1}\,\Delta(\sigma)^2 - 2\,\%3\,\Delta(S)\,\sigma_B^{\,2}\,\Delta(\sigma)^2$$
$$+ 2\,S_A\sqrt{\%1}\,\Delta(\sigma)^2\ln(\sigma_B) + \%3\,\Delta(S)\,\sigma_A^{\,4} + \Delta(S)\sqrt{\%1}\,\Delta(\sigma)^2\ln(\sigma_B)$$
$$- 2\,\%3\,\Delta(S)\,\sigma_A^{\,2}\,\sigma_B^{\,2} + \Delta(S)\,\sigma_A^{\,2}\sqrt{\%1}\,\ln(\sigma_B) + \%3\,\Delta(S)\,\sigma_B^{\,4}$$
$$- \Delta(S)\,\sigma_B^{\,2}\sqrt{\%1}\,\ln(\sigma_B) - 2\,\%3\,\Delta(S)\,\sigma_A^{\,2}\,\Delta(\sigma)^2 + \%3\,\Delta(S)\,\Delta(\sigma)^4) \Big/ (\sqrt{\%1}$$
$$\Delta(\sigma)^2) - (2\,\%2\,\Delta(S)\,\sigma_B^{\,2}\,\Delta(\sigma)^2 + 2\,S_A\sqrt{\%1}\,\Delta(\sigma)^2\ln(\sigma_A) - \%2\,\Delta(S)\,\sigma_A^{\,4}$$
$$+ \Delta(S)\sqrt{\%1}\,\Delta(\sigma)^2\ln(\sigma_A) + 2\,\%2\,\Delta(S)\,\sigma_A^{\,2}\,\sigma_B^{\,2} + \Delta(S)\,\sigma_A^{\,2}\sqrt{\%1}\,\ln(\sigma_A)$$

$$-\%2\,\Delta(S)\,\sigma_B^{\,4}-\Delta(S)\,\sigma_B^{\,2}\sqrt{\%1}\,\ln(\sigma_A)+2\,\%2\,\Delta(S)\,\sigma_A^{\,2}\,\Delta(\sigma)^2$$
$$-\%2\,\Delta(S)\,\Delta(\sigma)^4)\Big/(\sqrt{\%1}\,\Delta(\sigma)^2)$$

$$\%1 := 2\,\Delta(\sigma)^2\,\sigma_A^{\,2}-\Delta(\sigma)^4+2\,\Delta(\sigma)^2\,\sigma_B^{\,2}-\sigma_A^{\,4}+2\,\sigma_A^{\,2}\,\sigma_B^{\,2}-\sigma_B^{\,4}$$

$$\%2 := \arctan\left(\frac{\Delta(\sigma)^2+\sigma_A^{\,2}-\sigma_B^{\,2}}{\sqrt{\%1}}\right)$$

$$\%3 := \arctan\left(\frac{\Delta(\sigma)^2-\sigma_A^{\,2}+\sigma_B^{\,2}}{\sqrt{\%1}}\right)$$

SIMPLIFICATION

```
> simplify(");
  (B.6)
```

$$(2\,\Delta(S)\sqrt{\%1}\,\Delta(\sigma)^2-2\,\%3\,\Delta(S)\,\sigma_B^{\,2}\,\Delta(\sigma)^2+2\,S_A\sqrt{\%1}\,\Delta(\sigma)^2\ln(\sigma_B)$$
$$+\%3\,\Delta(S)\,\sigma_A^{\,4}+\Delta(S)\sqrt{\%1}\,\Delta(\sigma)^2\ln(\sigma_B)-2\,\%3\,\Delta(S)\,\sigma_A^{\,2}\,\sigma_B^{\,2}$$
$$+\Delta(S)\,\sigma_A^{\,2}\sqrt{\%1}\,\ln(\sigma_B)+\%3\,\Delta(S)\,\sigma_B^{\,4}-\Delta(S)\,\sigma_B^{\,2}\sqrt{\%1}\,\ln(\sigma_B)$$
$$-2\,\%3\,\Delta(S)\,\sigma_A^{\,2}\,\Delta(\sigma)^2+\%3\,\Delta(S)\,\Delta(\sigma)^4-2\,\%2\,\Delta(S)\,\sigma_B^{\,2}\,\Delta(\sigma)^2$$
$$-2\,S_A\sqrt{\%1}\,\Delta(\sigma)^2\ln(\sigma_A)+\%2\,\Delta(S)\,\sigma_A^{\,4}-\Delta(S)\sqrt{\%1}\,\Delta(\sigma)^2\ln(\sigma_A)$$
$$-2\,\%2\,\Delta(S)\,\sigma_A^{\,2}\,\sigma_B^{\,2}-\Delta(S)\,\sigma_A^{\,2}\sqrt{\%1}\,\ln(\sigma_A)+\%2\,\Delta(S)\,\sigma_B^{\,4}$$
$$+\Delta(S)\,\sigma_B^{\,2}\sqrt{\%1}\,\ln(\sigma_A)-2\,\%2\,\Delta(S)\,\sigma_A^{\,2}\,\Delta(\sigma)^2+\%2\,\Delta(S)\,\Delta(\sigma)^4)\Big/(\sqrt{\%1}$$
$$\Delta(\sigma)^2)$$

$$\%1 := 2\,\Delta(\sigma)^2\,\sigma_A^{\,2}-\Delta(\sigma)^4+2\,\Delta(\sigma)^2\,\sigma_B^{\,2}-\sigma_A^{\,4}+2\,\sigma_A^{\,2}\,\sigma_B^{\,2}-\sigma_B^{\,4}$$

$$\%2 := \arctan\left(\frac{\Delta(\sigma)^2+\sigma_A^{\,2}-\sigma_B^{\,2}}{\sqrt{\%1}}\right)$$

$$\%3 := \arctan\left(\frac{\Delta(\sigma)^2-\sigma_A^{\,2}+\sigma_B^{\,2}}{\sqrt{\%1}}\right)$$

APPENDIX C

PLASTIC STRAIN CALCULATION FOR A SEQUENCE OF LINEAR NONPROPORTIONAL LOADINGS

This appendix includes three items: 1) the subroutine that utilizes the total deformation formula given in Eq. (5.13) for calculation of plastic strain field, 2) MAPLE V.4 worksheet providing the integration results for materials obeying the Ramberg-Osgood relation, and 3) the FORTRAN code generated automatically by MAPLE V.4 based on the results of integration for the Ramberg-Osgood relation.

The MAPLE V.4 worksheet is a typical example for generating total deformation formula for nonhardening materials. In this example the Ramberg-Osgood relation in a form shown in Eq. (2.11) is used. The hardening exponent $n=0.287$, which is for stainless steel 304, is used. This Maple routine automatically generates a FORTRAN code shown at the end of this appendix.

```
**********************************************************************
C. THIS SUBROUTINE WILL ADJUST THE STRAIN FIELD FOR A
C. NONPROPORTIONAL LOADING USING THE DERIVED TOTAL
C. DEFORMATION FORMULATION
**********************************************************************
C. THE MAIN PROGRAM LISTING IS IN APPENDIX A
C. DEFINITION OF VARIABLES
      SUBROUTINE ADJUST
      IMPLICIT DOUBLE PRECISION (A-H,K,O-Z)
      DIMENSION DELSEQ(500),SRLPRM(500),STLPRM(500),SZLPRM(500)
     1  ,PETTL(500),PERRL(500),PERTL(500)
     2  ,SRPRM(500),STPRM(500),SZPRM(500),SIIL(500)
     3  ,SII(500),DELSRR(500),DELSZZ(500),DELSTT(500),DELSRT(500)
```

```
     4    ,DELERR(500),DELETT(500),DELEZZ(500),DELERT(500)
     5    ,EERRL(500),EETTL(500),EERTL(500)
          COMMON/BLK0/R(500),AR(500),MXITER,NELM,N,NITER,IUNLD,PII,POO,T
     .    ,MXITR,ITER,IDUM,IADJST,IBOUND
          COMMON/BLK1/K(2,2)
          COMMON/BLK2/A,B,AI,BO,YSTRES(500),SY,ERROR,ICURVE,ALPHA,M
          COMMON/BLK3/AA(500),BB(500),CC(500),U(500),P(500)
          COMMON/BLK4/SZZ(500),SRR(500),STT(500),SRT(500),SEQ(500)
          COMMON/BLK5/E(500),ANU(500),EELAS,ANUE,IPLANE,IYCRT
          COMMON/BLK6/SZZIN,SRRIN,STTIN,SRROUT
     .    ,STTOUT,ERRIN,ERROUT,ETTIN,ETTOUT
          COMMON/BLK7/EL(500),STTL(500),SRRL(500),SZZL(500),ETTL(500)
     .    ,ERRL(500)
     .    ,EZZL(500),UL(500),SEQL(500),SRRLIN,STTLIN,ERRLIN,ETTLIN,SRRLOT
     .    ,STTLOT,ERRLOT,ETTLOT,EEQL(500),SZZLIN,SRTL(500),ERTL(500)
          COMMON/BLK8/ERR(500),ETT(500),EZZ(500),ERT(500)
          COMMON/BLK9/NDAT,SIGDAT(20),ESTDAT(20),SYL(500),SLOPE(20)
          COMMON/BLK11/PERR(500),EERR(500),PETT(500),EETT(500)
     1    ,PERT(500),EERT(500)

          EEPLAS=SLOPE(2)
          IF(IADJST.EQ.0)THEN
C.SAVE THE STRESS VALUES OF THE FIRST LOADING
          DO 10 I=1,NELM
          EERRL(I)=(1.D0/EELAS)*SRRL(I)-(ANUE/EELAS)*(STTL(I)+SZZL(I))
          EETTL(I)=(1.D0/EELAS)*STTL(I)-(ANUE/EELAS)*(SRRL(I)+SZZL(I))
          EERTL(I)=2.D0*((1.D0+ANUE)/EELAS)*SRTL(I)
          PERRL(I)=ERRL(I)-EERRL(I)
          PETTL(I)=ETTL(I)-EETTL(I)
          PERTL(I)=ERTL(I)-EERTL(I)
C.FIND THE HYDROSTATIC PRESSURE AND THE DEVIATORIC STRESS OF
C.THE FIRST LOADING
          SIIL(I)=(1.D0/3.D0)*(SRRL(I)+STTL(I)+SZZL(I))
          SRLPRM(I)=SRRL(I)-SIIL(I)
          STLPRM(I)=STTL(I)-SIIL(I)
          SZLPRM(I)=SZZL(I)-SIIL(I)
 10       CONTINUE
          ELSE
          ENDIF
C.CALCULATE THE STRAINS
          DO 20 I=1,NELM
          IF(SEQ(I).GT.SY) THEN
```

```
C.FIND THE DEVIATORIC STRESS
        SII(I)=(1.D0/3.D0)*(SRR(I)+STT(I)+SZZ(I))
        SRPRM(I)=SRR(I)-SII(I)
        STPRM(I)=STT(I)-SII(I)
        SZPRM(I)=SZZ(I)-SII(I)
C.FIND THE CHANGES IN DEVIATORIC STRESS TENSOR
        DELSRR(I)=SRPRM(I)-SRLPRM(I)
        DELSTT(I)=STPRM(I)-STLPRM(I)
        DELSZZ(I)=SZPRM(I)-SZLPRM(I)
        DELSRT(I)=SRT(I)-SRTL(I)
C.FIND THE EQUIVALENT STRESS FOR STRESS CHANGES
        DELSEQ(I)=DSQRT(.5D0*((DELSTT(I)-DELSRR(I))**2
     .  +(DELSTT(I)-DELSZZ(I))**2+(DELSRR(I)-DELSZZ(I))**2
     .  +6.D0*DELSRT(I)**2))
C.FIND THE ELASTIC & PLASTIC STRAIN OF THE COMBINED PROPORTIONAL LOADING
        EERR(I)=(1.D0/EELAS)*SRR(I)-(ANUE/EELAS)*(STT(I)+SZZ(I))
        EETT(I)=(1.D0/EELAS)*STT(I)-(ANUE/EELAS)*(SRR(I)+SZZ(I))
        EERT(I)=2.D0*((1.D0+ANUE)/EELAS)*SRT(I)
        PERR(I)=ERR(I)-EERR(I)
        PETT(I)=ETT(I)-EETT(I)
        PERT(I)=ERT(I)-EERT(I)
C.CALL THE PLASTIC STRAIN CALCULATION SUBROUTINE GENERATED BY C.MAPLEV.4
        CALL PLSCAL(SRLPRM(I),DELSRR(I),SEQL(I),SEQ(I)
     1  ,DELSEQ(I),DELERR(I),M,ALPHA,EELAS,SY)
        CALL PLSCAL(STLPRM(I),DELSTT(I),SEQL(I),SEQ(I)
     1  ,DELSEQ(I),DELETT(I),M,ALPHA,EELAS,SY)
        CALL PLSCAL(SRTL(I),DELSRT(I),SEQL(I),SEQ(I)
     1  ,DELSEQ(I),DELERT(I),M,ALPHA,EELAS,SY)
        DELERT(I)=2.D0*DELERT(I)
C.ADD UP THE STRAINS
        PERR(I)=DELERR(I)+PERRL(I)
        PETT(I)=DELETT(I)+PETTL(I)
        PERT(I)=DELERT(I)+PERTL(I)
        ERR(I)=PERR(I)+EERR(I)
        ETT(I)=PETT(I)+EETT(I)
        ERT(I)=PERT(I)+EERT(I)
        ELSE
        PERR(I)=PERRL(I)
        PETT(I)=PETTL(I)
        PERT(I)=PERTL(I)
        ENDIF
 20     CONTINUE
```

```
CALL PRINT
IDUM=1
RETURN
END
```

MAPLE V.4

TOTAL DEFORMATION THEORY FOR A SEQUENCE OF LINEAR NONPROPORTIONAL LOADINGS
(RAMBERG-OSGOOD MATERIALS)
epsl(p)=(sig/H)^(1/n)

```
> restart;
```

DEFINITIONS OF THE PROPORTIONALITY VARIABLES

```
> EQ:=(sa+k*dels)*((2*k-1)*dsig^2-(siga^2-s
  igb^2))*(k*(-1+k)*dsig^2-k*(siga^2-sigb^2
  )+siga^2)^(7/2-3);
  (C.1)
```

$$EQ := \frac{(sa + k\,dels)\,((2k-1)\,dsig^2 - siga^2 + sigb^2)}{\sqrt{k(-1+k)\,dsig^2 - k\,(siga^2 - sigb^2) + siga^2}}$$

INTEGRATION FROM THE STARTING AND ENDING POINT OF NEXT PROPORTIONAL LOADING

```
> FC:=int(EQ,k=0..1);
  (C.2)
```

$$FC := \frac{1}{192}(3\,dels\,siga^8\ln(2) + 6\,dels\,siga^8\ln(dsig) + 3\,dels\,sigb^8\ln(2)$$
$$+ 6\,dels\,sigb^8\ln(dsig) - 3\,dels\,sigb^8\,\%2 - 3\,dels\,siga^8\,\%2$$
$$+ 112\,dels\,(sigb^2)^{3/2}\,dsig^4\sqrt{dsig^2} + 128\,sa\,(sigb^2)^{3/2}\,dsig^4\sqrt{dsig^2}$$
$$- 6\,dels\,sigb^2\sqrt{sigb^2}\,dsig^4\sqrt{dsig^2} - 18\,dels\,siga^2\sqrt{sigb^2}\,dsig^4\sqrt{dsig^2}$$
$$+ 6\,dels\,dsig^6\sqrt{sigb^2}\sqrt{dsig^2} - 6\,dels\,siga^6\sqrt{sigb^2}\sqrt{dsig^2}$$
$$- 16\,dels\,sigb^2\,(sigb^2)^{3/2}\,dsig^2\sqrt{dsig^2} - 6\,dels\,sigb^4\sqrt{sigb^2}\,dsig^2\sqrt{dsig^2}$$

$$
\begin{aligned}
&+ 16\,dels\,siga^2\,(sigb^2)^{3/2}\,dsig^2\sqrt{dsig^2} + 18\,dels\,siga^4\sqrt{sigb^2}\,sigb^2\sqrt{dsig^2}\\
&- 18\,dels\,siga^2\,sigb^4\sqrt{sigb^2}\sqrt{dsig^2} + 18\,dels\,siga^4\sqrt{sigb^2}\,dsig^2\sqrt{dsig^2}\\
&+ 6\,dels\,sigb^6\sqrt{sigb^2}\sqrt{dsig^2} - 12\,dels\,siga^2\sqrt{sigb^2}\,sigb^2\,dsig^2\sqrt{dsig^2}\\
&+ 3\,dels\,dsig^8\ln(2) - 3\,dels\,dsig^8\,\%2 + 6\,dels\,dsig^8\ln(dsig)\\
&+ 12\,dels\,siga^2\,sigb^6\,\%2 - 24\,dels\,siga^2\,sigb^6\ln(dsig) - 12\,dels\,siga^6\,sigb^2\ln(2)\\
&+ 12\,dels\,siga^6\,sigb^2\,\%2 - 24\,dels\,siga^6\,sigb^2\ln(dsig) + 18\,dels\,siga^4\,sigb^4\ln(2)\\
&- 18\,dels\,siga^4\,sigb^4\,\%2 + 36\,dels\,siga^4\,sigb^4\ln(dsig)\\
&- 12\,dels\,siga^2\,sigb^2\,dsig^4\,\%2 + 24\,dels\,siga^2\,sigb^2\,dsig^4\ln(dsig)\\
&- 12\,dels\,sigb^6\,dsig^2\ln(2) + 12\,dels\,sigb^6\,dsig^2\,\%2 - 24\,dels\,sigb^6\,dsig^2\ln(dsig)\\
&- 12\,dels\,dsig^6\,sigb^2\ln(2) + 12\,dels\,dsig^6\,sigb^2\,\%2 - 24\,dels\,dsig^6\,sigb^2\ln(dsig)\\
&- 12\,dels\,siga^6\,dsig^2\ln(2) + 12\,dels\,siga^6\,dsig^2\,\%2 - 24\,dels\,siga^6\,dsig^2\ln(dsig)\\
&+ 12\,dels\,siga^4\,sigb^2\,dsig^2\ln(2) - 12\,dels\,siga^4\,sigb^2\,dsig^2\,\%2\\
&+ 24\,dels\,siga^4\,sigb^2\,dsig^2\ln(dsig) + 18\,dels\,siga^4\,dsig^4\ln(2)\\
&- 18\,dels\,siga^4\,dsig^4\,\%2 + 36\,dels\,siga^4\,dsig^4\ln(dsig) + 18\,dels\,sigb^4\,dsig^4\ln(2)\\
&- 18\,dels\,sigb^4\,dsig^4\,\%2 + 36\,dels\,sigb^4\,dsig^4\ln(dsig) - 12\,dels\,dsig^6\,siga^2\ln(2)\\
&+ 12\,dels\,dsig^6\,siga^2\,\%2 - 24\,dels\,dsig^6\,siga^2\ln(dsig)\\
&+ 12\,dels\,siga^2\,sigb^4\,dsig^2\ln(2) - 12\,dels\,siga^2\,sigb^4\,dsig^2\,\%2\\
&+ 24\,dels\,siga^2\,sigb^4\,dsig^2\ln(dsig) + 12\,dels\,siga^2\,sigb^2\,dsig^4\ln(2)\\
&- 12\,dels\,siga^2\,sigb^6\ln(2))\Big/(dsig^4\sqrt{dsig^2}) + \frac{1}{192}(-3\,dels\,siga^8\ln(2)\\
&- 6\,dels\,siga^8\ln(dsig) - 3\,dels\,sigb^8\ln(2) + 3\,dels\,sigb^8\,\%1 + 3\,dels\,siga^8\,\%1\\
&+ 3\,dels\,dsig^8\,\%1 - 6\,dels\,sigb^8\ln(dsig) + 12\,dels\,siga^2\,sigb^2\,dsig^4\,\%1\\
&+ 12\,dels\,siga^2\,sigb^4\,dsig^2\,\%1 - 12\,dels\,sigb^6\,dsig^2\,\%1 + 18\,dels\,sigb^4\,dsig^4\,\%1\\
&- 12\,dels\,siga^6\,dsig^2\,\%1 - 12\,dels\,siga^2\,sigb^6\,\%1 + 18\,dels\,siga^4\,sigb^4\,\%1\\
&- 12\,dels\,dsig^6\,sigb^2\,\%1 + 18\,dels\,siga^4\,dsig^4\,\%1 + 12\,dels\,siga^4\,sigb^2\,dsig^2\,\%1\\
&- 12\,dels\,dsig^6\,siga^2\,\%1 - 12\,dels\,siga^6\,sigb^2\,\%1 - 3\,dels\,dsig^8\ln(2)\\
&- 6\,dels\,dsig^8\ln(dsig) + 24\,dels\,siga^2\,sigb^6\ln(dsig) + 12\,dels\,siga^6\,sigb^2\ln(2)\\
&+ 24\,dels\,siga^6\,sigb^2\ln(dsig) - 18\,dels\,siga^4\,sigb^4\ln(2)\\
&- 36\,dels\,siga^4\,sigb^4\ln(dsig) - 24\,dels\,siga^2\,sigb^2\,dsig^4\ln(dsig)\\
&+ 12\,dels\,sigb^6\,dsig^2\ln(2) + 24\,dels\,sigb^6\,dsig^2\ln(dsig)\\
&+ 12\,dels\,dsig^6\,sigb^2\ln(2) + 24\,dels\,dsig^6\,sigb^2\ln(dsig)\\
&+ 12\,dels\,siga^6\,dsig^2\ln(2) + 24\,dels\,siga^6\,dsig^2\ln(dsig)\\
&- 12\,dels\,siga^4\,sigb^2\,dsig^2\ln(2) - 24\,dels\,siga^4\,sigb^2\,dsig^2\ln(dsig)\\
&- 18\,dels\,siga^4\,dsig^4\ln(2) - 36\,dels\,siga^4\,dsig^4\ln(dsig)\\
&- 18\,dels\,sigb^4\,dsig^4\ln(2) - 36\,dels\,sigb^4\,dsig^4\ln(dsig)\\
&+ 12\,dels\,dsig^6\,siga^2\ln(2) + 24\,dels\,dsig^6\,siga^2\ln(dsig)
\end{aligned}
$$

$$
\begin{aligned}
&- 12\,dels\,siga^2\,sigb^4\,dsig^2\ln(2) - 24\,dels\,siga^2\,sigb^4\,dsig^2\ln(dsig)\\
&- 12\,dels\,siga^2\,sigb^2\,dsig^4\ln(2) + 12\,dels\,siga^2\,sigb^6\ln(2)\\
&+ 16\,dels\,sigb^2\,(siga^2)^{3/2}\,dsig^2\sqrt{dsig^2} - 18\,dels\,sigb^2\sqrt{siga^2}\,dsig^4\sqrt{dsig^2}\\
&- 6\,dels\sqrt{siga^2\,siga^2}\,dsig^4\sqrt{dsig^2} + 6\,dels\,siga^6\sqrt{siga^2}\sqrt{dsig^2}\\
&- 6\,dels\,siga^4\sqrt{siga^2\,dsig^2}\sqrt{dsig^2} - 12\,dels\,siga^2\sqrt{siga^2\,sigb^2\,dsig^2}\sqrt{dsig^2}\\
&+ 18\,dels\,sigb^4\sqrt{siga^2}\,dsig^2\sqrt{dsig^2} + 18\,dels\,siga^2\,sigb^4\sqrt{siga^2}\sqrt{dsig^2}\\
&- 16\,dels\,siga^2\,(siga^2)^{3/2}\,dsig^2\sqrt{dsig^2} - 18\,dels\,siga^4\sqrt{siga^2}\,sigb^2\sqrt{dsig^2}\\
&- 6\,dels\,sigb^6\sqrt{siga^2}\sqrt{dsig^2} - 16\,dels\,(siga^2)^{3/2}\,dsig^4\sqrt{dsig^2}\\
&- 128\,sa\,(siga^2)^{3/2}\,dsig^4\sqrt{dsig^2} + 6\,dels\,dsig^6\sqrt{siga^2}\sqrt{dsig^2}\Big) \Big/ \left(dsig^4\sqrt{dsig^2}\right)
\end{aligned}
$$

$$
\%1 := \ln\left(-\sqrt{dsig^2}\,dsig^2 - \sqrt{dsig^2}\,siga^2 + \sqrt{dsig^2}\,sigb^2 + 2\sqrt{siga^2}\,dsig^2\right)
$$

$$
\%2 := \ln\left(\sqrt{dsig^2}\,dsig^2 - \sqrt{dsig^2}\,siga^2 + \sqrt{dsig^2}\,sigb^2 + 2\sqrt{sigb^2}\,dsig^2\right)
$$

DEFINITION OF END POINTS STRESS AND STRAIN PARAMETER

```
> alias(S[A]=sa):
> alias(Delta(S)=dels):
> alias(sigma[A]=siga):
> alias(sigma[B]=sigb):
  (C.3)
> alias((Delta(epsilon[ij]))=FC1):
> alias((Delta(sigma))=dsig):
```

SUBSTITUTION

```
> FC1:=FC;
```

$$
\begin{aligned}
\Delta(\varepsilon_{ij}) := \frac{1}{192}\,&(3\,\Delta(S)\,\sigma_A^{\,8}\ln(2) + 6\,\Delta(S)\,\sigma_A^{\,8}\ln(\Delta(\sigma)) + 3\,\Delta(S)\,\sigma_B^{\,8}\ln(2)\\
&+ 6\,\Delta(S)\,\sigma_B^{\,8}\ln(\Delta(\sigma)) - 3\,\Delta(S)\,\sigma_B^{\,8}\,\%5 - 3\,\Delta(S)\,\sigma_A^{\,8}\,\%5\\
&+ 112\,\Delta(S)\,(\sigma_B^{\,2})^{3/2}\,\Delta(\sigma)^4\sqrt{\Delta(\sigma)^2} + 128\,S_A\,(\sigma_B^{\,2})^{3/2}\,\Delta(\sigma)^4\sqrt{\Delta(\sigma)^2}\\
&- 6\,\Delta(S)\,\sigma_B^{\,2}\sqrt{\sigma_B^{\,2}}\,\Delta(\sigma)^4\sqrt{\Delta(\sigma)^2} - 18\,\Delta(S)\,\sigma_A^{\,2}\sqrt{\sigma_B^{\,2}}\,\Delta(\sigma)^4\sqrt{\Delta(\sigma)^2}
\end{aligned}
$$

$$+6\,\Delta(S)\,\Delta(\sigma)^6\sqrt{\sigma_B^{\,2}}\sqrt{\Delta(\sigma)^2}-6\,\Delta(S)\,\sigma_A^{\,6}\sqrt{\sigma_B^{\,2}}\sqrt{\Delta(\sigma)^2}$$
$$-16\,\Delta(S)\,\sigma_B^{\,2}\,(\sigma_B^{\,2})^{3/2}\,\Delta(\sigma)^2\sqrt{\Delta(\sigma)^2}-6\,\Delta(S)\,\sigma_B^{\,4}\sqrt{\sigma_B^{\,2}}\,\Delta(\sigma)^2\sqrt{\Delta(\sigma)^2}$$
$$+16\,\Delta(S)\,\sigma_A^{\,2}\,(\sigma_B^{\,2})^{3/2}\,\Delta(\sigma)^2\sqrt{\Delta(\sigma)^2}+18\,\Delta(S)\,\sigma_A^{\,4}\sqrt{\sigma_B^{\,2}}\,\sigma_B^{\,2}\sqrt{\Delta(\sigma)^2}$$
$$-18\,\Delta(S)\,\sigma_A^{\,2}\,\sigma_B^{\,4}\sqrt{\sigma_B^{\,2}}\sqrt{\Delta(\sigma)^2}+18\,\Delta(S)\,\sigma_A^{\,4}\sqrt{\sigma_B^{\,2}}\,\Delta(\sigma)^2\sqrt{\Delta(\sigma)^2}$$
$$+6\,\Delta(S)\,\sigma_B^{\,6}\sqrt{\sigma_B^{\,2}}\sqrt{\Delta(\sigma)^2}-12\,\Delta(S)\,\sigma_A^{\,2}\sqrt{\sigma_B^{\,2}}\,\sigma_B^{\,2}\,\Delta(\sigma)^2\sqrt{\Delta(\sigma)^2}$$
$$+3\,\Delta(S)\,\Delta(\sigma)^8\ln(2)-3\,\Delta(S)\,\Delta(\sigma)^8\,\%5+6\,\Delta(S)\,\Delta(\sigma)^8\ln(\Delta(\sigma))$$
$$+12\,\Delta(S)\,\sigma_A^{\,2}\,\sigma_B^{\,6}\,\%5-24\,\Delta(S)\,\sigma_A^{\,2}\,\sigma_B^{\,6}\ln(\Delta(\sigma))-12\,\Delta(S)\,\sigma_A^{\,6}\,\sigma_B^{\,2}\ln(2)$$
$$+12\,\Delta(S)\,\sigma_A^{\,6}\,\sigma_B^{\,2}\,\%5-24\,\Delta(S)\,\sigma_A^{\,6}\,\sigma_B^{\,2}\ln(\Delta(\sigma))+18\,\Delta(S)\,\sigma_A^{\,4}\,\sigma_B^{\,4}\ln(2)$$
$$-18\,\Delta(S)\,\sigma_A^{\,4}\,\sigma_B^{\,4}\,\%5+36\,\Delta(S)\,\sigma_A^{\,4}\,\sigma_B^{\,4}\ln(\Delta(\sigma))-12\,\Delta(S)\,\sigma_A^{\,2}\,\sigma_B^{\,2}\,\Delta(\sigma)^4\,\%5$$
$$+24\,\Delta(S)\,\sigma_A^{\,2}\,\sigma_B^{\,2}\,\Delta(\sigma)^4\ln(\Delta(\sigma))-12\,\Delta(S)\,\sigma_B^{\,6}\,\Delta(\sigma)^2\ln(2)$$
$$+12\,\Delta(S)\,\sigma_B^{\,6}\,\Delta(\sigma)^2\,\%5-24\,\Delta(S)\,\sigma_B^{\,6}\,\Delta(\sigma)^2\ln(\Delta(\sigma))$$
$$-12\,\Delta(S)\,\Delta(\sigma)^6\,\sigma_B^{\,2}\ln(2)+12\,\Delta(S)\,\Delta(\sigma)^6\,\sigma_B^{\,2}\,\%5$$
$$-24\,\Delta(S)\,\Delta(\sigma)^6\,\sigma_B^{\,2}\ln(\Delta(\sigma))-12\,\Delta(S)\,\sigma_A^{\,6}\,\Delta(\sigma)^2\ln(2)$$
$$+12\,\Delta(S)\,\sigma_A^{\,6}\,\Delta(\sigma)^2\,\%5-24\,\Delta(S)\,\sigma_A^{\,6}\,\Delta(\sigma)^2\ln(\Delta(\sigma))$$
$$+12\,\Delta(S)\,\sigma_A^{\,4}\,\sigma_B^{\,2}\,\Delta(\sigma)^2\ln(2)-12\,\Delta(S)\,\sigma_A^{\,4}\,\sigma_B^{\,2}\,\Delta(\sigma)^2\,\%5$$
$$+24\,\Delta(S)\,\sigma_A^{\,4}\,\sigma_B^{\,2}\,\Delta(\sigma)^2\ln(\Delta(\sigma))+18\,\Delta(S)\,\sigma_A^{\,4}\,\Delta(\sigma)^4\ln(2)$$
$$-18\,\Delta(S)\,\sigma_A^{\,4}\,\Delta(\sigma)^4\,\%5+36\,\Delta(S)\,\sigma_A^{\,4}\,\Delta(\sigma)^4\ln(\Delta(\sigma))$$
$$+18\,\Delta(S)\,\sigma_B^{\,4}\,\Delta(\sigma)^4\ln(2)-18\,\Delta(S)\,\sigma_B^{\,4}\,\Delta(\sigma)^4\,\%5$$
$$+36\,\Delta(S)\,\sigma_B^{\,4}\,\Delta(\sigma)^4\ln(\Delta(\sigma))-12\,\Delta(S)\,\Delta(\sigma)^6\,\sigma_A^{\,2}\ln(2)$$
$$+12\,\Delta(S)\,\Delta(\sigma)^6\,\sigma_A^{\,2}\,\%5-24\,\Delta(S)\,\Delta(\sigma)^6\,\sigma_A^{\,2}\ln(\Delta(\sigma))$$
$$+12\,\Delta(S)\,\sigma_A^{\,2}\,\sigma_B^{\,4}\,\Delta(\sigma)^2\ln(2)-12\,\Delta(S)\,\sigma_A^{\,2}\,\sigma_B^{\,4}\,\Delta(\sigma)^2\,\%5$$
$$+24\,\Delta(S)\,\sigma_A^{\,2}\,\sigma_B^{\,4}\,\Delta(\sigma)^2\ln(\Delta(\sigma))+12\,\Delta(S)\,\sigma_A^{\,2}\,\sigma_B^{\,2}\,\Delta(\sigma)^4\ln(2)$$
$$-12\,\Delta(S)\,\sigma_A^{\,2}\,\sigma_B^{\,6}\ln(2))\Big/(\Delta(\sigma)^4\sqrt{\Delta(\sigma)^2})+\frac{1}{192}(-3\,\Delta(S)\,\sigma_A^{\,8}\ln(2)$$
$$-6\,\Delta(S)\,\sigma_A^{\,8}\ln(\Delta(\sigma))-3\,\Delta(S)\,\sigma_B^{\,8}\ln(2)+3\,\Delta(S)\,\sigma_B^{\,8}\,\%4+3\,\Delta(S)\,\sigma_A^{\,8}\,\%4$$
$$+3\,\Delta(S)\,\Delta(\sigma)^8\,\%4-6\,\Delta(S)\,\sigma_B^{\,8}\ln(\Delta(\sigma))+12\,\Delta(S)\,\sigma_A^{\,2}\,\sigma_B^{\,2}\,\Delta(\sigma)^4\,\%4$$
$$+12\,\Delta(S)\,\sigma_A^{\,2}\,\sigma_B^{\,4}\,\Delta(\sigma)^2\,\%4-12\,\Delta(S)\,\sigma_B^{\,6}\,\Delta(\sigma)^2\,\%4+18\,\Delta(S)\,\sigma_B^{\,4}\,\Delta(\sigma)^4\,\%4$$

$$
\begin{aligned}
&- 12\,\Delta(S)\,\sigma_A^{\,6}\,\Delta(\sigma)^2\,\%4 - 12\,\Delta(S)\,\sigma_A^{\,2}\,\sigma_B^{\,6}\,\%4 + 18\,\Delta(S)\,\sigma_A^{\,4}\,\sigma_B^{\,4}\,\%4 \\
&- 12\,\Delta(S)\,\Delta(\sigma)^6\,\sigma_B^{\,2}\,\%4 + 18\,\Delta(S)\,\sigma_A^{\,4}\,\Delta(\sigma)^4\,\%4 + 12\,\Delta(S)\,\sigma_A^{\,4}\,\sigma_B^{\,2}\,\Delta(\sigma)^2\,\%4 \\
&- 12\,\Delta(S)\,\Delta(\sigma)^6\,\sigma_A^{\,2}\,\%4 - 12\,\Delta(S)\,\sigma_A^{\,6}\,\sigma_B^{\,2}\,\%4 - 3\,\Delta(S)\,\Delta(\sigma)^8\ln(2) \\
&- 6\,\Delta(S)\,\Delta(\sigma)^8\ln(\Delta(\sigma)) + 24\,\Delta(S)\,\sigma_A^{\,2}\,\sigma_B^{\,6}\ln(\Delta(\sigma)) + 12\,\Delta(S)\,\sigma_A^{\,6}\,\sigma_B^{\,2}\ln(2) \\
&+ 24\,\Delta(S)\,\sigma_A^{\,6}\,\sigma_B^{\,2}\ln(\Delta(\sigma)) - 18\,\Delta(S)\,\sigma_A^{\,4}\,\sigma_B^{\,4}\ln(2) - 36\,\Delta(S)\,\sigma_A^{\,4}\,\sigma_B^{\,4}\ln(\Delta(\sigma)) \\
&- 24\,\Delta(S)\,\sigma_A^{\,2}\,\sigma_B^{\,2}\,\Delta(\sigma)^4\ln(\Delta(\sigma)) + 12\,\Delta(S)\,\sigma_B^{\,6}\,\Delta(\sigma)^2\ln(2) \\
&+ 24\,\Delta(S)\,\sigma_B^{\,6}\,\Delta(\sigma)^2\ln(\Delta(\sigma)) + 12\,\Delta(S)\,\Delta(\sigma)^6\,\sigma_B^{\,2}\ln(2) \\
&+ 24\,\Delta(S)\,\Delta(\sigma)^6\,\sigma_B^{\,2}\ln(\Delta(\sigma)) + 12\,\Delta(S)\,\sigma_A^{\,6}\,\Delta(\sigma)^2\ln(2) \\
&+ 24\,\Delta(S)\,\sigma_A^{\,6}\,\Delta(\sigma)^2\ln(\Delta(\sigma)) - 12\,\Delta(S)\,\sigma_A^{\,4}\,\sigma_B^{\,2}\,\Delta(\sigma)^2\ln(2) \\
&- 24\,\Delta(S)\,\sigma_A^{\,4}\,\sigma_B^{\,2}\,\Delta(\sigma)^2\ln(\Delta(\sigma)) - 18\,\Delta(S)\,\sigma_A^{\,4}\,\Delta(\sigma)^4\ln(2) \\
&- 36\,\Delta(S)\,\sigma_A^{\,4}\,\Delta(\sigma)^4\ln(\Delta(\sigma)) - 18\,\Delta(S)\,\sigma_B^{\,4}\,\Delta(\sigma)^4\ln(2) \\
&- 36\,\Delta(S)\,\sigma_B^{\,4}\,\Delta(\sigma)^4\ln(\Delta(\sigma)) + 12\,\Delta(S)\,\Delta(\sigma)^6\,\sigma_A^{\,2}\ln(2) \\
&+ 24\,\Delta(S)\,\Delta(\sigma)^6\,\sigma_A^{\,2}\ln(\Delta(\sigma)) - 12\,\Delta(S)\,\sigma_A^{\,2}\,\sigma_B^{\,4}\,\Delta(\sigma)^2\ln(2) \\
&- 24\,\Delta(S)\,\sigma_A^{\,2}\,\sigma_B^{\,4}\,\Delta(\sigma)^2\ln(\Delta(\sigma)) - 12\,\Delta(S)\,\sigma_A^{\,2}\,\sigma_B^{\,2}\,\Delta(\sigma)^4\ln(2) \\
&+ 12\,\Delta(S)\,\sigma_A^{\,2}\,\sigma_B^{\,6}\ln(2) + 16\,\Delta(S)\,\sigma_B^{\,2}\,(\sigma_A^{\,2})^{3/2}\,\Delta(\sigma)^2\sqrt{\Delta(\sigma)^2} \\
&- 18\,\Delta(S)\,\sigma_B^{\,2}\sqrt{\sigma_A^{\,2}}\,\Delta(\sigma)^4\sqrt{\Delta(\sigma)^2} - 6\,\Delta(S)\sqrt{\sigma_A^{\,2}\,\sigma_A^{\,2}}\,\Delta(\sigma)^4\sqrt{\Delta(\sigma)^2} \\
&+ 6\,\Delta(S)\,\sigma_A^{\,6}\sqrt{\sigma_A^{\,2}}\sqrt{\Delta(\sigma)^2} - 6\,\Delta(S)\,\sigma_A^{\,4}\sqrt{\sigma_A^{\,2}}\,\Delta(\sigma)^2\sqrt{\Delta(\sigma)^2} \\
&- 12\,\Delta(S)\,\sigma_A^{\,2}\sqrt{\sigma_A^{\,2}\,\sigma_B^{\,2}}\,\Delta(\sigma)^2\sqrt{\Delta(\sigma)^2} + 18\,\Delta(S)\,\sigma_B^{\,4}\sqrt{\sigma_A^{\,2}}\,\Delta(\sigma)^2\sqrt{\Delta(\sigma)^2} \\
&+ 18\,\Delta(S)\,\sigma_A^{\,2}\,\sigma_B^{\,4}\sqrt{\sigma_A^{\,2}}\sqrt{\Delta(\sigma)^2} - 16\,\Delta(S)\,\sigma_A^{\,2}\,(\sigma_A^{\,2})^{3/2}\,\Delta(\sigma)^2\sqrt{\Delta(\sigma)^2} \\
&- 18\,\Delta(S)\,\sigma_A^{\,4}\sqrt{\sigma_A^{\,2}\,\sigma_B^{\,2}}\sqrt{\Delta(\sigma)^2} - 6\,\Delta(S)\,\sigma_B^{\,6}\sqrt{\sigma_A^{\,2}}\sqrt{\Delta(\sigma)^2} \\
&- 16\,\Delta(S)\,(\sigma_A^{\,2})^{3/2}\,\Delta(\sigma)^4\sqrt{\Delta(\sigma)^2} - 128\,S_A\,(\sigma_A^{\,2})^{3/2}\,\Delta(\sigma)^4\sqrt{\Delta(\sigma)^2} \\
&+ 6\,\Delta(S)\,\Delta(\sigma)^6\sqrt{\sigma_A^{\,2}}\sqrt{\Delta(\sigma)^2}\Big) \Big/ \left(\Delta(\sigma)^4\sqrt{\Delta(\sigma)^2}\right)
\end{aligned}
$$

$$\%1 := \sqrt{\Delta(\sigma)^2}\,\sigma_B^{\,2}$$

$$\%2 := \sqrt{\Delta(\sigma)^2}\,\sigma_A^{\,2}$$

$$\%3 := \sqrt{\Delta(\sigma)^2}\,\Delta(\sigma)^2$$

$$\%4 := \ln(-\%3 - \%2 + \%1 + 2\sqrt{\sigma_A^{\,2}}\,\Delta(\sigma)^2)$$

$$\%5 := \ln(\%3 - \%2 + \%1 + 2\sqrt{\sigma_B^{\,2}}\,\Delta(\sigma)^2)$$

```
> append to(general);
```

CREAT A FORTRAN PROGRAM AND ADD IT TO THE CODE CALLED GENERAL

```
> fortran(");
```

```
C....THIS ROUTINE IS GENERATED BY MAPLE V.4
C....PLASTIC STRAIN CALCULATION
      SUBROUTINE PLSCAL(SA,DELS,SIGA,SIGB,DSIG,T0,M,ALPHA,EE,SY)
      DELPHI=(3./4.)*ALPHA*M/(EE*(SY**(M-1)))
      S2 = DELPHI/192
      S6 = 3*DELS*SIGA**8*ALOG(2.E0)+6*DELS*DSIG**8*ALOG(DSIG)-3*DELS*DS
     ,IG**8*ALOG(SQRT(DSIG**2)*DSIG**2-SQRT(DSIG**2)*SIGA**2+SQRT(DSIG**
     ,2)*SIGB**2+2*SQRT(SIGB**2)*DSIG**2)+3*DELS*DSIG**8*ALOG(2.E0)+6*DE
     ,LS*SIGA**8*ALOG(DSIG)+3*DELS*SIGB**8*ALOG(2.E0)+6*DELS*SIGB**8*ALO
     ,G(DSIG)-3*DELS*SIGB**8*ALOG(SQRT(DSIG**2)*DSIG**2-SQRT(DSIG**2)*SI
     ,GA**2+SQRT(DSIG**2)*SIGB**2+2*SQRT(SIGB**2)*DSIG**2)-3*DELS*SIGA**
     ,8*ALOG(SQRT(DSIG**2)*DSIG**2-SQRT(DSIG**2)*SIGA**2+SQRT(DSIG**2)*S
     ,IGB**2+2*SQRT(SIGB**2)*DSIG**2)-12*DELS*SIGB**6*DSIG**2*ALOG(2.E0)
     ,+6*DELS*DSIG**6*SQRT(SIGB**2)*SQRT(DSIG**2)+112*DELS*SQRT(SIGB**2)
     ,**3*DSIG**4*SQRT(DSIG**2)-18*DELS*SIGA**2*SQRT(SIGB**2)*DSIG**4*SQ
     ,RT(DSIG**2)+128*SA*SQRT(SIGB**2)**3*DSIG**4*SQRT(DSIG**2)
      S7 = S6-16*DELS*SIGB**2*SQRT(SIGB**2)**3*DSIG**2*SQRT(DSIG**2)+18*
     ,DELS*SIGA**4*SQRT(SIGB**2)*DSIG**2*SQRT(DSIG**2)-12*DELS*SIGA**2*S
     ,QRT(SIGB**2)*SIGB**2*DSIG**2*SQRT(DSIG**2)-6*DELS*SIGB**2*SQRT(SIG
     ,B**2)*DSIG**4*SQRT(DSIG**2)-6*DELS*SIGA**6*SQRT(SIGB**2)*SQRT(DSIG
     ,**2)-6*DELS*SIGB**4*SQRT(SIGB**2)*DSIG**2*SQRT(DSIG**2)+18*DELS*SI
     ,GA**4*SQRT(SIGB**2)*SIGB**2*SQRT(DSIG**2)
      S5 = S7+16*DELS*SIGA**2*SQRT(SIGB**2)**3*DSIG**2*SQRT(DSIG**2)-18*
     ,DELS*SIGA**2*SIGB**4*SQRT(SIGB**2)*SQRT(DSIG**2)+12*DELS*SIGA**2*S
     ,IGB**6*ALOG(SQRT(DSIG**2)*DSIG**2-SQRT(DSIG**2)*SIGA**2+SQRT(DSIG*
     ,*2)*SIGB**2+2*SQRT(SIGB**2)*DSIG**2)-12*DELS*SIGA**2*SIGB**6*ALOG(
     ,2.E0)-24*DELS*SIGB**6*DSIG**2*ALOG(DSIG)+12*DELS*SIGB**6*DSIG**2*A
     ,LOG(SQRT(DSIG**2)*DSIG**2-SQRT(DSIG**2)*SIGA**2+SQRT(DSIG**2)*SIGB
     ,**2+2*SQRT(SIGB**2)*DSIG**2)+6*DELS*SIGB**6*SQRT(SIGB**2)*SQRT(DSI
     ,G**2)-12*DELS*SIGA**6*SIGB**2*ALOG(2.E0)
      S7 = 36*DELS*SIGA**4*SIGB**4*ALOG(DSIG)-18*DELS*SIGA**4*SIGB**4*AL
     ,OG(SQRT(DSIG**2)*DSIG**2-SQRT(DSIG**2)*SIGA**2+SQRT(DSIG**2)*SIGB*
     ,*2+2*SQRT(SIGB**2)*DSIG**2)+18*DELS*SIGA**4*SIGB**4*ALOG(2.E0)-24*
     ,DELS*SIGA**2*SIGB**6*ALOG(DSIG)-24*DELS*SIGA**6*SIGB**2*ALOG(DSIG)
     ,+12*DELS*SIGA**6*SIGB**2*ALOG(SQRT(DSIG**2)*DSIG**2-SQRT(DSIG**2)*
     ,SIGA**2+SQRT(DSIG**2)*SIGB**2+2*SQRT(SIGB**2)*DSIG**2)+24*DELS*SIG
     ,A**4*SIGB**2*DSIG**2*ALOG(DSIG)
      S6 = S7-12*DELS*SIGA**4*SIGB**2*DSIG**2*ALOG(SQRT(DSIG**2)*DSIG**2
     ,-SQRT(DSIG**2)*SIGA**2+SQRT(DSIG**2)*SIGB**2+2*SQRT(SIGB**2)*DSIG*
     ,*2)+12*DELS*SIGA**4*SIGB**2*DSIG**2*ALOG(2.E0)-24*DELS*DSIG**6*SIG
```

```
     ,A**2*ALOG(DSIG)+12*DELS*DSIG**6*SIGA**2*ALOG(SQRT(DSIG**2)*DSIG**2
     ,-SQRT(DSIG**2)*SIGA**2+SQRT(DSIG**2)*SIGB**2+2*SQRT(SIGB**2)*DSIG*
     ,*2)-12*DELS*DSIG**6*SIGA**2*ALOG(2.E0)-12*DELS*SIGA**2*SIGB**4*DSI
     ,G**2*ALOG(SQRT(DSIG**2)*DSIG**2-SQRT(DSIG**2)*SIGA**2+SQRT(DSIG**2
     ,)*SIGB**2+2*SQRT(SIGB**2)*DSIG**2)+12*DELS*SIGA**2*SIGB**4*DSIG**2
     ,*ALOG(2.E0)+36*DELS*SIGB**4*DSIG**4*ALOG(DSIG)
      S7 = S6-18*DELS*SIGB**4*DSIG**4*ALOG(SQRT(DSIG**2)*DSIG**2-SQRT(DS
     ,IG**2)*SIGA**2+SQRT(DSIG**2)*SIGB**2+2*SQRT(SIGB**2)*DSIG**2)+18*D
     ,ELS*SIGB**4*DSIG**4*ALOG(2.E0)+36*DELS*SIGA**4*DSIG**4*ALOG(DSIG)-
     ,18*DELS*SIGA**4*DSIG**4*ALOG(SQRT(DSIG**2)*DSIG**2-SQRT(DSIG**2)*S
     ,IGA**2+SQRT(DSIG**2)*SIGB**2+2*SQRT(SIGB**2)*DSIG**2)+18*DELS*SIGA
     ,**4*DSIG**4*ALOG(2.E0)+12*DELS*SIGA**6*DSIG**2*ALOG(SQRT(DSIG**2)*
     ,DSIG**2-SQRT(DSIG**2)*SIGA**2+SQRT(DSIG**2)*SIGB**2+2*SQRT(SIGB**2
     ,)*DSIG**2)-12*DELS*SIGA**6*DSIG**2*ALOG(2.E0)
      S4 = S7-12*DELS*DSIG**6*SIGB**2*ALOG(2.E0)-24*DELS*DSIG**6*SIGB**2
     ,*ALOG(DSIG)+12*DELS*DSIG**6*SIGB**2*ALOG(SQRT(DSIG**2)*DSIG**2-SQR
     ,T(DSIG**2)*SIGA**2+SQRT(DSIG**2)*SIGB**2+2*SQRT(SIGB**2)*DSIG**2)+
     ,24*DELS*SIGA**2*SIGB**2*DSIG**4*ALOG(DSIG)-12*DELS*SIGA**2*SIGB**2
     ,*DSIG**4*ALOG(SQRT(DSIG**2)*DSIG**2-SQRT(DSIG**2)*SIGA**2+SQRT(DSI
     ,G**2)*SIGB**2+2*SQRT(SIGB**2)*DSIG**2)+12*DELS*SIGA**2*SIGB**2*DSI
     ,G**4*ALOG(2.E0)+24*DELS*SIGA**2*SIGB**4*DSIG**2*ALOG(DSIG)-24*DELS
     ,*SIGA**6*DSIG**2*ALOG(DSIG)+S5
      S5 = 1/DSIG**4/SQRT(DSIG**2)
      S3 = S4*S5
      S1 = S2*S3
      S3 = -DELPHI/192
      S8 = 12*DELS*SIGB**6*DSIG**2*ALOG(-SQRT(DSIG**2)*DSIG**2-SQRT(DSIG
     ,**2)*SIGA**2+SQRT(DSIG**2)*SIGB**2+2*SQRT(SIGA**2)*DSIG**2)+12*DEL
     ,S*SIGA**6*SIGB**2*ALOG(-SQRT(DSIG**2)*DSIG**2-SQRT(DSIG**2)*SIGA**
     ,2+SQRT(DSIG**2)*SIGB**2+2*SQRT(SIGA**2)*DSIG**2)-12*DELS*SIGA**4*S
     ,IGB**2*DSIG**2*ALOG(-SQRT(DSIG**2)*DSIG**2-SQRT(DSIG**2)*SIGA**2+S
     ,QRT(DSIG**2)*SIGB**2+2*SQRT(SIGA**2)*DSIG**2)-18*DELS*SIGB**4*DSIG
     ,**4*ALOG(-SQRT(DSIG**2)*DSIG**2-SQRT(DSIG**2)*SIGA**2+SQRT(DSIG**2
     ,)*SIGB**2+2*SQRT(SIGA**2)*DSIG**2)+3*DELS*SIGA**8*ALOG(2.E0)+6*DEL
     ,S*DSIG**8*ALOG(DSIG)+12*DELS*SIGA**2*SIGB**6*ALOG(-SQRT(DSIG**2)*D
     ,SIG**2-SQRT(DSIG**2)*SIGA**2+SQRT(DSIG**2)*SIGB**2+2*SQRT(SIGA**2)
     ,*DSIG**2)
      S9 = S8-18*DELS*SIGA**4*SIGB**4*ALOG(-SQRT(DSIG**2)*DSIG**2-SQRT(D
     ,SIG**2)*SIGA**2+SQRT(DSIG**2)*SIGB**2+2*SQRT(SIGA**2)*DSIG**2)+12*
     ,DELS*DSIG**6*SIGA**2*ALOG(-SQRT(DSIG**2)*DSIG**2-SQRT(DSIG**2)*SIG
     ,A**2+SQRT(DSIG**2)*SIGB**2+2*SQRT(SIGA**2)*DSIG**2)-18*DELS*SIGA**
     ,4*DSIG**4*ALOG(-SQRT(DSIG**2)*DSIG**2-SQRT(DSIG**2)*SIGA**2+SQRT(D
```

```
,SIG**2)*SIGB**2+2*SQRT(SIGA**2)*DSIG**2)
 S7 = S9-12*DELS*SIGA**2*SIGB**4*DSIG**2*ALOG(-SQRT(DSIG**2)*DSIG**
,2-SQRT(DSIG**2)*SIGA**2+SQRT(DSIG**2)*SIGB**2+2*SQRT(SIGA**2)*DSIG
,**2)+3*DELS*DSIG**8*ALOG(2.E0)-12*DELS*SIGA**2*SIGB**2*DSIG**4*ALO
,G(-SQRT(DSIG**2)*DSIG**2-SQRT(DSIG**2)*SIGA**2+SQRT(DSIG**2)*SIGB*
,*2+2*SQRT(SIGA**2)*DSIG**2)+12*DELS*SIGA**6*DSIG**2*ALOG(-SQRT(DSI
,G**2)*DSIG**2-SQRT(DSIG**2)*SIGA**2+SQRT(DSIG**2)*SIGB**2+2*SQRT(S
,IGA**2)*DSIG**2)
 S8 = S7-3*DELS*SIGB**8*ALOG(-SQRT(DSIG**2)*DSIG**2-SQRT(DSIG**2)*S
,IGA**2+SQRT(DSIG**2)*SIGB**2+2*SQRT(SIGA**2)*DSIG**2)+6*DELS*SIGA*
,*8*ALOG(DSIG)+18*DELS*SIGA**4*SQRT(SIGA**2)*SIGB**2*SQRT(DSIG**2)-
,16*DELS*SIGB**2*SQRT(SIGA**2)**3*DSIG**2*SQRT(DSIG**2)+6*DELS*SIGB
,**6*SQRT(SIGA**2)*SQRT(DSIG**2)+3*DELS*SIGB**8*ALOG(2.E0)+6*DELS*S
,IGB**8*ALOG(DSIG)
 S6 = S8-3*DELS*SIGA**8*ALOG(-SQRT(DSIG**2)*DSIG**2-SQRT(DSIG**2)*S
,IGA**2+SQRT(DSIG**2)*SIGB**2+2*SQRT(SIGA**2)*DSIG**2)+6*DELS*SIGA*
,*4*SQRT(SIGA**2)*DSIG**2*SQRT(DSIG**2)-6*DELS*SIGA**6*SQRT(SIGA**2
,)*SQRT(DSIG**2)+16*DELS*SIGA**2*SQRT(SIGA**2)**3*DSIG**2*SQRT(DSIG
,**2)-18*DELS*SIGB**4*SQRT(SIGA**2)*DSIG**2*SQRT(DSIG**2)+128*SA*SQ
,RT(SIGA**2)**3*DSIG**4*SQRT(DSIG**2)+16*DELS*SQRT(SIGA**2)**3*DSIG
,**4*SQRT(DSIG**2)+12*DELS*DSIG**6*SIGB**2*ALOG(-SQRT(DSIG**2)*DSIG
,**2-SQRT(DSIG**2)*SIGA**2+SQRT(DSIG**2)*SIGB**2+2*SQRT(SIGA**2)*DS
,IG**2)
 S7 = -18*DELS*SIGA**2*SIGB**4*SQRT(SIGA**2)*SQRT(DSIG**2)+S6-12*DE
,LS*SIGB**6*DSIG**2*ALOG(2.E0)-12*DELS*SIGA**2*SIGB**6*ALOG(2.E0)-2
,4*DELS*SIGB**6*DSIG**2*ALOG(DSIG)-12*DELS*SIGA**6*SIGB**2*ALOG(2.E
,0)+36*DELS*SIGA**4*SIGB**4*ALOG(DSIG)+18*DELS*SIGA**4*SIGB**4*ALOG
,(2.E0)-24*DELS*SIGA**2*SIGB**6*ALOG(DSIG)-3*DELS*DSIG**8*ALOG(-SQR
,T(DSIG**2)*DSIG**2-SQRT(DSIG**2)*SIGA**2+SQRT(DSIG**2)*SIGB**2+2*S
,QRT(SIGA**2)*DSIG**2)-24*DELS*SIGA**6*SIGB**2*ALOG(DSIG)+24*DELS*S
,IGA**4*SIGB**2*DSIG**2*ALOG(DSIG)+12*DELS*SIGA**4*SIGB**2*DSIG**2*
,ALOG(2.E0)-24*DELS*DSIG**6*SIGA**2*ALOG(DSIG)-12*DELS*DSIG**6*SIGA
,**2*ALOG(2.E0)
 S5 = S7+12*DELS*SIGA**2*SIGB**4*DSIG**2*ALOG(2.E0)+36*DELS*SIGB**4
,*DSIG**4*ALOG(DSIG)+18*DELS*SIGB**4*DSIG**4*ALOG(2.E0)+36*DELS*SIG
,A**4*DSIG**4*ALOG(DSIG)+18*DELS*SIGA**4*DSIG**4*ALOG(2.E0)-12*DELS
,*SIGA**6*DSIG**2*ALOG(2.E0)-12*DELS*DSIG**6*SIGB**2*ALOG(2.E0)-24*
,DELS*DSIG**6*SIGB**2*ALOG(DSIG)+24*DELS*SIGA**2*SIGB**2*DSIG**4*AL
,OG(DSIG)+12*DELS*SIGA**2*SIGB**2*DSIG**4*ALOG(2.E0)+24*DELS*SIGA**
,2*SIGB**4*DSIG**2*ALOG(DSIG)-24*DELS*SIGA**6*DSIG**2*ALOG(DSIG)+6*
,DELS*SQRT(SIGA**2)*SIGA**2*DSIG**4*SQRT(DSIG**2)+12*DELS*SIGA**2*S
,IGB**2*SQRT(SIGA**2)*DSIG**2*SQRT(DSIG**2)-6*DELS*DSIG**6*SQRT(SIG
```

```
,A**2)*SQRT(DSIG**2)+18*DELS*SQRT(SIGA**2)*SIGB**2*DSIG**4*SQRT(DSI
,G**2)
 S6 = 1/DSIG**4/SQRT(DSIG**2)
 S4 = S5*S6
 S2 = S3*S4
 T0 = S1+S2
 RETURN
 END
```

REFERENCES

Alder, W. F., and Dupree, D. M., 1974, "Stress Analysis of Coldworked Fastener Holes," *AFML-TR-74-44*, Air Force Materials Laboratory, Wright-Patterson AFB, Ohio.

Allen, D. N., and Sopwith, D. G., 1951, "The Stresses and Strains in Partly-Plastic Thick Tube Under Internal Pressure and End Load," *Proceedings of the Royal Society of London*, Ser. A, Vol. 205, p. 69.

Avitzur, B., 1994, "Autofrettage-Stress Distribution under Load Retained Stress after Depressurization," *Int. J. Pres. Ves. & Piping*, pp. 271-287.

Ball, D. L., 1995, "Elastic-Plastic Analysis of Cold Expanded Fastener Holes," *Fatigue Fract. Engng Mater. Struct.*, Vol. 18, No. 1, pp. 47-63.

Barber, J. R., 1992, *Elasticity*, Kluwer Academic Publishers.

Bernard, M., Bui-Quoc, T. and Burlat, M., 1995, "Effect of Re-Coldworking on Fatigue Life Enhancement of a Fastener Hole," *Fatigue Fract. Engng Mater. Struct.*, Vol. 18, No. 7/8, pp. 765-775.

Bland, D. R., 1956, "Elastoplastic Thick-Walled Tubes of Work-Hardening Materials Subjected to Internal and External Pressure and Temperature Gradient," *J. Mech. Phys. Solids*, pp. 209-229.

Bonn, R., and Haupt, P., 1995, "Exact Solution for Large Elastoplastic Deformation of a Thick-Walled Tube under Internal Pressure," *Int. J. Plasticity*, Vol. 11, No. 1, pp. 99-118.

Budiansky, B., 1959, "A Reassessment of Deformation Theories of Plasticity," *ASME Journal of Applied Mechanics*, Vol. 26, pp. 259-264.

Budiansky, B., 1971, "An Exact Solution to an Elastic-Plastic Stress Concentration Problem," *Prikl. Mat. Phys.*, Vol. 35, pp. 40-48.

Budiansky, B., and Mangasarian, O. L., 1961, "Plastic Stress Concentration at a Circular Hole in an Infinite Sheet Subjected to Equal Biaxial Tension," *ASME Journal of Applied Mechanics* , pp. 59-64.

Budiansky, B., and Videnšek, R. J., 1953, "Analysis of Stresses in the Plastic Range Around a Circular Hole Subjected to Uniaxial Tension," *National Advisory Committee for Aeronautics*, Technical Note No. 3542.

Buxbaum, O., and Huth, H., 1987, "Expansion of Cracked Fastener Holes as a Measure of Lifetime to Repair," *Journal of Engineering Fracture Mechanics*, Vol. 28, pp. 689-698.

Carter, A. E. and Hanagud, S., 1975, "Stress Corrosion Susceptibility of Stress-Coined Fastener Holes in Aircraft Structures," *AIAA Journal*, Vol. 13, No. 7, pp. 858-863.

Chaaban, A., 1985, *Static and Fatigue Design of High Pressure Vessels With Blind-End and Cross-Bores*, Ph.D. Thesis, Dept. Of Mech. Eng., University of Waterloo, Ontario, Canada.

Chakrabarty, J., 1987, *Theory of Plasticity*, McGraw-Hill Book Company.

Champoux, R. L., 1986, "An Overview of Cold Expansion Methods," in *Fatigue Prevention and Design*, Ed. J. T. Barnby, Chameleon Press, London, pp. 35-45.

Chang, J. B., 1974, "Analytical Prediction of Fatigue Crack Growth at Cold Worked Fastener Holes," *AIAA Paper*, No. 75-805.

Chen, P. C. T., 1972, "The Finite Element Analysis of Elastic-Plastic Thick-Walled Tubes," *Proceedings of Army Symposium on Solid Mechanics, The Role of Mechanics in Design-Ballistic Problems*, pp. 243-253.

Chen, P. C. T., 1973,"A Comparison of Flow and Deformation Theories in a Radially Stressed Annular Plate," *ASME Journal of Applied Mechanics*, Vol. 40, pp. 283-287.

Chen, P. C. T., 1980, "A Finite Difference Approach to Axisymmetric Plane-Strain Problems Beyond the Elastic Limit," *Transaction of the 25th Conference of Army Mathematician*, pp. 661-674.

Chen, P. C. T., 1980, "Generalized Plane-Strain Problems in an Elastic-Plastic Thick-Walled Cylinder," *Transaction of the 26th Conference of Army Mathematicians*, pp. 265-275.

Chen, P. C. T., 1986, "The Bauschinger and Hardening Effect on Residual Stresses in an Autofrettaged Thick-Walled Cylinder," *J. Pres. Ves. Tech., Trans. ASME*, Vol. 108, pp. 108-112.

Chen, P. C. T., 1992, "Nonlinear Stress Analysis of Composite-Jacketed Steel Cylinders Subjected to High Internal Pressure," *ASME PVP*-Vol. 40, pp. 283-287.

Chen, P. C. T., and O'Hara, G. P., 1984, "Finite Element Results of Pressurized Thick Tubes Based on Two Elastic-Plastic Material Models," *Trans. First Army Conf. on Applied Mathematics and Computing*, ARO Report 84-1, pp. 535-549.

Chen, R., 1996, *Constraint-Based Fracture Assessment of Pipeline Surface Cracks*, MASc Thesis, Department of Mechanical Engineering, University of Waterloo, Canada.

Chen, W. F., and Han D. J., 1988, *Plasticity for Structural engineers*, Springer-Verlag.

Chu, C. C., and Conle, F. A., 1994, "Multiaxial Neuber-Type of Elastic-Plastic Stress-Strain Correction," *Fourth International Conference on Biaxial/Multiaxial Fatigue*, Paris, France.

Chu, S. C., 1972, "A More Rational Approach to the Problem of an Elastoplastic Thick-Walled Cylinder," *J. Franklin Inst.*, Vol. 294, pp. 57-65.

Chu, S. C., and Vasilakis, J. D., 1973, "Inelastic Behavior of Thick-Walled Cylinders Subjected to Nonproportional Loading," *Experimental Mechanics SESA*, pp. 113-119.

Clark, G., 1982, "Residual Stress in Swage-Autofrettaged Thick-Walled Cylinders," *MRL-R-847*, Materials Research Laboratories, Ascot Vale.

Clark, G., 1991, "Modeling Residual Stress and Fatigue Crack Growth at Cold-Expanded Fastener Holes," *Fatigue Fract. Engng Mater. Struct.*, Vol. 14, No. 5, pp. 579-589.

Conle, A., and Nowack, H., 1977, "Verification of a Neuber-Based Notch Analysis by the Companion-Specimen method," *Experimental Mechanics*, Vol. 23, pp. 57-63.

Cook, G., 1934, "The Stresses in Thick-Walled Cylinders of Mild Steel Overstrained by Internal Pressure," *Proceedings of Institution of Mechanical Engineers*, Vol. 126, p. 407.

Cook, R. and Holdway, P., 1993, "Residual Stresses Induced by Hole Cold Expansion," *Proceedings of the I[st] International Conference on Computer Methods and Experimental Measurements for Surface*, Ed. M. H. Aliabadi and C. A. Brebbia, pp. 91-99.

Davis, E. A., 1943, "Increase of Stress with Permanent Strain and Stress-Strain Relations in the Plastic State for Copper under Combined Stresses," *ASME Journal of Applied Mechanics*, Vol. 65, pp. A187-A196.

Davis, E. A., 1945, "Yielding and Fracture of Medium-Carbon Steels under Combined Stresses," *ASME Journal of Applied Mechanics*, Vol. 67, pp. A13-A24.

Davis, E. A., 1964, "Extension of Iteration Method for Determining Strain Distribution to the Uniformly Stressed Plate with a Hole," *ASME Journal of Applied Mechanics*, Vol. 30, pp. 210-214.

Dhalla, A. K., 1981, "Simplified Inelastic Analysis Procedure to Evaluate a Butt-Welded Elbow End," *ASME PVP*-Vol. 50, pp. 109-127.

Dhalla, A. K., Jones, G. L., 1986, "ASME Code Classification of Pipe Stresses: A Simplified Elastic Procedure," *Int. J. Pres. Ves. & Piping*, Vol. 26, pp. 145-166.

Dowling, N. E., 1993, *Mechanical Behavior of Materials*, Prentice Hall, New Jersey.

Dowling, N. E., Brose, W. R. , and Wilson, W. K., 1977, "Notched Member Fatigue Life Predictions by Local Strain Approach, " *Fatigue under Complex Loading: Analyses and Experiments, Advanced in Engineering*, Vol. 6, Ed. R. M. Wetzel, Society of Automotive Engineers, Warrendale, Pa., pp. 55-84.

Durban, D., 1979," Large Strain Solution for Pressurized Elasto/Plastic Tubes," *ASME Journal of Applied Mechanics*, Vol. 64, pp. 228-230.

Durban, D., and Kubi, M., 1992, "A General Solution for the Pressurized Elastoplastic Tubes," *ASME Journal of Applied Mechanics*, Vol. 59, pp. 20-26.

Endo, T., and Morrow, J., 1969, "Cyclic Stress-Strain and Fatigue Behavior of Representative Aircraft Metals," *Journal of Materials, JMLSA*, Vol. 4, No. 1, pp. 159-175.

Fourgues, S., A., Bernard, M. and Bui-Quoc, T., 1993, "3-D Axisymmetric Numerical Analysis and Experimental Study of the Fastener Hole Coldworking Process," *Proceedings of 1st International Conference on Computer methods and Experimental measurements for Surface*, Ed. Aliabadi and Brebbia.

Franklin, G., Morrison, J. L. M., 1960, "Autofrettage of Cylinders: Prediction of Pressure/External Expansion Curves and Calculation of Residual Stresses," *Proc. Instn Mech. Engrs*, Vol. 174, No. 35, pp. 947-965.

Gao Xin-Lin, Wei Xue-xia, and Wang Zi-Kung, 1991, "A General Analytical Solution of a Strain-Hardening Plate Containing a Circular Hole Subjected to Biaxial Loading-With Applications in Pressure Vessels," *Int. J. Press. Vess. & Piping*, Vol. 47, pp. 35-55.

Gerdeen, J., C., 1979, "A Critical Evaluation of Plastic Behavior Data and a United Definition of Plastic Load for Pressure Components," *WRC Bulletin*, Vol. 254.

Glinka, G., 1985, "Energy Density Approach to Calculation of Inelastic Strain-Stress Near Notches and Cracks," *Engineering Fracture Mechanics*, Vol. 22, No. 3, pp. 485-508.

Hencky, H., 1924, "Zur Theorie Plastischer Deformationen und der Hierdurch im Material Hervorgerufenen Nachspannungen," *Z. Angew. Math. Mech.* Vol. 4, pp. 323.

Hibbitt, Karlsson & Sorensen, 1996, *ABAQUS / Standard*, Users Manual, Ver. 5.5.

Hill, R, 1950, *The Mathematical Theory of Plasticity*, Oxford University Press, London.

Hill, R., Lee, E. H., and Tupper, S. J., 1947, "The Theory of Combined Plastic and Elastic Deformation," *Proceeding of the Royal Society of London A*, Vol. 191, pp. 278-303.

Hill, R., Lee, E. H., and Tupper, S. J., 1951, "Plastic Flow in Closed-End Tube with Internal Pressure," *Proceeding of the First US National Congress on Applied Mechanics*, Chicago, Illinois.

Hodge, P. G., White, Jr., G. N., and Providence, R. I., 1952, "A Quantitative Comparison of Flow and Deformation Theories of Plasticity," *ASME Journal of Applied Mechanics*, Vol. 17, N0. 2, pp. 180-184.

Hoffman, O., and Sachs, G., 1953, *Introduction to the Theory of Plasticity for Engineers*, McGraw Hill, New York, pp. 80-95.

Hoffmann, M., Amstutz, H., and Seeger, T., 1991, "Local Strain Approach in Nonproportional Loading," *Fatigue under Biaxial and Multiaxial Loading ESIS10*, Ed. K. Kussmaul, D. McDiarmid, and D. Socie, Mechanical Engineering Publication, London, pp. 357-376.

Hoffmann, M., and Seeger, T., 1985, "A Generalized Method for Estimating Multiaxial Elastic-Plastic Notch Stresses and Strains Part 1: Theory," *ASME Journal of Engineering Materials and Technology*, Vol. 107, pp. 250-254.

Holdway, P., Cook, R., and Bowen, A. W., 1994, "Mapping of Residual Stresses Around Fastener Holes in High Strength Aluminum Alloy," *Surface Engineering*, Vol. 10, No. 4, pp. 292-295.

Hsu, Y. C., and Forman, R. G., 1975, "Elastic-Plastic Analysis of an Infinite Sheet Having a Circular Hole Under Pressure," *ASME Journal of Applied Mechanics*, Vol. 42, No. 2, pp. 347-352.

Huang, W. C., 1972, "Theoretical Study of Stress Concentrations at Circular Holes and Inclusions in Strain Hardening Materials," *Int. J. of Solids & Struct.*, pp. 149-192.

Hundy, B. B., and Green, A. P., 1954, "A Determination of Plastic Stress-Strain Relations," *J. Mech. Phys. Solids*, Vol. 3, p. 16.

Hunsaker, B., Vaughan, D. K., and Stricklin, J. A., 1976, "A Comparison of the Capability of Four Hardening Rules to Predict a Material's Plastic Behavior," *J. Pres. Ves. Tech., Trans. ASME*, pp. 66-74.

Hutchinson, J. W., 1968, "Singular Behavior at the End of a Tensile Crack in a Hardening Material," *J. Mech. Phys. Solids*, Vol. 16, pp. 13-31.

Ilyushin, A. A., 1946, "Some Problems in the Theory of Plastic Deformation," *RMB-12*, translation from *Prikl. Math. Mech.*, Vol. 7, 1943, pp. 245-272, by Grad. Div. Appl. Math., Brown University.

Ince, E. L., 1944, *Ordinary Differential Equation*, Dover, New York.

Jacob, L., 1907, "La Resistane et L'equilibre Elastique des Tubes Frettes," *Memorial de L'artillerie Naval*, Vol. 1, pp. 43-155.

Jahed, H., and Dubey R. N., 1996, "A Consistent Inelastic Formulation Analogous to Elastic Problems with Variable Coefficients," *ASME PVP-Vol. 343*, Development Validation, and Application of Inelastic methods for Structural Analysis and Design, pp. 215-223.

Jahed, H., and Dubey R. N., 1996, "Residual Stresses Calculation in Autofrettage Using Variable Material Properties Method," *ASME PVP-Vol. 327*, Residual Stress in Design, Fabrication, Assessment and repare, pp. 181-188.

Jahed, H., and Dubey, R. N., 1997, "An Axisymmetric Method of Elastic-Plastic Analysis Capable of Predicting Residual Stress Field," *J. Pres. Ves. Tech., Trans. ASME*, Vol. 119, in print.

Jahed, H., Sethuraman, R. and Dubey R. N., 1997, "A Variable Material Property Approach for Solving Elastic-Plastic Problems," accepted for publication in *Int. J. Pres. Ves. & Piping*.

Jahed, H., Sethuraman, R., and Dubey R. N., 1996, "Variable Material Properties Approach in Elastic-Plastic Solution of Thick-Walled Cylinders," *Mechanics in Design*, Ed. S. A. Meguid, Toronto, pp. 187-197.

Johnson, W., and Mellor, P. B., 1983, *Engineering Plasticity*, Ellis Horwood Limited, second edition.

Jost, G. S., 1988, "Stresses and Strains in a Cold Worked Annulus," *Australian Dept. Of Def., Aeronautical Research Laboratory, Tech. Rep. ARL-STRUC-R-434.*

Kalnins, A., and Updike, D. P., 1991, "Role of Plastic Limit and Elastic-Plastic Analyses in Design," *ASME PVP*-210-2, pp. 135-142.

Kendall, D. P., 1984, "A Simple Fracture Mechanics Based Method for Fatigue Life Prediction in Thick-Walled Cylinders," *Benet Weapons Laboratory, U. S. Army, Technical Report*, ARLCB-TR-84023.

Koiter, W. T., 1953, "On Partially Plastic Thick-Walled Tubes," *Biezeno Anniversary Volume on Applied Mechanics,* N. V. De Technische Uitgeverij H. Stam Harlem, Antwerpen, Djakarta, pp. 233-251.

Kottgen, V., Schon, M., and Seeger, T., 1993, "Application of a Multiaxial Load-Notch Strain Approximation Procedure to Autofrettage of Pressurized Components," *Advances in Multiaxial Fatigue, ASTM STP* 1191, pp. 375-396.

Landgraf, R., W., Morrow, J. and Endo, T., 1969, "Determination of the Cyclic Stress-Strain Curve," *Journal of Materials, JMLSA*, Vol. 4, No. 1, pp. 176-188.

Langlais, T. E., 1994, *Computer Method for Multiaxial Cyclic Plasticity*, MSc. Thesis, University of Minnesota.

Levy, M., 1870, *C. R. Acad. Sci., Paris*, Vol. 70, 1323.

Link, R. E., and Sanford, R. J., 1990, "Residual Strain Surrounding Split-Sleeve Cold Expanded Holes in 7075-T651 Aluminum," *Journal of Aircraft*, Vol. 27, No. 7, pp. 599-604.

Loghman, A., and Wahab, M. A., 1994, "Loading and Unloading of Thick-Walled Cylindrical Pressure Vessels of Strain-Hardening Material," *J. Pres. Ves. Tech., Trans. ASME*, Vol. 116, pp. 105-109.

Lowak, H., 1981, *Fraunhofer-Inst. Betriebs.*, Ber. No. FB-157.

MacGregor, C. W., Coffin, L. F., and Fisher, J. C., 1948, "Partially Plastic Thick-Walled Tubes," *J. Franklin Inst.*, p. 245.

Mackenzie, D., Boyle, J. T., 1993, "A Method of Estimating Limit Loads by Iterative Elastic Analysis. I- Simple Examples," *Int. J. Pres. Ves. & Piping*, Vol. 53, pp. 77-95.

Mann, J. Y., and Jost, G. S., 1983, "Stress Fields Associated with Interference Fitted and Cold-Expanded Holes," *Metal Forum*, Vol. 6, No. 1, pp. 43-53.

MAPLE V, 1996, Waterloo Maple Inc., Waterloo, Canada.

Marriott, D. L., 1988, "Evaluation of Deformation or Load Control of Stress under Inelastic Conditions using Elastic Finite Element Stress Analysis," *ASME PVP*-Vol. 136, Pittsburgh.

Megahed, M. M., and Abbas, A. T., 1991, "Influence of Reverse Yielding on Residual Stresses Induced by Autofrettage," *Int. J. Mech. Sci.*, Vol. 33, No. 2, pp. 139-150.

Mendelson, A., 1968, *Plasticity: Theory and Application*, The MacMillan Company, New York.

Mendelson, A., and Manson, S. S., 1959, "Practical Solution of Plastic Deformation in the Elastic-Plastic Range," *NACA Technical Report R-28.*

Milligan, R. V., Koo, W. H., and Davidson, T. E., 1966, "The Bauschinger Effect in a High-Strength Steel," *ASME Journal of Basic Engineering*, pp. 480-488.

Mises, R., Von, 1913, "Mechanik der Festen Koeper im Plastisch Deformablen Zustant," *Gottinger Nachr.*, Math.-Phys. Kl., pp. 582-592.

Moftakhar, A., 1994, *Calculation of Time Independent and Time Dependent Strains and Stresses in Notches*, PhD Thesis, Department of Mechanical Engineering, University of Waterloo, Canada.

Moftakhar, A., Buczynski, A., and Glinka, G., 1995, "Calculation of Elasto-Plastic Stress and Strain in Notches under Multiaxial Loading," *International Journal of Fracture*, Vol. 70, pp.357-373.

Molski, K., and Glinka, G., 1981, "A Method of Elastic-Plastic Stress and Strain Calculation at a Notch Root," *Materials Science and Engineering*, Vol. 50, pp. 93-100.

Mroz, E., and Olszak, A. H., 1963, *Recent Advancement in the Mathematical Theory of Plasticity*," Pergamon Press.

Nadai, A., 1943, "Theory of the Expanding of Boiler and Condenser Tube Joints Through Rolling," *Trans. ASME*, Vol. 65, pp. 865-880.

Nadai, A., 1950, *Theory of Flow and Fracture of Solids*, McGraw-Hill, London.

Nadarajah, C., Mackenzie, D., and Boyle, J. T., 1993, "A Method of Estimating Limit Loads by Iterative Elastic Analysis. II - Nozzle Sphere Intersections with Internal Pressure and Radial Load," *Int. J. Pres. Vess. & Piping*, Vol. 53, pp. pp. 97-115.

Naghdi, P. M., Essenburg, F., and Koff, W., 1958, "An Experimental Study of Initial and Subsequent Yield Surfaces in Plasticity," *ASME Journal of Applied Mechanics*, Vol. 25, pp. 201-213.

Neuber, H., 1961, "Theory of Stress Concentration for Shear-Strained Prismatical Bodies with Arbitrary Nonlinear Stress-Strain Law," *ASME Journal of Applied Mechanics*, Vol. 28, pp. 554-550.

Ozdemir, A. T., and Edwards, L., 1996, "Measurement of the Three-Dimensional Residual Stress Distribution Around Split-Sleeve Cold-Expanded Holes," *Journal of Strain Analysis*, Vol. 31, No. 6, pp. 413-420.

Ozelton, M. W., and Coyle, T. G., 1986, "Fatigue Life Improvement by Cold Working Fastener Holes in 7050 Aluminum," in *Fatigue in Mechanically Fastened Composite and Metallic Joints*, ASTM STP 927, pp. 53-71.

Parker, A. P., and Farrow, J. R., 1981, "Stress Intensity Factors for Multiple Radial Cracks Emanating from the Bore of an Autofrettage or Thermally Stressed Thick Cylinder," *Engng Fracture Mech.*, Vol. 14, pp. 278-303.

Perl, M., and Arone, R., 1988, "Stress Intensity Factors for a Radially Multicracked Partially Autofrettaged Pressurized Thick-Walled Cylinder," *J. Pres. Ves. Tech., Trans. ASME*, Vol. 110, pp. 147-154.

Perl, M., and Arone, R., 1994, "An Axisymmetric Stress Release Method for Measuring the Autofrettage Level in Thick-Walled Cylinders- Part I: Basic Concept and Numerical Simulation," *J. Pres. Ves. Tech., Trans. ASME*, Vol. 116, pp. 384-388.

Phillips, A., and Lee, C. W., 1979, "Yield Surfaces and Loading Surface: Experiments and Recommendations," *International Journal of Solids and Structures*, Vol. 15, pp. 715-729.

Pintschovius, L., Macherauch, E., and Scholets, B., 1986, "Determination of Residual Stress in Autofrettaged Steel Tubes by Neutron and X-ray Diffraction," *Residual Stress in Science and Technology*, pp. 159-165.

Poolsuk, S., and Sharpe, W. N., 1978, "Measurement of the Elastic-Plastic Boundary Around Coldworked Fastener Holes," *ASME Journal of Applied Mechanics*, Vol. 45, pp. 515-520.

Potter, R. M., Ting, T. W., and Grandt, A. F., 1978, "An Analysis of Residual Stresses and Displacements Due to Radial Expansion of Fastener Holes," *Air force Material Laboratory, Tech. Rep. AFML-TR-79-4048.*

Poussard, C. G. C., Pavier, M., J., and Smith, D. J., 1994, "Prediction of Residual Stresses in Cold Worked Fastener Holes Using the Finite Element Method," *Engineering Systems Design and Analysis, PD-Vol. 64-8.1*, Vol. 8, Part A, pp. 47-53.

Poussard, C., Pavier, M. and Smith, D., J., 1995, "Analytical and Finite Element Predictions of Residual Stresses in Cold Worked Fastener Holes," *Journal of Strain Analysis*, Vol. 30, No. 4, pp. 291-304.

Prager, W., 1957, "A New Method of Analyzing Stress and Strains in Work-Hardening Plastic Solids," *ASME Journal of Applied Mechanics*, Vol. 23, pp. 493-496.

Prager, W., and Hodge, P. G, 1951, *The Theory of Perfectly Plastic Solids*, Wiley, New York.

Prandtl, L., 1924, *Proc. Ist Int. Congr. App. Mech.*, Delft, pp. 43.

Priest, M., Poussard, C. G., Pavier, M. J., and Smith D. J., 1995, "An Assessment of Residual-Stress Measurements Around Cold-Worked Holes in Al 2024," *The 4th International Conference on Residual Stresses*, Baltimore, Md., pp. 324-332.

Ramberg, W., and Osgood, W. R., 1943, " Description of Stress-Strain Curves by Three Parameters," *National Advisory Committee on Aeronautics*, Technical Note, 902.

Rees, D. W. A., 1987, "A Theory of Autofrettage with Applications to Creep and Fatigue," *Int. J. Prss. Vess. & Piping*, Vol. 30, pp. 57-76,.

Reuss, A., 1930, *Z. Angew. Math. Mech.* Vol., 10, pp. 266.

Rich, D. L., and Impelizzerri, L. F., 1977, "Fatigue Analysis of Cold-Worked and Interference Fit Fastener Holes," *Cyclic Stress-Strain and Plastic Deformation Aspects of Fatigue Growth, ASTM STP 637,* pp. 153-175.

Roach, D. P., and Priddy, T. G., 1994, "Effect of Material Properties on the Strain to Failure of Thick-Walled Cylinders Subjected to Internal Pressure," *J. Pres. Ves. Tech., Trans. ASME,* Vol. 116, pp. 96-104.

Sachs, G., 1927 "Der Nachweis Immerer Spannungen in Stangen und Rohen", *Zeit. Metall.,* 19, pp. 352-357.

Schulte, C. A., 1960, "Predicting Creep Deflection of Plastic Beam," *ASTM*, Vol. 60, pp. 895-904.

Seeger, T., 1985, "A Generalized Method for Estimating Multiaxial Elastic-Plastic Notch Stresses and Strains Part 1: Theory," *ASME Journal of Engineering Materials and Technology,* Vol. 107, pp. 250-254.

Seshadri, R., 1990, "The Effect of Multiaxiality and Follow-Up on Creep Damage," *J. Pres. Ves. Tech., Trans. ASME,* Vol. 112, pp. 378-385.

Seshadri, R., 1991, "Simplified Methods for Determining Multiaxial Relaxation and Creep Damage," *Proceedings of ASME Pressure Vessels and Piping Conference,* San Diego, *ASME PVP* 210-2, pp. 173-180.

Seshadri, R., 1991, "The Generalized Local Stress Strain (GLOSS) Analysis- Theory and Applications," *J. Pres. Ves. Tech., Trans. ASME*, Vol. 113, pp. 219-227.

Seshadri, R., and Fernando, C. P. D., 1992, "Limit Loads of Mechanical Components and Structures Using the GLOSS R-Node Method," *J. Pres. Ves. Tech., Trans. ASME,* Vol. 114, pp. 201-208.

Seshadri, R., Marriott, D. L., 1992, "On Relating the Reference Stress, Limit Load and the ASME Stress Classification Concepts," *ASME PVP* Vol. 203, pp. 135-149.

Sharp, W. N. Jr., and Wang, K. C., 1991, "Evaluation of a Modified Monotonic Neuber Relation," *Journal of Engineering Materials and Technology,* Vol. 113, pp. 350-353.

Sharpe, W. N., Jr., Yang, C. H., and Tregoning, R. L., 1992, "An Evaluation of Neuber and Glinka Relations for Monotonic Loading," *ASME Journal of Applied Mechanics*, Vol. 59, pp. S50-S56.

Shi, J., Mackenzie, D., and Boyle, J. T., 1993, "A Method of Estimating Limit Loads by Iterative Elastic Analysis. III-Terispherical Heads Under Internal Pressure," *Int. J. Pres. Ves. & Piping*, Vol. 53, pp. 121-142.

Sidebottom, O. M., and Chu, S. C., 1975, "Bursting Pressure of Thick-Walled Cylinders Subjected to Internal and External Pressure, Axial Load and Torsion," *Experimental Mechanics SESA*, pp. 209-218.

Smith, J. O., and Sidebottom, O. M., 1952, *Inelastic Behavior of Load Carrying Members*, Wiley, New York.

Sokolovsky, W. W., 1969, *Theory of Plasticity*, Moscow.

Stacey, A., and Webster, G. A., 1988, "Determination of Residual Stress Distribution in Autofrettaged Tubing," *Int. J. Pres. Ves. & Piping*, Vol. 31, pp. 205-220.

Stacey, A., MacGillivary, H. J., Webster, G. A., Webster, P. J., and Ziebeck, K. R. A., 1985, "Measurement of Residual Stress by Neutron Diffraction," *Journal of Strain Analysis*, Vol. 20, No 2, pp. 93-100.

Steel, M. C., 1952, "Partially Plastic Thick-Walled Cylinder Theory," *ASME Journal of Applied Mechanics*, Vol. 74, pp. 133-140.

Stowell, E. Z., 1950, "Stress and Strain Concentration at a Circular Hole in an Infinite Plate," *NACA TN 2073*.

Taylor, G. L., 1947, "The Formation and Enlargement of a Circular Hole in a Thin Plastic Sheet," *Quarterly Journal of Mechanics and Applied Mathematics*, Series 7, No. 1, pp. 103-124.

Tresca, H., 1864, "Notes on Yield of Solid Bodies under Strong Pressure," *Comptes Rendus del' Academie des Science*, Vol. 59, p. 754.

Tuba, I. S., 1965, "Elastic-Plastic Stress and Strain Concentration Factors at a Circular Hole in a Uniformly Stressed Infinite Plate," *ASME Journal of Applied Mechanics*, Vol. 32, pp. 710-711.

Tuba, I. S., 1966, "A Method of Elastic-Plastic Plane Stress and Strain Analysis," *Journal of Strain Analysis*, Vol. 1, No. 2, pp. 115-120.

Walker, K., 1977, "Multiaxial Stress-Strain Approximation for Notch Fatigue Behavior," *Journal of Testing and Evaluation*, Vol. 5, No. 2, pp. 106-113.

Wang, G. S., 1988, "An Elastic-Plastic Solution for a Normally Loaded Center Hole in a Finite Circular Body," *Int. J. Pres. Ves. & Piping*, Vol. 33, pp. 269-284.

Wanlin, G., 1993, "Elastic-Plastic Analysis of a Finite Sheet With a Cold-Worked Hole," *Engineering Fracture Mechanics*, Vol. 45, No. 6, pp. 857-864.

Wieland, D. H., Cutshall, J. T., Burnside, O. H., and Cardinal, J. W., 1994, "Analysis of Cold Worked Holes for Structural Life Extension," *FAA/NASA International Symposium on Advanced Structural Integrity Methods for Airframe Durability and Damage Tolerance*, Ed. C. E. Harris, NASA Langley research Center, pp. 947-961.

Wood, H. A., 1975, "Application of Fracture Mechanics to Aircraft Structural Safety," *Journal of Engineering Fracture Mechanics*, Vol. 7, pp. 557-564.

Yong, L., and Naiji, S., 1991, "Residual Stress Analysis for Actual Material Model of Autofrettaged Tube by Non-Linear Boundary Element Method," *Int. J. Pres. Ves. & Piping*, Vol. 48, pp. 21-35.

Ziegler, H., 1959, "A Modification of Prager's Hardening Rule," *Quarterly of Mathematics*, Vol. 17, No. 1, pp. 55-65.